SYNTHESIS AND CHARACTERIZATION OF SEMIORGANIC POTASSIUM HYDROGEN OXALATE OXALIC ACID DIHYDRATE SINGLE CRYSTALS

Thesis

Submitted in partial fulfilment of the requirements for the degree of

DOCTOR OF PHILOSOPHY

By

MAHENDRA K

(Reg.No. 138023PH13F06)

DEPARTMENT OF PHYSICS

NATIONAL INSTITUTE OF TECHNOLOGY KARNATAKA

SURATHKAL, MANGALORE - 575025

May, 2020

DECLARATION

By the Ph.D Scholar

I hereby declare that the Research Thesis entitled **"Synthesis and characterization of semiorganic potassium hydrogen oxalate oxalic acid dihydrate single crystals"** which is being submitted to the **National Institute of Technology Karnataka, Surathkal** in partial fulfilment of the requirements for the award of the Degree of **Doctor of Philosophy** in **Physics** is a bonafide report of the research work carried out by me. The material contained in this Research Thesis has not been submitted to any University or Institution for the award of any degree.

Mahendra K

(Register No.: 138023PH13F06)

Department of Physics

Place: NITK, Surathkal

Date:

CERTIFICATE

This is to certify that the Research Thesis entitled **"Synthesis and characterization of semiorganic potassium hydrogen oxalate oxalic acid dihydrate single crystals"** submitted by **Mahendra K** (**Register Number: 138023PH13F06**) as the record of the research work carried out by him, is accepted as the ***Research Thesis*** submission in partial fulfilment of the requirements for the award of degree of ***Doctor of Philosophy***.

Prof. N.K. Udayashankar
Research Supervisor
Department of Physics
N.I.T.K., Surathkal – 575025

Chairman – DRPC
(Signature with Date and Seal)

ACKNOWLEDGEMENTS

Completion of this doctoral research work is possible with the support of several people. I would like to express my sincere gratitude to all of them. First of all, I am extremely grateful to my research guide, Prof. N. K. Udayashankar, for his valuable guidance, scholarly inputs and consistent encouragement I received throughout the research work. This accomplishment is possible only because of the unconditional support provided by him.

I sincerely thank the members of RPAC Dr. Ravishankar K.S and Dr. Partha Pratim Das for their valuable suggestions and excellent advice in pursuing this research work.

I am grateful to the Head of Department for supporting me to attend various conferences and workshops, which in turn helped me to understand the current research work.

I heartily thank my fellow lab mates Dr. Naveen, Dr. Kiran P, Dr. Brian Jeevan Fernandes, Dr. Ramana Reddy, Dr. Suchitra S.M., Ms. Anupriya James, Ms. Navaneeta and Mr. Sindhur Joshi for their cooperation and best wishes. I also thank MSc students Ms. Anita, Mr. Ifthekar, Ms. Kavya, Ms. Swathi, Mr. Gajendra and Mr. Sebastian for their best wishes.

I am greatly indebted to companionship of circle of friends outside the lab and institute, who have continuously supported me in many aspects throughout these years. I owe a lot to Dr. Bindu, Dr. Bharath, Ms. Amudha, Mr. Dhanush Shanbhag, Mr. Achyutha, Mr. Biswajith and Mr. Brijesh for being there for me when I was in need of support.

I thank Dr. Raghavendra Hebbar, Mr. Makesh, Mr. Shreyas, Mr. Karthik Hegde, Mr. Karthik S Bhat, Mr. Mukhesh, Mr. Sachin, Mr. Nitish, Mr. Arjun Nayak, Mr. Sumant, Mr. Prakash, Mr. Nandakumar, Mr. Vijeth, Ms. Soujanya, Ms. Pavitra, Mr. Laxmisagar, Ms. Lavanya and Ms. Megha. I appreciate their friendly encouragement and making my experience a lot better.

I owe special thanks to my parents K. Kanthappa and Vishalakshi K., sister Akshatha K. A special thanks to family members, Yathish, Vinith and Sandeep, for their care and support along the way.

There are many more whom I must remember with gratitude. Their names, though I might have failed to mention here, shall never be forgotten.

Mahendra K

Abstract

A metal-organic hybrid compound named potassium hydrogen oxalate oxalic acid dihydrate (KHOOD) single crystal is synthesized using solvent evaporation technique at room temperature. Synthesized crystals are thoroughly characterized using various methods such as single crystal XRD (SCXRD), powder XRD (PXRD), UV-vis analysis, FTIR, TGA-DTA, DSC, photoluminescence, Vickers microhardness, SEM-EDAX, I-V and dielectric measurements. The synthesized crystal belongs to centro-symmetric space group P-1 with triclinic crystal system and from I-V studies negative photoconductivity effect is observed suggesting their use as photoresistors. Further, doping studies were carried out for the synthesized KHOOD crystals where, commercially purchased Amaranth dye and pre-synthesized $Co(OH)_2$ nanoparticles were used for doping KHOOD single crystals. The presence of $Co(OH)_2$ nanoparticles in the crystal system were confirmed through XRD, EDAX and PL measurements. The effect of nanoparticle incorporation on the optical, thermal and electrical properties of the crystals were studied with the help of UV-vis, TGA-DTA, I-V and dielectric measurements. From I-V and dielectric measurements it was confirmed that the conductivity increases as the dopant concentration increased. Influence of amaranth dye on the KHOOD single crystal was also investigated. The effect of dye molecule on the crystal of KHOOD was studied using XRD, UV-vis, SEM-EDX, PL, TGA-DTA and I-V measurements.

The defect induced studies were performed for different dosage of Gamma irradiations. The structural, optical and electrical properties of the irradiated crystals were studied and results were analyzed. The effect of irradiation on the crystal lattice for different dosage was investigated. As the irradiation dosage increased, the crystal conductivity decreases which consequently led to increase in its resistivity which is also true in case of light irradiated crystals.

Further, a detailed study is conducted to understand the differences between Oxalic acid dihydrate (OAD), Potassium oxalate hydrate (KOH), Potassium hydrogen oxalate oxalic acid dihydrate (KHOOD) for comparing their physical properties. The crystals of these compounds were studied using PXRD, UV-vis, PL, TGA-DTA, I-V and Vickers microhardness studies to understand the physio chemical changes brought about by the complexation of the oxalic acid.

CONTENTS

List of Figures

List of Tables

CHAPTER 1

INTRODUCTION

Overview

This chapter provides a detailed description of crystals, importance of crystals and, different methods used for crystal growth. This chapter gives a detailed literature survey on metal oxalate single crystals using solution method. Further, the research objectives and the organization of the thesis is mentioned.

1.1 Background and motivation

Ancient Greeks used the word 'crystal (krustallos)' to imply clear, transparent and hard ice. Pythagoras used the word 'crystal' to imply perfection, harmony and beauty. The enchanting appearance of crystals through their colour, transparency, shape and healing power as believed by some have always fascinated humans from the beginning of the Stone Age. Crystals were seen as mesmerizing work of nature, their internal structure ultimately bestow them with their unique external appearance or morphology. The crystal is a solid formed through three-dimensional periodic array of identical building blocks of a material (atoms, molecules or ions). Crystals may contain imperfections and impurities affecting their properties. The early crystallization experiments in 18^{th} and 19^{th} century formed the basis for the fundamental aspects of crystal growth. However, theoretical understanding of the process was not known until the development of thermodynamics in the late 19^{th} century. Further, in the 20^{th} century, nucleation and crystal growth theories gave a better understanding of the process [Kittel 2012].

A crystal is a solid material in which constituent atoms, molecules or ions are arranged in a regular repeating pattern in all three spatial directions, showing long range periodicity and symmetry. The building blocks may be ions, atoms or group of atoms. Further, a crystal is always characterized by anisotropy [Pring 2006]. In single crystals, distribution of basic constituents like atoms is continuous throughout the crystal without any discontinuous boundaries. Single crystals are difficult to grow when compared to polycrystalline materials. Perfect single crystals are rare in nature and they

have to be grown in laboratory in well controlled experimental conditions. They possess long range ordering and symmetry. The extra effort taken in growing single crystals is formidable due to the uniformity in composition and absence of grain boundaries. The aggregation of many small crystals with different orientations gives polycrystalline solid. These crystals in polycrystalline solid are microscopic and are known as crystallites. Polycrystals contain grain boundaries. If one desires to know some bulk properties of a material and measures those properties on a polycrystalline specimen, then the measured property would be that of the grain boundaries and not the bulk material. Electrical conductivity of semiconductors is always impurity-sensitive. Impurities tend to segregate at grain boundaries and thereby affecting the electrical properties of the semiconductors. Similarly, grain boundaries and associated voids cause light scattering, and thus single crystals are often required in optical studies. Good quality single crystals are needed for fabrication of high performance devices. Much better frequency stability and lower acoustic losses can be achieved in single crystals than in polycrystalline aggregates. Thus single-crystal piezoelectric crystals, such as quartz are used for frequency-control elements. The existence of lasers and masers has created new demands for single crystals for research and applications.

"Today, man lives on the boundary between the Iron Age and a new Materials Age" said the Cocke and Clearfield [Cocke and Clearfield 1987]. Nobel laureate Sir George Thomson in 1987 made us aware of the upcoming material revolution which is still accelerating. Technology demands efficient materials for its implementation. Best example is the growth of electronics industry witnessed by advancement of semiconductor materials like silicon, germanium, gallium arsenide, etc. Crystal growth is an interdisciplinary subject which involves physics, chemistry, metallurgy, chemical engineering, crystallography, mineralogy and so on. The scientific study of crystal structure and symmetry is called crystallography. They are essential part of electronic industry, photonic industry and fiber optic communications. Good quality crystals are required for the production of semiconductors, superconductors, polarizers, transducers, radiation detectors, ultrasonic amplifiers, ferrites, solid state lasers, electro-optic devices, acousto-optic devices, crystalline films for microelectronics and computer industries. The recent rapid advancements in microelectronics, photonics and fiber optic communications shows the strong impact of single crystals in the present

day technology. Growth of defect free single crystals and their characterization towards device fabrication have received great impetus due to their importance in both applied and academic research.

1.2 Importance of Crystals

Optoelectronics and laser technology are boosted with new optical materials especially nonlinear optical materials like lithium niobate, lithium tantalate, KDP, etc. It is difficult to imagine the photonic industry without crystals. Dr. Tadahiro Sekimoto, a Japanese businessman and scientist has accurately put forward the necessity of developing novel materials for advancement of technology as, "one who dominates materials dominates technology" [Sass 2011]. The rapid development of new materials has established materials science as a well-established discipline. As crystal is a basic building block of a solid-state material, growing newer and better crystals from existing and future techniques is inevitably important. Some recently developed types of crystals like photonic crystals and quasi crystals are gaining their ground.

Over the past few decades there has been significant advancement in the field of opto- electronic device fabrication and to achieve highly efficient devices, good quality single crystals are needed. Growth and characterization of defect free single crystals has assumed great scope and significance in view of their importance for both scientific research as well as cutting edge industrial applications.

The stages involved in the synthesis of single crystals include proper selection of growth technique, understanding growth behavior, setting up optimized growth parameters, characterization and utilization of these crystals in devices and finally extension from laboratory to commercial production.

The search for newer crystals and faster crystallization techniques has driven the scientific community to understand the growth methodology better and design improved growth equipments. Hence there exists unending scope for crystal growth theory and technology.

1.3 WHAT IS A CRYSTAL?

A crystal is a solid composed of atoms or other microscopic particles arranged in an orderly repetitive array. The three general types of solids - amorphous, polycrystalline and single crystal are distinguished by the size of ordered regions within the materials. Order in amorphous solids is limited to a few molecular distances. In

polycrystalline materials, the solid is made up of grains which are highly ordered crystalline regions of irregular size and orientation. Single crystals have long range order and possess translational symmetry. The atomic arrangement in a crystal is called crystal structure. In a perfect crystal, there is a regular arrangement of atoms. This periodicity in arrangement generally varies in different directions. It is very convenient to imagine points in space about which these atoms are located. Such points in space are called lattice points and the totality of such points forms a crystal space lattice. If all the lattice points are identical, the lattice is called Bravais lattice. Thus, the three-dimensional space lattice may be defined as a finite array of points in three dimensions in which every point has identical environment as any other point in the array.

For a three-dimensional lattice

$$\vec{T} = n_1\overrightarrow{a_1} + n_2\overrightarrow{a_2} + n_3\overrightarrow{a_3}$$

Where, n_1, n_2 and n_3 are integers and $\overrightarrow{a_1}$, $\overrightarrow{a_2}$, $\overrightarrow{a_3}$ are fundamental translation vectors which are characteristic of the array [Cubillas and Anderson 2010].

A crystal is likely to exhibit an external morphology of planes which make characteristic angles with each other if the sample being studied happens to be a single crystal. In three dimensions, triclinic is the most general lattice. The simplest primitive cell of triclinic is a parallelepiped with all angles different from 90° and primitive translation vectors $\vec{a}$, $\vec{b}$ and $\vec{c}$ are of different lengths. However, thirteen "special lattice types" are generated by considering relationships between sides and angles. Thus, in total, there are 14 Bravais lattices which can be grouped into seven crystal systems as shown in Table 1.1.

Table. 1.1. The seven crystal systems and the fourteen Bravais space lattices.

System	**Interfacial angles (α, β, γ)**	**Axial length of unit cell**	**Bravis lattices**	**Examples**
Cubic	α=β=γ=90°	a=b=c	Primitive (P) Face centered (F) Body centered (I)	Sodium chloride (NaCl) Cesium chloride (CsCl)
Tetragonal	α=β=γ=90°	a=b≠c	Primitive (P) Body centered (I)	Nickel sulphate ($NiSo_4$)

Orthorhombic	α=β=γ=90°	a≠b≠c	Primitive (P) Face centered (F) Body centered (I) Base centered (C)	Ammonium sulphate ($(NH_4)_2SO_4$) Iodine (I_2)
Monoclinic	α=γ=90°≠ β	a≠b≠c	Primitive (P) Base centered (C)	Potassium chlorate ($KClO_3$)
Hexagonal	α=β=90° γ=120°	a=b≠c	Primitive (P)	Graphite (C)
Rhombohedral	α=β=γ≠90°	a=b≠c	Primitive (P)	Sodium nitrate ($NaNO_3$)
Triclinic	α≠β≠γ≠90°	a≠b≠c	Primitive (P)	Copper sulphate ($CuSO_4$)

1.4 THEORY OF CRYSTAL GROWTH

Matter in the universe is present in different states or phases in which it can attain maximum stability. A system always prefers most stable state through energy transfer with surroundings. Different phases in which a matter can exist at particular pressure and temperature can be explained by a phase diagram. Each phase has chemical potential (Δμ) or energy associated with it which is used as work done while phase transition. Chemical potential is defined as amount of work done in order to change number of particles in a phase by unity. Two phases are in equilibrium when their potentials coincide. Consider two phases of a matter as A and B, with potential energies $\Delta\mu_A$ and $\Delta\mu_B$ respectively. These phases will be in equilibrium when

$$\Delta\mu_A\,(P, T) = \Delta\mu_B\,(P, T) \qquad 1.1$$

If there arises difference in chemical potentials of these phases, phenomena of mass transport take place which continues until both phases acquire equilibrium again. This imbalance of chemical potentials works as the driving force for phase transition.

$$\Delta\mu * Number\ of\ molecules\ transported = Work\ done \qquad 1.2$$

It is a known fact that all thermodynamic process strives to minimize the free energy. A system always prefers to be in most stable state by energy transfer with its surroundings. Different phases of matter exist at different temperature and pressure which can be represented

by a phase diagram Figure 1.1. During the process of crystal growth, phase transition occurs due to lowering of free energy of the system. In any system, the fraction of energy available to be converted into work is termed as Gibb's free energy and the remaining energy is called bound energy. From thermodynamic point of view Gibbs free energy establishes relation between enthalpy (H) and entropy (S) of the system through temperature (T) as,

$$G = H - TS \quad (1.3)$$

It is the measure of stability of a phase. Lesser the free energy more stable would be the phase of the system. For a phase transition, change in free energy would be

$$\Delta G = \Delta H - T\Delta S \quad (1.4)$$

Where, ΔH is change in enthalpy and ΔS is change in entropy. The free energy difference between the solid and supercooled liquid is the driving force for crystallization. Phase transition occurs such that there is decrease in free energy of the system [Rudolph 2003].

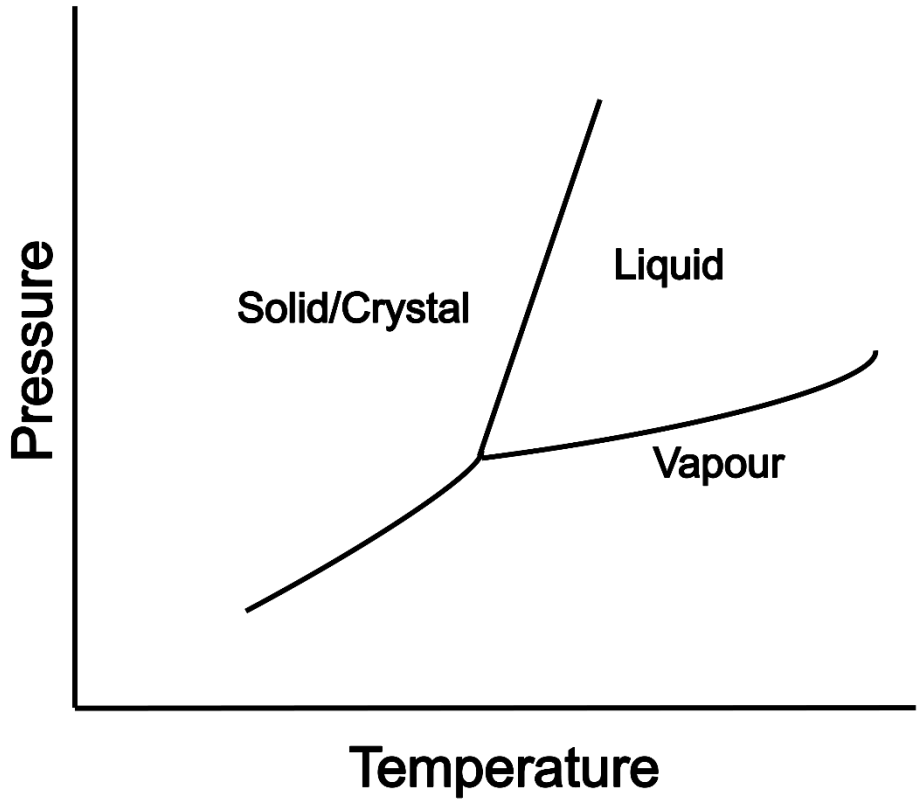

Figure. 1.1. Phase diagram of a crystal.

Along the line separating two phases, both phases are in equilibrium due to equality of their chemical potentials at corresponding values of pressure and temperature. This

balance can be disturbed through change in pressure or temperature in one of the phases which makes transition to other phase to attain stability. In crystal growth technique such a state is obtained through supersaturation or supercooling of the initial available phase often referred as metastable state or mother phase. Energy associated with metastable state is intermediate of stable and unstable states. Growth is a result of highly one directional flow of substituents from one phase to another which is obtained as transition from metastable to stable state.

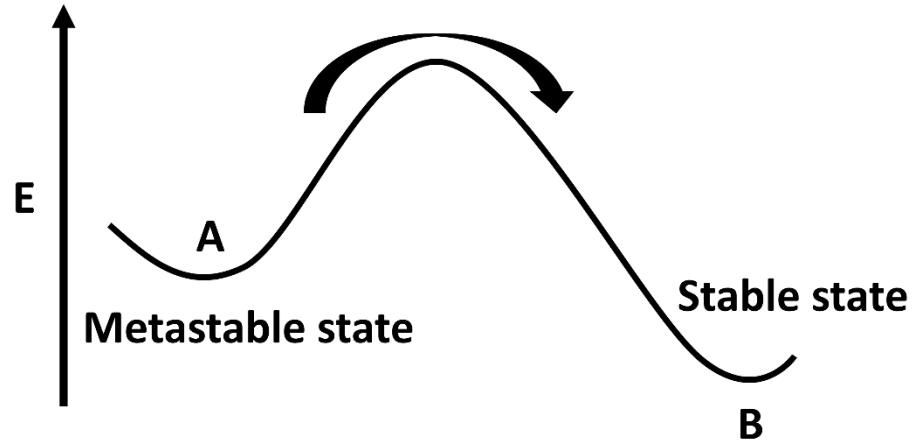

Figure. 1.2. Transition from metastable to stable state.

In Figure 1.2, net growth from A to B is not obtained at equilibrium temperature as transition from A to B is equal to transition from B to A. But at lower temperature, if B has lower free energy than A, net growth from A to B is observed as transition from B to A puts higher energy barrier to overcome.

1.5 GROWTH OF SINGLE CRYSTALS

There are wide variety of methods ranging from simple inexpensive techniques to complex sophisticated techniques. The time taken for crystallization may range from few hours to few months. The main principle behind the crystal growth is the formation of nucleus which grows into single crystal by assembling ions or molecules with specific interactions and bonding. Crystal growth can be classified under following categories [Spring-Thorpe and Pamplin 1968] :

1. Solid growth which involves solid to solid phase transition.
2. Melt growth which involves liquid to solid phase transition.
3. Vapour growth which involves vapour to solid phase transition.
4. Liquid growth which involves liquid to solid phase transition.

A particular material may be grown by number of techniques. One method may yield high purity crystal while other may yield large single crystals. The choice of appropriate method depends not only on the characteristics of the material but also on the requirements for specific applications.

1.5.1 SOLID GROWTH

The conversion of a polycrystalline piece of material into single crystal by causing the grain boundaries to be swept through and pushed out of the crystal takes place in the solid growth of crystals. Solid state growth requires atomic diffusion in the given material. If a polycrystalline material is held at an elevated temperature, below the melting point for many hours, some grains grow at the expense of their neighbors.
There are five principal methods of Solid- Solid growth,

1. Recrystallization by annealing out strain
2. Recrystallization by sintering
3. Recrystallization by polymorphic transition
4. Crystallization by devitrification
5. Recrystallization by solid-solid precipitation

The main advantages of solid- solid growth methods are the following: They permit growth at low temperatures without the presence of additional components, the shape of the grown crystal is fixed beforehand so that wires, foils etc., are easily grown. The main disadvantage of this technique is that as the growth process takes place in the solid, density of sites for nucleation is high and is difficult to control nucleation to produce large single crystals.

1.5.2 Growth from melt

Melt growth is the process of crystallization by fusion and resolidification of the pure material from a melt on cooling it below its freezing point. The materials which melt congruently, do not decompose before melting and do not undergo a phase transition between the melting point and room temperature can be grown into a single crystal from the melt. The rate of growth is much higher than any other methods of crystal growth. Hence this method is widely used method of crystal growth for commercial purposes.
Melt growth involves following techniques:

a) Bridgeman technique

b) Czochralski technique

c) Flame fusion technique

d) Zone melting method

e) Float zone method

1.5.2(a) Bridgeman method

It is the simplest technique for growth of crystals from melt and it was developed by Bridgman in 1925. A large range of materials are grown by this technique. A boat containing molten material with seed crystal at one end is withdrawn through temperature gradient. The slow cooling from the end containing seed crystal results in the formation of single crystal along the length of the container. The process can be carried out in horizontal or vertical geometry. This technique is often used for the growth of metals, semiconductors, and alkali and alkaline earth metals.

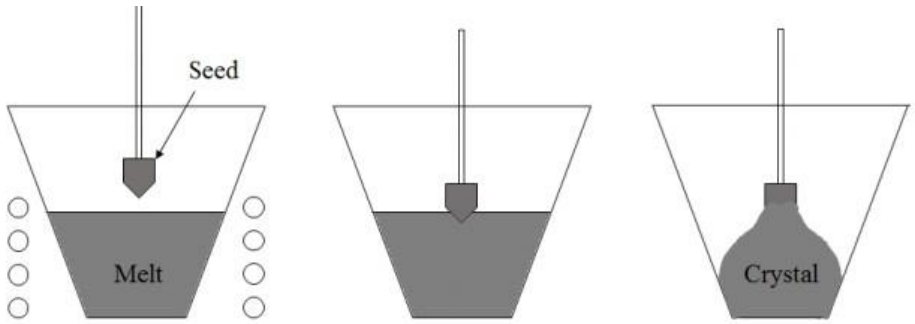

Figure 1.3. Schematic diagram of Bridgman crystal growth setup

1.5.2 (b) Czochralski technique

The technique is named after Jan Czochralski who accidently invented this method in 1915 when instead of dipping his pen into the ink, he did so in molten tin and obtained a tin filament which was later proved to be a single crystal. In this method, the molten charge is kept in crucible at temperature just above its melting point. The seed crystal which is mounted on a rod is suspended vertically downwards which is schematically indicated in Figure 1.4. Initially, the seed and charge are not in contact. The process of nucleation is initiated by dipping the rod into molten charge and it is then slowly pulled upwards to avoid re-melting. The seed crystal is simultaneously pulled and rotated to maintain homogeneity in the crystal grown. Cylindrical ingots are obtained as final

products. This method is mainly used in semiconductor industries to obtain single crystal silicon ingots.

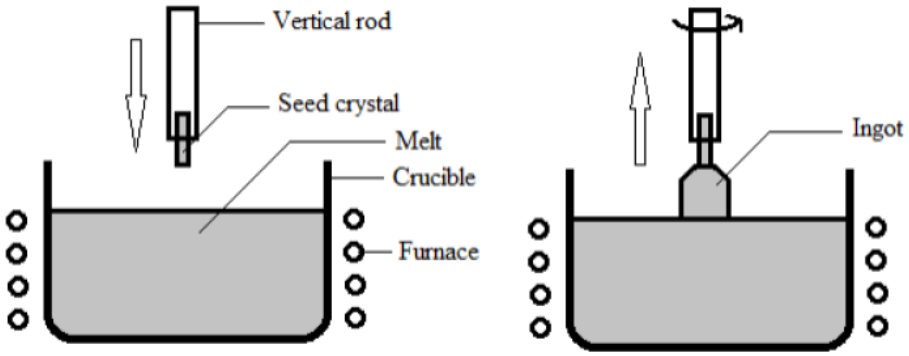

Figure. 1.4. Schematic representation of Czochralski growth setup.

1.5.2 (c) Flame fusion technique

Flame fusion technique also called as Verneuil process, was originally developed by a French chemist, August Verneuil in 1902. This technique is used for the growth of large number of materials with high melting point such as ZrO_2, SrO, Y_2O_3 etc and was the first commercially successful method of manufacturing synthetic gemstones. The starting material for the production of crystals in this method is in the form of a fine grained powder. The powder is scatter by a tapping mechanism out of the supply container through a sieve into the oxy-hydrogen flame. There the powder is melted and a single crystal grows progressively around a seed crystal as the seed crystal is slowly lowered.

1.5.2 (d) Zone melting method

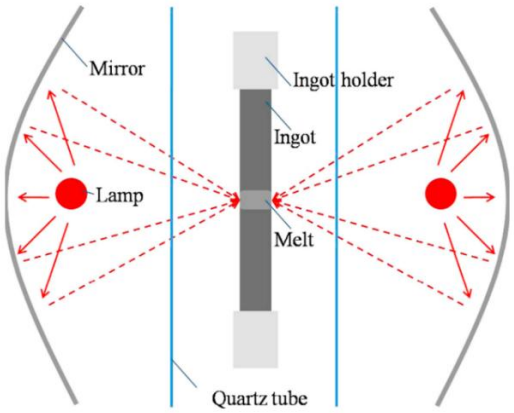

Figure. 1.5. Schematic representation of zone melting setup.

Zone melting is probably thought of as a purification technique. However, it may

be used as a method for the growth of single crystals. In this method, a zone or part of the solid material is melted and this molten zone travels together with the heating elements. This is schematically shown in Figure 1.5. The advantage of zone technique is that multiple recrystallization is possible which permits chemical purification of the substance [Zhang et al. 2017].

1.5.2 (e) Float zone method

Float zone technique was first described by Keck and Golay and its first application was in the purification of silicon. In this technique, surface tension holds a molten zone of liquid in a sample whose axis is vertical. Since this method needs no container, reactivity with the boat is no longer a problem. This technique is especially suitable for the preparation of high purity silicon and germanium.

1.5.3 Vapour growth

This technique is the most versatile among all the available crystal growth techniques and is often used to produce bulk crystals and to prepare thin layers on crystals with a high degree of purity. Growth from vapour phase may be broadly classified as:

1. Physical Vapour Deposition (PVD)
2. Chemical Vapour Deposition (CVD)
3. Chemical Vapour Transport (CVT)

1.5.3 (a) Physical Vapour Deposition

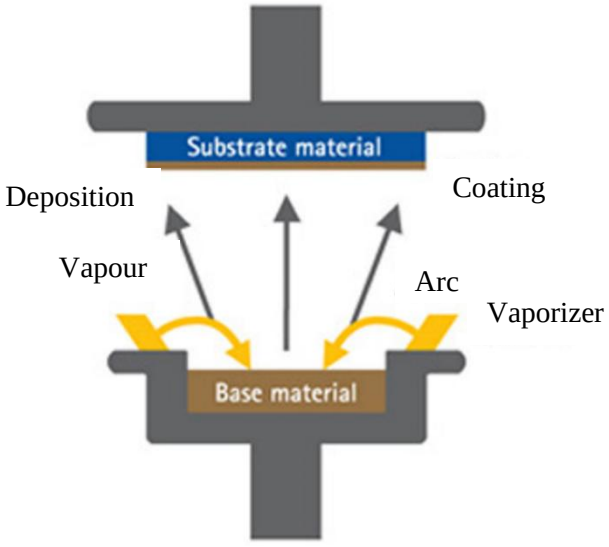

Figure. 1.6. Schematic representation of PVD system.

In the Physical vapour deposition (PVD) process, the material to be evaporated is kept on an evaporation source (can be either a filament or boat or crucible) and a substrate is located at an appropriate distance facing the evaporation source as shown in Figure 1.6. The material used to fabricate the evaporation source should be having a higher melting temperature than the material to be evaporated. Generally, the evaporation sources are made up of tungsten or molybdenum. Both the source and the substrate are located inside a high vacuum chamber. The substrate can also be heated or electrically biased or rotated during deposition. The desired vapor pressure of source material can be generated by simply heating the source to elevated temperatures, and the concentration of the growth species in the gas phase can be easily controlled by varying the source temperature and the flux of the carrier gas.

1.5.3 (b) Chemical Vapour Deposition (CVD)

CVD is a chemical process of producing high quality solid materials. The precursor gases are delivered into the reaction chamber at approximately ambient temperature. As they come into contact with heated substrate, they react and decompose to form a solid phase. This method is advantageous because controlled doping of impurities is possible and deposition rates are generally higher.

1.5.3 (c) Chemical Vapour Transport

It is a process where a condensed phase, typically a solid, is volatilised in the presence of gaseous reactant (transport agent) and deposited elsewhere in the form of crystal. The solid phase reacts with transporting agents like iodine, bromine etc., at the source zone to form vapour phase products. Hence this technique mainly depends on the reaction between source material to be crystallised and a transporting agent. The reaction product which is volatile can be transported in the vapour phase [Feigelson 2015]. Initially, a random deposition takes place forming seed crystals. Thus, initial seed crystals are not required prior to the process.

1.5.4 Growth from solution

Materials showing variation of solubility with temperature and higher solubility can be grown by this method. In this method, a saturated solution of the material in appropriate solvent is used from which crystallization takes place as the solution becomes critically supersaturated. The supersaturation can be achieved either by lowering the temperature or by slow evaporation. The advantage of this method is that

crystals can be prepared from a solution even at room temperature and therefore it turns out to be more applicable in many cases.

Solution growth can be broadly classified into:

a) High temperature solution growth

b) Hydrothermal method

c) Gel growth

d) Low temperature solution growth

1.5.4 (a) High temperature solution growth

This method is mostly used for growth of oxide crystals. Flux method is the most widely used high temperature solution growth technique. In this method, the constituents of the material to be crystallized are dissolved in suitable solvent, the so called flux. Under controlled condition, crystallization occurs. In this process the temperature is maintained for several hours and then the temperature is lowered very slowly.

1.5.4 (b) Hydrothermal methods

Hydrothermal method is suited for the growth of certain class of materials which are practically insoluble in water. Hydrothermal growth implies conditions of high pressure and high temperature. Substances like calcite, quartz are insoluble in water but at high temperature and pressure they become soluble. Temperatures involved in this technique is in the range of 150º C to 600º C and the pressure involved ranges from few hundreds to thousands of atmospheres. Growth is usually carried out in steel autoclaves with gold or silver linings. The requirement of high pressures presents practical difficulties and there are only a few crystals of good quality and large dimensions which are grown by this technique. One major disadvantage of this technique is the frequent incorporation of OH^- ions into the crystal which makes them unsuitable for many applications.

1.5.4 (c) Gel growth

All the methods mentioned above will fail in the case of growth of certain class of materials having poor solubility and unstable thermal behaviour. Such class of materials can be grown successfully by gel growth method. In this technique, growth occurs due to reaction between two suitable reactants in a gel medium or achieving supersaturation by diffusion in gel medium. Crystals of dimensions of several millimeter can be grown

in a period of 3 to 4 weeks.

1.5.4 (d) Low temperature solution growth

This is the most effective and easy way for growing crystals. A variety of crystals can be grown by this technique at room temperature. This technique is preferred when the starting materials are unstable at high temperatures and also undergo phase transformation. The growth of crystals by this method involves weeks, months or sometimes years. In this method, a saturated solution of the material is prepared in a suitable solvent and crystallization is initiated by slow cooling of the solution or by slow evaporation of the solvent. Good quality crystals with low thermal stresses can be produced by this method. The materials which undergo decomposition or phase transition at high temperatures are suited for low temperatures solution growth. This method allows to grow variety of different morphologies and polymorphic forms of the same substance by variations of growth conditions or due to change of solvent. The main disadvantage of this method is slow growth rate and possibility of solvent inclusion into the growing crystal. The solvent inclusion can be minimized by controlling conditions of growth. The high quality of crystal obtained compensates the disadvantage of much longer growth periods. After many modifications and refinements, this method yields good variety of crystals for different applications. Since growth is carried out at room temperature, structural imperfections in the grown crystal is low. In this method, crystals can be grown from the solution if the solution is supersaturated, that is, solution should contain more solute than its equilibrium state. The principal methods used to produce the required supersaturated solution:

1. Slow cooling of the solution
2. Slow evaporation of the solvent
3. The temperature gradient method

1.5.4 (e) Slow cooling technique

It is the best method to grow bulk single crystals from solution. This technique needs only a vessel for the solutions, in which the crystals grow. The temperature at which crystallization begins is in the range of 45º C to 75º C and the lower limit is the room temperature.

"Mason-jar method" is the one of the simplest techniques of slow cooling. It is

easiest method of growing crystals and is cheap enough to permit many parallel attempts to be made. A saturated solution is heated slightly above its saturation temperature and poured into a screw-cap jar and a seed tied to a piece of thread is introduced as shown in Figure 1.7. Well-formed crystals are obtained provided the solubility is high enough and the cooling rate is slow enough. No stirring is possible in this technique. But the simplicity of this method essentially makes it attractive, particularly when modest size crystals essentially satisfies our purpose.

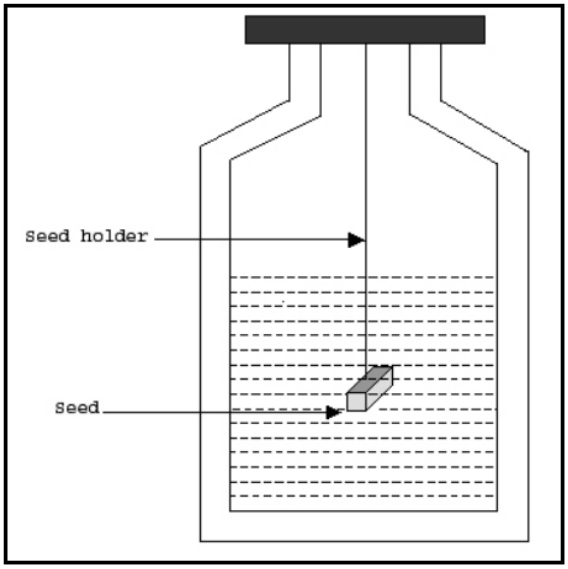

Figure. 1.7. Schematic representation of mason-jar setup.

1.5.4 (f) Slow solvent evaporation technique

This method is similar to slow cooling technique as far as apparatus requirements are concerned. In this method, the saturated solution is kept at a particular temperature and provision is made for its evaporation. If the solvent is non-toxic like water, then evaporation into the atmosphere is allowed. The advantage of this technique is that crystals grow at fixed temperature and hence the problem of variation in the properties due to variation in temperature does not arise here. But evaporation of solvent from the surface of solution produces high local supersaturation resulting in the formation of unwanted nuclei. Small crystals are formed on the walls of the vessel near the surface of the liquid and these crystals when fall into the solution can hinder the growth rate of the crystal. The major limitation is the control of rate of evaporation. Changing rate of evaporation may vary the quality of the crystal. Inspite of all these disadvantages, this

method still remains as simple and convenient method to grow large-sized single crystals.

1.5.4 (g) The temperature gradient method

This method involves transport of the materials from the hot region containing the source material to a cooler region where the solution is supersaturated and the crystal begins to grow. The main advantage of this method is that crystals grow at a fixed temperature and this method is insensitive to temperature changes provided both source and growing crystal are undergoing same change. Excellent quality crystals of ferroelectric and piezo-electric materials such as potassium dihydrogen phosphate (KDP) and triglycine sulphate (TGS) are commercially grown for use in devices by this method.

1.6 Factors governing crystal growth

The growth of crystals is governed by following factors:

1. Nucleation
2. Supersaturation
3. Habit modification

1.6.1 Nucleation

The physical and chemical processes involved in the formation of crystals occurs through nucleation. Nucleation is an important phenomenon in crystal growth and is the precursor of the overall crystallization process. It is the extremely localized budding of a distinct thermodynamic phase. It occurs when the solution is supersaturated. Nucleation is associated with aggregation of fragments in the supersaturated mother solution and it is also associated with the change in free energy of the system. It is the process in which ions, atoms, or molecules arrange themselves in a pattern characteristic of a crystalline solid, forming a site in which additional particles deposit as the crystal grows.

When the size of the nucleus exceeds the size of critical nucleus, crystals are developed by the attachment of growth species (molecules or atoms or ions) at energetically favorable growth sites such as kinks in the edges of surface. Nucleation may be either of the following,

a) spontaneous / homogeneous nucleation: it occurs without intervention of particles.

b) heterogeneous nucleation: It occurs due to the intervention of other factors (surface

wall of vessel or foreign particle or impurity component).

1.6.2 Supersaturation

A solution is said to be supersaturated if the concentration of solute in it exceeds that of the equilibrium condition at a given temperature. Such a solution is thermodynamically unstable. Supersaturation can be achieved by slow evaporation of solvent or by slow cooling of solution. More amount of solute is dissolved in a solvent than its actual equilibrium concentration. On slow cooling in the absence of agitations or fluctuations, nucleation occurs which is followed by the growth of crystal. Supersaturation can also be achieved by adding impurities. The presence of impurities reduces solubility of solute and the growth proceeds.

1.6.3 Habit modification

The growth rate of crystal plane depends on a set of parameters like temperature, degree of supersaturation of solution, pH of solution, concentration of impurities in the solution. This dependence can be represented by following relation

$$R = F(t, s, pH, c) \quad 1.5$$

where, R expresses the growth rate of crystal plane, t is temperature, s is supersaturation of solution, c is concentration of impurities in the solution. Different crystal faces grow at different rates at different environment conditions.

1.7 Optimising solution growth

The optimized conditions for the growth of good quality single crystals may be achieved using following norms:

1. Material purification
2. Solvent selection
3. Solubility
4. Solution preparation
5. Seed preparation
6. Agitation

1.7.1 Material purification

The availability of highest purity material is an essential prerequisite for the growth of good quality crystals. The impurities may get incorporated into the crystal lattice resulting in the formation of flaws and defects in the crystal. The impurities may also

get adsorbed on the growing face of the crystal thereby changing the crystal habit. Hence solute and solvents of high purity are required. Standard purification methods involving recrystallization followed by filtration of the solution would increase the level of purity.

1.7.2 Solvent selection

A solution is a homogeneous mixture of a solute in a solvent. The component which is present is smaller quantity is called solute and the one in which it is dissolved is called solvent. For a given solute, different solvents can be chosen. The solvent chosen should have good solubility for the given solute, less viscosity, less volatility, less toxicity, chemically inert nature and should be cost effective. Water, ethanol, methanol, acetone, carbon tetrachloride, hexane and xylene are some of the commonly used solvents.

1.7.3 Solubility

The solubility of the material in a solvent determines the amount of material available for the growth and hence determines the size of the crystal. If the solubility is too high, it is difficult to grow bulk crystal and lower solubility imposes restriction on size and growth rate of the crystal. The solubility of solute in solvent is determined by chemical similarity between them. Experiments reveal that the solvent in which solubility of compound is in between 10 and 60% at a given temperature is economically suitable for crystal growth. Very low and very high solubility decreases growth rate due to low solute concentration and increased viscosity respectively.

1.7.4 Solution preparation

For solution preparation, it is necessary to have solubility data of the material at various temperatures. Sintered glass fibres of different pore size are used for solution filtration. The clear solution, saturated at the desired temperature is taken in a growth vessel. For growth by slow cooling, the vessel is sealed to prevent evaporation. Solvent evaporation at constant temperature is achieved by providing a controlled vapour leak. A small crystal is suspended in the solution is used to test the solution. By varying the temperature, a situation where neither the occurrence of growth nor dissolution is established. The test seed is then replaced with a good quality seed. All unwanted nuclei and the surface damage on the seed are removed by dissolving at a temperature above the saturation point. Growth is initiated after saturation.

1.7.5 Seed preparation

Seed crystals are prepared by self-nucleation under slow evaporation from a saturated solution. Seeds of good visual quality, free from any inclusion and imperfections are chosen for growth.

1.7.6 Agitation

The level of supersaturation has to be maintained equally around the surface of the growing crystal so that regular and even growth occurs. An uneven growth leads to localized stresses at the surface generating imperfection in the bulk crystal. The degree of formation of concentration gradients around the crystal depends on the efficiency of agitation of the solution. The saturated solution is agitated in either direction at an optimized speed using a stirrer motor.

1.8 Literature Survey

Bride et al. synthesized a new compound called Cadmium oxalate single crystals using gel growth method [Bridle and Lomer 1965]. The obtained crystals were thoroughly studied using single crystal XRD measurements. The crystal structure is solved and crystal informations such as lattice parameters, bonding informations were extracted for their possible applications.

Erikson et al. synthesized single crystals of $K_2C_2O_4 \cdot H_2O$ and $K_2C_2O_4 \cdot D_2O$ at room temperature [Eriksson and Nielsen 1978]. The synthesized crystals were studied using Raman measurements. The change in the functional bonds of $K_2C_2O_4$ in the presence of deuteriated water is studied and confirmed the presence of deuteriated water in $K_2C_2O_4 \cdot D_2O$ crystal system.

Arora et al. grew Cadmium oxalate trihydrate single crystals using silica hydrogel at ambient temperatures by using different nucleation control methods [Arora and Abraham 1981]. From the obtained results it was observed that different parameters like gel aging, concentration programming, two-gel technique. Seeding, etc are inadequate in the controlled nucleation process of CdC_2O_4 crystals. The crystals of larger and perfect shape was achieved using impregnation of NH4Cl in the gel mixture. From the chemical etching method, the crystal is proved to be of higher perfection. The crystals were characterized using thermal and mechanical measurements.

Dharmaprakash et al. synthesized the crystals of barium oxalate single crystals using gel growth technique [Dharmaprakash and Rao 1985]. Effect of the pH and concentration on the growth of barium oxalate crystals were also investigated. pH 3.175 to 3.3 gel mixture and 0.5 M supernatant feed ($BaC1_2$) solution gave the best results. The functional vibrations were studied by IR spectrometer.

Varghese et al. synthesized rare earth element doped lanthanum copper oxalate La_{1-x} Cu_x $3(C_2O_4)$ nH_2O crystals using gel technique [Varghese et al. 1990]. The synthesized crystals were characterized using powder XRD, FTIR and magnetic studies. From the magnetic measurements the crystal nature is observed to be diamagnetic.

Bangera et al. synthesized Barium copper oxalate single crystals using silica hydrogel at ambient temperature. The various parameters like gel density, gel aging, gel pH and concentrations of reactants were studied to analyze the growth of these crystals [Bangera and Rao 1992]. It is found that well-developed single crystals are obtained at 0.5 M concentrations of feed solution in the pH range 2.9 to 3.1 of the gel.

Jagannatha et al. studied metal atoms doped cadmium oxalate single crystals [Jagannatha and Rao 1993]. The metal atoms such as (Na, Li^+, K^+, NH_4^+, Zn^{2+}, Co^{2+}, Ni^{2+}, and Ca^{2+}) cation impurities are studied. Single diffusion method is employed to synthesize these compounds. Effect of dopant molecules on the structural and morphological changes were studied. Results revealed that the impurity cations led to the change in colour of the crystal and such materials are useful in tuning the bandgap of the materials for optical filter applications.

Raju et al. synthesized Neodymium copper oxalate (NCO) single crystals using gel method [Raju et al. 1994]. The synthesized crystal was investigated for the physical properties of the material. Interestingly, IR spectrum confirms the presence of water molecules in the crystal structure and from EDAX spectrum it was noticed that the Nd dominates over copper in the crystal. Further, the material is studied using XPS measurements and the results revealed that Nd and Cu in their oxide states (XPS) and

the elements linked to O- of oxalate groups. The dominance of Nd in the crystal was confirmed by the XPS and EDAX spectrum.

Deepa et al. synthesized Calcium oxalate dihydrate single crystals using gel growth technique [Deepa et al. 1995]. The double diffusion technique is employed for the synthesis process. The crystal nucleation starts after 4 days interval. The optimized parameters are with 1.03 g/cc sodium metasilicate, 1 M calcium chloride, 3 M acetic acid, 1 M calcium chloride, 1 M magnesium acetate gave better quality crystals. The obtained crystal crystallizes in tetragonal structure.

Isac et al. grew single crystals of Praseodymium barium molybdate (PBM) using gel method [Isac et al. 1996]. The synthesized crystals were studied for its various physical properties. From XRD measurements the crystal belongs to tetragonal system. The presence of $(MoO_4)^{2-}$ ions in PBM were confirmed using IR spectroscopy. The thermal stability of the crystal was studied using TGA analysis and loses molybdenum oxide component around 420°C. The presence of Ba, Pr and Mo in the sample was confirmed EDAX analysis. Presence of Ba, Pr and Mo in the sample was confirmed using EDAX analysis. The metal atoms are linked to the O- of oxalate groups and the elements Ba, Pr and Mo are in their oxide states which was confirmed by XPS analysis.

John et al. grew Lanthanum samarium oxalate (LSO) single crystals using gel technique [John et al. 1997]. The synthesized crystals were characterized using powder XRD, FTIR, TGA-DSC, EDAX and XPS studies. From the results it was confirmed that La and Sm are present in oxide state and linked to O^- of oxalate groups (XPS).

Joseph et al. synthesized the mixed crystals of Neodymium praseodymium oxalate (NPO) using gel diffusion technique [Joseph et al. 1997]. NPO samples are well-ordered crystalline materials and belonging to monoclinic crystal system. The presence of oxalate complex was confirmed using FTIR measurements. The thermal stabilities of the crystal was studied using TGA and DSC analysis and the crystal is stable till 420 °C. The presence of Nd and Pr are confirmed using EDAX and XPS studies. From XPS it is noted that the elements are in its oxide form by linking to O^- of oxalate groups.

Girija et al. synthesized Calcium oxalate monohydrate ($CaC_2O_4 \cdot H_2O$) single crystals using double diffusion technique [Girija et al. 1998]. The grown crystals were characterized using XRD, TGA-DTA, FTIR and microhardness studies. From the mechanical studies it was observed that the synthesized crystal could withstand up to 200 g load and which is a higher value for the crystals.

John et al. synthesized a new crystal named Cerium oxalate single crystals using gel method [John and Ittyachen 1998]. The synthesized crystals were characterized using powder XRD, FTIR and TGA-DTA analysis. From the results it was noticed that the crystal belongs to orthorhombic crystal system and the crystal is thermally stable upto 180 °C.

Dalal et al. grew Barium oxalate single crystals in agar gel medium at ambient temperature [Dalal and Saraf 2006]. The different parameters like gel setting time, gel concentration and reactant concentration on growth parameters of these crystals were investigated. The grown crystals were characterized using powder X-ray diffractometry, thermogravimetric, differential thermal analysis, infrared spectroscopy. The crystal growth parameters were optimized and concluded that single and double diffusion methods show differences in growth mechanisms.

Krishnakumar et al. synthesized L-Alanine oxalate ($C_5H_9NO_6$) single crystals for frequency conversion applications [Krishnakumar and Nagalakshmi 2006]. The crystals were grown using slow evaporation technique. The crystal was characterized using IR, Raman, UV-vis, fluorescence and NLO measurements. The essential vibrations were foreseen by using group theoretical analysis. The theoretically predicted modes were matching with the observed spectra and the spectral vibrations were assigned. The crystals show maximum absorption of Nd:YAG laser fundamental wavelength and the crystal emits green light (532 nm) confirming NLO activity.

Korah et al. grew single crystals of Gadolinium Samarium Oxalate (GSO) using gel method [Korah et al. 2007]. The obtained crystals are pale yellowish in colour.

Morphology and size of the crystals depends on gel density, concentration of the reactants, pH of the medium and acidity of the feed solution. Powder XRD confirms the crystalline nature of the synthesized compound. The presence of oxalate and water molecules were confirmed using IR spectroscopy. The presence of Sm and Gd in the crystal was confirmed using EDAX analysis. Thermal studies are conducted to analyze thermal decomposition of the samples using TGA and DTA analysis. The stable residual of rare earth oxides are stable beyond 600 ºC confirms the GdSm in the system.

Raj et al. synthesized Barium oxalate monohydrate ($BaC_2O_4.H_2O$) single crystals using controlled diffusion of Ba^{2+} using gel technique at different temperature [Raj et al. 2008]. The synthesis of BaC2O4.H2O single crystals are studied by varying the parameters such as pH, crystallization temperature and gel aging. It was noticed that the growth rate of the crystals were less initially, irrespective of all temperatures and once the supersaturation is achieved the growth rate increased drastically. The single crystals were grown on gel medium for higher pH values.

Jananakumar et al. grew Potassium hydrogen oxalate (KHO) single crystal using solvent evaporation technique [Jananakumar and Mani 2014]. From single crystal X-ray diffraction analysis the crystal structure is solved and the crystal belongs to monoclinic crystal system. The crystal possess bandgap of 5.62 eV and the crystal is thermally stable upto 211.4 °C. The KHO crystal showed SHG property and can be of use in NLO device applications.

Manikandan et al. synthesized single crystals of glycinium oxalate (GOX) and Cu^{2+} doped GOX using solvent evaporation technique [Manikandan et al. 2019]. The bandgap of the crystal decreased after the doping 4.83 eV to 4.68 eV. Both the crystals possess NLO activity and the third order nonlinear susceptibility ($\chi(3)$) was calculated to be 2.33×10^{-6} esu and 4.42×10^{-6} esu for GOX and Cu^{2+} doped GOX crystals. Further, laser damage threshold is measured and the obtained values are 46.87 MW/cm^2 (pure GOX) and 49.32 MW/ cm^2 for GOX and Cu^{2+} doped GOX crystals.

Punniyamoorthy et al. synthesized the new semiorganic Potassium sulphato oxalate (KSO) single crystals at room temperature using slow evaporation technique [Punniyamoorthy et al. 2019]. From single crystal X-ray diffraction, the crystal structure was solved and the crystal belongs to triclinic (P1) crystal system. The crystal optical band gap is measured to be 3.2 eV and the crystal emits in green region (576 nm). The SHG stability is measured to be 1.16 times higher than that of KDP crystal. Further, the laser damage threshold studies show KSO crystal possess higher laser damage threshold stability (6.135 GW cm^{-2}) which is greater than KDP crystal.

Elangovan et al. grew single crystals of 2-Methylimidazolium hydrogen oxalate dihydrate (2MIO) by slow evaporation method [Elangovan et al. 2019]. 2MIO crystallizes in monoclinic space group P21/n. The crystal bandgap is obtained to be 3.94 eV and fro mechanical studies the crystal classified as a soft material (n = 2.7). The crystal shows NLO activity and the third order NLO susceptibility $\chi(3)$ is observed to be 8.86×10^{-8} esu.

Dardar et al. synthesized a new layered Gallium phosphonate-oxalate single crystals using mild hydrothermal conditions (150 °C) in the presence of ethylenediammonium ion $(H_2en)^{2+}$ as structure-directing agent [Dardar et al. 2019]. The compound crystallizes in Monoclinic P21/n crystal system with cell values a = 8.7530(5) Å; b = 16.3427(8) Å; c = 14.7522(8) Å; β = 93.284(1) °, V = 2106.8(2) $Å^3$ and Z = 4. The synthesized compound provides the opportunity to prepare new types of layered material, which may find widespread application in intercalation reactions and catalysis.

1.9 Scope and objectives

Semiorganic or metal-organic hybrids have attracted many researchers to synthesize materials in the field of crystal engineering due to their vast applications in high ionic or mixed conductors, solid-state batteries, sensors, capacitors, photovoltaic cells, electroluminescent diodes, electrochemical transistors and so on [Zhang et al. 2002 Sanchez et al. 2005 Matulková et al. 2012 Chouaib et al. 2016].

Oxalic acid is an interesting organic matrix modifier and forms complexes with

inorganic salts. Oxalic acid exists in anhydrous and dehydrated forms. Oxalic acid links to the metal atoms and forms stable metal oxalates. Many oxalate related complexes are synthesized and studied due to their vast applications in optoelectronic industries. This inspired us to synthesize the titled compound (potassium hydrogen oxalate oxalic acid dihydrate). Synthesized compound is studied for their structural, optical, thermal, electrical and mechanical properties.

Apart from studying pure material, incorporation of foreign particles (dye molecules and nanoparticles) and defect induced studies were also performed. This is because doping or defect induced studies changes their properties like optical absorption, energy band gap, thermal properties etc. which may be either due to the difference in the crystal structure or bonding between the atoms in the crystal.

Objectives

- To synthesize oxalate based complexes with inorganic salts.
- To determine the molecular structure using single crystal XRD method.
- To determine the elemental compositions by EDAX analysis.
- To perform the structural characterizations using powder XRD and FTIR.
- To study optical properties using UV-vis Spectroscopy.
- To study the dielectric properties of the grown crystals for practical applications.

1.10 Organization of Thesis

Chapter 1 and its sub-sections provide the background and motivation for the present work. This chapter includes a brief introduction to crystals and the crystal growth techniques. It also provides a summary of the literature review on oxalate based crystals and its properties. The scope and objectives of the present work is given at the end of the chapter.

Chapter 2 provides the details of experimental procedure used to synthesize KHOOD single crystals and also, presents the synthesis of doped KHOOD single crystals. This is followed by a brief description of different characterization techniques, their theoretical description and formulae used for calculations.

Chapter 3 presents the investigation of structure determination of the crystal followed by results and discussions on optical, structural, thermal, mechanical and electrical properties.

Chapter 4 presents effect of $Co(OH)_2$ nanoparticles on the properties of the KHOOD single crystals. The nanoparticle doped crystals are compared with those of undoped crystals for their optical, structural, thermal and electrical properties.

Chapter 5 presents effect of Amaranth dye doping on the crystal properties of KHOOD. The synthesized doped crystals are studied for their optical, structural, electrical and thermal properties.

Chapter 6 presents effect of Gamma irradiation on the properties of the KHOOD single crystals. Radiation dosage effect on structural, optical, electrical properties of the crystals were discussed in detail.

Chapter 7 presents the comparison between Oxalic acid dihydrate, potassium hydrogen oxalate, potassium hydrogen oxalate oxalic acid dihydrate single crystals via structural, optical, thermal and mechanical properties.

Chapter 8 summarizes the conclusions drawn from the present work. Further, the scope for further work in this field is indicated. An appendix is followed by list of references and a brief profile with publications in international journals and conferences presented at the end of the thesis.

Chapter 2

EXPERIMENTAL TECHNIQUES

Overview

This chapter gives detailed description on the preparation of KHOOD single crystals. This chapter also contains the details regarding experimental setup used for the synthesis and characterization of KHOOD single crystals.

2.1 Synthesis of KHOOD single crystal

The potassium oxalate oxalic acid dihydrate (KHOOD) single crystals were grown from an aqueous solution by dissolving the raw materials of analytical grade, namely oxalic acid dihydrate and potassium dihydrogen phosphate, in equimolar ratio in deionized water. The solution was stirred well using magnetic stirrer for 5 hours to ensure that the material is dissolved in the solution. The solution was then filtered to remove the suspended particles using Whatman filter paper of pore size around 10 µm. The prepared saturated solution was transferred to a Petri dish and kept in vibration free environment to obtain the seeds of KHOOD single crystals. The crystals were formed in a time duration of 20 days and the grown crystals were characterized.

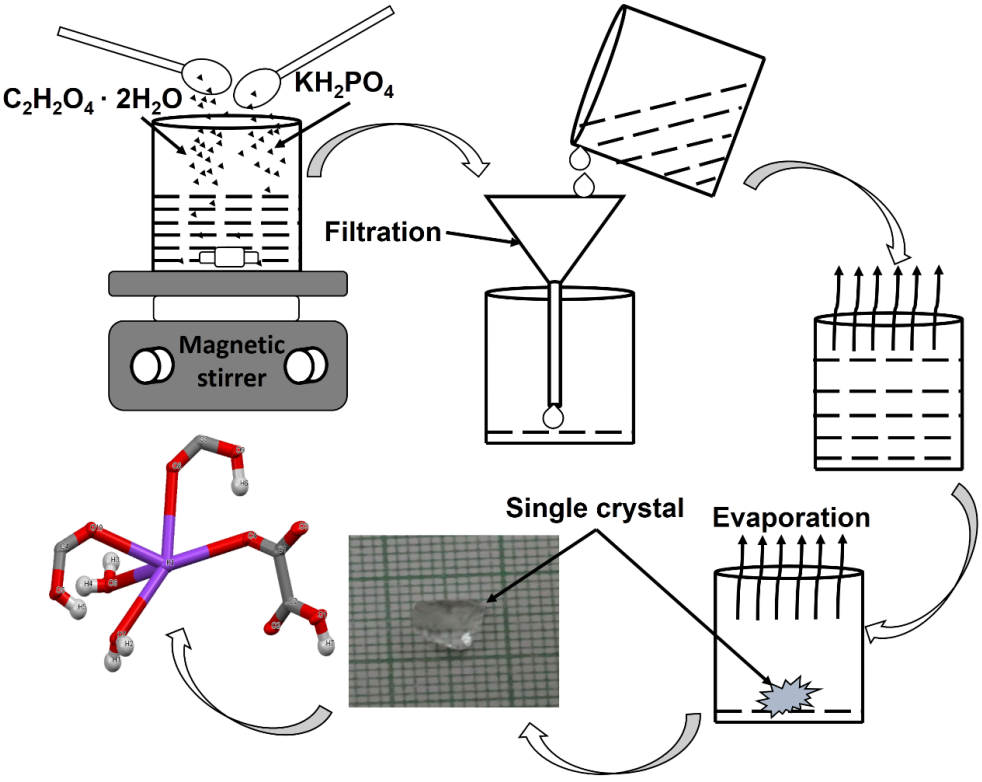

Figure. 2.1. Synthesis of KHOOD single crystal.

2.1.1 Synthesis of $Co(OH)_2$ nanoparticles

In a typical process, a pink colored solution was formed by adding 0.582 g of Cobalt nitrate hexahydrate ($Co(NO_3)_2 .6H_2O$) in 40 ml of DI water at room temperature. Next, 3 ml of triethylamine ($C_6H_{15}N$) was added dropwise to the pink solution which resulted in an immediate color change to dark blue. The solution was made to reach a total volume of 80 ml by adding 37 ml of excess DI water and allowed to stir for 10 min. the final solution was then transferred into a 120 ml Teflon-lined stainless-steel autoclave, sealed and hydrothermal process was carried out a temperature of 180 ºC for 24 h. After the autoclaves cooled down naturally, the black colored precipitates were collected by washing with excess DI water and ethanol under centrifugation, after which they were dried overnight at 60 ºC.

2.1.2 Synthesis of nanoparticle doped KHOOD single crystal

For the synthesis of $Co(OH)_2$ nanoparticles doped KHOOD single crystals, three beakers containing the equimolar ratios of potassium dihydrogen phosphate and oxalic acid were taken, followed by magnetic stirring and filtration as explained in the previous step. Next, different volumes of $Co(OH)_2$ nanoparticle solutions (20 µl, 40 µl, and 60 µl) were added to the filtered solutions and ultrasonicated for 40 min to ensure the complete dispersion of nanoparticles in the solution. The solution was subjected to slow evaporation and pure quality of $Co(OH)_2$ nanoparticles doped single crystals were obtained over a period of 40 to 45 days.

2.1.3 Synthesis of Amaranth doped KHOOD crystal

Equmimolar quantities of potassium dihydrogen phosphate and oxalic acid dihydrate salts are used to obtain single crystals of KHOOD. Two beakers containing equimolar concentrations of KHOOD materials were taken and for one beaker containing KHOOD solution, 0.1 mM concentration amaranth dye was added and stirred for 2 hr. After the solute was dissolved the solutions were kept for evaporation. After a week the crystals started to form in that solution and the crystals were removed once they attain the reasonable size.

2.2 Characterization techniques

The synthesized single crystals of KHOOD is characterized using different techniques. The crystal structure was determined using single crystal X-ray diffraction (SCXRD) technique and the molecular structure was solved. The crystals were studied using

powder X-ray diffraction (PXRD), Fourier transform infrared spectroscopy (FTIR), Raman Spectroscopy, scanning electron microscopy (SEM), energy dispersive x-ray analysis (EDAX) and other techniques. The optical properties were investigated using UV-visible spectroscopy and Photoluminescence spectroscopy (PL). The thermal properties were studied using Thermal Gravimetric Analysis (TGA), Differential Thermal Analysis (DTA), Differential Thermal Calorimetry (DSC). Mechanical properties were investigated using Vickers microhardness Tester. The electrical properties were explored using light dependent I-V measurements and dielectric measurements. The crystal was also exposed to gamma irradiation and studied.

2.2.1 Single crystal X-ray diffraction (SC-XRD)

Single crystal X-ray diffraction data for the crystal were collected on a Bruker Apex II duo diffractometer with CCD detector. Monochromatic Molybdenum (Mo) Kα radiation (λ=0.7107 Å) was used as a source of radiation. Data collection was done at ambient conditions (296 K). All the structures were solved by the direct method using SHELXL-2007/2014 software and refinement was carried out by full-matrix least squares technique. Anisotropic displacement parameters were calculated for all non-hydrogen atoms except for disordered atoms. H atoms attached to the O/N atoms were located in a difference Fourier density map and refined anisotropically. In some cases, hydrogen atoms were fixed geometrically. All the diagrams were prepared using mercury 3.5.1/3.8 software.

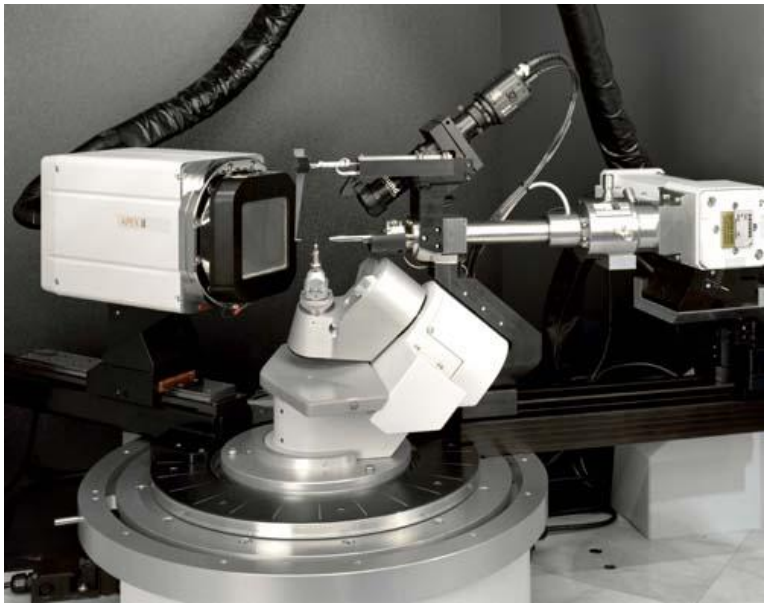

Figure. 2.2. Image of the SCXRD instrument.

2.2.2 X-ray Diffraction (XRD)

Diffraction is a scattering phenomenon where the atoms scatter incident X-rays in all directions. In some directions, the scattered beams will be in phase and hence they reinforce giving rise to diffraction. The technique began when von Laue, in 1912, discovered that crystals diffract X-rays. Since then it has been applied to chemical analysis, stress and strain measurement, measurement of particle size as well as crystal structure [Whittaker 1981]. X-rays have wavelength comparable with interatomic spacing hence results in the interference of deflected rays. The diffraction of X-rays by crystal is defined by Bragg's law given as

$$n\lambda = 2d \sin\theta \qquad 2.1$$

where, d is the distance between two planes, λ is the X-ray wavelength, θ is the angle which incident photon makes with the incident plane. Different 'd' spacing of the crystal satisfies Bragg's condition at different angles giving rise to XRD spectrum which is the fingerprint of the sample. Each crystal has many planes and alignment of these planes determines the crystal structure. These relationships are used in X-ray diffraction to determine specific properties about the specimen.

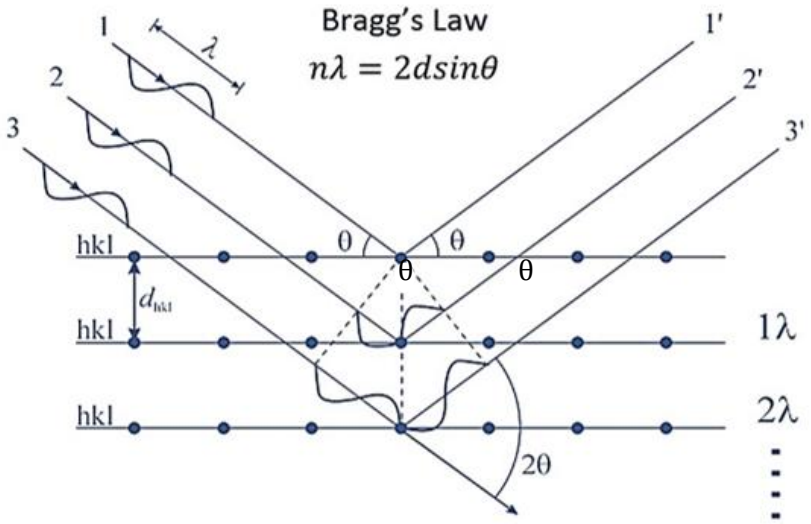

Figure. 2.3. Schematic representation of deflection of X-rays from atomic planes.

2.2.2 (a) Powder X-ray diffractometer

Powder X-ray diffraction (XRD) uses X-rays to investigate and quantify the crystalline nature of materials by measuring the diffraction of X-rays from the planes of atoms within the material. It is sensitive to both the type of atoms and relative position of

atoms in the material as well as the length scale over which the crystalline order persists. It can, therefore, be used to measure the crystalline content of materials, identify the crystalline phases and determine spacing between lattice planes and length scales over which they persist. The schematic diagram of powder X-ray diffractometer is shown in Figure. 2.4. The sample for analysis is taken in the form of finely divided powder. The materials can be of a vast array of types, including inorganic, organic, polymers, metals or composites and the potential applications cover almost all research fields. In this work, the X-ray diffraction study of pure and doped crystals was carried out using Rigaku 600 Powder X-ray diffractometer using CuK_{α} radiation (λ = 1.5405 Å). The diffractometer is shown in Figure. 2.5. The X-ray is generated by a cathode ray tube, filtered to produce monochromatic radiation, collimated to concentrate and then directed towards the sample. The interaction of the incident rays with the sample produces constructive interference when Bragg's law is satisfied. These diffracted X-rays are then detected, processed and counted. By scanning the sample through a range of 2θ angles, all possible diffraction directions of the lattice should be attained due to random orientation of the powdered material. Conversion of diffraction peaks to d-spacings helps in the identification of the material because every material has a unique set of d-spacings. Typically this is achieved by comparison of d-spacing with standard reference patterns i.e. JCPDF files.

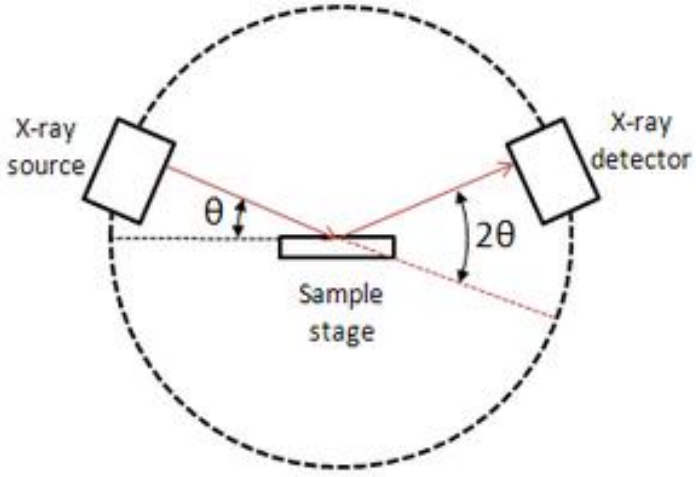

Figure. 2.4. Schematic representation of powder X-ray diffractometer.

Figure. 2.5. Powder X-ray diffractometer (Rigaku MiniFlex600).

2.2.3 Scanning Electron Microscopy (SEM)

The scanning electron microscope (SEM) is a powerful and frequently used instrument in both academia and industry to study the surface topography, composition, crystallography and properties on a local scale. SEM has better spatial resolution than the ordinary optical microscopes. Due to its extremely large depth of focus, it is well suited for topographic imaging. By using focused beam of electrons, SEM reveals levels of details and complexity inaccessible by light microscopy. SEM can magnify an object from about 10 times to about 3,00,000 times.

SEM uses electrons emitted from tungsten or Lanthanum hexaboride thermionic emitters. The filament is heated resistively by a current to achieve a temperature between 2000-2700 K. This results in the emission of thermionic electrons from the tip. These electrons are accelerated to an energy in the range of 0.1-30 keV towards the sample. A series of electromagnetic lenses focus the electron beam on to the sample where the interaction takes place. The electrons in the beam interact with the sample, producing various signals that can be used to obtain information regarding topography and composition. The electron beam is scanned in a raster scan pattern, and the beam's signal is combined with the detected signal to produce an image. The most common SEM mode is detection of secondary electrons emitted by atoms excited by the electron beam. The number of secondary electrons emitted depends on specimen topography. By scanning the sample and collecting the secondary electrons that are emitted using a detector, an image displaying the topography of the surface is created.

The highest resolution obtainable is limited by factors like diameter of the electron beam, scattering within the specimen, signal-to-noise ratio, external disturbances like electric or magnetic fields and mechanical vibrations. In the SEM, the specimen resides in a high vacuum chamber to prevent scattering of the electron beam and to avoid damage to the microscope. However, operating in a high vacuum poses some limitations on the types of specimens that could be observed with the SEM. Specimens should be electrically conductive, otherwise the electron beam may build up a static charge in the material due to the inability to dissipate the charge. Furthermore, the specimen must not contain water or other volatile components as that may destroy the vacuum in the sample chamber and potentially damage the microscope. Specimens that do not meet these requirements may still be observed after suitable sample preparation like metal coating with a conductive layer to avoid charging or drying to remove water. External morphology of crystals on nanometer or micrometer scale can be observed and characterized using SEM, obtaining a three dimensional images of the crystal surface. The schematic representation of SEM and typical SEM instrument are shown in Figure. 2.6 and Figure. 2.7 respectively.

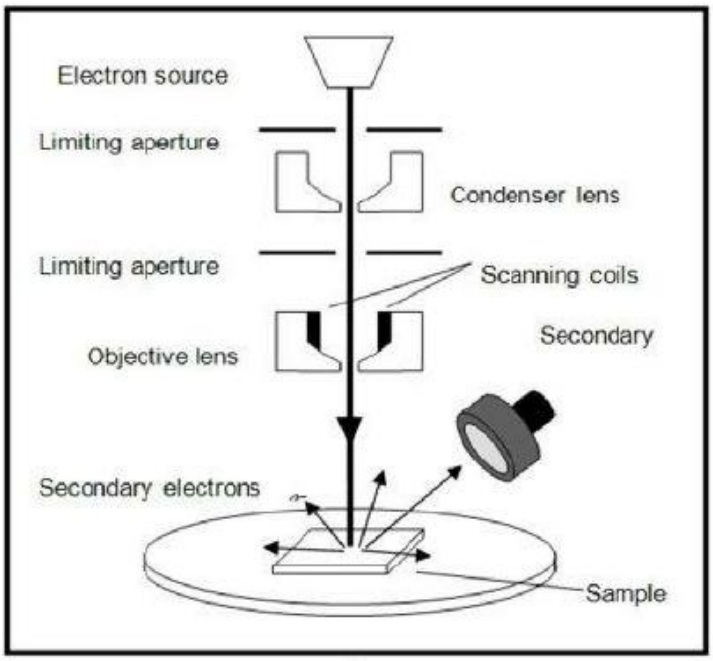

Figure. 2.6. Schematic of Scanning Electron Microscopy.

Figure. 2.7. Field Emission Scanning Electron Microscopy (FESEM) (Carl Zeiss).

2.2.4 Energy Dispersive X-ray Analysis (EDAX)

EDAX is a technique used to analyze elemental composition of the material. It is based on the investigation of a sample by means of interactions between electromagnetic radiation and matter. The X-rays emitted by the matter in response to being hit by electromagnetic radiation are analyzed. The fact that each element has a unique atomic structure allows emitted X-rays that are characteristic of an element's atomic structure to be identified uniquely from each other.

To stimulate the emission of characteristic X-rays from a specimen, a high energy beam of charged particles such as electrons or a beam of X-rays, is focused with the sample being studied. At rest, an atom within sample contains ground state electrons in discrete energy levels or electron shells bound to the nucleus. The incident beam may excite an electron from an inner shell, ejecting it from the shell and creates a vacancy. This positive vacancy is eventually occupied by a higher energy electron from an outer shell and the difference in energy between the higher energy shell and lower energy shell may be released in the form of an X-ray as shown in Figure. 2.8. The amount of energy released by transferring electron depends on which shell it is transferring from and which shell it transferring to. The energy of the X-rays emitted from a specimen can be

measured by an energy dispersive spectrometer. Since, the emitted X-ray is characteristic of the difference in energy between the two shells and of the atomic structure of the element form which they are emitted, this allows the elemental composition of the specimen to be measured. The position of the peak gives information about the qualitative composition of the sample.

EDAX systems are attachments to Scanning Electron Microscopy (SEM), Transmission Electron Microscopy (TEM) or Field Emission Scanning Electron Microscopy (FESEM) instruments where the imaging capability of the instrument identifies the specimen of interest. The data generated by EDAX analysis consists of spectra showing peaks corresponding to the elements making up the true composition of the sample being analyzed. Elemental mapping of the sample and image analysis are also possible.

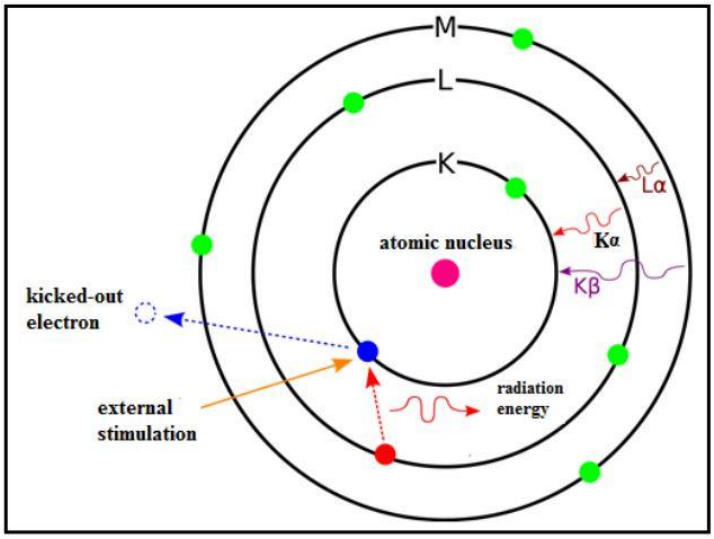

Figure. 2.8. Principle of EDAX.

2.2.5 UV-Visible studies

Ultra-Violet and visible (UV-Vis) absorption spectroscopy is the measurement of the attenuation of a beam of light when it passes through a sample or after reflection from a sample surface. When light passes through a sample, some amount of light will be transmitted and some amount will be absorbed. The amount of light absorbed can be calculated by finding out difference between intensities of incident and transmitted light. The values of absorption intensities can be plotted against the wavelength of the light to obtain the absorption spectra of the desired sample.

The instrument used in UV-Visible studies is called UV-Vis Spectrophotometer which is schematically represented in Figure. 2.9. In the present work, UV-Visible studies were carried out using Ocean Optics USB 4000 over a spectral range of 200 to 800 nm. The instrument operates by passing a beam of light through a sample and measuring wavelength of light reaching a detector. Light is quantized in tiny packets called as photons, the energy of which can be transferred to an electron upon collision. However, transfer occurs only when the energy level of photon equals the energy required for the electron to get promoted to the next energy state, for example from ground state to first excited state. This process forms the basis for absorption spectroscopy. Generally, light of a certain wavelength and energy is illuminated on the sample, which absorbs a certain amount of energy from the incident light. The energy of the light transmitted from the sample is measured using a photodetector, which registers the absorbance of the sample. A UV-Vis spectrophotometer measures absorbance or transmittance from the UV range to visible wavelength range. Further, from this data, optical constants like absorption coefficient, extinction coefficient, reflectance and band gap can be calculated.

UV-visible spectrophotometer consists of a number of fundamental components: Light Sources (UV and Visble), monochromator (wavelength selector), sample holder, a detector, signal processor and read out. The radiation source used is usually a tungsten filament, a deuterium arc lamp which is continuous over the ultraviolet region and more recently light emitting diodes (LED) and xenon arc lamps for the visible wavelengths. The detector use is typically a photodiode or charge coupling device (CCD).

Optical characterization is one of the methods to determine different electronic and optical transitions in the material and its band gap under the illumination of light. The incident light may get reflect, some part of the incident light may get absorb and some part may get transmitted through the sample. The amount of reflection, absorption, and transmission depend on the band structure and energy of the incident light. The transmittance and absorption measurements reveal valuable information about the energy band gap ($E_{a.}$) and band structure of the semiconductor material. The result of band to band transition is fundamental absorption, remaining mechanisms are important if the energy of the incident light is less than the energy band gap of semiconductor material.

The energy dependence of optical absorption coefficient (α) is as per Tauc's relation given in Equation 2.2.

$$(\alpha h\nu)^m = A(h\nu - E_g) \quad 2.2$$

where E_g is optical band gap, A is a constant, m is a constant that can take value 2 or $\frac{1}{2}$ corresponding to direct or indirect transition respectively [Karthigha and Krishnamoorthi 2018]. Direct transition is chosen and the plot of $(\alpha h\nu)^2$ versus hυ and extrapolating the linear portion of the graph, optical band gap E_g is calculated.

Optical absorption coefficient (α) is a measure of decrease in the energy of incident radiation per unit distance as the electromagnetic wave propagates through the crystal. It is calculated from the absorption spectrum using the Eqn. 2.3.

$$\alpha = \frac{2.303\ A}{t} \quad 2.3$$

where A is absorbance and t is thickness of the crystal [Ma et al. 2018].

Extinction coefficient (K) can be derived from the absorption coefficient using the relation given in Equation 2.4.

$$K = \frac{\lambda\alpha}{4\pi} \quad 2.4$$

where λ is the wavelength [Bincy and Gopalakrishnan 2014b].

Reflectance (R) is defined as the ration of the reflected intensity to the incident intensity and is the measure of ability of sample to reflect light from its surface [Kittel 2012]. Reflectance in terms of absorption coefficient is calculated from the Equation 2.5.

$$R = \frac{1 \pm \sqrt{1 - \exp(-\alpha t) + \exp(\alpha t)}}{1 + \exp(-\alpha t)} \quad 2.5$$

where t is thickness of sample and α is absorption coefficient [Girisun and Dhanuskodi 2009].

Refractive index (n) of a material determines how the light propagates through it. It is calculated from the relation given in Equation 2.6

$$n = \frac{-(T-2) \pm \sqrt{-3R^2 + 10R - 3}}{2\ (R-1)} \quad 2.6$$

Electric susceptibility (χ_c) indicates the degree of polarization of the material in response to applied field of electromagnetic wave. It is given by Equation 2.7.

$$\chi_c = \frac{n^2 - K^2 - \epsilon_0}{4\pi} \quad 2.7$$

where is the electric permittivity of free space [Rathika et al. 2016].

Optical conductivity of a crystal is a powerful tool to determine its optical response. Shankar Joseph equation for optical conductivity [Subramani et al. 2013] is given as shown in Equation 2.8.

$$\sigma_{op} = \frac{Knc}{\lambda} \qquad 2.8$$

where K is optical extinction coefficient, n is refractive index, c is the velocity of light and λ is the wavelength of light.

The real dielectric constant (ε_r) and imaginary dielectric constant (ε_i) are related to refractive index and extinction coefficient by the Equation 2.9 and 2.10 [Bincy and Gopalakrishnan 2014b].

$$\varepsilon_r = n^2 - K^2 \qquad 2.9$$

$$\varepsilon_i = 2nK \qquad 2.10$$

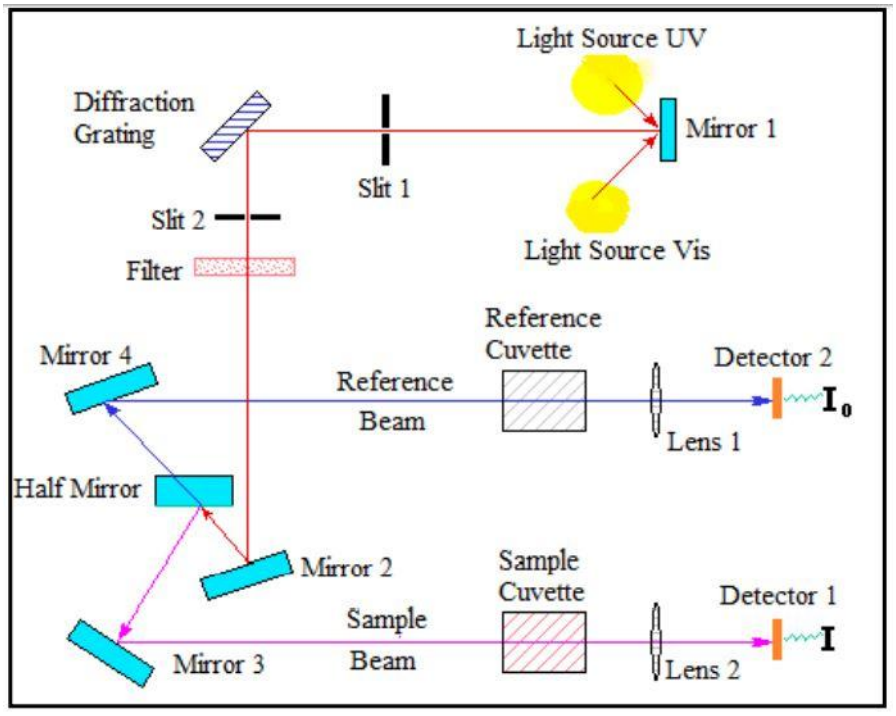

Figure. 2.9. Schematic diagram of UV-Vis spectrophotometer.

Figure. 2.10. The schematic of UV-Visible spectrophotometer.

2.2.6 Photoluminescence studies

Photoluminescence (PL) spectroscopy is contactless, versatile, nondestructive, powerful optical method of probing the electronic structure of materials. Light is directed onto a sample, where it is absorbed and imparts excess energy into the material in a process called photo-excitation. One way this excess energy can be dissipated by the sample through the emission of light or luminescence. In the case of photo-excitation, this luminescence is called photoluminescence. Thus, photoluminescence is the spontaneous emission of light from a material under optical excitation [Aoki 2002]. This light can be collected and analyzed spectrally. The intensity and spectral content of this photoluminescence is a direct measure of various important material properties. Photo-excitation causes electrons within a material to move into permissible energy levels. These electrons when return to ground states, the excess energy is released and may or may not involve emission of light. The energy of the emitted light relates to the difference in energy between two electron states involved in the transition. The principle of photoluminescence is shown in Figure. 2.11. The quantity of emitted light is related to the relative contribution of the radiative process. The spectral dependence of intensity gives information about properties of the material. The time dependence of emission provides information about energy levels in the material. Since PL emission involves defect level transitions, the presence of defects in the material can also be estimated. Hence the quality of material can be studied.

The photoluminescence spectra of pure and doped crystals in the present work were recorded using Horiba scientific Fluromax-4-spectrophotometer shown in Figure 2.12.

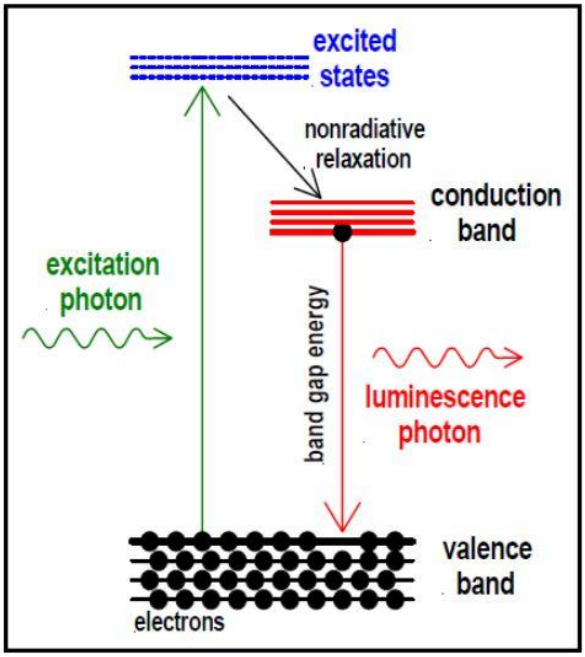

Figure. 2.11. Principle of Photoluminescence spectroscopy.

Figure. 2.12. Horiba scientific Fluromax-4-spectrophotometer instrument used for the PL studies.

2.2.7 Fourier Transform Infrared Spectroscopy (FTIR)

A molecule is a collection of atoms. These atoms have different types of vibrational motion. The energy corresponding to most of these vibrations is quantized and lies in infrared region of the electromagnetic spectrum. When infrared radiation is allowed to fall on the molecule, the system absorbs energy causing excitation of the molecule to higher vibrational levels. This gives rise to band characteristic of the molecule. Each functional group has characteristic vibrational frequency. This fact helps us to identify various functional groups. This has been achieved using infrared spectra which has been one of the most reliable methods for understanding the structure of molecules.

Infrared spectroscopy has been a technique for material analysis for over seventy years. An infrared spectrum represents a fingerprint of a sample with absorption peaks corresponding to frequencies of vibration of bonds between the atoms. Since each material is a different combination of atoms, no two compound produces same infrared spectrum. Hence infrared spectroscopy plays an important role in identification of the material. In addition, the size of the peaks is a direct indication of the amount of material present. Thus infrared spectroscopy is an excellent tool for both qualitative and quantitative analysis.

The original infrared instruments were of dispersive type where the individual frequencies of the infrared source was separated and the amount of energy at each frequency after passing through the sample was measured by the detector. Fourier Transform Infrared (FTIR) spectroscopy was developed in order to overcome the limitations of older infrared spectroscopic method. It consists of an interferometer that produces a unique type of signal which has all the infrared frequencies encoded into it. The signal can be measured very quickly thereby overcoming the drawback of slow scanning of the older technique. Most interferometers use a beam splitter which divides the incoming infrared beam into two optical beams. One reflects off from a mirror that is fixed and the other reflects off from a mirror which can be moved over a very short distance. The signal that exits the interferometer is the result of two reflected beams interfering with each other. The resulting signal is called interferogram which has the unique property that every data point that makes up the signal has information about every infrared frequency that comes from the source. As the interferogram is measured, all the frequencies are measured simultaneously resulting in extremely fast

measurements. The measured interferogram cannot be interpreted directly. A method of decoding the individual frequencies is required which is accomplished by a well-known mathematical technique called as Fourier transformation which is performed by the computer giving the desired spectral information for analysis. The schematic diagram for FTIR is shown in Figure. 2.13.

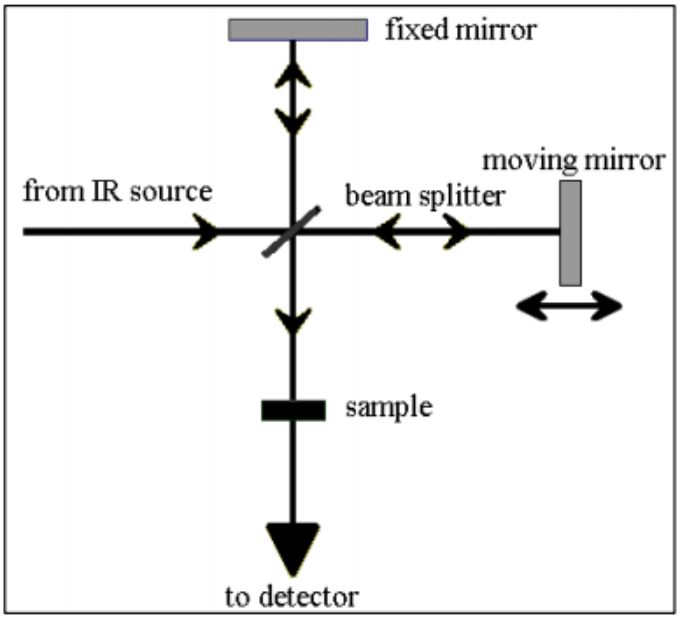

Figure. 2.13. Schematic representation of FTIR Spectrometer.

Figure. 2.14. FTIR instrument.

2.2.8 Thermo Gravimetric and Differential Thermal Analysis (TG-DTA)

Thermal analysis is a branch of materials science where the properties of materials are studied as a function of temperature. The techniques used in the present study are thermogravimetric analysis (TGA) and differential thermal analysis (DTA). TGA is a technique in which the mass of a substance is monitored as a function of temperature under controlled atmosphere. A simple TGA concept is TGA measures a sample's weight as it is heated or cooled in a furnace. It consists of a sample pan that is supported by a precision balance. That pan resides in a furnace and is heated or cooled during the experiment. The mass of the sample is monitored during the experiment. A sample purge gas controls the sample environment. This gas may be inert or a reactive gas that flows over the sample and exits through an exhaust. The schematic diagram for TGA technique is shown in Figure. 2.15. These instruments can quantify loss of water, loss of solvent, loss of plasticizer, decarboxylation, pyrolysis, oxidation and decomposition.

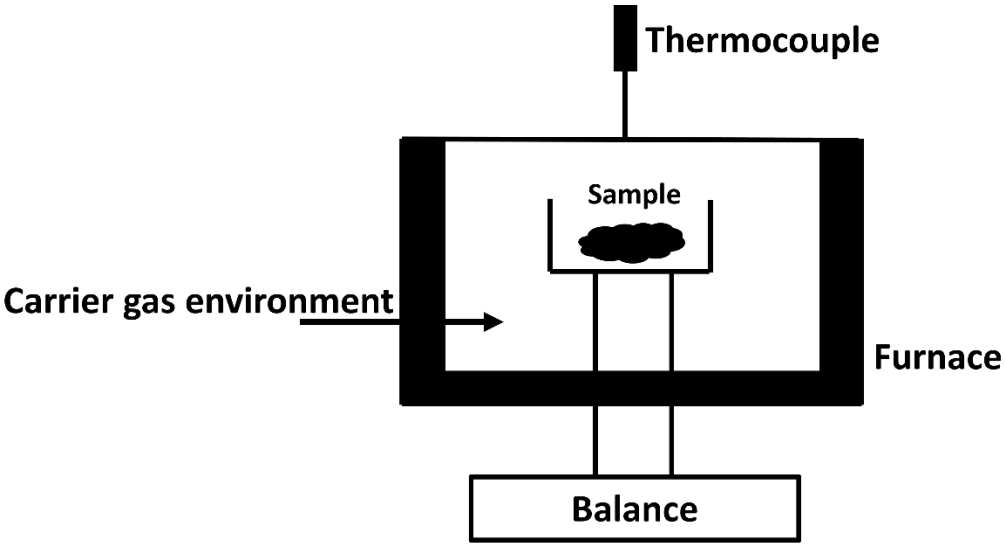

Figure. 2.15. Schematic diagram for TGA technique.

DTA consists of heating the sample and reference material at the same rate and monitoring the temperature difference between the sample and reference. In this method, the sample is heated along with the reference standard under identical thermal conditions in the same oven. The temperature difference between the sample and reference substance is monitored during the period of heating. As the sample undergoes any change in state, the latent heat of transition will be evolved or absorbed and the

temperature of the sample will differ from that of the reference material. This difference in temperature is recorded. Hence, any change in state can be detected along with the temperature at which it occurs. The schematic diagram for DTA technique is shown in Figure. 2.16. The measured weight loss curve gives information on changes in sample composition and thermal stability. The derivative weight loss curve can be used to tell the point at which the weight loss is most apparent.

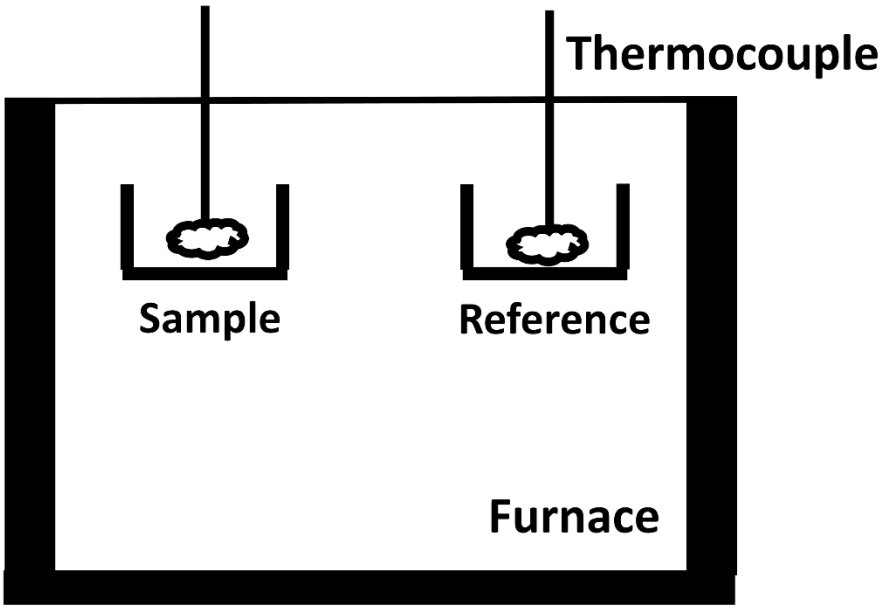

Figure. 2.16. Schematic diagram for DTA technique.

2.2.9 DIFFERENTIAL SCANNING CALORIMETRY (DSC)

The thermal studies presented in this thesis have been performed using a differential scanning calorimeter (DSC). DSC is a thermal analysis technique that measures the heat flow into or out of a sample as a function of temperature and is used to detect thermodynamic transitions such as glass transition, crystallization or melting. A DSC measures the temperature difference between the sample under study (S) and an inert reference (R). Thus, DSC is a calorimetric method in which differences in energy are measured. Generally, the temperature program for a DSC analysis is designed such that the sample holder temperature increases linearly as a function of time. The reference sample should have a well-defined heat capacity over the range of temperatures to be scanned. The DSC operates under the simple assumption that the heat flow rate between two points is proportional to the temperature difference between

those two points. The Figure 2.17 shows the schematics of a DSC and the image of the instrument used in the present work (Figure 2.18). The calorimeter consists of a sample holder and a reference holder (beneath their respective pans) as shown in Figure 2.17. Both are constructed of platinum to allow high temperature operation.

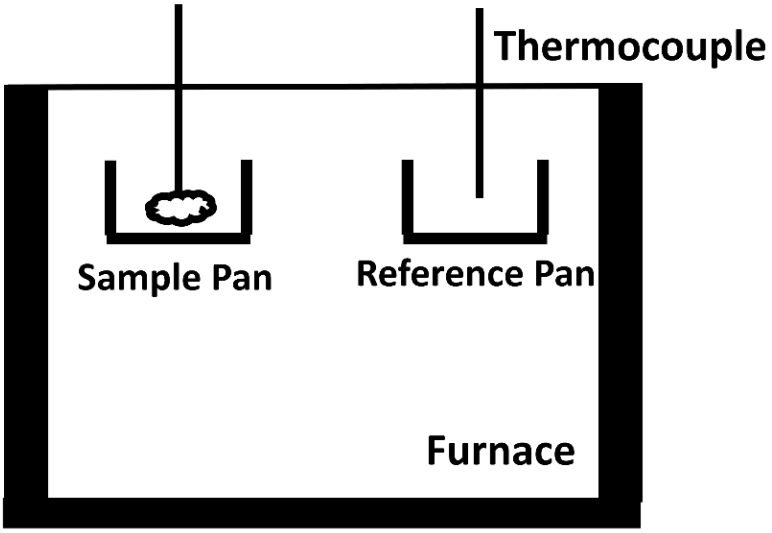

Figure. 2.17 Schematics of a Differential Scanning Calorimeter.

Figure. 2.18. Image of the Perkin Elmer DSC 8000 used for thermal studies.

Under each holder is a resistance heater and a temperature sensor. Currents are applied to the two heaters to increase the temperature at a selected rate. The difference in the power to the two holders is necessary to maintain the holders at the same temperature. A flow of nitrogen gas is maintained over the samples to create a reproducible and dry atmosphere. The nitrogen atmosphere also eliminates air oxidation of the samples at high temperatures. The sample is sealed into a small aluminum pan. The reference is an inert material such as alumina or just an empty aluminum pan. The pans hold up to about 10 mg of material. Since the DSC is at constant pressure, heat flow is equivalent to enthalpy changes:

$$\left(\frac{dq}{dt}\right)_p = \frac{dH}{dt} \qquad 2.11$$

Here dH/dt is the heat flow measured in mcal sec^{-1}. The heat flow difference between the sample and the reference is:

$$\frac{\Delta dH}{dt} = \left(\frac{dH}{dt}\right)_{sample} - \left(\frac{dH}{dt}\right)_{reference} \qquad 2.12$$

and can be either positive or negative. In endothermic processes such as most phase transitions, heat is absorbed and therefore, heat flow to the sample is higher than that to the reference. Hence, ΔdH/dt is positive. For example, as a solid sample melts into a liquid, it requires more heat flowing to the sample to increase its temperature at the same rate as the reference. This is due to the absorption of heat by the sample as it undergoes the endothermic phase transition from solid to liquid. In an exothermic process such as crystallization, some cross-linking processes, oxidation reactions, and some decomposition reactions, the opposite is true and ΔdH/dt is negative. When the sample undergoes exothermic processes, less heat is required to raise the sample temperature. By observing the difference in heat flow between the sample and the reference, differential scanning calorimeters are able to measure the amount of heat absorbed or released during such transitions.

2.2.10 Hardness Measurements

Vickers hardness number (VHN) is given by the relation [Gao et al. 2003 Tyagi et al. 2015]

$$H_v = 108544 \frac{P}{d^2} \qquad 2.13$$

Where, P is the applied test load in kg and d is the mean diagonal length of indentation impression in mm. In an ideal crystal, the hardness does not vary with the applied load whereas in a real crystal this variation is observed. The diamond indenter is as shown in the Figure 2.19.

$C_{11} = H_v^{7/4}$ 2.14

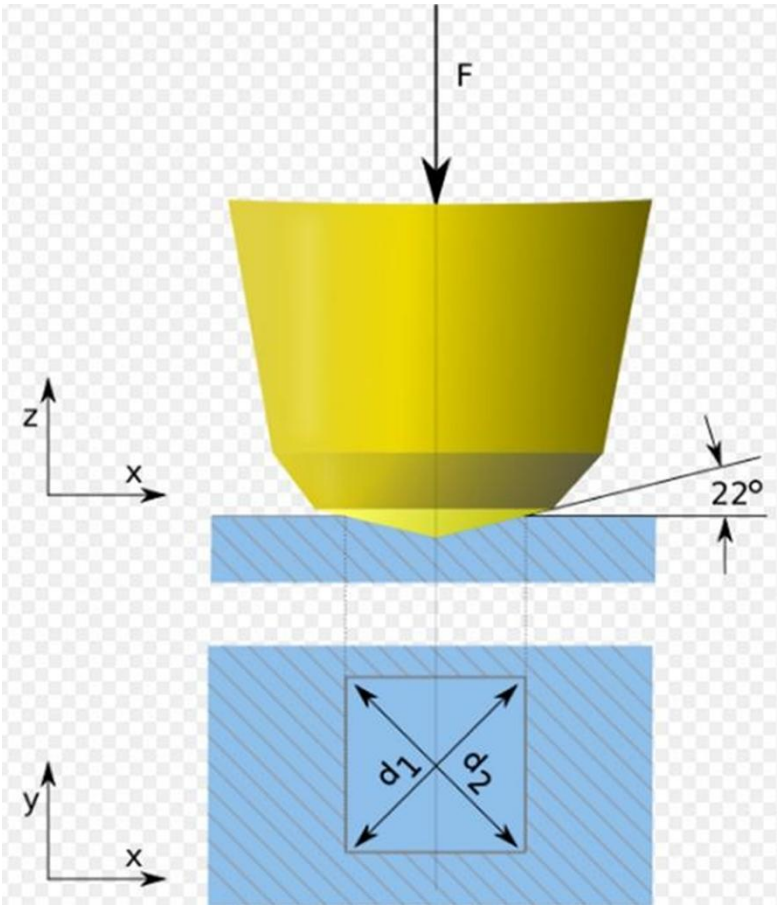

Figure. 2.19. Schematic representation of Vicker's pyramidal indenter.

The size of the indentation and the load applied can be related using Meyer's law [Sangwal 2000] as shown in Equation 2.15.

$P = Kd^n$ 2.15

Where n is Mayer's index and K is the material constant. The n value can be calculated by taking the slope from log P versus log d graph.

The yield strength values are computed using the relation 2.16 [Suresh et al. 2018]

$\sigma_y = \frac{H_v}{3}$ 2.16

The Fracture toughness of the crystals are calculated using the relation.

$K_c = \beta_0 C^{3/2}$ 2.17

Where C is crack length and β_0 is taken as 7 for Vickers indenter [Vizhi and Vijayalakshmi 2016].

The relative measure of the material brittleness is obtained by the crack produced on the indented surface and calculated using the Equation 2.18.

$B_i = \frac{H_v}{K_c}$ 2.18

Where, H_v is the Vicker's hardness number and K_c is Fracture toughness of the crystal.

2.2.11 I-V studies

2.2.11(a) Preparing samples

The synthesized crystals with parallel surface were chosen and polished on both sides using two different grade polishing papers of 1200 grade paper for removing the rougher surfaces and 3000 grade paper to polish the samples to get smoother surfaces. The thickness of the crystals were measured using Digital Vernier callipers having a least count of 0.01 mm. For I-V characterization experiments, smooth surfaces on the both the sides of the crystals are required to obtain the better I-V results without any current loss due to the contacts on both the surface. The electrical response of the crystal depends on the electrode in contact with the crystal.

The same I-V measurements were carried out in dark as well as illuminated conditions in order to measure the photo response of the material. A white light source of 50W capacity is used to illuminate the crystal and the I-V response is studied.

2.2.11(b) I-V ANALYZER

The current-voltage characteristic of a solid can be studied either by scanning along the voltage axis with variable voltage source and measuring the current induced in the sample, or by scanning the current axis with the variable current source and measuring the voltage developed across the sample. The selection of the source depends on the characteristics to be measured. In the case of ohmic samples, either of these methods produces the same result.

A customized setup is used to study the Photo response of the material. The setup consists of a closed wooden box with provision to insert sample holder to study the response of the crystal. A white light source of 50W is fitted in the one top end of the wooden board and the light is aligned in such a way that the illuminated light

directly falls on the sample holder (where the sample is studied).

The crystals were studied by sourcing voltage and measuring the current developed across the sample. The photo response of the crystal was studied by exposing the crystal to the illuminated source for 2 min and sourcing the voltage and measuring the current. Schematic diagram of the PC based I-V analyzer system used to study the electrical I-V and Photo response of the crystals is shown in the Figure. 2.20. It consists of two main parts:

(i) Source meter :- A Keithley Source - Meter (Model 2410) controlled through IV Lab Tracer 2.0 is used as an excitation source to study the I-V characteristics. It can deliver a maximum current of 20mA at a compliance voltage of 1100V. The current source mode of this instrument is employed for the switching analyses as it is possible to obtain the complete I-V curve in this mode.

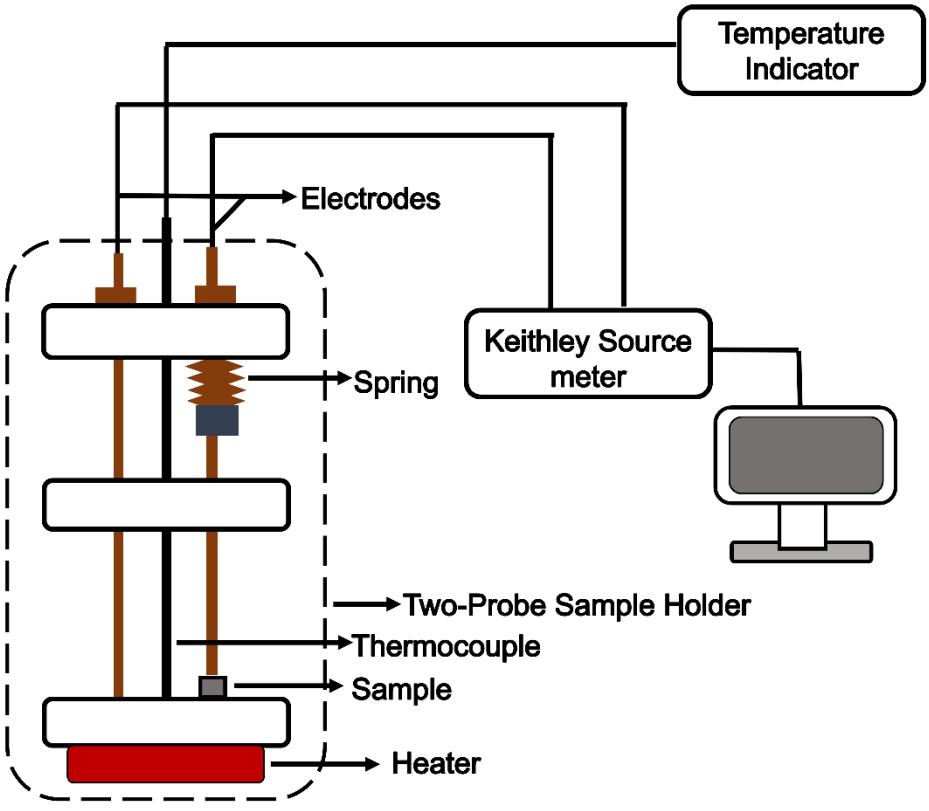

Figure. 2.20. Schematic of PC controlled set-up used for I-V characteristics of the crystals.

(ii) Sample holder :- The sample whose I-V characteristic is to be studied is placed in a sample holder cell. Basically, the design comprises of an inter changeable two probe holder assembly comprising of a four hole high purity Alumina Sheathing with overall

diameter not exceeding 8 mm. This is integrated with alumina plates of diameter not exceeding 20mm at the bottom with suitable holding assembly on which the specimen to be tested is placed. The brass electrodes are inserted through the holes of the alumina sheathing for making contact with that of the sample. The design is such that the measuring probes will run through the individual holes of the Alumina sheathing duly fitted with a spring loading system provided at the top. By just applying adequate hand pressure on the spring loading system, the contacts between the probes and the specimen are developed. To study the I-V characteristics, flat contacts are taken from the two electrodes as shown in Figure. 2.21.

Figure. 2.21. Image of the experimental setup used for electrical conductivity studies.

(iii) Photoconductivity setup

Sample was polished in both the ends and placed between a two-probe sample holder. Customized set up has been used in order to characterize the sample in both dark and illuminated condition. We have used a Halogen dichroic lamp of 50 W capacity which is a white light source for the present study. An input voltage has been applied to the sample and the resultant current has been measured. The wavelength dependent I-V studies of the crystal was carried out by illuminating the crystal with different frequencies of visible light radiation using suitable filters. The time dependent I-V studies were performed by setting the bias voltage at +3 V and measuring the current with respect to time.

The resistivity of the crystal is calculated using the Equation 2.19

$$\rho_{dc} = \frac{RA}{d} \qquad 2.19$$

where, ρ is the resistivity, A is the area of contact and d is the thickness of crystal.

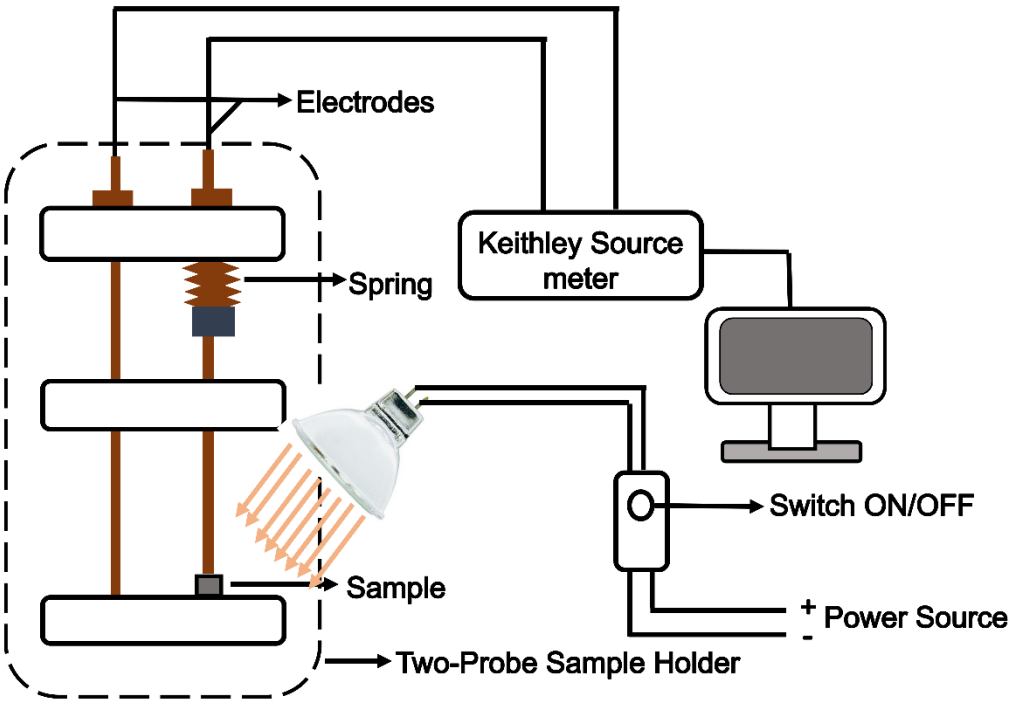

Figure. 2.22. Schematic of PC controlled set-up used for Photoconductivity studies of the crystals.

2.2.12 Dielectric Studies

The electrical properties and dynamics of semiorganic crystals at the metal-crystal interface or in their bulk form can be easily investigated using a relatively new and powerful electrical characterization method called Impedance Spectroscopy (IS). This is a purely electrical and non-destructive technique which does not require expensive experimental setup. The general approach in Impedance Spectroscopy of single crystals is to apply an external stimulus (*ac* voltage or current) to the electrodes and observe the response. The nature of the external stimulus can be varied and the standard approach is to apply a single-frequency voltage or current to the interface and measure the phase shift and amplitude, or real and imaginary parts of the resulting current at that frequency, using either analog circuit or fast Fourier transform (FFT) analysis of the response [Macdonald and Johnson 2005]

In Impedance spectroscopy measurements, a small sinusoidal voltage $v(t)$ =

$V_m\sin(\omega t)$ of amplitude V_m and frequency $\omega = 2\pi f$ is applied to the sample along with a constant bias voltage V. The response of the sample is given by the resulting measured current $i(t) = I_m\sin(\omega t+\phi)$ with a phase shift ϕ and amplitude I_m. The small sinusoidal voltage is in the order of millivolts so that the current response is almost linear and does not perturb the sample very much. For purely resistive behavior, $\phi = 0$. When the system involves capacitive and inductive elements, the relation between the properties of the system and its response to the external stimuli becomes very complex in time domain. The frequency dependent complex impedance $Z(\omega)$ is defined according to Ohm's law as the ratio of the complex voltage $V(\omega)$ to complex current $I(\omega)$ and is given by the following expression

$$Z(\omega) = \frac{V(\omega)}{I(\omega)} = \mathrm{Re}[Z(\omega)] + i\mathrm{Im}[Z(\omega)] \qquad 2.20$$

where $\mathrm{Re}[Z(\omega)]$ is the real part and $\mathrm{Im}[Z(\omega)]$ is the imaginary part of the complex impedance. The plot of $-\mathrm{Im}[Z(\omega)]$ versus $\mathrm{Re}[Z(\omega)]$ is called as the Cole – Cole plot and is shown in Figure 2.23.

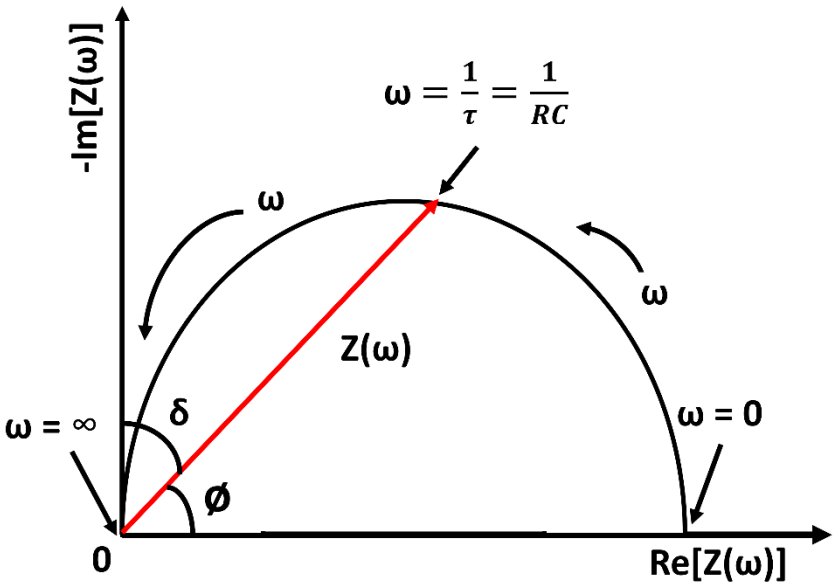

Figure. 2.23. Cole-cole Plot.

The modulus $|Z(\omega)|$ is given by the expression

$$|Z(\omega)| = \sqrt{\{(\mathrm{Re}[Z(\omega)])^2 + (\mathrm{Im}[Z(\omega)])^2\}} \qquad 2.21$$

And the phase angle is given by the following expression

$$\phi = \tan^{-1}\left[\frac{\mathrm{Im}[Z(\omega)]}{\mathrm{Re}[Z(\omega)]}\right] \quad 2.22$$

The IS data is represented and modeled using different equivalent circuits consisting of resistors and capacitors, depending on the structure and type of devices studied.

The *RC* circuit as shown in Figure 2.24 consisting of a resistor R_S in series with a parallel resistor R_P and parallel capacitor C_P is used to represent a single semicircle of radius $R_P/2$ and height $\tau = 1/R_P C_P$ in the Cole - Cole plot. The negligible value of series resistor R_S can be obtained from the distance between the origin and $\omega = \infty$ on the x-axis of the Cole – Cole plot.

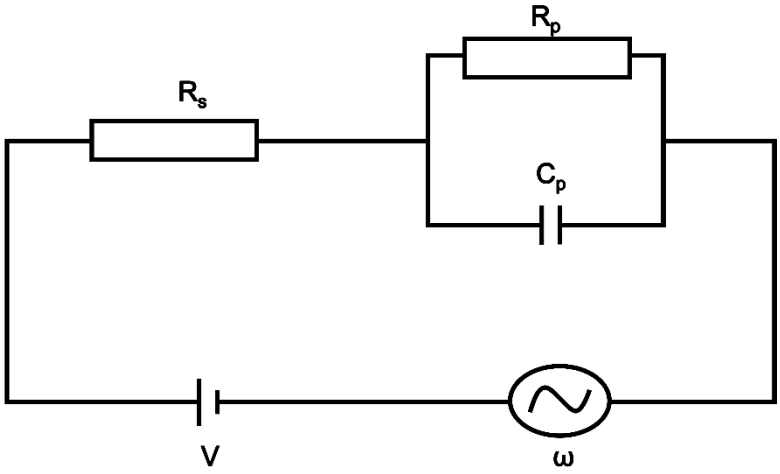

Figure. 2.24. Equivalent circuit model.

The values of R_P and C_P are given by the following equations

$$R_p = (\mathrm{Re}[Z(\omega)] - R_s) + \frac{(\mathrm{Im}[Z(\omega)])^2}{(\mathrm{Re}[Z(\omega)]) - R_S} \quad 2.23$$

$$C_p = -\left[\frac{1}{\omega R_p}\right] + \frac{((\mathrm{Im}[Z(\omega)])}{(\mathrm{Re}[Z(\omega)] - R_S} \quad 2.24$$

2.2.12(a) Dielectric calculations

The complex dielectric constant of a system subjected to an oscillating electric field is given by

$$\varepsilon^* = \varepsilon' + \varepsilon'' \quad 2.25$$

where, ε' and ε'' are real and imaginary parts of dielectric constants [Elwej and Hlel 2016].

ε' is calculated from the parallel capacitance value (C_p) as shown in Equation 2.26.

$$\varepsilon' = \frac{C_p d}{\varepsilon_0 A} \quad 2.26$$

where $\varepsilon_0$is permittivity of free space, A is area of cross-section of the sample and d is the thickness of the sample [Shoba and Kaleemulla 2017].

ε'' is calculated using the relation shown in Equation 2.27

$$\varepsilon'' = \frac{\varepsilon'}{2\pi f C_p R_p} \quad 2.27$$

where R_p is parallel resistance and f is frequency of applied electric field.

The dielectric loss tangent ($\tan\delta$) which represents dielectric loss of the material is calculated using the relation 2.28 [Bindu et al. 2018a],

$$\tan\delta = \frac{\varepsilon''}{\varepsilon'} \quad 2.28$$

The ac conductivity of pure and doped crystals was calculated using the formula given in Equation 2.29.

$$\sigma_{ac} = \omega\varepsilon_0\varepsilon' \tan\delta \quad 2.29$$

where $\omega = 2\pi f$ is the angular frequency of the applied field and ε_0 is permittivity of free space [Sagadevan 2016a].

The frequency dependence impedance consisting of the real (Z') and imaginary (Z') parts are calculated using the relation 2.30 and 2.31, respectively.

$Z' = Z \times \text{Sin (Phase)}$ 2.30

$Z'' = Z \times \text{Cos (Phase)}$ 2.31

CHAPTER 3

SYNTHESIS AND CHARACTERIZATION OF ORGANOMETALLIC POTASSIUM HYDROGEN OXALATE OXALIC ACID DIHYDRATE SINGLE CRYSTAL

Overview

In this chapter, the description of the preparation of potassium oxalate oxalic acid dihydrate ($KH_3(C_2O_4)_2.2H_2O$) single crystals using the slow solvent evaporation technique at room temperature was given in sufficient detail. The structural, optical, thermal, mechanical and electrical properties of the crystal were discussed.

3.1 Introduction

Great efforts have been made in the area of research and design of highly efficient materials for various applications such as high speed information processing, optical communication, optical data storage, etc. [Shahil Kirupavathy et al. 2008 Saritha 2013 Santhi and Alagar 2016]. Many research works were carried to overcome the drawbacks of the existing host materials by combining them with the other materials. The organic materials are having excellent optical properties, but they are brittle in nature [Rajasekaran et al. 2001 Senthil Pandian and Ramasamy 2010 Thaila and Kumararaman 2012]. Polishing those materials to the potential need is difficult because they are soft in nature which is due to the weak hydrogen bonds [Ramajothi and Dhanuskodi 2007]. The organic materials, due to their low thermal stabilities, poses difficulty during device fabrications. On the other hand, inorganic materials possess higher mechanical and thermal stabilities but moderate optical properties. An alternate class of materials have been developed to overcome the drawbacks of organic and inorganic materials by combining both the materials, giving rise to semiorganic materials which possess higher optical properties of organic materials and mechanical and thermal stabilities of the inorganic materials. The titled compound was first synthesized using potassium hydrogen oxalate $K(HC_20_4)$ and aluminium hydroxide $Al(OH)_3$ and the obtained compound was $KH_3(C_4O_8).2H_2O$ [Haas 1964]. The $KH_3(C_4O_8).2H_2O$ single crystal was refined to R factor of 0.05. The crystal structure was further solved to the R value of 0.03 and the synthesis method was not described in the paper [Gilmore and Speakman 1982]. In the present work, the potassium

hydrogen oxalate oxalic acid dihydrate $KH_3(C_4O_8).2H_2O$ single crystals were synthesized using oxalic acid and potassium dihydrogen phosphate and structure was solved which is in close agreement with the reported values [Haas 1964 Gilmore and Speakman 1982]. The method employed to synthesize the titled compound is completely different and the structure is solved to the R value of 0.024. The synthesized crystal was further characterized structurally, optically, thermally and electrically using powder XRD, UV-vis analysis, FTIR analysis, photoluminescence, Vickers hardness, TGA-DTA, I-V and dielectric analysis.

3.2 Results and Discussions

3.2.1 Solubility, density and growth rate studies

The solubility studies of KHOOD crystal was determined at 6 different temperatures starting from room temperature (27 °C) to 50 °C. A Constant volume of double distilled water was used for the experiment (10 ml). The measurement was performed by dissolving a known quantity of KHOOD crystal in double distilled water taken in an air tight container kept at a constant temperature with continuous stirring. The solution was stirred for 2 hrs with magnetic stirrer for homogenization. The obtained solid samples are weighed to obtain the solubility of the material. The solubility as a function of temperature is given in Fig. 3.1.

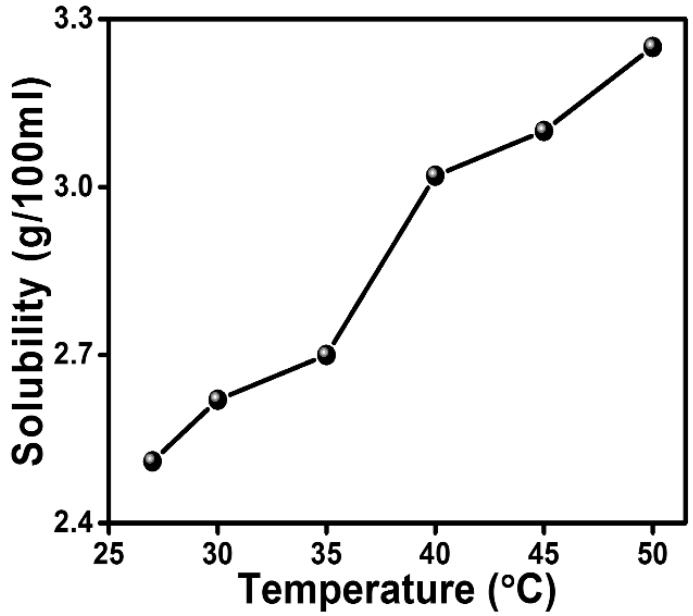

Figure. 3.1. Solubility Curve of $KH_3(C_4O_8).2H_2O$ single crystal.

The density measurements are carried for the KHOOD crystal using Contech Density measurement unit and the obtained density value is 1.83 g/cm^3. The crystal growth rate was also measured at room temperature and the growth rate is observed to be 0.09232 g/day.

3.2.2 Single Crystal X-ray diffraction (SCXRD) analysis

The crystal was subjected to SCXRD analysis and the structure of the molecule is solved using direct method which is shown in Fig. 3.1. The crystal belongs to triclinic crystal system with P-1 space group (Table 1). Unit cell parameters are a = 6.3632(5) Å, b = 7.0291(5) Å, c = 10.5984(7) Å, α = 93.835(3)°, β = 101.358(3)°, γ = 100.174(3)° and V = 454.90(6) Å^3. Asymmetric unit of the titled compound consists of one molecule of potassium oxalate, 2 hemi oxalic acid molecule and 2 molecules of water. Potassium in the crystalline materials form bond with carbonyl group of oxalic acid and H_2O molecule. Oxalic acid in the crystal bonds with water molecule and carboxylate group of potassium oxalate with O—H···O bond distance 2.484 Å and 2.503 Å respectively. Bond lengths between K^+, oxalic acid and water molecules. The molecule expands in 3D manner by utilizing interactions associated with oxalic acid, oxalate and water molecule. Oxalic acid acts as a bridge between the packing units via –C=O···K^+ and O—H···O interactions leading to a 3D structure of $KH_3(C_4O_8).2H_2O$. The packing view of $KH_3(C_4O_8).2H_2O$ single crystal was shown in Fig. 3.2

Table. 3.1. Crystal information, data collection and refinement details.

Crystal structure details	**KHOOD**
CCDC number	1547829
Molecular Formula	$C_4H_7KO_{10}$
Molecular weight	254.20
crystal system	triclinic
Space group	$P\bar{1}$
a /Å	6.3632(5)
b /Å	7.0291(5)
c /Å	10.5984(7)
α / °	93.835(3)

β / °	101.358(3)
γ / °	100.174(3)
Volume/ Å ^{3}	454.90(6)
Z	2
Density [g/cm^3]	1.856
μ (MoKα) [mm^{-1}]	0.627
T/K	296 (2)
Reflns collected	2270
Unique rflns	1953
Parameter refined	165
$R_1(I > 2\sigma)$	0.0240
wR_2 (I>2σ)	0.0645
GOF	1.007

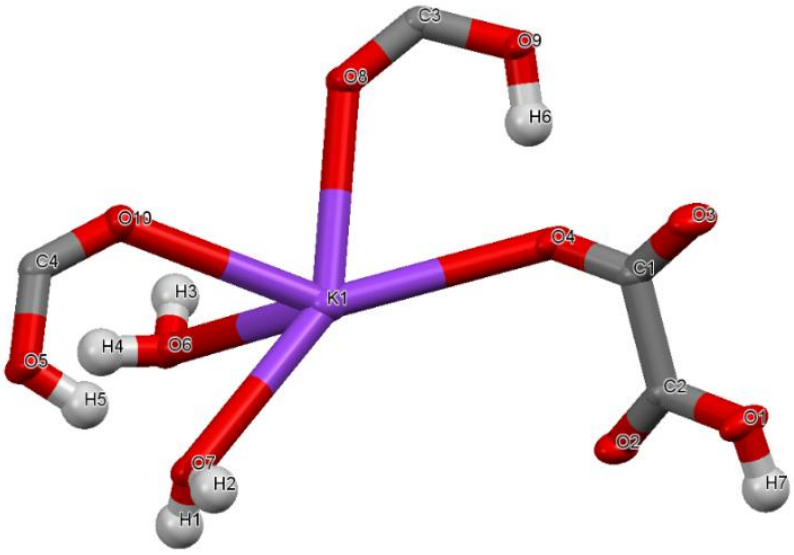

Figure. 3.2. Asymmetric unit of $KH_3(C_4O_8).2H_2O$ single crystal.

Table. 3.2. Bond lengths.

Number	Atom1	Atom2	Length
1	K1	O10	2.9127(9)
2	K1	O8	2.8778(9)
3	K1	O7	2.896(1)

4	K1	O4	3.042(1)
5	K1	O6	2.922(1)
6	O10	C4	1.208(1)
7	O5	C4	1.296(2)
8	O5	H5	0.89(3)
9	O9	C3	1.285(1)
10	O9	H6	0.97(2)
11	C2	O1	1.300(1)
12	C2	C1	1.553(2)
13	C2	O2	1.210(1)
14	O8	C3	1.215(1)
15	O1	H7	0.90(2)
16	O7	H1	0.82(2)
17	O7	H2	0.81(2)
18	O3	C1	1.232(1)
19	O4	C1	1.256(1)
20	O6	H4	0.86(2)
21	O6	H3	0.81(2)

Table. 3.3. Hydrogen bonds in the $KH_3(C_4O_8).2H_2O$ single crystal.

D*—H⋯*A	***D*—H**	**H⋯*A***	***D*⋯*A***	***D*—H⋯*A***
O1—H7⋯O6	0.90(2)	1.63(2)	2.5272(12)	175(2)
O9—H6⋯O4	0.97(3)	1.53(3)	2.5032(11)	175(2)

O5—H5···O7	0.89(3)	1.59(3)	2.4839(13)	175(2)
O6—H3···O5	0.81(2)	2.42(2)	2.8415(13)	113.4(19)
O6—H3···O10	0.81(2)	2.01(2)	2.7917(12)	163(2)
O6—H4···O8	0.87(2)	2.03(2)	2.8402(13)	154(2)
O6—H4···O9	0.87(2)	2.27(2)	2.8933(13)	129.0(19)
O7—H2···O2	0.81(2)	1.94(2)	2.7403(13)	169.2(18)
O7—H2···O4	0.81(2)	2.626(19)	3.0799(13)	116.9(15)
O7—H1···O3	0.82(2)	1.91(2)	2.7106(12)	166.4(19)

Symmetry codes: (i) −*x*+1, −*y*, −*z*+1; (ii) *x*+1, *y*, *z*; (iii) −*x*, −*y*, −*z*; (iv) *x*−1, *y*−1, *z*; (v) *x*−1, *y*, *z*.

3.2.3 Powder XRD analysis

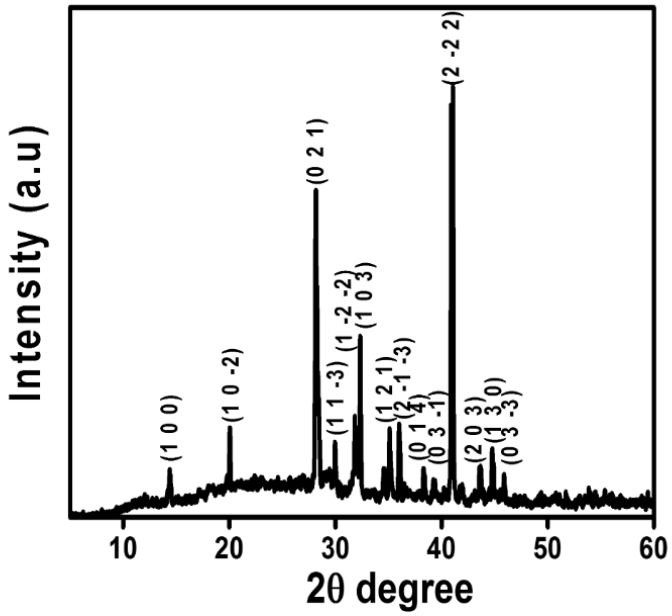

Figure. 3.3. Powder XRD pattern of KHOOD single crystal.

The synthesized single crystals were crushed using motor and pestle to obtain fine powder. The obtained powder was subjected to powder XRD analysis and the plot is as shown in Fig. 3.3. The presence of crystalline peaks indicates the crystalline nature of the synthesized material. The crystals were indexed using the miller indices obtained from the SXRD which was extracted using the mercury software. The powder XRD

data was further analyzed using X-pert highschore software and the crystal obtained belongs to triclinic crystal system which is in good agreement with the single crystal XRD data (Table 3.4).

Table 3.4. Structural details of $KH_3(C_2O_4)_2.2H_2O$ crystal.

Cell parameters	SXRD	PXRD
a (Å)	7.029(5)	7.031(3)
b (Å)	10.598(5)	10.611(5)
c (Å)	6.363(7)	6.367(3)
Alpha (°)	101.358(3)	101.360(3)
Beta (°)	100.174(3)	100.180(5)
Gamma (°)	93.835(3)	93.820(5)
Volume of cell ($Å^3$)	454.90(3)	455.84(7)

3.2.4 SEM and Energy Dispersive X-ray (EDAX) analysis

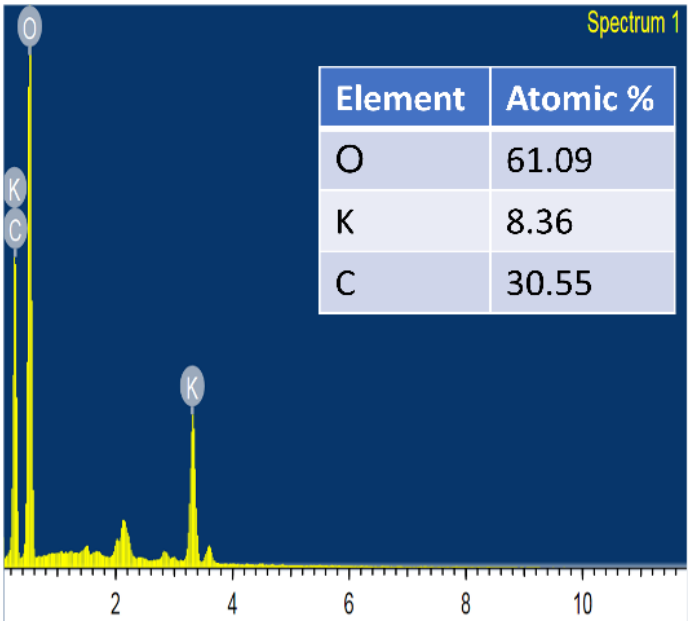

Figure. 3.4. EDAX spectrum of $KH_3(C_2O_4)_2.2H_2O$ single crystal.

From the SEM micrograph of $KH_3(C_2O_4)_2.2H_2O$ single crystal, it was observed that the crystal surface consists of pits and microcrystals. The elemental composition of the synthesized crystal can be determined using a micro analytical technique known as EDAX analysis. In the present work, elemental analysis of $KH_3(C_2O_4)_2.2H_2O$

crystals was carried out. Fig. 3.4 shows the recorded EDAX spectrum which confirms the presence of potassium, carbon and oxygen in the synthesized crystal. The mapping spectra shown in Fig. 3.5 further depicts the distribution of these elements in the crystal.

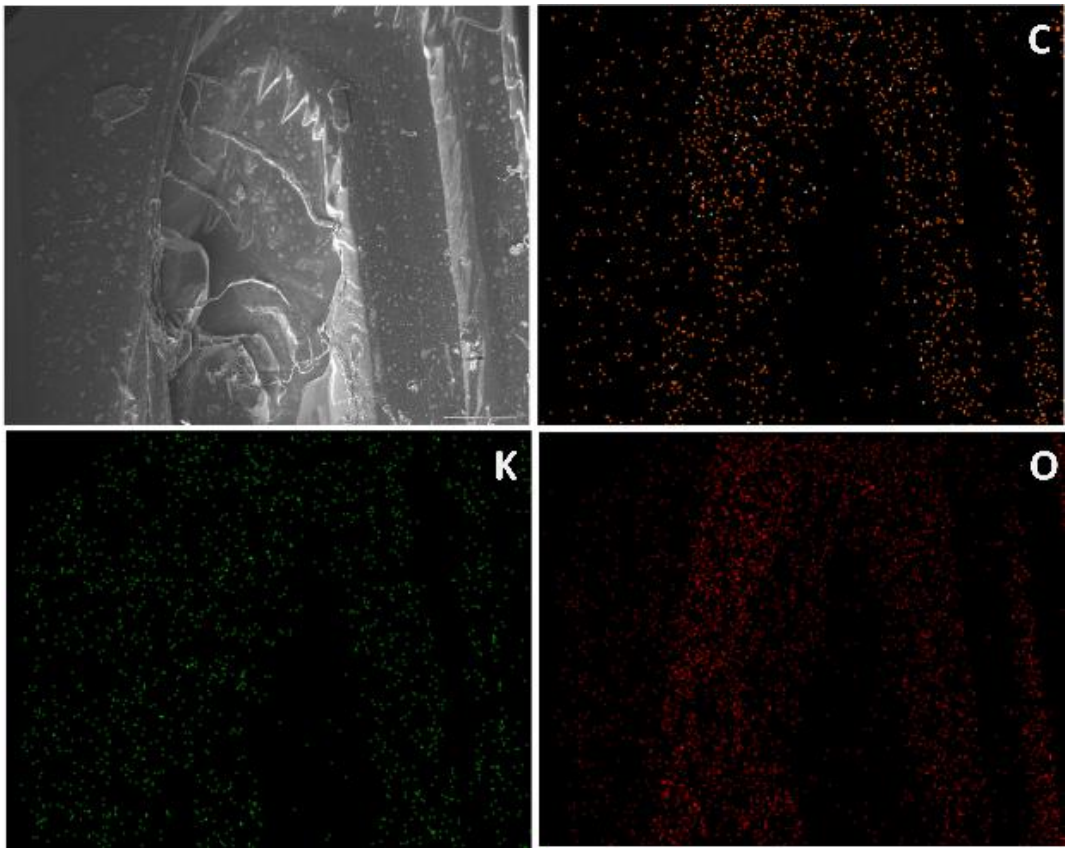

Figure. 3.5. FESEM and elemental mapping of $KH_3(C_2O_4)_2.2H_2O$ single crystal.

3.2.5 UV-visible studies

The crystals were characterized using UV-vis spectrometer and the absorption spectrum was recorded in the spectral range of 200-900 nm. As obtained crystals were polished on both the sides to obtain smooth surface to measure UV-vis measurements. The crystal shows strong absorbance in the UV region and transmits in the visible region, which is shown in the Fig. 3.6. The crystal absorption peak was observed at around 280 nm which corresponds to the UV region of the electromagnetic spectrum. The crystal exhibits excellent transmittance in the visible region.

The interaction between the electromagnetic radiation and the material decides the optical property of the material [Job et al. 2016a]. The UV-visible transmittance spectrum of the synthesized crystal is recorded and is shown in Fig. 3.7. The crystal

exhibits excellent transmittance in entire visible region and near IR region with lower cut-off wavelength lying in UV region at 333 nm. The wide optical window suggests its application in optoelectronic industries.

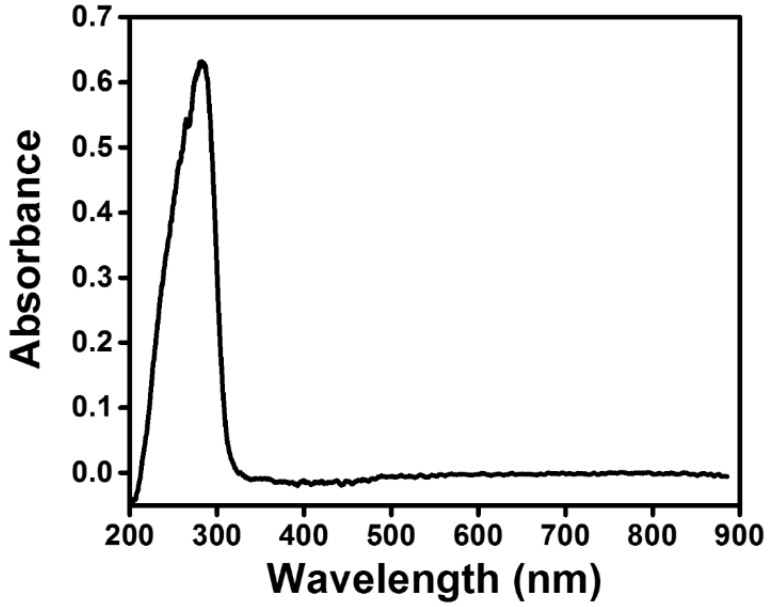

Figure. 3.6. UV-vis absorption spectrum.

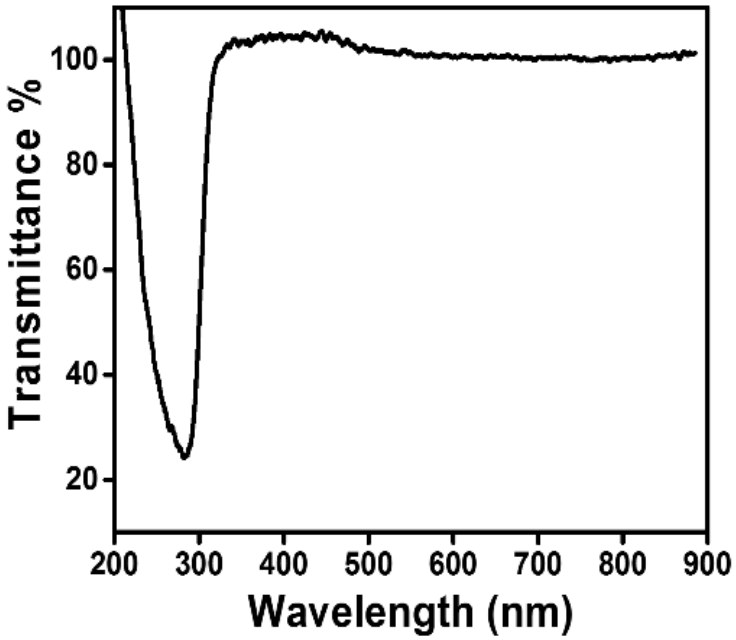

Figure. 3.7. UV-vis transmittance spectrum.

Optical absorption coefficient (α) can be calculated from the UV-transmittance spectra using Equation 2.4.

Being a direct band gap material, the absorption coefficient is related to photon energy

(hν) by the relation given in Equation 2.2.

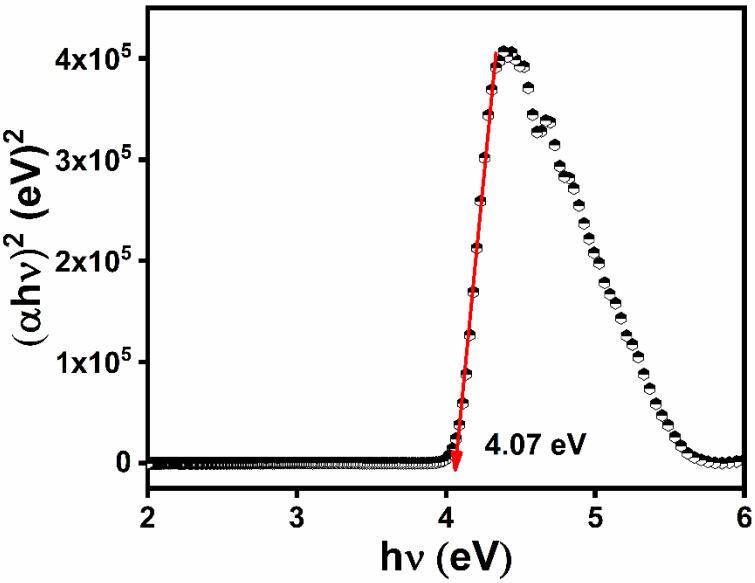

Figure. 3.8. Tauc's plot.

The variation of $(\alpha h\nu)^2$ versus photon energy (hν) is shown in Tauc's plot presented in Fig. 3.8. The intercept of linear portion of the graph on the x-axis gives the value of optical band gap which is found to be 4.07 eV. As a consequence of the wide band gap, the synthesized crystal has high transmittance in visible region.

3.2.6 FTIR analysis

The IR absorption of the $KH_3(C_4O_8).2H_2O$ single crystal was studied using FTIR analysis using ATR method, which is shown in Fig. 3.9. The peaks corresponding to 3663 cm^{-1} and 3350 cm^{-1} can be attributed to the O-H stretching and bending vibrations [Ezhil Raj et al. 2008 Mahalakshmi et al. 2012 Vimal et al. 2014]. The vibrational frequency corresponding to the 1760 cm^{-1} is due to the C=O stretching mode [Sagadevan 2016a Ramki and Ezhil Vizhi 2017]. The asymmetric stretching vibrations of C=O was present at 1286 cm^{-1} [Ezhil Raj et al. 2008 Mary C et al. 2016]. The presence of K-O stretching vibration was witnessed at around 887 cm^{-1} [Sagadevan 2016a]. The C-O-H bending mode was observed at 1495 cm^{-1} [Sagadevan 2016a].

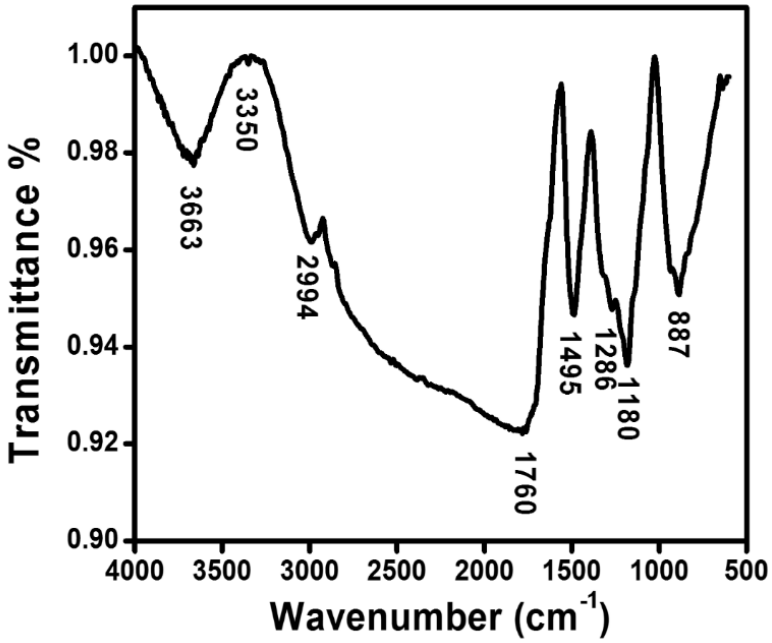

Figure. 3.9. FTIR spectrum of $KH_3(C_4O_8).2H_2O$ single crystal.

3.2.7 Photoluminescence studies

When the crystal is exposed to light of particular energy, electronic states are excited and the energy of excitation is emitted as light of different wavelength. This process is termed as photoluminescence. The photoluminescence (PL) spectrum of $KH_3(C_2O_4)_2.2H_2O$ single crystal is shown in Fig. 3.10. The recorded emission spectrum when analyzed gives information regarding intrinsic impurities, electronic transition states, defect states and roughness of the material [Anis et al. 2016 Sasi et al. 2016]. In present study, the $KH_3(C_2O_4)_2.2H_2O$ single crystal is photo-excited at a wavelength of 280 nm and the emission spectrum is recorded in the range of 300-500 nm. Three distinct emission peaks are observed at 324 nm, 366 nm and 426 nm. The sharp peak at 426 nm points out that the synthesized crystal has fluorescence emission in the violet region of visible spectrum which may be due to the processes like charge transfer and electron trapping. The other peaks present in the emission spectra may be attributed to the existence of various energy levels between ground and excited states due to the delocalization of the O-C=O bond of oxalic acid [Dalal and Kumar 2016]. The distinct nature of PL peaks clearly indicates that the synthesized crystal has good optical quality which is of great importance in optoelectronic applications.

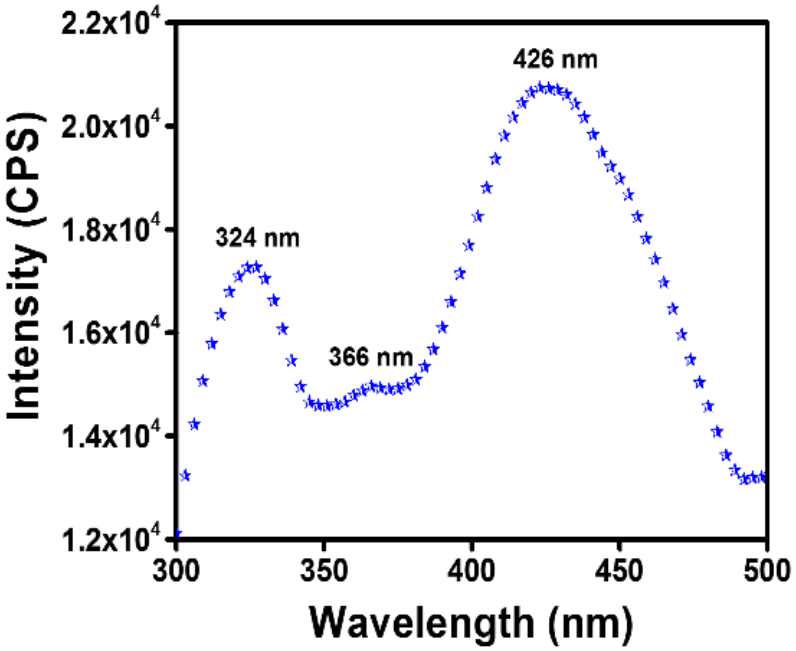

Figure. 3.10. Photoluminescence spectrum.

3.2.8 Differential Scanning Calorimetry

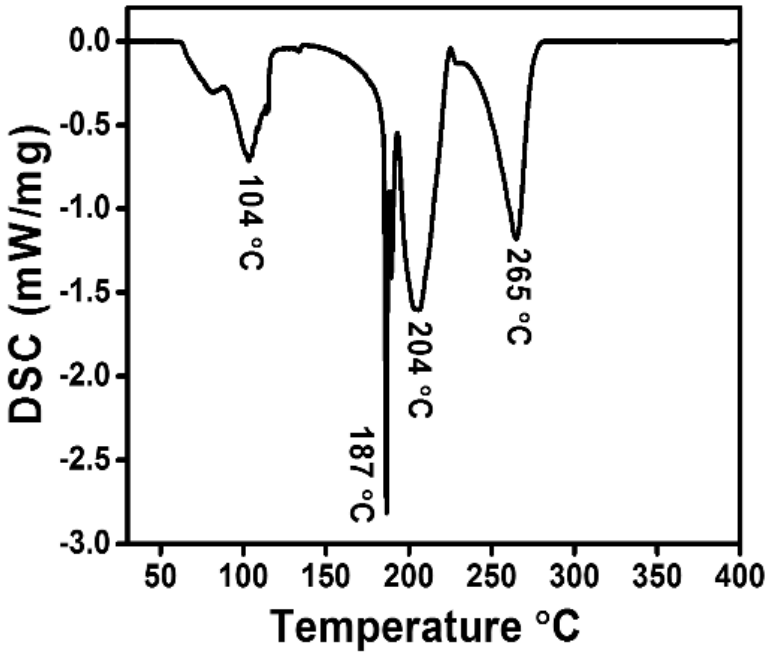

Figure. 3.11. DSC plot of $KH_3(C_2O_4)_2.2H_2O$.

The thermal stability of the crystal was studied using DSC analysis by taking 2 g of the crystal in the nitrogen atmosphere. The crystal was studied thermally in the temperature range of 32 ºC to 400 ºC in heating rate of 10º/minute shown in Fig. 3.11. The endothermic peaks are observed and the peak at 104 ºC corresponds to the loss of

water molecules. Further, sharp peak at 187 ºC and 204 ºC is attributed to the release of water molecules which are entrapped inside the crystal lattice. In addition to these, peak at the 265 ºC can be attributed to the release of CO_2 and H_2 gas molecules. The endothermic peak from the DTA at 265 ºC can be attributed to the melting point of the sample.

3.2.9 TGA-DTA analysis

The melting point, decomposition temperature, purity and crystalline nature of the materials were studied using the TGA and DTA analysis. The crystal of 2 mg was taken for the thermal analysis of $KH_3(C_4O_8).2H_2O$ single crystal in the nitrogen atmosphere. The TGA and DTA curves of the synthesized crystals were shown in the Fig. 3.12. The crystal is observed to be stable till 80º C and the temperature is increased till 116 ºC mass loss is observed and these mass losses can be due to the liberation of H_2O adsorbed [Vimal et al. 2014 Chandran et al. 2017]. The second mass loss is observed at around 165 ºC to 220 ºC can be attributed to the dehydration of water molecule from the crystal [Vimal et al. 2014]. Phase transformation happens in the region where the water molecules from the crystal is dehydrated completely [Mahalakshmi et al. 2012]. The mass loss at 240 ºC to 275 ºC can be attributed to the liberation of CO_2 and HCOOH gas molecules and the product remaining is $K_2C_2O_4$. The endothermic peak from the DTA at 266.5 ºC can be attributed to the melting point of the sample. The presence of endothermic peak at 394.4 ºC suggests that the crystal undergoes physical transformation and no mass loss is observed in this region [Higashiyama and Hasegawa 1971a Dinnebier et al. 2005]. The mass loss observed after 530 ºC and the mass loss in the range 530 ºC to 600 ºC is attributed to the liberation of CO gas and formation of K_2CO_3 [Mahalakshmi et al. 2012].

$$2(KH_3C_4O_8 \cdot 2H_2O) \rightarrow 2KH_3C_4O_8 + 4H_2O\uparrow \quad (3.1)$$

$$2KH_3(C_2O_4)_2 \rightarrow 2KHC_2O_4 + 2CO_2\uparrow + 2HCOOH \quad (3.2)$$

$$2KHC_2O_4 \rightarrow K_2C_2O_4 + CO_2\uparrow + HCOOH \quad (3.3)$$

$$K_2C_2O_4 \rightarrow K_2CO_3 + CO\uparrow \quad (3.4)$$

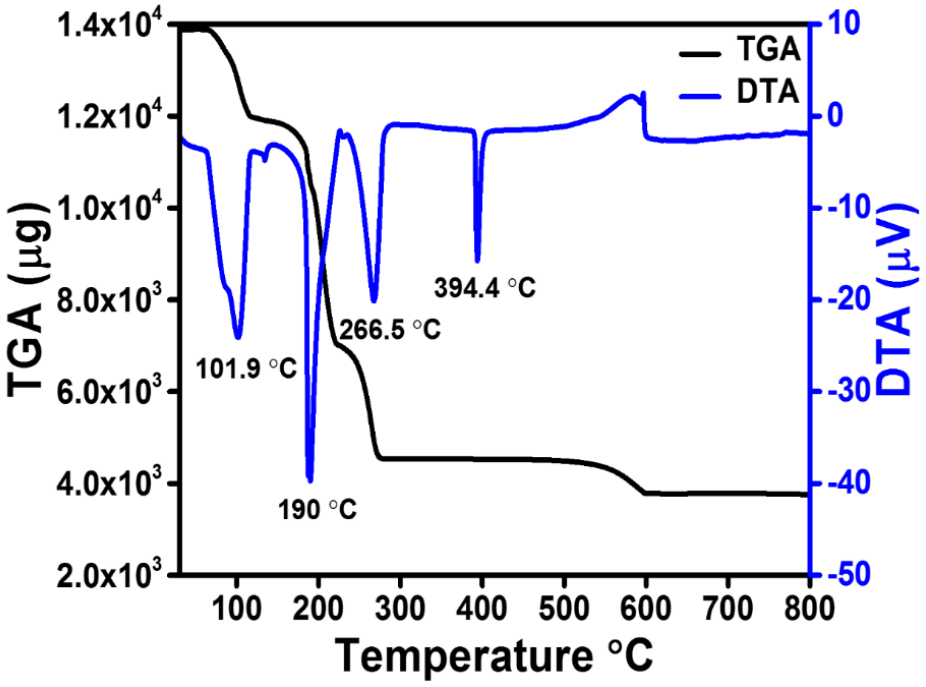

Figure. 3.12. TGA-DTA plots of $KH_3(C_4O_8).2H_2O$ single crystal.

3.2.10 Hardness studies

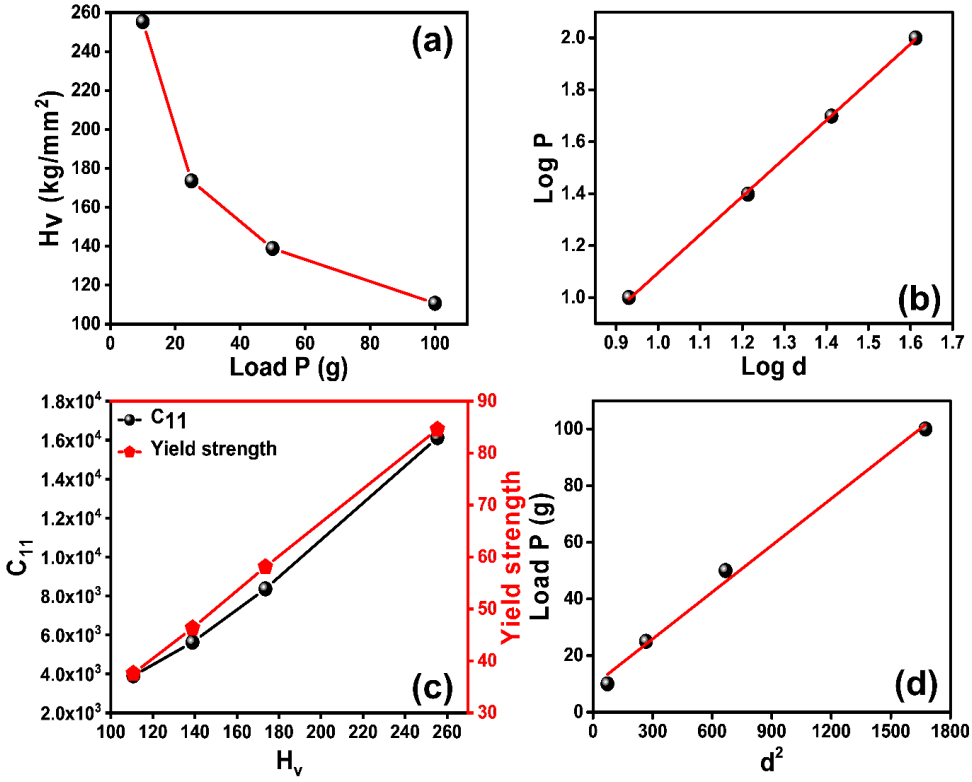

Figure. 3.13. The variation of (a) applied load (P) Vs Hardenss number (H_v) (b) Log d Vs Log P (c) Stiffness constant (C_{11}) and Yield strencgth Vs H_v (d) Load P Vs d^2.

The mechanical hardness of a crystal is related to the structure and composition of the crystalline materials. Vickers microhardness measurement technique is employed to characterize the hardness of the KHOOD single crystal. Hardness measurements were carried out on well-polished (0 0 1) plane of KHOOD single crystals, which is free from any visible inclusions or cracks.

However, it was interesting to note that the hardness value (H_v) decreased as the applied load increased (ISE) [Goel et al. 2013]. Similar results showing deterioration in hardness number as a result of applied load is reported elsewhere [Cyrac Peter et al. 2010 Sujatha et al. 2010 Adhikari and Kar 2013 Baskaran et al. 2017 Ramki and Ezhil Vizhi 2018].

The Vickers H_v microhardness value is computed using the Equation 2.13 [Gao et al. 2003 Tyagi et al. 2015]

The estimated values of Vickers microhardness numbers for the KHOOD single crystal is plotted and shown in Fig. 3.13(a). The indentation was made on the top surface of the KHOOD crystal by applying 10, 25, 50 and 100 g loads respectively with a 15 sec indentation time.

In KHOOD single crystal, it was noted that the microhardness number decreased as the applied load increased (10-100 g).

The elastic stiffness (C_{11}) of the material gives information about the molecular bond strength in crystals. The C_{11} can be calculated using the Wooster's relation (Equation. 2.14) [Ray et al. 2017b] and C_{11} with respect to hardness number is plotted and shown in Fig. 3.13(c). The C_{11} values are tabulated in Table 3.5.

The indentation size and the applied loads are related, which is given by Meyer's law [Sangwal 2000]

The n value can be calculated by taking the slope from log P versus log d graph. The obtained n value is 1.47 and the crystal belongs to hard material category.

The material with $n < 2$, it exhibits a normal indentation size effect (ISE) behaviour and for $n > 2$ the material behaves reverse indentation size effect (RISE) [Sangwal 2000 Hanumantharao et al. 2013]. The obtained n value is less than 2 thus, KHOOD crystal belongs to hard material category which is experimentally confirmed.

Yield strength (σ_y) of the crystal is explored using the Eqn. 2.16. The hardness of the material mainly depends on chemical bonding between the molecules which is

responsible for its distinct hardness. From the result, we concluded that the hardness of the material got increased as the strength of the chemical bonding consequently increased.

Table. 3.5. Hardness number, Elastic stiffness (C11) and yield strength for different applied loads for KHOOD single crystal.

Load (P) (g)	Hardness (H_v)	C_{11} (Pa)	Yield Strength (Kg/mm^2)
10	253.7	16127.27	84.57
25	174.34	8364.59	58.11
50	139.02	5628.40	46.34
100	112.82	3905.49	37.61

3.2.11 I-V studies

Fig. 3.14. shows I-V plots of $KH_3(C_2O_4)_2.2H_2O$ single crystal in the illuminated and in the dark condition. A linear increment of dark current as well as photocurrent as a function of applied field was observed in the experiments. Dark current was observed to be greater than the photocurrent at each applied field. This phenomenon is known as negative photoconductivity which may be due to the fall in the number of charge carriers or decrease in their lifetime on illumination [Ashraf et al. 2004a]. When light is illuminated on the sample, recombination of electrons and holes takes place, reducing the number of mobile charge carriers leading to negative photoconductivity. This leads to the decrease in lifetime of the charge carriers. According to the Stockmann model, two energy levels are present in the forbidden gap of the material, one of these levels is positioned between the conduction band and the Fermi level, whereas the other level is present near to the valence band. The capture cross-sections for electrons and holes in the second level is high. The capturing of electrons and holes from the conduction and the valence band respectively reduces the number of charge carriers in the conduction band consequently decreasing the current in the presence of illumination. Thus, the crystal is said to exhibit a negative photo-conducting effect. Calculated resistivity values herein, 1.78×10^4 ($\Omega\cdot m$) in the dark and 4.27×10^4 ($\Omega\cdot m$) when illuminated with light serves as an additional experimental evidence. Aforementioned observation may lead us to use this material for photo-resistive applications.

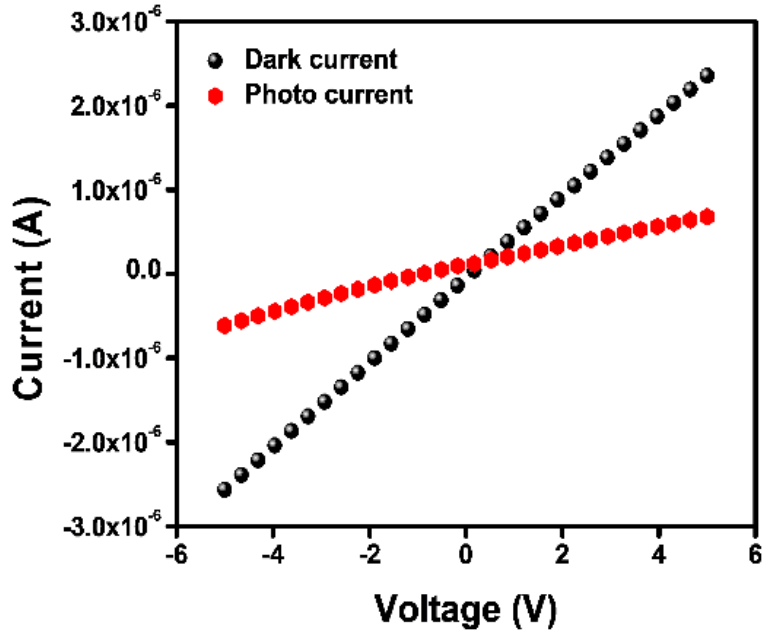

Figure. 3.14. Photoconductivity measurement.

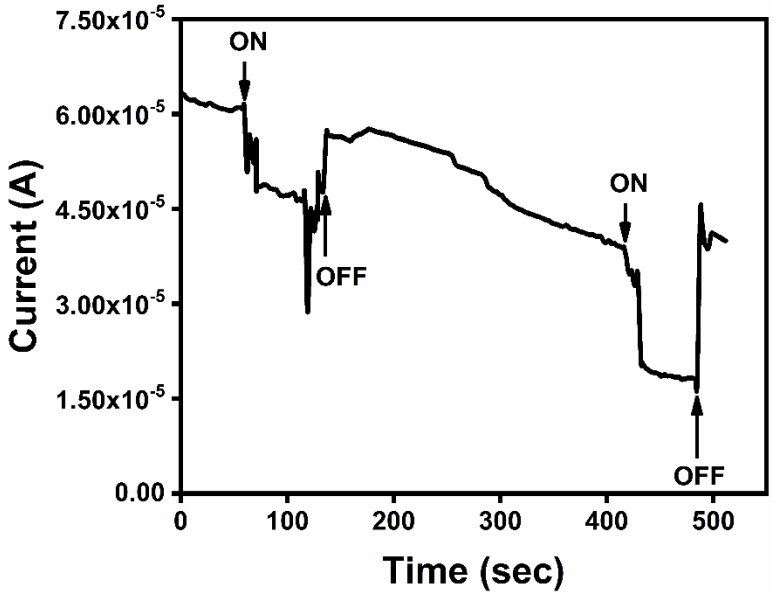

Figure. 3.15. Time dependent photocurrent response of $KH_3(C_2O_4)_2.2H_2O$ single crystal.

The crystal was subjected to time dependent photo response with the light source switched on for 1 min duration and then switched off for a time interval of 4 minutes alternately. The crystal shows negative photoconductivity and increased resistivity with the light source switched on and the resistivity decreases in the absence of illumination.

3.2.12 Electrical resistivity studies

I-V studies were carried out to explore the electrical conductivity and resistivity of the KHOOD single crystal. The synthesized crystals were polished using Emery Polishing paper III Grade 3/0 to ensure flat surface on both the sides to get uniform thickness. The crystals were characterized by varying the voltage and measuring current using 2 probe method. The current is measured in the range of -3 V to +3 V and the resistance is calculated by inversing slope of the curve. The IV curve of the crystals for different temperatures are shown in the Fig. 3.18. The following studies are repeated for different temperatures till 85 ºC. The resistivity of the KHOOD crystals for different temperatures was calculated using the relation given in Equation. 2.19. and the conductivity was calculated by inversing the resistivity.

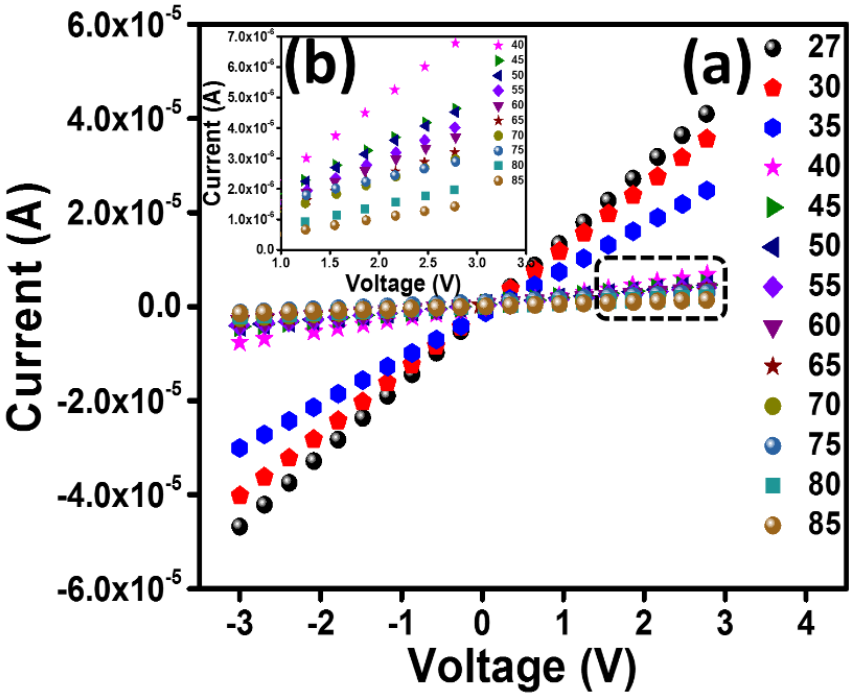

Figure. 3.16. The I-V plot of KHOOD single crystal for different temperatures.

The crystal resistivity is found to be in the range of $10^4\Omega$m whereas the conductivity is in the range of S/m. The resistivity and conductivity values for the KHOOD crystal with respect to different temperatures are tabulated and shown in Table 3.6. The resistivity value increases as a function of temperature. Conductivity follows the decreasing trend as the temperature increased.

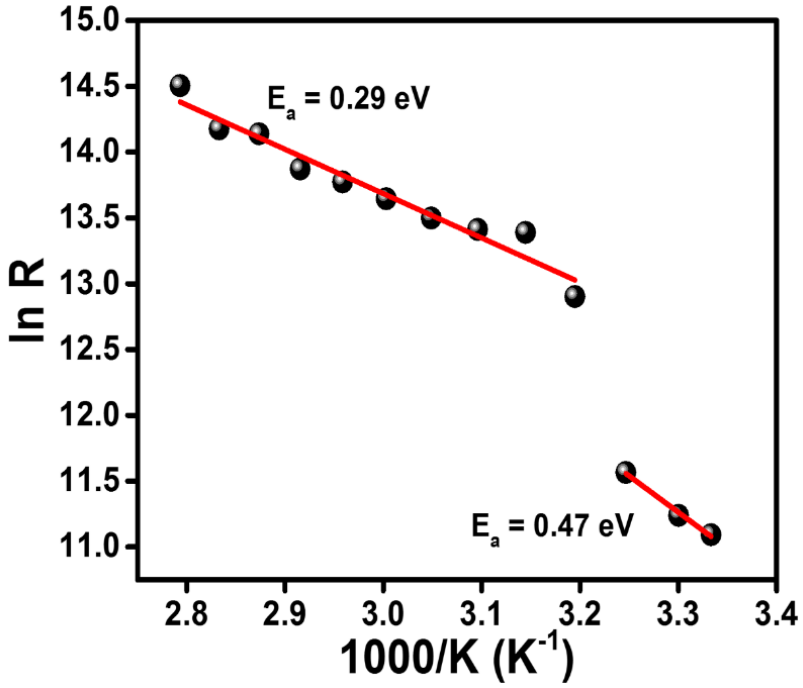

Figure. 3.17. Activation energy of the KHOOD single crystal.

Table. 3.6. Resistivity and conductivity of the KHOOD crystals for different temperatures.

Temperature (°C)	**Resistivity (×10⁴ Ωm)**	**Conductivity (S/m)**
27	1.82	5.49×10^{-5}
30	2.024	4.94×10^{-5}
35	2.6	3.84×10^{-5}
40	6.151	1.62×10^{-5}
45	13.35	7.48×10^{-6}
50	13.64	7.33×10^{-6}
55	14.82	6.74×10^{-6}
60	17.09	5.84×10^{-6}
65	19.33	5.17×10^{-6}
70	21.28	4.69×10^{-6}

75	27.66	3.61×10^{-6}
80	28.74	3.47×10^{-6}
85	39.65	2.52×10^{-6}

The activation energy plots show two linear regions with increase in resistance with increase in temperature. Activation energy (E_a) was calculated from the slope of linear parts of the plots. It is noticed that activation energy increases from 0.476 eV and 0.290 eV.

3.2.13 Dielectric studies

Dielectric properties of a material reveal significant information regarding the storage and dissipation of electric and magnetic fields in the material and also provides insight into feasibility of implementing the material in potential applications. Dielectric studies of the synthesized crystals were carried out at frequency range of 4 Hz to 1 MHz at room temperature. The variation of dielectric constant of $KH_3(C_4O_8).2H_2O$ single crystal with respect to log frequency is plotted and shown in the Fig. 3.20. The dielectric constant of a material is a complex quantity in which, the real part represents the polarization energy stored in the material. The ε_r magnitude mainly depends on charge displacement due to the degree of polarization in the crystals. The material experiences dielectric constant due to the contribution of space charge, orientational, electronic and ionic polarizations which depends on the applied frequency [De and Rao 1988].

The real part of dielectric constant (ε') is a measure of amount of energy from external field stored in the material and ε' is calculated from the parallel capacitance value (C_p) as (Equation 2.26)

From the Fig. 3.20. it can be observed that real part of dielectric constant has high dielectric values at low frequencies and it decreases as the frequency increases. This characteristic behavior of dielectric constant can be attributed to the dielectric relaxation [Anand et al. 2017 Chand et al. 2017a]. The lower dielectric constant at higher frequencies is due to low polarization activity in the higher frequency region [Devmunde et al. 2016 Lahlali et al. 2017]. An applied electric field at low frequencies influences the buildup of localized charge leading to accumulation of the space charge polarization which causes high dielectric constant. As the applied frequency increases,

charge accumulation at the grain boundary reduces, which reduces the polarization, resulting in the reduction of dielectric constant. The lower dielectric constant is a vibrant parameter for designing electro-optic modulators, microelectronics, terahertz wave generators, field detectors, and photonic devices [Ma et al. 2018]. The relatively lower dielectric loss confirms the presence of a minimum defect density and the enhanced optical quality of the $KH_3(C_4O_8).2H_2O$ single crystal [Ma et al. 2018].

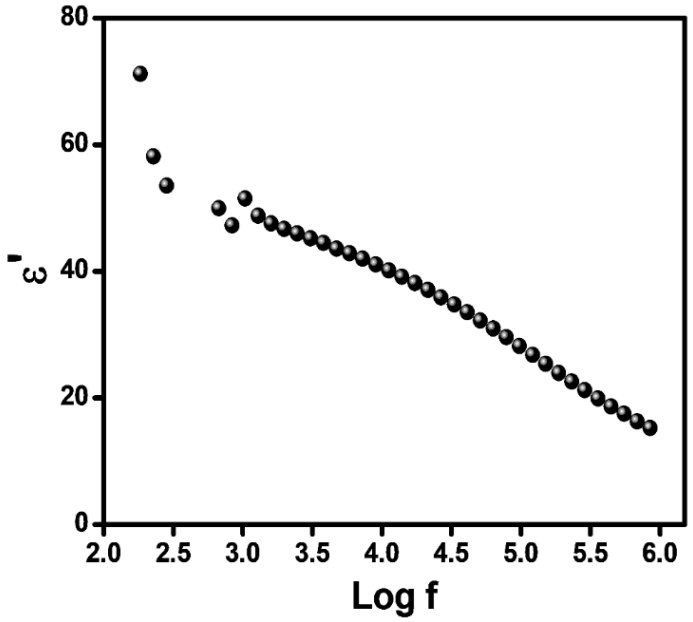

Figure. 3.18. Real part of dielectric constant versus log frequency.

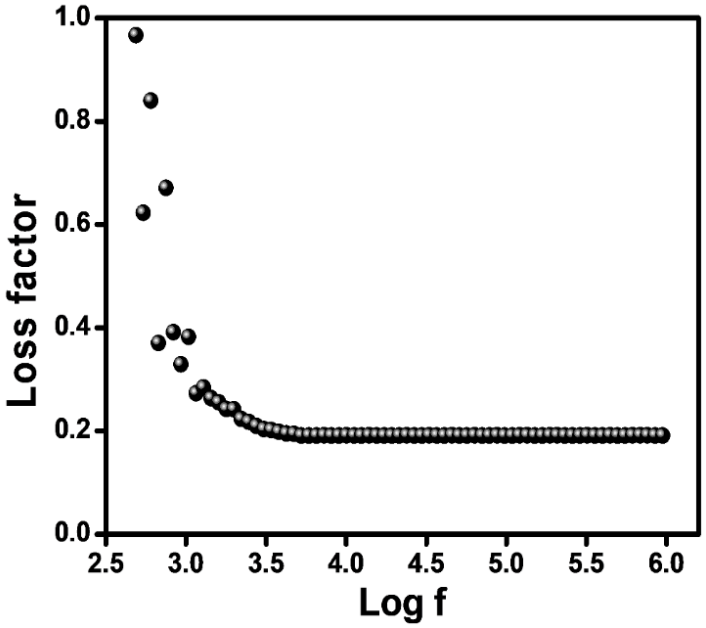

Figure. 3.19. Loss factor versus log frequency.

The dielectric loss factor or loss tangent ($\tan\delta$) of the synthesized $KH_3(C_4O_8).2H_2O$ single crystal was calculated using the Equation. 2.28.

The variation of loss factor with respect to applied frequencies is shown in Fig. 3.21. It was noticed that the loss factor decreases rapidly and becomes almost constant at higher frequencies because the polarized material cannot keep up for higher frequencies. The dielectric loss tangent arises when the polarization lags behind the applied altering field and is a result of the presence of structural inhomogeneities and impurities and crystal lattice imperfections [Singh et al. 2014]. The low value of loss tangent at high frequencies suggest the suitability of $KH_3(C_4O_8).2H_2O$ single crystal in high frequency device applications [Aravind et al. 2015].

The electrical conduction at alternating frequencies was primarily a defect-controlled process at room temperature region. From Fig. 3.22, it was noted that the electrical conductivity of $KH_3(C_4O_8).2H_2O$ single crystal is minimum at lower frequency regions. The lower conductivity in the lower applied frequency region is due to the trapping mechanism. As the frequency increased, the space charge mechanism reduces which leads to the decrease in the trapping of electrons leading to increase in conductivity at higher frequency regions.

It is observed that the electrical conductivity of $KH_3(C_4O_8).2H_2O$ single crystal is low at lower frequencies due to trapping of some carriers at defect sites. The increase in conductivity at higher frequencies can be attributed to the reduction mechanism in the space charge polarization.

The ac conductivity of $KH_3(C_4O_8).2H_2O$ single crystal was calculated using the Equation 2.29.

The ac conductivity with respect to the applied frequencies are shown in Fig. 3.22. The ac conduction of the material reveals information regarding the nature of conduction mechanism and the type of polarons accountable for the conduction process [Hamdi et al. 2018]. The increase in ac conductivity values with increase in applied frequencies may be due to the pumping force of the applied field. The ac field helps to increase the movements of charge carriers from the various trapping centers. For higher frequencies the electron hopping improves between charge carriers which leads to increased conductivity of the crystal.

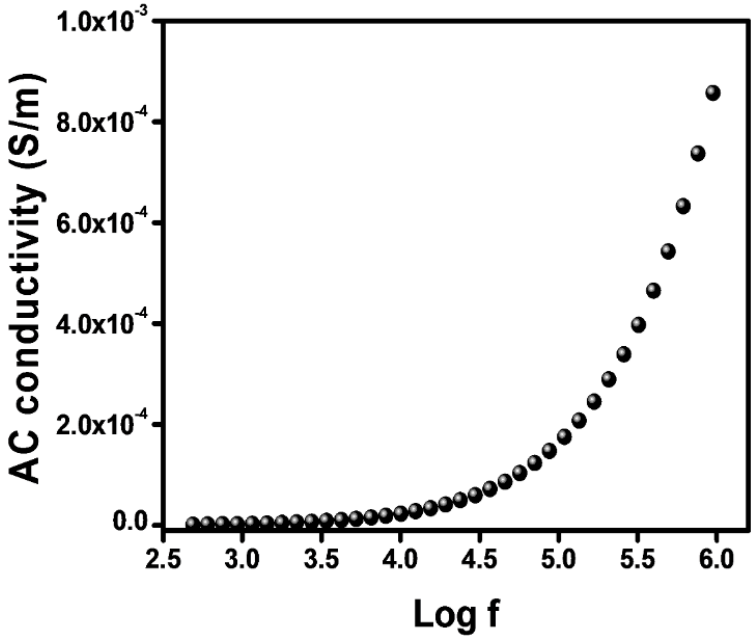

Figure. 3.20. Ac conductivity versus log frequency.

The higher frequencies the ac conductivity increases linearly suggesting that the conduction takes place by hopping of charge carriers in between the localized states which confirms the small polaron type of conduction mechanism in $KH_3(C_4O_8).2H_2O$ single crystal [Singh et al. 2014]. The small decrease in conductivity value for lower frequency region suggests the conduction mechanism by mixed (small and large) polarons [Devan et al. 2006 Khader et al. 2015].

Complex impedance spectra of polycrystalline solids can be interpreted using the equivalent circuit model (resistance and capacitance). In general, when represented in the diagram of the negative of the imaginary part (Z'') versus the real part (Z'), the impedance data of materials depends on the resistive and capacitive components leading to a succession of semicircles [Macdonald 1992]. As observed in Fig. 3.23, where the spectra represent typical semicircles, whose center lies below the abscise axe by an angle $(\pi\alpha)/2$, suggesting the departure from ideal Debye behavior [Chouaib et al. 2015, 2016 Helen and Kanchana 2015].

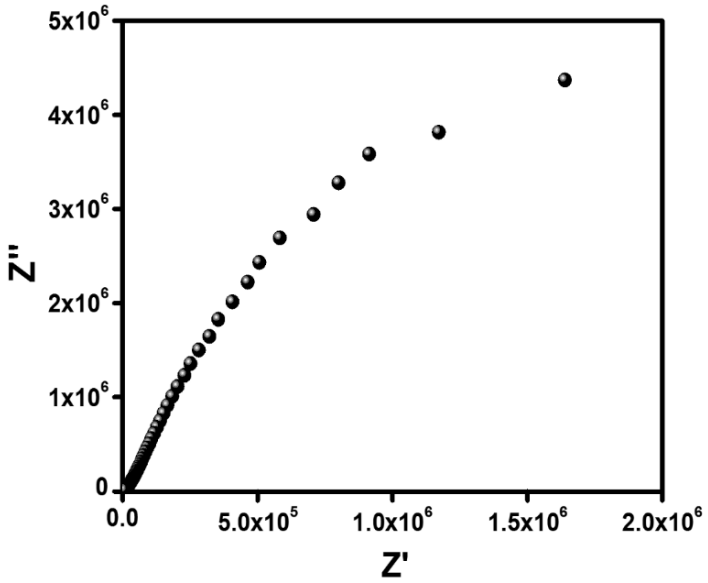

Figure. 3.21. Cole-cole plot of the synthesized $KH_3(C_4O_8).2H_2O$ single crystal.

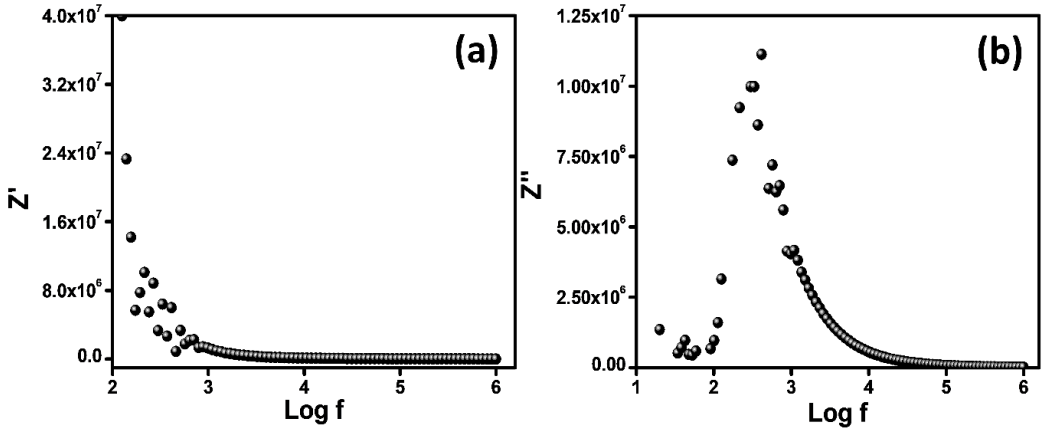

Figure. 3.22. (a) Variation of Z' and **(b)** Z'' with respect to log frequency.

The frequency dependence impedance consisting of the real (Z') and imaginary (Z') parts as shown in Fig. 3.24(a) and Fig. 3.24(b), respectively.

It is noticed that the extent of decrease in values of Z' with respect to applied frequency, indicating a decrease in the resistivity of the material. However, a maxima is obtained in the imaginary part of the impedance and the presence of such peak (maxima) is due to the dielectric relaxation process [Haque et al. 2017 Bindu et al. 2018b].

3.3 Conclusions

Hybrid class metal organic $KH_3(C_4O_8).2H_2O$ single crystals were synthesized successfully via solvent evaporation technique. The solved crystal structure belongs to

centrocymmetric triclinic crystal system with P-1 space group. The unit cell parameters were determined using powder XRD technique which shows good agreement with data obtained from single crystal XRD. EDAX analysis confirmed the presence of potassium, carbon and oxygen in the synthesized crystal. The optical absorption and emission properties were investigated and results presented that the crystal absorbs in the UV region (280 nm) and emits in blue region (427 nm). The functional vibrations were also studied using FTIR analysis and the vibrational modes present in the crystal were identified. It is worth noting that the crystal sustains till 266 ºC and for the farther temperatures it decomposes. The Vickers microhardness study reveals that the hardness number decreases as the applied load increases which explains the indentation side effect (ISE) behaviour of the crystal. From Meyer's law the value of 'n' is evaluated to be 1.47 and it belongs to hard material category. The elastic stiffness of the crystal was studied using Wooster's relation which gives information about the bonding and tightness of the neighbouring ions. The electrical resistivity measurements show increasing trend as the temperature increased. The activation energy of the crystal is also estimated and the crystal shows activation energy of 0.476 eV and 0.290 eV. I-V studies have shown the increase in the resistivity of the crystal on illumination suggesting their use as photoresistors. Time dependent I-V studies have shown negative photoconductivity of the crystal with the resistance being increased on illumination and decreasing under dark condition. Frequency dependent dielectric studies suggested the decrease in dielectric constant with respect to frequency. In addition, the low values of dielectric parameter and dielectric loss suggest its potential application in optoelectronic device fabrications. From the dielectric measurements it is noticed that space charge phenomenon acts on the crystal as the frequency is varied. Single semicircle from the cole-cole plot justifies the dielectric behavior obtained due to grain boundaries.

CHAPTER 4

Effect of $Co(OH)_2$ nanoparticle on the semiorganic potassium hydrogen oxalate oxalic acid dihydrate single crystal

Overview

In this chapter, the effect of $Co(OH)_2$ nanoparticles on the structural, optical and electrical properties of the KHOOD single crystals is discussed.

4.1 Introduction

The development of novel materials of technicalogical importance has been the topic of considerable interest in the field of materials sciences. The advance research in the field of crystallography has modernized the optoelectronic industries. Crystal growth and analysis of novel materials have been strongly encouraged due to their possible use in the field of optical communication and laser technology [Prabukanthan et al. 2018]. Development of optoelectronic devices at low costs that are more efficient than the existing ones has been one of the important goals in the field of photonics [Mangaiyarkarasi et al. 2018]. The researchers from all over the world have shown interest to develop materials which have a wide range of applications in lasers, light emitting diodes and in the field of telecommunication, optical signal processing and optical modulation [Shahil Kirupavathy et al. 2008 Saritha 2013 Santhi and Alagar 2016]. Materials with low absorption coefficient, good optical quality, high laser damage threshold, high thermal stability and ability to take high polish are of great interest due to their immense applications in day-to-day technological requirements [Ramajothi and Dhanuskodi 2007 Mahendra et al. 2019]. Designing devices that use photons instead of electrons in acquiring, storing, processing and transmitting data has become an active field of research these days [Martin Britto Dhas et al. 2008].

Organic and inorganic materials have been developed and extensively studied either from the research point of view or for the purpose of industrial growth. The choice of the material depends on technological applications. Organic materials due to their high electro-optic coefficients and greater ease of synthesis were investigated for their use in technology [Panchapakesan et al. 2018]. However, most of the organic materials have poor thermal and mechanical stabilities and are easily prone to damage during device fabrication. The weak van der Waal's bonding in organic compounds creates difficulty in growing large sized organic crystals [Rajasekaran et al. 2001 Senthil

Pandian and Ramasamy 2010 Thaila and Kumararaman 2012]. Furthermore, cutting and polishing of these materials is difficult which hampers their use in practical device applications [Sankar et al. 2007]. In contrast to organic materials, inorganic materials possess better thermal properties and higher mechanical stability [Albert Irudayaraj et al. 2014]. An effort of combining advantages of both organic and inorganic materials have led to the development of a new class of organic-inorganic hybrid compounds termed as metalorganics which have revolutionized optoelectronic industries [Anbuselvi et al. 2014]. These materials with higher optical transparency and greater thermal and mechanical stabilities have been studied extensively and topics of research interest these days [Krishnakumar et al. 2010]. Thus, an alternate approach to overcome inherent limitations of both organic as well as inorganic materials has been successful and is gaining more importance due to their attractive properties that have allowed their innovative industrial application [Karuppasamy et al. 2018]. One of such hybrid materials is potassium hydrogen oxalate oxalic acid dihydrate whose excellent transmittance in the visible region and the optical and electrical properties suggest its candidature in optoelectronic applications. Electrical studies of this material has revealed its photo-resistive behavior and its candidature in technological applications [Mahendra et al. 2018]. Very few reports are available in the literature on KHOOD materials and thus leaving great scope to investigate their properties by addition of dopants.

Impurities generally get incorporated into crystallization processes. These impurities may be either undesirable when present unintentionally or may be purposefully added to investigate their effect on host crystal lattice [Hottenhuis and Lucasius 1988 Kuznetsov et al. 1998]. In recent years, the crystals with additives have been studied extensively owing to their modified functional properties in comparison with pure crystals. Growth of crystals in the presence of impurities in the form of dopants or additives has been ever more interesting on account of the fact that the addition of impurities affects both habit modification and crystal properties [Hottenhuis and Lucasius 1986, 1989 Hottenhuis and Oudenampsen 1988 S. and E.k. 2018 Mahendra et al. 2019]. Dye doping in some of the crystals has been found to vary their optical, thermal, electrical and mechanical properties [Enculescu 2010 Kushwaha et al. 2010 Sinha et al. 2012, 2015 Raja et al. 2014 Bamini et al. 2015 Nandhakumar and

Radhakrishnan 2016 Raguram et al. 2016 Rao et al. 2017 Ray et al. 2017]. The inclusion of nanoparticles have also reported to alter the properties of the host crystal [Balasubramanian et al. 2008 Grachev et al. 2012 V Mary Sheeja 2013 Kosinova et al. 2014]. The doped crystals with better optical transmittance, electrical properties, higher thermal and mechanical stabilities are promising candidates for optoelectronic applications.

Recently, doping single crystals with metallic nanoparticles have gained attention to tune their various physical, optical and electrical properties. However, successful doping and doping control is difficult due to the various complications associated with metallic nanoparticles such as agglomeration, charge centers etc. In this case, the synthesized $Co(OH)_2$ nanoparticles are free from agglomeration, which comfort the pathway for doping. In addition, the sparingly solubility of $Co(OH)_2$ is one more advantage, which ease the compound formation while doping [Vidotti et al. 2006 Wu et al. 2018].

So far very less work has been reported on nanoparticle doping on Potassium hydrogen oxalate oxalic acid dihydrate (KHOOD) single crystals. In the present work, the synthesis of potassium hydrogen oxalate oxalic acid dihydrate single crystals doped with cobalt hydroxide ($Co(OH)_2$) nanoparticles of size 15 nm is given. The details of characterization of these crystals using powder XRD analysis, UV-visible spectroscopy, photoluminescence studies, EDAX mapping, FTIR analysis, thermo gravimetric analysis, I-V and dielectric studies are also presented. The studies carried out on pure and doped crystals were intended to determine the influence of nanoparticle doping on the properties of pure KHOOD crystal.

4.2 Results and discussions

4.2.1 Powder XRD analysis

The synthesized crystals were fine powdered and studied using X-ray diffraction technique. The indexed XRD patterns for pure and $Co(OH)_2$ doped crystals are shown in Figure. 4.1. The sharp peaks in the diffraction pattern confirms the crystalline nature of the synthesized materials. The unchanged peak positions suggest that the crystal system is unaffected by doping. The slight variation in intensity and shift in the XRD pattern indicates the incorporation of nanoparticles into the host lattice. In the system of KHOOD the ionic radius of K^+ is 1.38 Å and Co^{2+} is 0.70 Å since the

possibility of replacing the K^+ is higher. The K^+ is replaced by the Co^{2+} could be the reason behind the peak shift obtained.

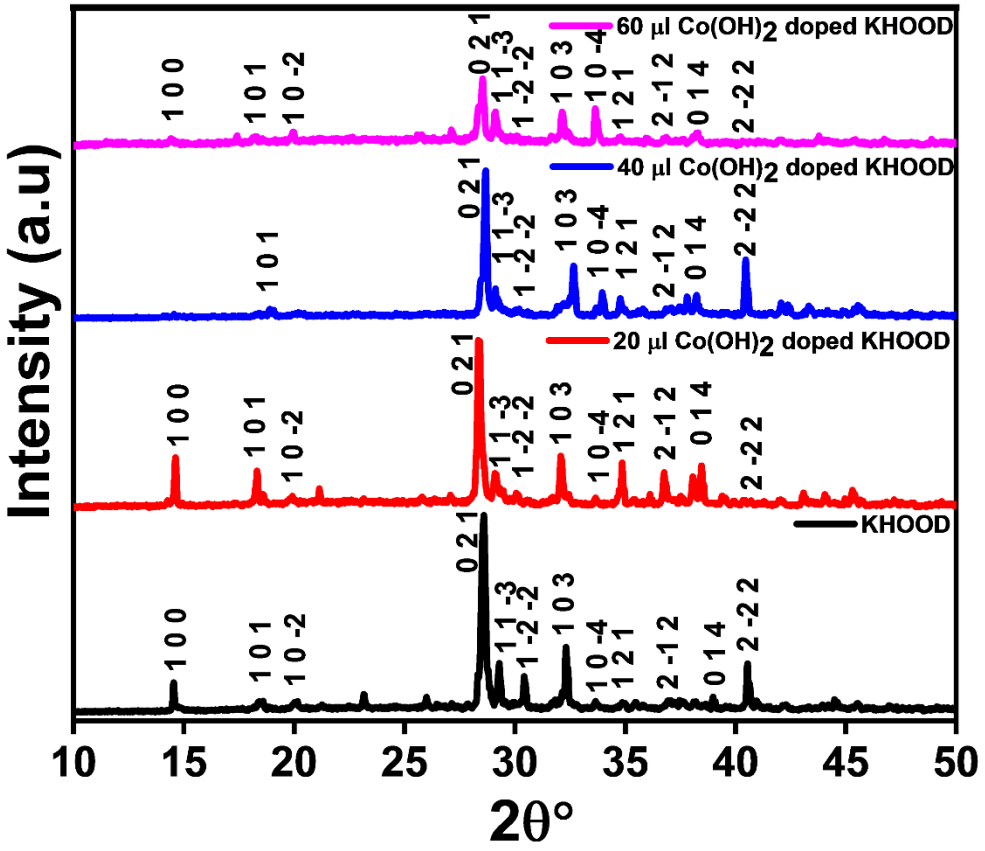

Figure. 4.1. Powder XRD pattern of the pure and $Co(OH)_2$ doped KHOOD single crystals.

4.2.2 EDAX mapping

The elemental distribution in the crystals are analyzed by EDAX mapping and the mapping spectrum is shown in the Figure. 4.2. The presence of individual elements were mapped and the elemental distributions were observed confirming all the elements of the KHOOD crystal. In addition, nanoparticle incorporation in the KHOOD crystal after doping was confirmed by the presence of Co particles in the crystal. The $Co(OH)_2$ nanoparticles are distributed randomly in the crystal leading to the change in properties of the crystal by inducing stress due to interstitial substitutions. The elemental composition of the pure and $Co(OH)_2$ doped crystals are provided as Table. 4.1.

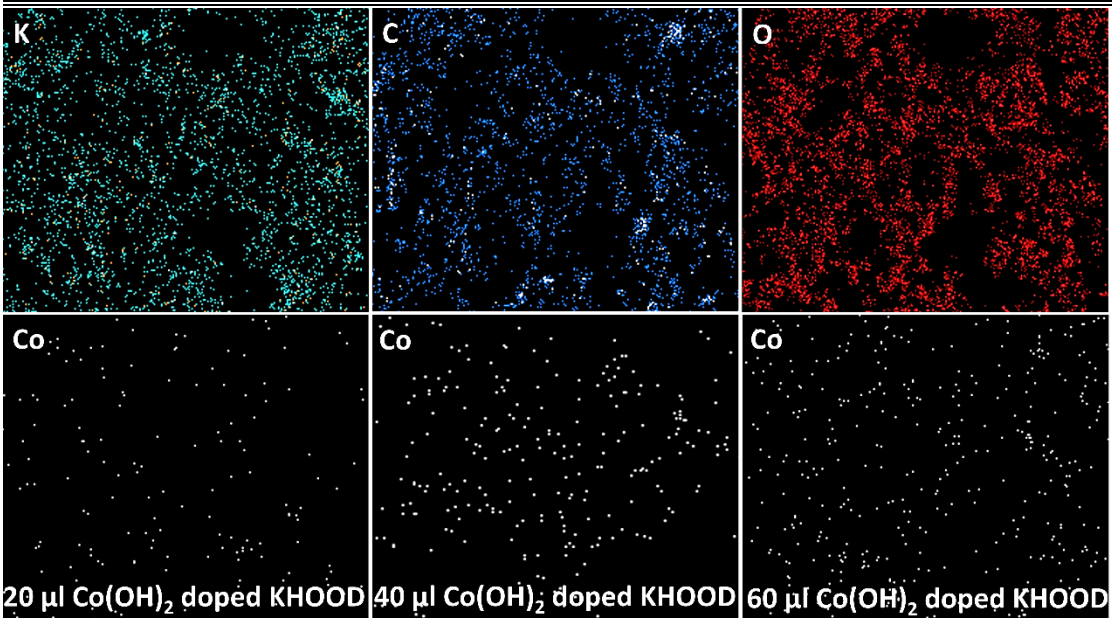

Figure. 4.2. Mapping of elements in the and $Co(OH)_2$ doped KHOOD single crystals.

Table. 4.1. Elemental compositional of pure and $Co(OH)_2$ doped KHOOD single crystals.

Element	Atomic %			
	KHOOD	**20 µl $Co(OH)_2$ doped KHOOD**	**40 µl $Co(OH)_2$ doped KHOOD**	**60 µl $Co(OH)_2$ doped KHOOD**
O	60.56	60.64	60.71	61.09
K	9.17	9.03	9.02	8.36
C	30.27	30.16	29.98	30.17
Co	--	0.17	0.29	0.38

4.2.3 Optical studies

Electromagnetic radiation affects all the particles making up the crystal – the lattice atoms, the electrons and holes in the valence and conduction bands, and the impurity atoms. The optical properties of any crystal is governed by the interaction of electric and magnetic field of the electromagnetic radiation with the crystal [Perkowitz 1993]. Absorbance and transmittance data, optical constants like absorption coefficient, extinction coefficient, reflectance, refractive index, band gap and optical conductivity

are necessary factors those decide the suitability of the crystal in optoelectronic applications.

When a crystal is exposed to electromagnetic radiation, a part of light is absorbed, a part is transmitted and the rest is reflected at the surface of the crystal [Job et al. 2016]. UV-visible spectrum of pure and doped crystals gives absorbance and transmittance data. The optical absorption and transmittance spectra of pure and doped crystals were recorded in the wavelength range of 200 nm to 800 nm as shown in Figure. 4.3(a) and 3 (b). The pure crystals have UV cut-off wavelength of 300 nm, while a shift is observed towards higher wavelengths for $Co(OH)_2$ NPs doped crystals. Few works have been reported which show the shift in absorption peak on doping [Hasmuddin et al. 2014 Rajyalakshmi et al. 2016]. The shift in absorption peaks implies that the electronic structure of the material has been modified by the nanoparticle dopant. Both pure as well as $Co(OH)_2$ doped crystals show excellent transmittance in the entire visible region of electromagnetic spectrum which is an essential criteria for any material to be used in optoelectronic industries [Uma and Rajendran 2016].

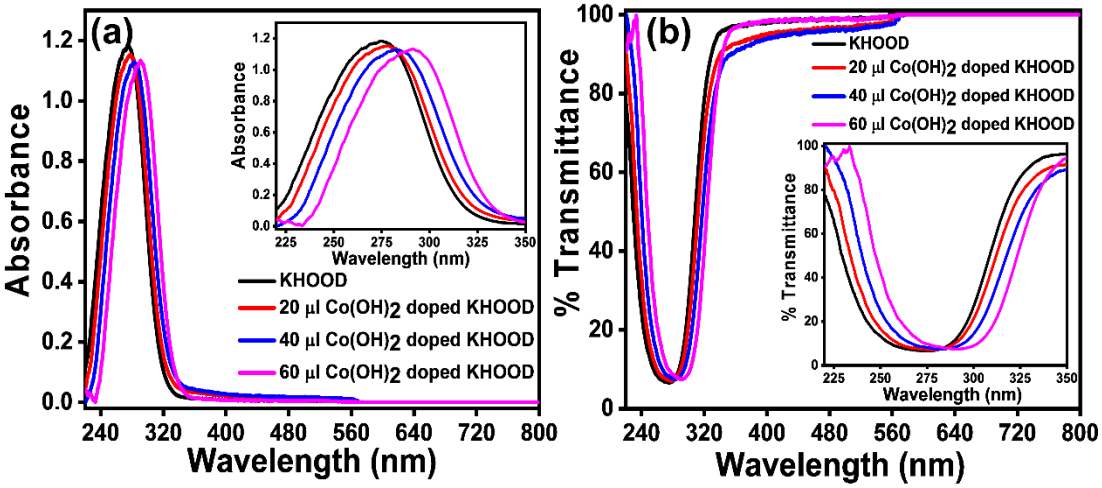

Figure. 4.3. (a) Absorbance (b) Transmittance spectrum of pure and $Co(OH)_2$ doped KHOOD single crystal.

4.2.3 (a) Determination of optical constants

Optical absorption coefficient (α) is a measure of decrease in the energy of incident radiation per unit distance as the electromagnetic wave propagates through the crystal [Mahendra et al. 2017]. It is calculated from the absorption spectrum using the Eqn. 1.

The variation of optical absorption coefficient with the incident wavelength for pure

and doped crystals is shown in Figure. 4.5(a). A steep rise appearing in UV region is a consequence of absorption of radiation by the molecules over a range of wavelengths [Jerusha et al. 2016].

Extinction coefficient (K) can be derived from the absorption coefficient using the relation given in Equation. 2.4.

It indicates the loss of electromagnetic radiation by means of absorption and scattering during its propagation through the crystal [Bincy and Gopalakrishnan 2014]. Figure. 4.5(c) (Supplementary content) shows the variation of extinction coefficient with wavelength.

Reflectance (R) is defined as the ratio of the reflected intensity to the incident intensity and is the measure of ability of sample to reflect light from its surface [Kittel 2012]. Reflectance in terms of absorption coefficient is calculated from the Equation. 2.5.

Reflectance spectrum for pure and doped crystals is as shown in Figure. 4.5(b). Both pure and doped crystals show very low reflectance in visible region signifying their use in antireflection coatings [Shaikh et al. 2013].

Refractive index (n) of a material determines how the light propagates through it. It is calculated from the relation given in Eqnuation. 2.6. The profile of variation of refractive index with wavelength is depicted in Figure. 4.5(d).

The energy dependence of optical absorption coefficient (α) is as per Tauc's relation given in Equation. 2.3.

Band gap of doped crystals shows decreasing trend with increase in dopant concentration. Pure crystal has a band gap value of 4.39 eV which further decreases to 4.33 eV, 4.24 eV and 4.16 eV for 20 µl, 40 µl and 60 µl nanoparticle doped crystals. The decrease in bandgap or red shift of absorption peak obtained as the increase in dopant concentration is due to the formation of donor levels caused by doped impurities in the crystal [Chen et al. 2012 Shenoy et al. 2018]. The wide band gap of the crystals is an evidence for their transmittance nature in visible region. This is because only photons having energy greater than band gap energy will be absorbed by the crystal [Dhanjayan et al. 2017]. By tailoring absorption coefficient and by tuning band gap, the material can be made to meet suitable requirements for its use in fabrication of optoelectronic devices.

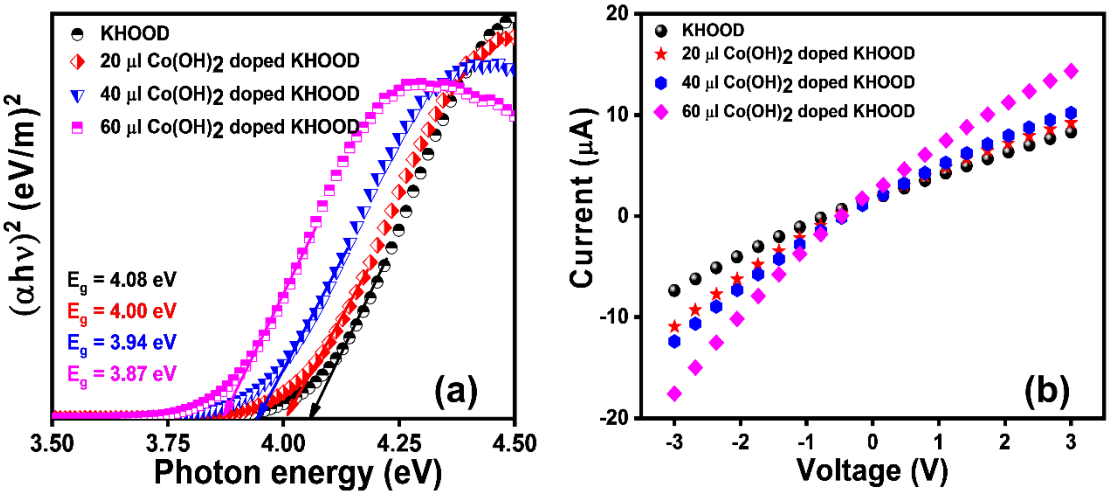

Figure. 4.4. (a) Tauc's plot of pure and $Co(OH)_2$ doped KHOOD single crystals (b) I-V curves of pure and $Co(OH)_2$ doped KHOOD single crystals.

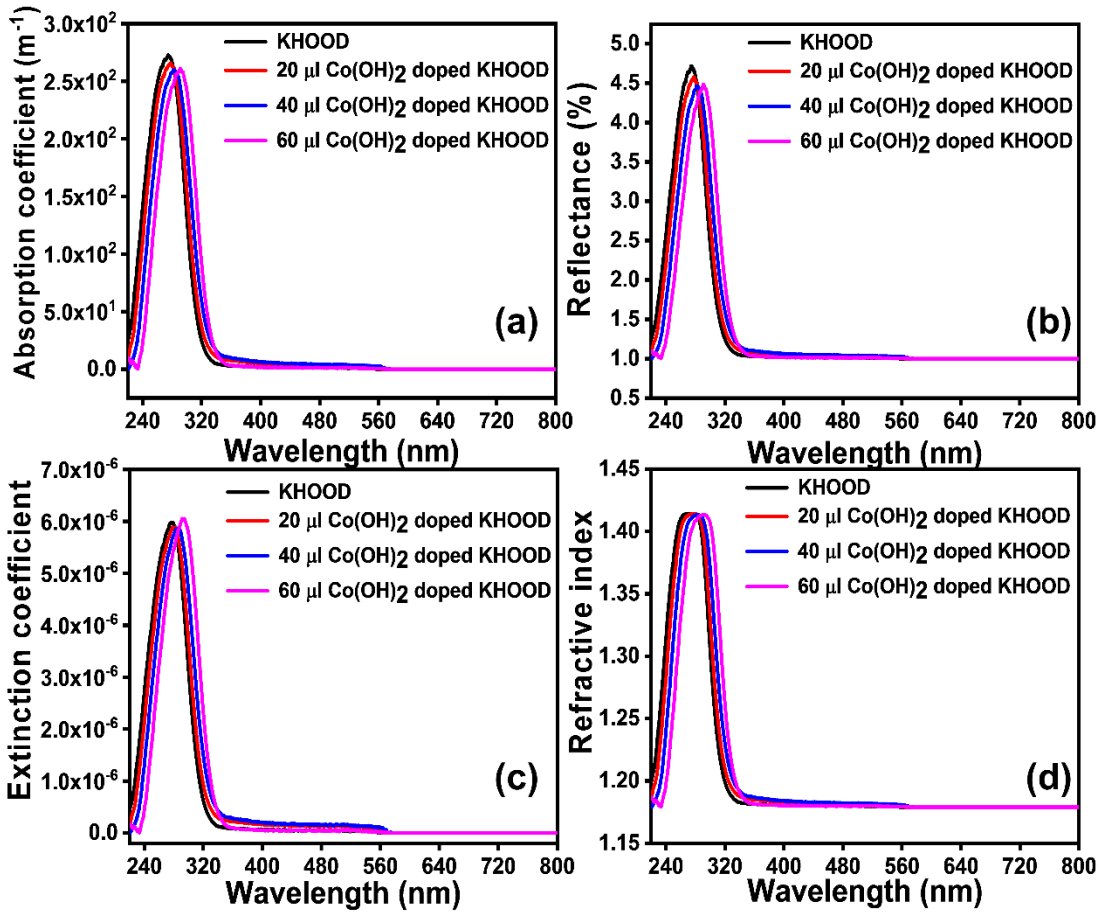

Figure. 4.5. (a) Absorption coefficient (b) Reflectance (c) Extinction coefficient (d) Refractive index of pure and $Co(OH)_2$ doped KHOOD single crystals as a function of wavelength.

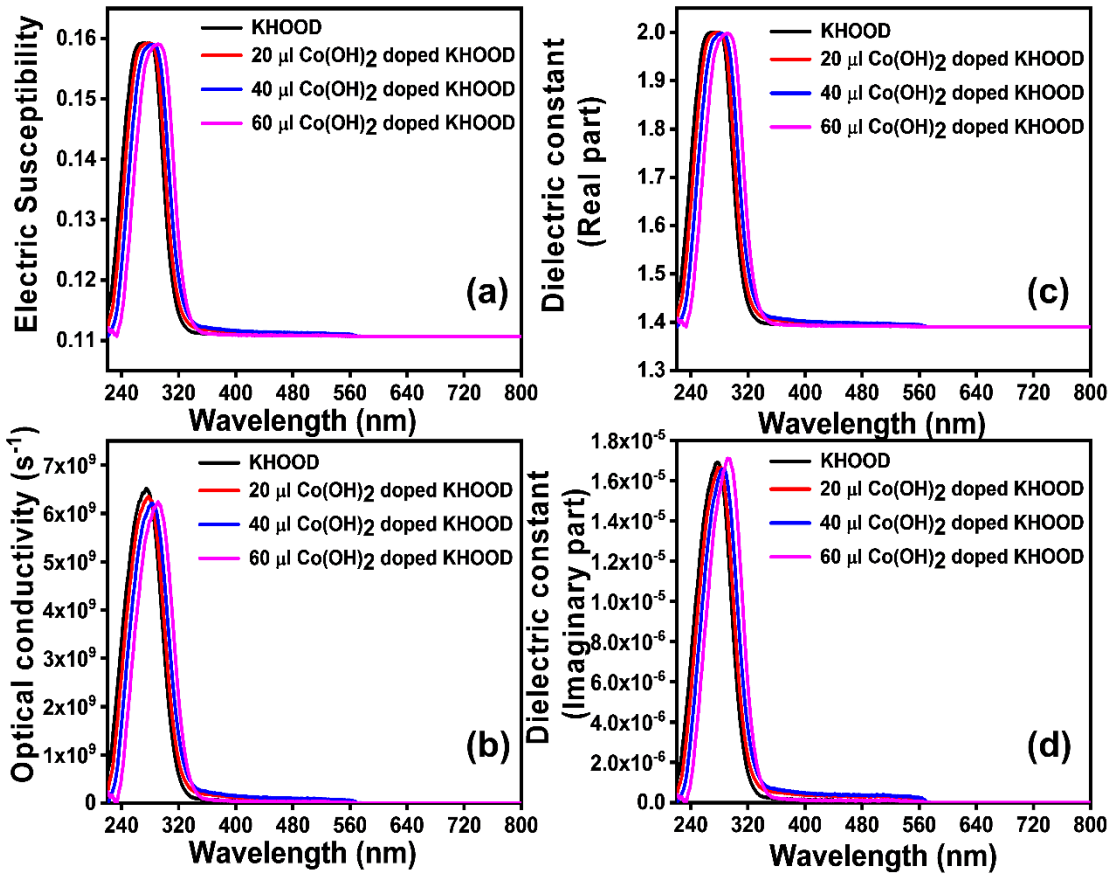

Figure. 4.6. (a) Electric susceptibility (b) Optical conductivity (c) Real dielectric constant (d) Imaginary dielectric constant of pure and Co(OH)2 doped KHOOD single crystals with respect to wavelength.

Electric susceptibility (χ_c) indicates the degree of polarization of the material in response to applied field of electromagnetic wave.

The variation of electric susceptibility with wavelength is shown in Figure. 4.6(a).

Optical conductivity of a crystal is a powerful tool to determine its optical response. Shankar Joseph equation for optical conductivity [Subramani et al. 2013] is given as shown in Eqn. 7 which is shown in Figure. 4.6(b).

Optical conductivity is in the order of 10^9 s^{-1} and remains almost constant in visible region. The higher value of optical conductivity is an indicative of the application of crystals in signal processing and computing [Anis et al. 2016].

The real dielectric constant (ε_r) and imaginary dielectric constant (ε_i) are related to refractive index and extinction coefficient by the Equation. 8 and 9 [Bincy and

Gopalakrishnan 2014]. The variation of ε_r and ε_i with wavelength are shown in Figure. 4.6(c) and (d).

4.2.4 I-V studies

The as synthesized crystals were polished to obtain uniform surfaces on the both sides of the crystals and the thickness of 1.25 mm was maintained for all crystals to perform I-V measurements. I-V measurements were performed in the voltage range from -3 V to +3 V, and the current generated are measured using Keithley 2410-c 1100V source measuring unit. The crystals were swept in the voltage range from -3 V to +3 V and the current is measured which is shown in Figure. 4.4(b). The dc resistivity (ρ_{dc}) of pure and $Co(OH)_2$ nanoparticles doped KHOOD single crystals are obtained by the relation, $\rho_{dc} = RA/d$ [Freeda and Mahadevan 2000]. Wherein, R is the measured resistance, d is the thickness of the sample and A is the area of contact. The conductivity of the crystal was calculated by the inverse of calculated resistivity.

On $Co(OH)_2$ nanoparticles doping by small amount (20 µl), the conductivity of the crystals are increased by the order of 0.8×10^{-5} $(\Omega.m)^{-1}$. Further increase in the doping amount, enhanced the conductivity to almost twice in comparison to the conductivity of pure KHOOD single crystals. The enhancement in the conductivity maybe due to the incorporation of metallic sites through doping. The I-V studies are also supported by bandgap analysis as discussed and plotted in Figure. 4.4(a), in which the declination in the bandgap as the function of dopant concentration were observed. The calculated values of resistivity and electrical conductivities are tabulated in Table. 4.2.

Table. 4.2. The resistivity and conductivity values of pure and $Co(OH)_2$ doped KHOOD single crystals.

Name	**Resistivity (Ω.m)**	**Conductivity $(\Omega.m)^{-1}$**
KHOOD	2.021×10^{4}	4.947×10^{-5}
20 µl $Co(OH)_2$ doped KHOOD	1.712×10^{4}	5.841×10^{-5}
40 µl $Co(OH)_2$ doped KHOOD	1.509×10^{4}	6.626×10^{-5}
60 µl $Co(OH)_2$ doped KHOOD	1.074×10^{4}	9.310×10^{-5}

4.2.5 FTIR spectral analysis

The FTIR spectral studies is a widely used scientific technique to effectively identify the functional groups and to determine the structure of synthesized compound. FTIR spectra reveals details regarding bond type and bond strength in the material. The FTIR spectra of pure and doped crystals were recorded over a mid-infrared range of 500 cm^{-1} to 4000 cm^{-1} which are shown in Figure. 4.7(b). The absorption peak observed at 3438 cm^{-1} is attributed to OH stretching of oxalic acid molecule which is shifted to 3438 cm^{-1}, 3436 cm^{-1} and 3438 cm^{-1} for 20 µl, 40 µl and 60 µl $Co(OH)_2$ nanoparticle doped KHOOD crystals [Jananakumar and Mani 2014]. The symmetric and asymmetric stretching vibrations of O-H bonds of water molecule are observed at 3015 cm^{-1}. The peaks at 2525 cm^{-1} and 1701 cm^{-1} indicates C=O stretching vibrations. The absorption peak at 1633 cm^{-1} is attributed to COO^- asymmetric stretching. The peak at 1403 cm^{-1} is assigned to K-O symmetric stretching. The peak at 1231 cm^{-1} corresponds to C-O-H bending vibrations. The C-C stretching vibrations were identified at 1109 and 909 cm^{-1}. The peak at 803 cm^{-1} and 720 cm^{-1} shows the presence of K-O stretching vibrations and O-C=O deformation. As such, there are no noticeable differences in the FTIR spectra of pure and doped KHOOD samples which supports the fact that addition of small amount of nanoparticle dopant in the host lattice does not affect the functional groups of KHOOD crystal [Chandran et al. 2015]. The amount of $Co(OH)_2$ nanoparticles added in the KHOOD crystal are very less (ranging from 20µL to 60 µL) and the peaks corresponding to $Co(OH)_2$ nanoparticles are not observed in the FT-IR spectrum. However, interestingly we observed a 'red shift' in the wavenumber, corresponding to O-H stretching in the FT-IR spectrums of $Co(OH)_2$ doped KHOOD single crystals, confirming the successful doping of $Co(OH)_2$ in the KHOOD system. Minor changes observed in the peak positions of FTIR spectra of doped samples suggest the incorporation of dopants into the KHOOD lattice [Goel et al. 2017]. The assigned vibrational frequencies are listed in Table. 4.3, which confirm the presence of different functional groups in the synthesized pure and $Co(OH)_2$ doped single crystals.

Table. 4.3. FTIR spectral assignments for pure and $Co(OH)_2$ nanoparticle doped KHOOD single crystals.

Pure KHOOD Wavenumber (cm^{-1})	**KHOOD 20 µl Co Wavenumber (cm^{-1})**	**KHOOD 40 µl Co Wavenumber (cm^{-1})**	**KHOOD 60 µl Co Wavenumber (cm^{-1})**	**Assignment**
3438.32	3436.92	3432.20	3430.80	OH stretching [of oxalic acid]
3015.31	3015.31	3016.45	3016.72	H_2O symmetric and asymmetric stretching
2525.18	2525.53	2525.44	2525.96	C=O stretching vibrations
1701.03	1702.43	1701.25		C=O stretching vibrations
1633.63	1639.77	1636.94	1640.28	Presence of H_20 molecule / C=O absorption band / COO^- symmetric stretching [of hydrogen oxalate]
1403.60	1404.21	1403.61	1404.67	K-O asymmetric stretching
1231.33	1232.26	1232.12	1231.89	C-O-H bending in plane [of hydrogen oxalate]
1109.61	1113.6	1115.7	1111.7	C-C stretching
909	907	905	903	C-C stretching
803.65	801.61	799.57	797.53	K-O stretching
720.02	722.06	724.10	726.14	O-C=O deformation

4.2.6 Photoluminescence studies (PL)

Photoluminescence (PL) is an optical phenomenon where the electronic states present in a material are excited by the absorption of light of particular energy and then

undergo radiative relaxation [Rajesh et al. 2014 Shanthi et al. 2016 Shkir et al. 2017b]. The PL emission is sensitive to change in local atomic configuration and defect states in a crystal structure. It depends on the perfection of the crystal [Goel et al. 2017]. The pure and doped samples were excited at a wavelength of 280 nm and PL emission spectrum was recorded in the range 360 nm to 550 nm as shown in Figure. 4.7(a). The pure crystal showed a broad peak whereas the peak width decreased with increase in dopant concentration. These doped impurities create defect levels which act as energy traps causing a rise in the emission intensity [Yadav et al. 2015 Shkir et al. 2017a]. It is worth noting that, the peak intensity increased with the doping level, indicates the successful doping of $Co(OH)_2$ nanoparticles in the interstitial positions of the host KHOOD lattice. The blue emission of the pristine and doped crystals can be of importance in fabrication of blue LEDs [Patil et al. 2017].

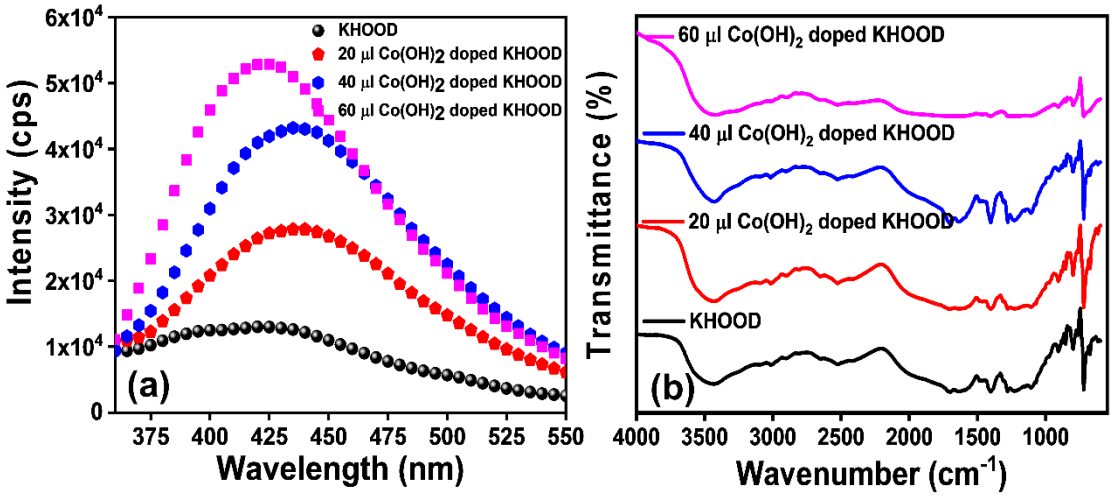

Figure. 4.7. (a) PL spectrum of pure and $Co(OH)_2$ doped single crystals. (b) FTIR spectrum of pure and $Co(OH)_2$ doped KHOOD single crystals.

4.2.7 Thermal analysis

In the present investigation, Thermogravimetry (TG) and Differential Thermal Analysis (DTA) of synthesized crystals have been carried out in inert atmosphere from room temperature to 800º C with a heating rate of 10 ºC per minute. TG-DTA curves of pure and doped samples are shown in Figure. 4.8. These curves are analyzed to get information regarding the effect of nanoparticles on the thermal stability and dissociation of the samples. The crystal weighing nearly 2 mg was taken for the TGA-

DTA measurements under nitrogen inert atmosphere. The initial mass loss in the pure and doped crystals occurs nearly around 80 ºC and the mass loss is observed till 117 ºC. The observed mass loss can be accredited to the liberation of H_2O adsorbed [Vimal et al. 2014 Chandran et al. 2017]. The second mass loss is observed at around 167 ºC to 224 ºC, which can be attributed to the liberation of lattice H_2O molecules [Vimal et al. 2014]. The crystal further undergoes mass loss from 239 ºC to 273 ºC, which is due to the liberation of HCOOH and CO_2 gas. The crystal melting point is observed to be at 263.4 ºC and it was observed to be enhanced for increased dopant concentration. The melting point for the doped crystals are 266.2 ºC, 267.9 ºC and 270.7 ºC for 20, 40, 60 µl $Co(OH)_2$ doped KHOOD single crystals. The DTA peak observed at 396.1 ºC for Pure KHOOD single crystal suggests the phase transformation at this temperature since TGA curve shows no mass loss in that range [Higashiyama and Hasegawa 1971 Dinnebier et al. 2005]. The mass loss after 534ºC to 600 ºC is assigned to the liberation of CO from the crystal at that temperature, [Mahalakshmi et al. 2012] which is true for all the doped crystals.

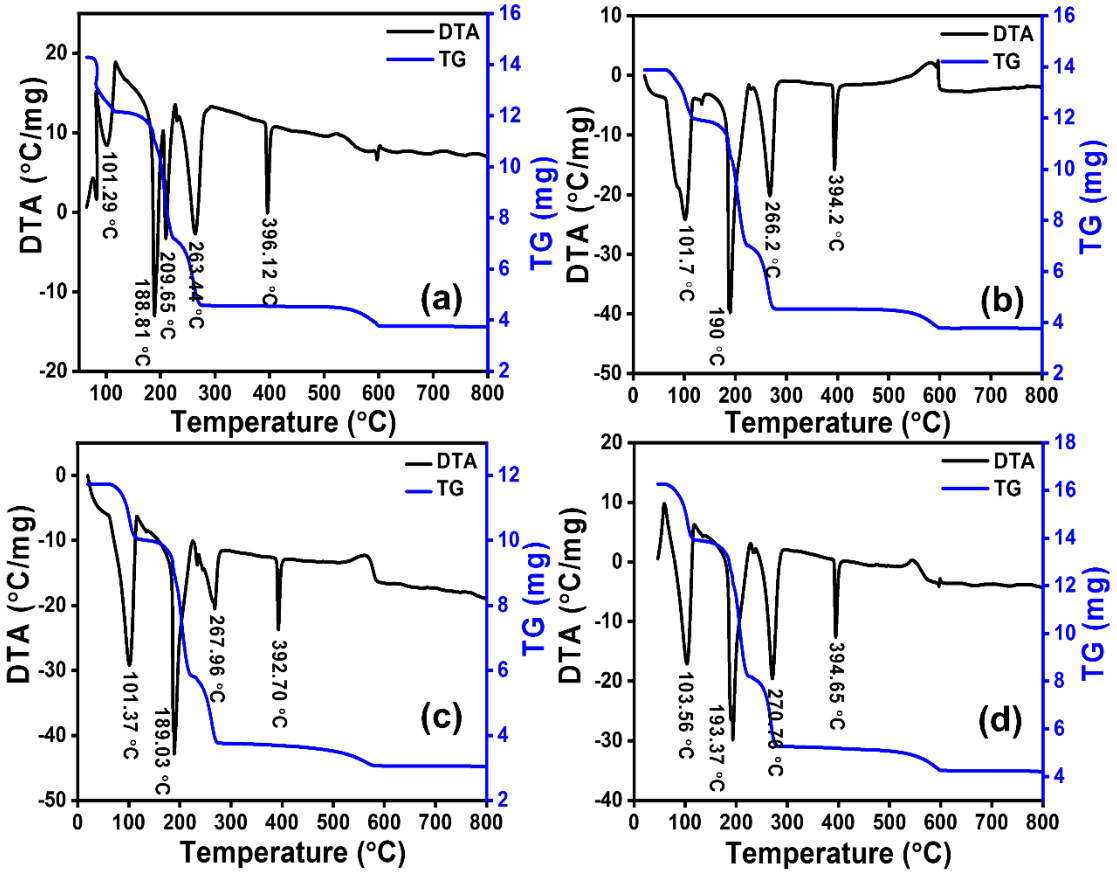

Figure. 4.8. TGA-DTA curves of pure and $Co(OH)_2$ doped KHOOD single crystals.

The chemical reaction followed in the higher temperatures are shown below

$2(KH_3C_4O_8 \cdot 2H_2O) \rightarrow 2KH_3C_4O_8 + 4H_2O\uparrow$ (1)

$2KH_3(C_2O_4)_2 \rightarrow 2KHC_2O_4 + 2CO_2\uparrow + 2HCOOH$ (2)

$2KHC_2O_4 \rightarrow K_2C_2O_4 + CO_2\uparrow + HCOOH$ (3)

$K_2C_2O_4 \rightarrow K_2CO_3 + CO\uparrow$ (4)

4.2.8 Impedance spectroscopy

The impedance study of the synthesized crystals was carried out by applying an ac field in the frequency range of 10 Hz to 1 MHz at room temperature. The study of frequency-dependent impedance spectroscopy helps in determining the contribution of grain boundaries on the electrical properties of the synthesized material [Chand et al. 2017a]. The variation of real part and imaginary part of the complex impedance with frequency for different doping concentration is shown in Figure. 4.9(a) and Figure. 4.9(b). Z′, the resistive part of impedance, is found to decrease with increase in frequency and also with increase in nanoparticle dopant concentration. The decrease in Z′ is an indicative of increase in ac conductivity which is clearly depicted by ac conductivity studies [Bindu et al. 2018a]. Z″ shows a maxima and starts to decrease after that and the maxima can be explained due to the dielectric relaxation process in the material [Tsay et al. 2016a]. It was noticed that the height of the Z″ value decreased as the dopant concentration increased and also shift in the peak position to higher frequencies indicating the decrease in relaxation time [Rahman and Hossain 2014 Tsay et al. 2016a].

The Nyquist plot (Z′ versus Z″) gives only one semicircle in the low frequency region as shown in Figure. 4.9(c). This suggests that the grain boundaries predominantly contribute to the conductivity in the samples [Tsay et al. 2016b]. The diameter of semicircle gives the measure of resistance of grain boundaries while the frequency of semicircle maximum helps in determining grain capacitance [Tsay et al. 2016b]. The diameter of semicircle decreased with increase in nanoparticle dopant concentration signifying the drop in grain interior resistance with increase in doping concentration [Kambale et al. 2009].

4.2.8 (a) Dielectric studies

Dielectric measurement is a vital tool to understand material behavior especially at high frequencies. Dielectric properties of a material reveal significant information

regarding the storage and dissipation of electric and magnetic fields in the material and also provides insight into feasibility of implementing the material in potential applications [Kanchana et al. 2013]. Dielectric studies of the synthesized crystals were carried out at frequency range of 10 Hz to 1 MHz at room temperature.

The real part of dielectric constant is a measure of amount of energy from external field stored in the material while the imaginary part of dielectric constant quantifies the amount of energy loss from the material.

The variation of loss tangent with frequency and dopant concentration is shown in Figure 4.9(d). The variation in dielectric constant in the synthesized KHOOD crystal can be explained on the basis of space charge polarization phenomenon [Ray et al. 2017]. A dielectric material is composed of well conducting grains with highly resistive grain boundaries between them. At lower frequencies, the mobile charge carriers accumulate at the grain boundaries giving rise to high value of dielectric constant [Anand et al. 2017 Chand et al. 2017b]. The space charge carriers require a finite time to line up along the direction of the applied field.

As the frequency of the applied field increases, the charge carriers cannot rotate rapidly and their oscillations deviate from that of the applied field. With a continuous increase in frequency, more number of charge carriers will not be capable to keep up the pace with the oscillations of the applied field. As a result, they do not add to polarization. Thus ε' decreases with increasing frequency and becomes constant at higher frequencies [Lahlali et al. 2017]. The low value of dielectric constant at higher frequencies is a suitable factor for the application of the crystals in electro-optic devices [Ma et al. 2018]. Further, ε' increases with increase in dopant concentration. This may be attributed to the fact that the presence of Co^{2+} ions may increase the number of grain boundaries where the electrons pile up resulting in polarization [Fadhil et al. 2017].

ε'' and $\tan\delta$ also show a decreasing trend with increase in applied frequency and remain constant at higher frequencies similar to ε'. Also, the values of $\varepsilon''$and $\tan\delta$ have found to increase with increase in nanoparticle dopant concentration. The dielectric loss tangent arises when the polarization lags behind the applied altering field and is a result of the presence of structural inhomogeneities, impurities and crystal lattice imperfections [Singh et al. 2014]. The low value of loss tangent at high frequencies suggest their suitability in high frequency device applications [Aravind et al. 2015].

Figure. 4.9(e) shows the variation of ac conductivity with applied frequency and nanoparticle dopant concentration at room temperature. The calculation of ac conductivity helps in determining the nature of conduction mechanism and the type of polarons responsible for conduction [Hamdi et al. 2018]. The ac conductivity is found to increase with increase in frequency of applied field at higher frequencies. This may be due to the pumping force of the applied ac field which helps in the transfer of charge carriers between different localized states and also facilitates the liberation of trapped charge carriers from various trapping centers. An increase in frequency would improve the electron hopping frequency between the charge carriers which would in turn increase the conductivity [Singh et al. 2014].

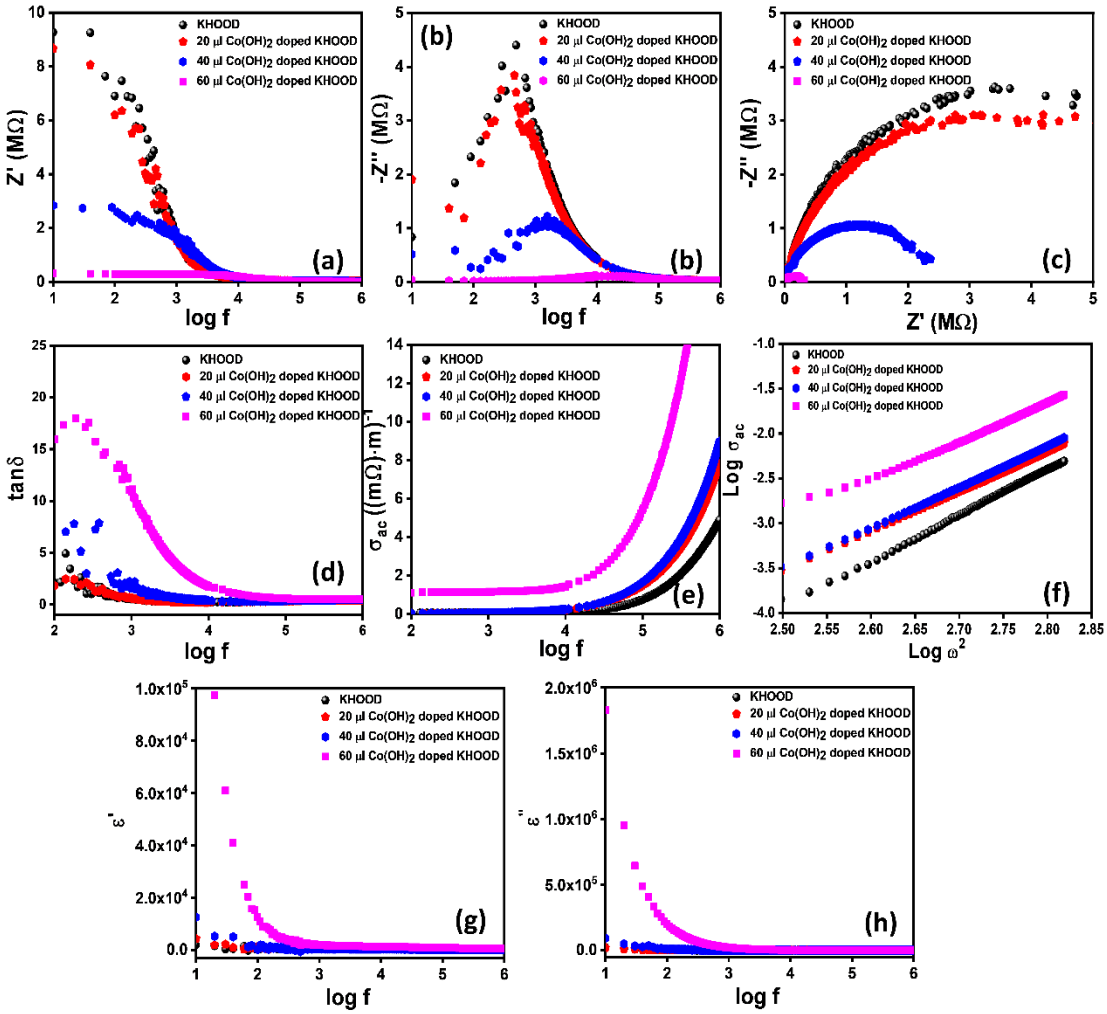

Figure. 4.9. (a) Z' and (b) $-Z''$ variation with respect to log frequency (c) Nyquist plots (d) loss factor (tanδ) versus log frequency (e) σ_{ac} versus log frequency (f) log σ_{ac} versus log ω^2 (g) Real part (dielectric) versus log frequency (h) Imaginary part (dielectric)

versus log frequency.

The linear variation of σ_{ac} at higher frequencies suggests that the conduction occurs by hopping of charge carriers between the localized states thereby confirming small polaron type of conduction. The decrease in σ_{ac} at lower frequencies implies the conduction by mixed (small and large) polarons [Devan et al. 2006 Khader et al. 2015]. Also, from Figure. 4.9(f). it was noticed that the plot of log (σ_{ac}) vs log(ω^2) shows a linear behaviour for all the synthesized crystals confirming that small polarons are responsible for the conduction mechanism in frequency dependent ac conductivity [Rosso et al. 2003 Kadam et al. 2004 Ashwini et al. 2017 Bindu et al. 2018b]. The enhanced properties of doped crystals can be of use in optoelectronic device fabrications.

4.3 Conclusions

The single crystals of potassium oxalate oxalic acid dihydrate (KHOOD) and $Co(OH)_2$ doped KHOOD crystals were synthesized using slow evaporation technique. The shift in the XRD peaks and the variation of overall peak intensities through doping confirms the nanoparticle incorporation in the host lattice. The declination in optical bandgap and enhancement of electrical conductivities were observed as the function of $Co(OH)_2$ doping in the KHOOD system. In addition, PL measurements displayed enhanced emission peaks and the FTIR spectra portrayed the redshift in the O-H stretching, once again confirming the successful doping of $Co(OH)_2$ in the KHOOD system. From the nyquist plot the radius of the semicircle decreased as the dopant concentration increased showing observable decrease in the resistivity of the material. From ac conductivity studies it was observed that the hopping mechanism is the reason behind the conductivity process. The conductivity mechanism was attributed to small polaron hopping mechanism.

CHAPTER 5

A STUDY ON STRUCTURAL, OPTICAL, THERMAL AND ELECTRICAL PROPERTIES OF THE DYE DOPED KHO SINGLE CRYSTAL

Overview

In this chapter the effect of Amaranth dye on the structural, optical, and electrical properties of the KHOOD single crystals is discussed.

5.1 Introduction

The advancement in the optoelectronic industries have promoted many researchers in exploring material properties and their suitability for device fabrications. In this regard, it is well known that organic materials possess excellent optical properties but lack thermal and mechanical stabilities[Rajasekaran et al. 2001 V. Kannan 2004 Ruby Nirmala and Thomas Joseph Prakash 2013]. Organic crystal growth is a challenging task and it is very difficult to grow those crystals into bigger sizes. On the other hand inorganic materials can be grown easily to bigger sizes and also they possess higher melting point and higher hardness values when compared with those of organic crystals [Shakila and Kalainathan 2015 Mahendra et al. 2018]. In order to overcome drawbacks of organic and inorganic materials, a new class of materials was developed by combining organic molecules with inorganic salts to attain semiorganic or organometallic complexes [Ahlam et al. 2012 Shkir et al. 2015 Ramki and Ezhil Vizhi 2017 Mahendra et al. 2019b, 2019a]. Oxalic acid is an organic compound having a large dipole moment and has an affinity to bind with several metal atoms to form complexes. Oxalic acid combined with metal atom forms a complex and it is found to possesses better properties when compared with the base material [Bridle and Lomer 1965 Hodgson and Ibers 1969 Pedersen 1972 Nancollas and Gardner 1974 Eriksson and Nielsen 1978 Bangera and Rao 1992 Raju et al. 1994 Joseph et al. 1997 Dalal and Saraf 2006 Ramki and Ezhil Vizhi 2017].

A dye is basically an organic aromatic chemical assembly which is water soluble and it strongly absorbs or emits light in visible region, Thus affecting the optical, mechanical, electrical and thermal properties of the material into which it is incorporated and therefore suitable for device fabrication [Weber and Eagen 1979 Murakoshi et al. 1995 Eggeling et al. 1998 L. Parker et al. 2012]. However, various dyes are classified according to their chemical composition and chromophore group. Furthermore, the

dyes of aryl and azo groups were extensively used for industrial applications.

The study on host material and dye interaction is a current trend in research since it influences the materials in optoelectronic devices [Sinha et al. 2015 Kahr and G. Shtukenberg 2016]. Small quantity of dye molecules can influence the properties of the host drastically [Muenster et al. 1997]. However, there is little work reported on the dye incorporated KHOOD single crystals. KHOOD single crystal is doped with water soluble azo dye (Amaranth) and properties of the material after dye incorporation was explored. The dye doped crystal was subjected to several other characterizations to study the variation of physical properties due to the dye incorporation into the host crystal.

5.2 Results and discussions

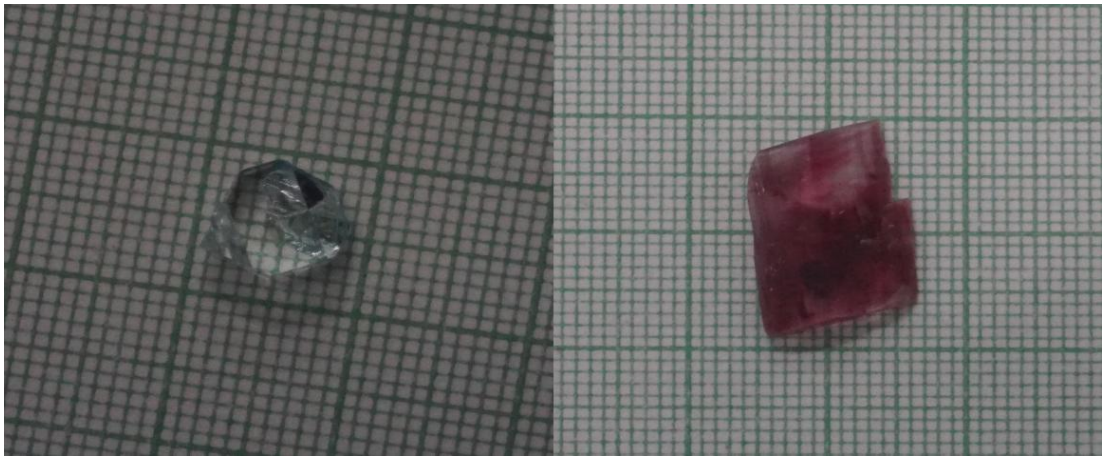

Figure. 5.1. Images of KHOOD and 0.1 mM Amaranth dye doped KHOOD crystal.

Crystal morphology and size changes drastically with addition of dye molecule onto the KHOOD crystal. A characteristic coloring pattern observed for 0.1 mM Amaranth doped KHOOD crystal provided an evidence of dye incorporation in to KHOOD matrix. The morphological changes in the crystal was due to the adsorption of dye molecules into the KHOOD crystal lattice affecting the interfacial surface tension and anisotropic growth rate during crystal formation [Sinha et al. 2012a Bhandari et al. 2014]. For higher concentrations of the amaranth dye molecule, the KHOOD crystal morphology changed and irregular shaped clusters were formed.

5.2.1 Powder XRD

Synthesized KHOOD and amaranth dye doped KHOOD crystals were investigated structurally using powder X-Ray diffraction (PXRD) analysis to study the

crystalline nature of the samples. The fine powders of the samples were studied over 10º - 70º with the scanning speed of 2º per minute (Rigaku 600 miniflex). The PXRD patterns of KHOOD and dye doped KHOOD crystals were shown in Figure. 5.2. Small variations in the XRD peaks were seen but all the peaks of KHOOD crystal was also present in amaranth doped KHOOD crystal signifying the fact that the crystal structure was not altered, though the dye molecule incorporation was assisted with the lattice strain in the crystal structure of KHOOD [Sinha et al. 2012b].

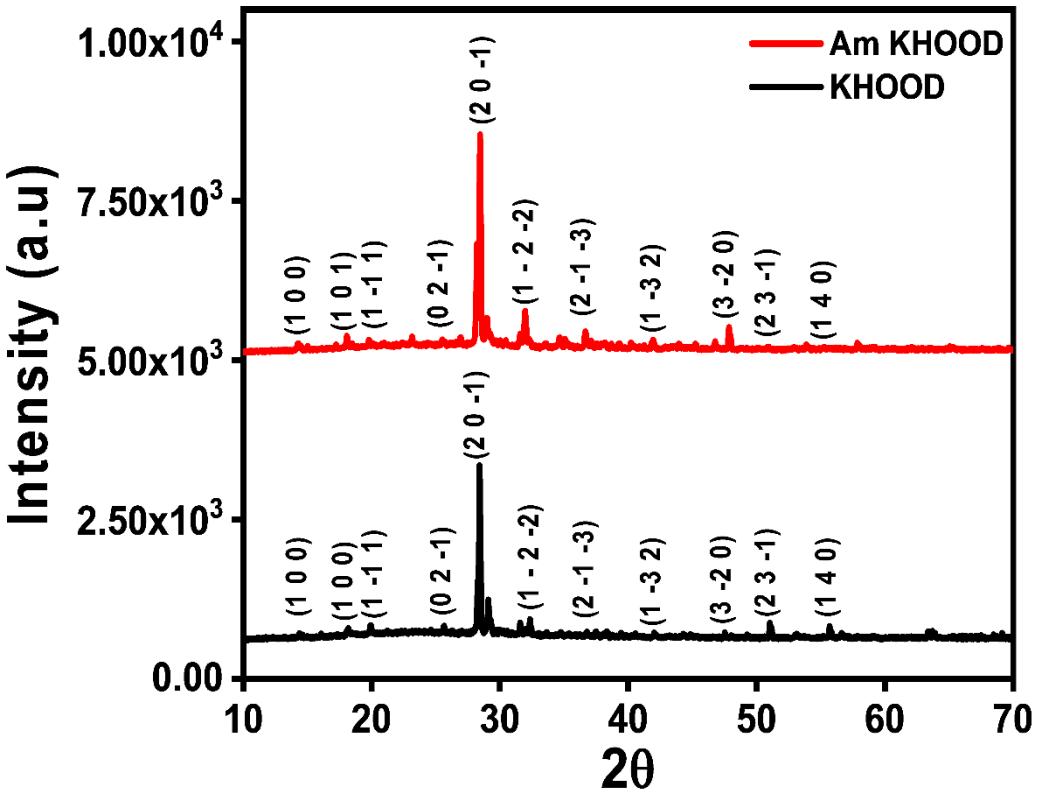

Figure. 5.2. PXRD pattern of KHOOD and 0.1 mM Amaranth dye doped KHOOD crystal.

5.2.2 Optical Studies

Absorption is an important parameter, which decides the suitability of the crystal for desired applications [Thaila and Kumararaman 2012]. The absorption spectrum of crystals were analyzed using ocean optic USB 4000 spectrometer in spectral range of 180 - 900 nm. The pure KHOOD crystal shows absorption peak at 278 nm whereas, amaranth dye doped KHOOD crystal shows absorption at 291 nm. The amaranth dye molecule was also studied for its optical absorption and it was seen that the amaranth absorption is present at 280 nm (major) 330 nm (minor) in UV region.

Further, it is interesting to note that, amaranth doped KHOOD crystal shows one more absorption peak at 532 nm, which was not present in undoped KHOOD crystal. The presence of 532 nm absorption is also observed in amaranth dye, confirming the presence of the dye molecule in the crystal. The absorption spectrum of amaranth dye, KHOOD and amaranth doped KHOOD crystals are shown in Figure. 5.3.

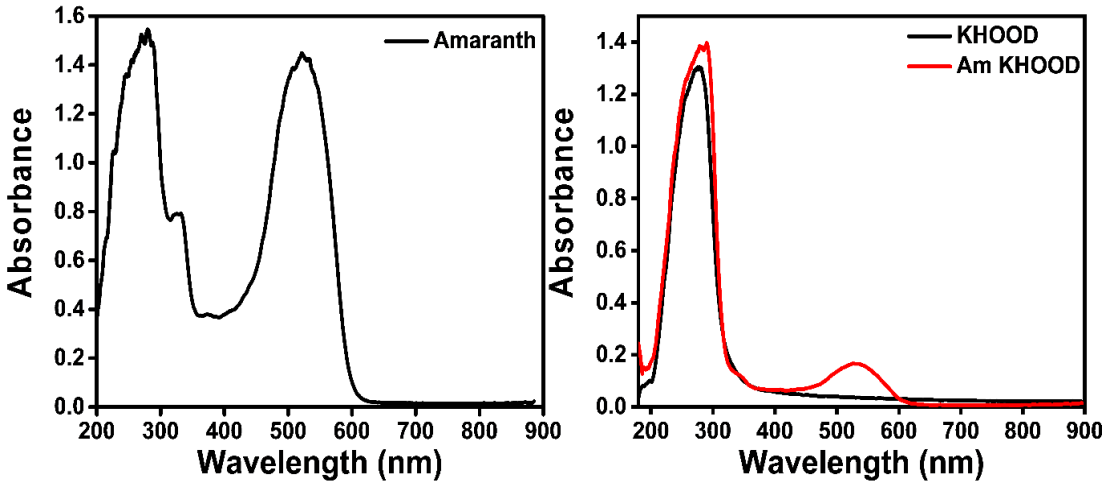

Figure. 5.3. Absorption spectrum of Amaranth dye, KHOOD and 0.1 mM Amaranth dye doped KHOOD crystal.

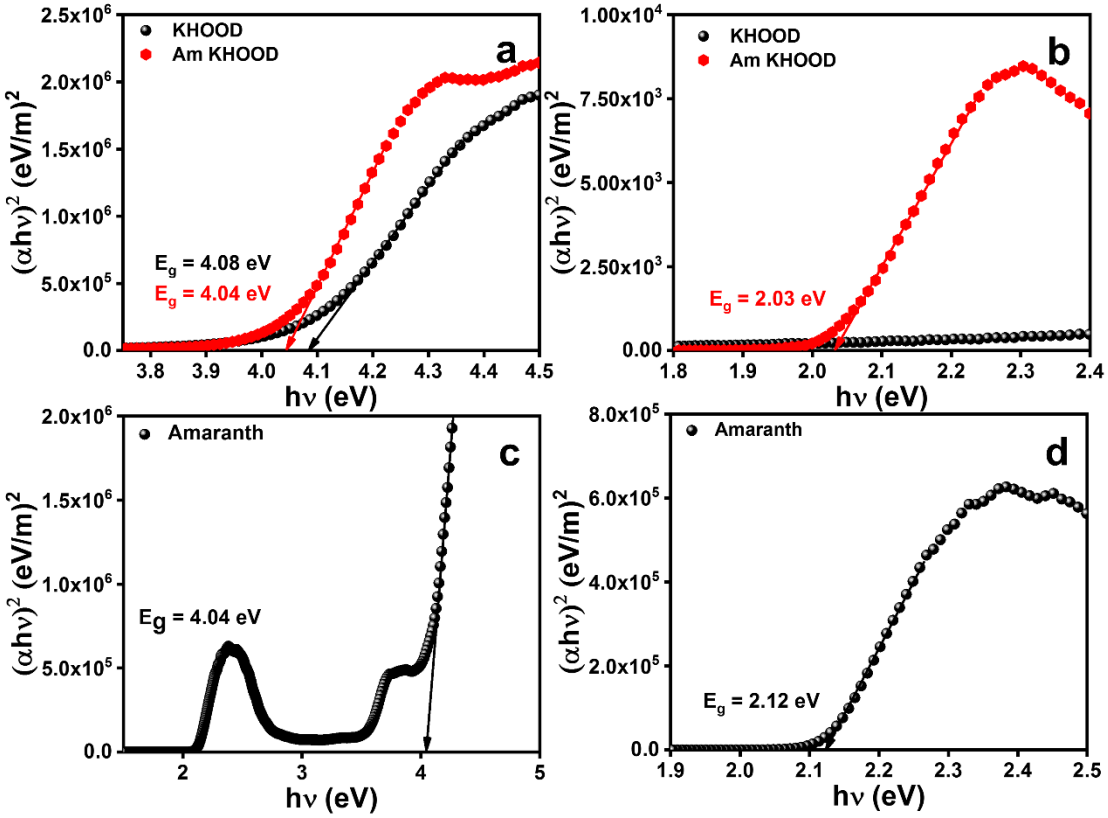

Figure. 5.4. Tauc's plot of (a) KHOOD and Amaranth dye doped crystal at higher energy values (b) KHOOD and Amaranth dye doped crystal lower energy values (c) Amaranth dye (d) Amaranth dye at lower energy values.

The crystal absorption is also used to calculate optical bandgaps of the crystals. The optical bandgap of the crystals are also compared with the bandgap obtained for the amaranth dye doped KHOOD crystal.

The absorption coefficient (α) is determined by the help of optical absorption of the crystal as shown in Equation. 2.3.

where A is a constant and E_g is optical band gap. The tauc's plot of dye molecule, KHOOD and dye doped KHOOD are presented in Figure. 5.4. It was noticed that KHOOD crystal possess a bandgap of 4.08 eV and the dye doped KHOOD crystal shows 4.04 eV. The decrease in bandgap after doping may be due to the formation of donor levels caused by doped impurities in the crystal [Chen et al. 2012 Shenoy et al. 2018] It is inferred that the amaranth dye incorporation decreases the bandgap of KHOOD crystal. Further, there is another linear portion was observed corresponding to the dye doped KHOOD crystal, which was not observed for KHOOD crystal. The linear portion in tauc's plot was due to the absorption of dye molecule in the crystal, also present in the amaranth dye molecule. The presence of another linear portion in the dye doped KHOOD crystal is a clear indication that the dye molecule is incorporated into the crystal lattice of KHOOD.

5.2.3 SEM and EDAX analysis

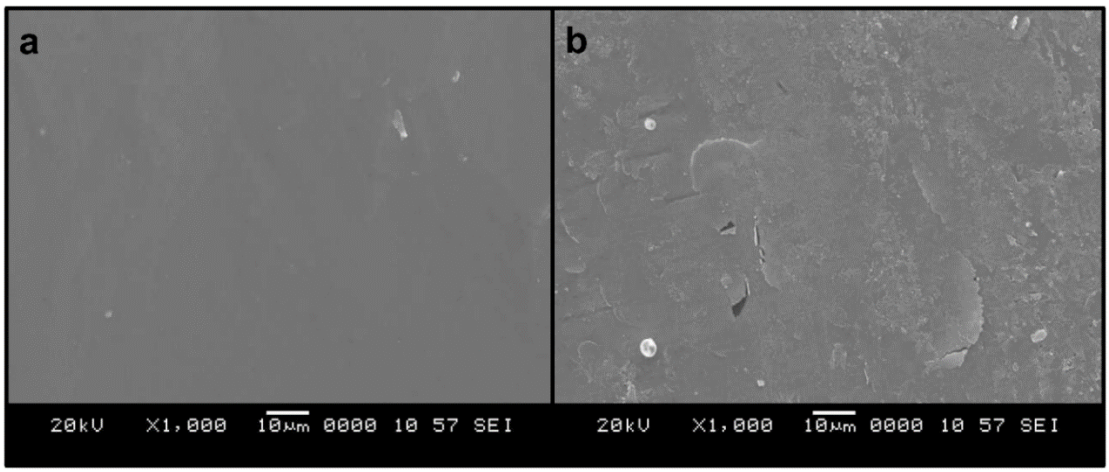

Figure. 5.5. SEM micrographs of (a) KHOOD (b) 0.1 mM Amaranth dye doped KHOOD crystal.

The surface studies are carried out using scanning electron microscope (SEM) (JOEL-JSM-6380LA) and the EDX studies were performed to confirm the elements present in the crystal after the doping and distribution of each elements in the crystal (Mapping). The recorded SEM micrographs of KHOOD and dye doped KHOOD crystals were shown in Figure. 5.5. Interestingly, a smooth surface is witnessed in the case of KHOOD single crystal and as the dye incorporation the crystal surface is altered and a rough surface was obtained. The elements of dye molecule in the crystal was confirmed using EDAX analysis (Figure. 6) and the elemental distribution in the crystal is shown in the Figure. 5.5.

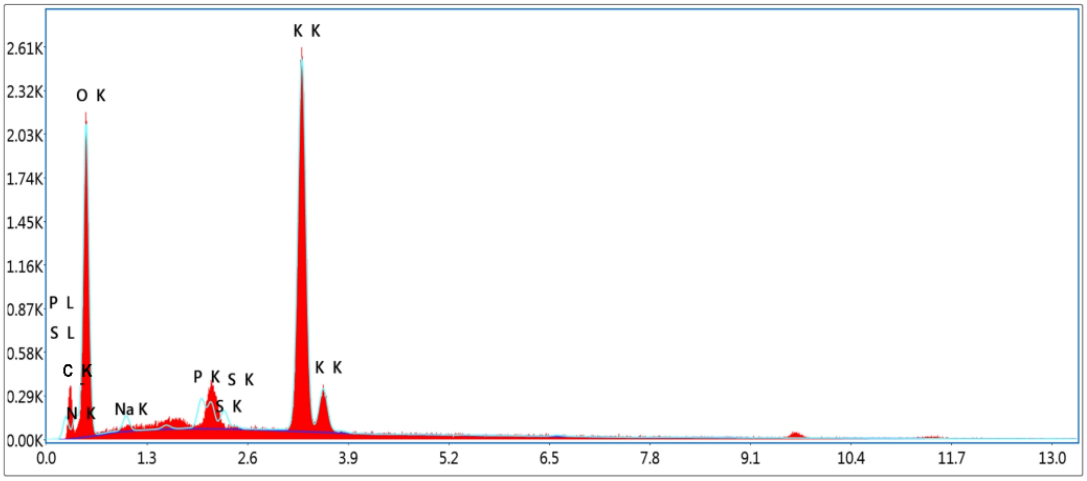

Figure. 5.6. EDX spectrum of 0.1 mM Amaranth dye doped KHOOD crystal.

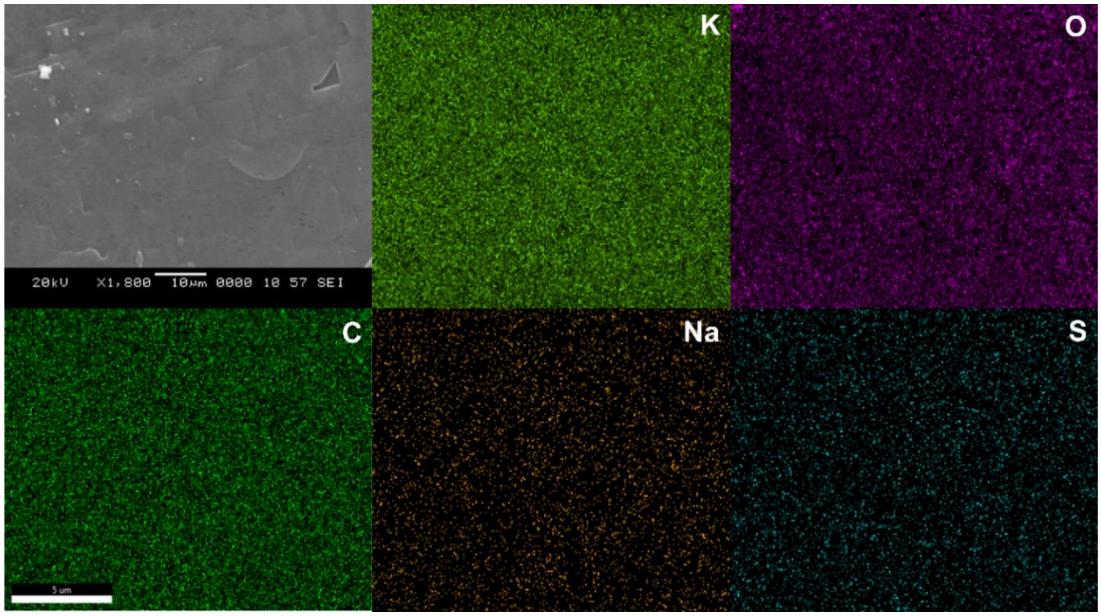

Figure. 5.7. EDX Mapping of 0.1 mM Amaranth dye doped KHOOD crystal.

5.2.4. Thermal analysis

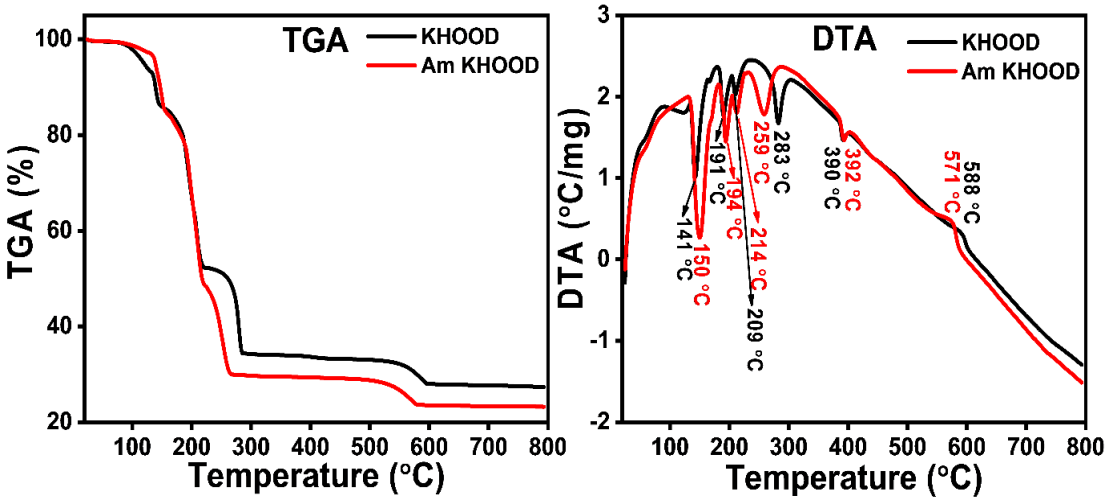

Figure. 5.8. TGA-DTA curves of KHOOD and 0.1 mM Amaranth dye doped KHOOD crystal.

Thermal degradation mechanism of KHOOD and dye doped KHOOD crystals were studied using TGA-DTA analysis. 8 mg samples of KHOOD were used for thermal analysis in the presence of nitrogen atmosphere. The TGA-DTA curves were plotted and shown in Figure. 5.8. The initial mass loss was higher for dye doped KHOOD crystal compared with that of KHOOD crystal. Initial mass loss begins at 89 ºC and the mass loss was observed till 154 ºC and 144 ºC for dye doped KHOOD and pure KHOOD crystal respectively. The endothermic peak corresponding to150 ºC and 141 ºC in DTA curves of dye doped KHOOD and pure KHOOD crystals are due to the liberation of water molecules [Vimal et al. 2014 Chandran et al. 2017]. The second mass loss observed can be attributed to the liberation of water molecules and also liberation of CO_2 gas from the crystal corresponding to endothermic peak observed at 194 ºC and 191 ºC in DTA curve. Till this temperature the decomposition rate for dye doped KHOOD crystal is less. Furthermore, the temperature is increased to 283 ºC and 256 ºC in DTA corresponding to the pure KHOOD and dye doped KHOOD are due to the liberation of CO_2 and H_2 gases respectively. Further increase in the temperature leads to exothermic peaks at 390 ºC and 392 ºC for pure and dye doped KHOOD crystals but no weight loss was observed in TGA curve suggesting the phase transformation of the material [Higashiyama and Hasegawa 1971 Dinnebier et al. 2005]. Further, the increase in temperature at 588 ºC and 571 ºC for KHOOD and dye

doped KHOOD crystals show an exothermic peak due to liberation of CO gas from the crystals and the mass loss obtained for dye doped KHOOD crystal is comparatively more than the pure crystal. The decreased mass loss of the pure crystal may be due to the formation of Na_2CO_3, which is having higher melting point (>800 ºC). Hence carbonates of the salts are left behind in that temperatures [Mahalakshmi et al. 2012].

5.2.5 Photoluminescence Studies

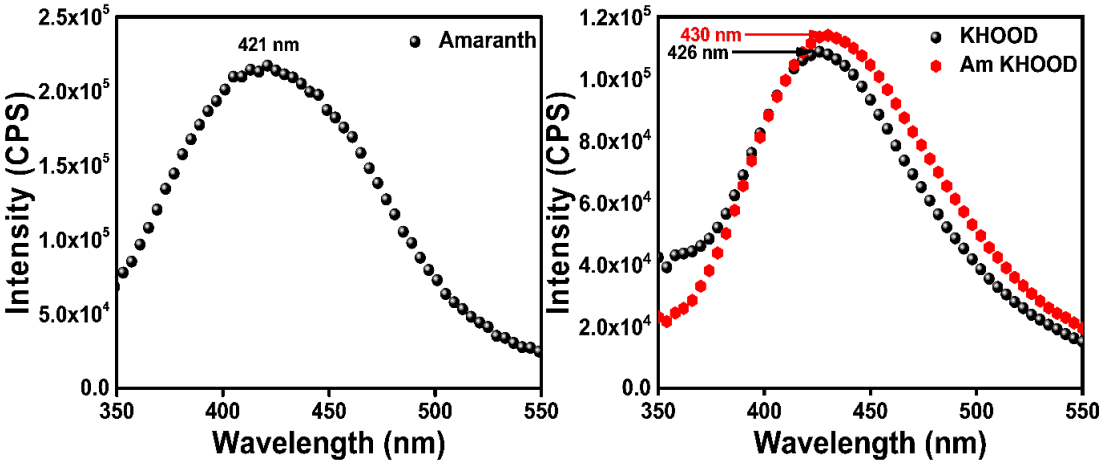

Figure. 5.9. Emission spectra of Amaranth dye, KHOOD and 0.1 mM Amaranth dye doped KHOOD crystal.

The emission properties of Amaranth dye, KHOOD and Amaranth dye doped crystal is studied using Horiba Scientific-Fluoromax-4 spectrophotometer TCSPC. All the samples are excited by 320 nm wavelength and the emission is measured in between 350 – 550 nm. It was observed that the amaranth dye doped KHOOD crystal shows enhanced emission when compared with the KHOOD crystal. In order to understand this behavior, we have also recorded the emission spectrum of Amaranth dye molecule. It was observed that the emission intensity of dye molecule is higher than that of KHOOD crystal leading to the enhancement in the emission of Amaranth dye doped KHOOD crystal. The enhancement in the emission of the crystal is achieved using doping and such an increase in the emission are desirable for optoelectronic applications.

5.2.6. Field dependent current versus voltage characteristics

Well-polished samples are used to study the current versus voltage response of the material. Custom-made 2 probe setup is used to produce contact from the sample surface. The current versus voltage characteristics are measured in the field range of 0

– 100 V/cm and plotted in Figure. 10. From the Figure. 5.10 it was understood that the crystal shows a linear variation as the applied field is varied and also it is worth noting that the current value is more in the case of dye doped KHOOD crystal as compared to pure KHOOD crystal indicating dye incorporation increased the conductivity of the crystal by effectively occupying the defect sites. The field dependent current characteristics also corroborate with the bandgap of the crystal. The bandgap of dye doped crystal is lesser than the pure KHOOD crystal and which reflected in the IV measurements, where conductivity increased for dye doped KHOOD crystal. The enhanced conductivity for the doped crystals are the necessary criteria for using these materials for industrial applications.

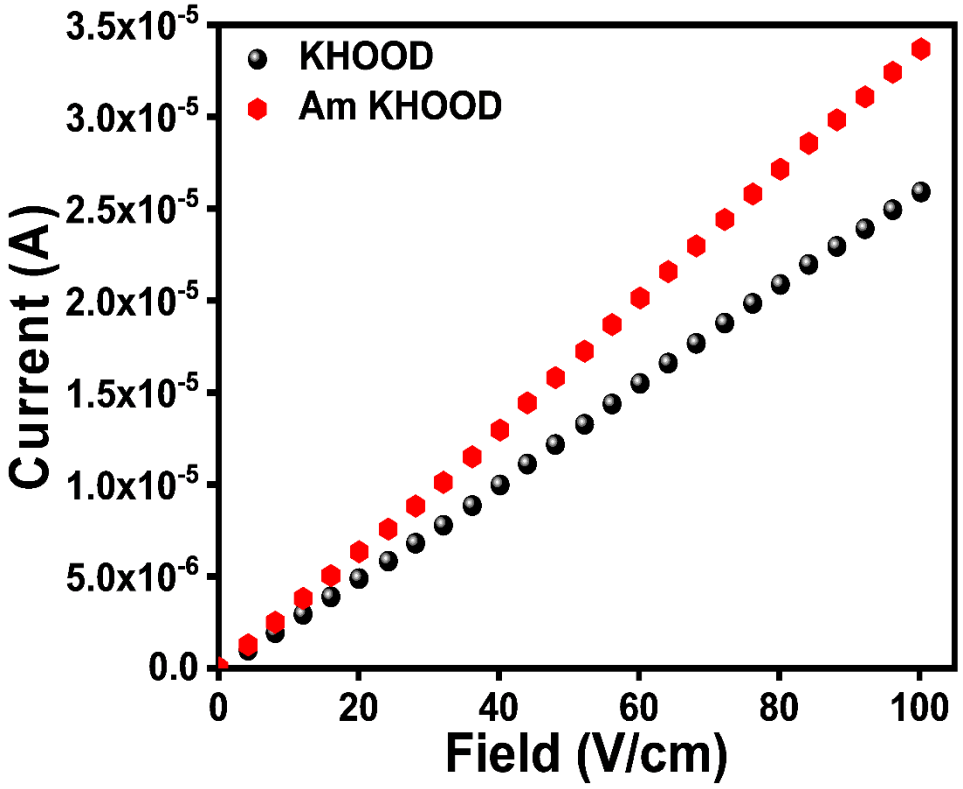

Figure. 5.10. Field dependent current characteristics of KHOOD and 0.1 mM Amaranth dye doped KHOOD crystal.

5.3 Conclusions

KHOOD single crystals were successfully doped with amaranth dye molecules and the results are presented systematically. It was observed that the dye incorporation in KHOOD matrix retained the KHOOD crystal structure. The extra absorption peak observed for the doped crystal was also present in the absorption spectrum of amaranth

dye indicating incorporation of dye molecules in KHOOD lattice. The optical bandgap of KHOOD crystal was observed to be 4.08 eV and that of dye doped crystal was 4.04 eV. Increased surface roughness was obtained for the dye doped crystals implying the presence of larger molecules of dye molecule in the crystal is the reason behind the roughness obtained. From the thermal studies, the melting point of the crystal shifted slightly and the pure crystal is stable at higher temperatures. Enhanced and broader emission was noticed for dye doped KHOOD crystal with emission peak of 426 nm and 430 nm for pure and amaranth dye doped KHOOD crystal, respectively. The dye incorporation resulted in subsequent increase in the conductivity of the crystal for the applied fields and supported the bandgap calculations. Hence, reasonable enhancement is observed when the crystal is doped with dye molecule that promises usefulness of these crystals for optoelectronic applications.

CHAPTER 6

Gamma irradiation effect on structural, optical and electrical properties of organometallic potassium oxalate oxalic acid dihydrate single crystal

Overview

In this chapter, gamma irradiated effect on the optical, structural and electrical properties of potassium hydrogen oxalate oxalic acid dihydrate ($KH_3(C_2O_4)_2.2H_2O$) single crystals is discussed.

6.1 Introduction

Metalorganic single crystals are gaining importance because of the applications in the field of optoelectronic industries [Ramki and Ezhil Vizhi 2017b]. Organic materials possess good optical properties but its mechanical and thermal stabilities are very less [Rajasekaran et al. 2001b V. Kannan 2004 Ruby Nirmala and Thomas Joseph Prakash 2013b]. Inorganic materials possess higher mechanical strength and can sustain more heat [Shakila and Kalainathan 2015]. Growing organic crystals into bigger size is difficult but inorganic materials can be grown into bigger sizes. The merits and demerits from the organic and inorganic materials have led to the development of a class of material where a metal atom is combined with organic molecules to overcome the drawbacks of each. The optoelectronic materials need to work in the strong external fields of ionizing radiations. In the space, these materials need to work in the presence of high-energy photons (> 30 MeV) (space radiations). The high energy radiations in space can damage the material by ionizing the atoms and changing the structural properties of the materials [Raju et al. 2016]. Understanding the effects of high energy radiations are of importance to study the usage of materials in space, to sustain these high energy radiations and to avoid the changes in the properties in a radiation rich environment. The heavy ions and gamma irradiation on crystalline materials changes the physical, optical, electrical properties of the materials [Kanagasekaran et al. 2008, 2010 Ahlam et al. 2012a]. The degradation mechanism, the resistance towards the high energy radiations and the lifetime of the material in the presence of radiation environments were studied using irradiating the samples with high energy radiations, at present gamma irradiated crystals were investigated. In recent years the optoelectronic materials are gaining importance because of its potential application in

the space fields such as space based light detecting systems, orbital space missions and space based ranging systems [Dong et al. 2007 Ahlam et al. 2012b].

In the present work, single crystals of triclinic organometalic KHOOD were grown using slow evaporation technique at room temperature. The grown crystals were irradiated using Co-60 gamma radiation in the total doses ranging from 5 kGy to 20 kGy. For the first time, we report the effect of gamma irradiation on the optical, structural and electrical properties of the grown KHOOD single crystals.

6.2 Results and discussions

6.2.1 Powder XRD

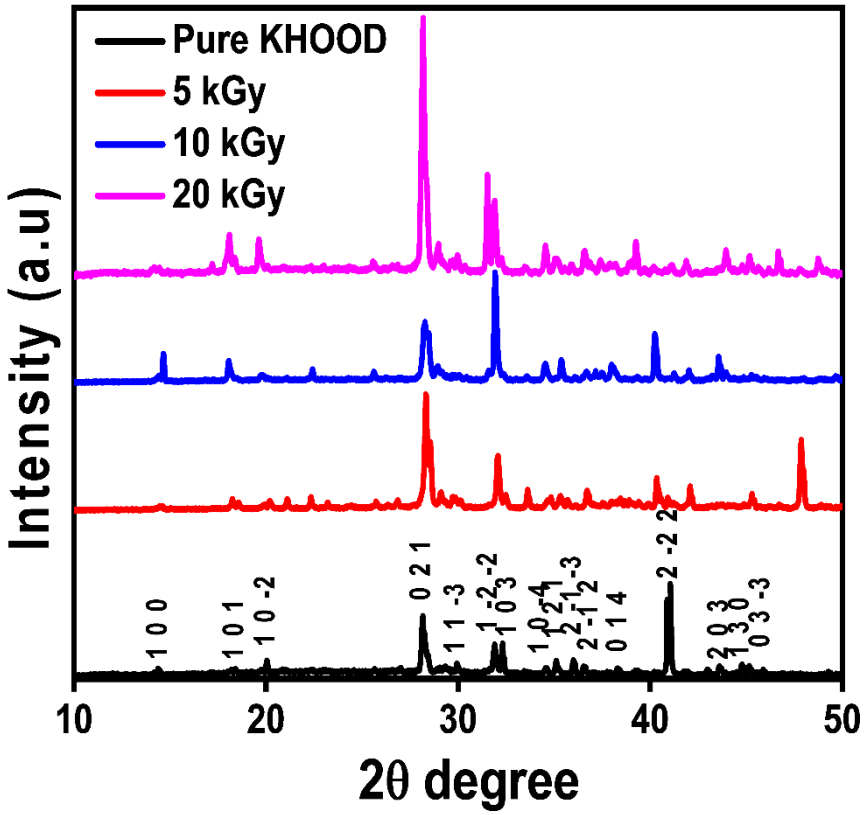

Figure. 6.1. Powder XRD pattern of pure and Gamma irradiated KHOOD single crystals.

Pure and Gamma irradiated crystals were characterized using powder X-Ray diffraction analysis to study the impact of irradiation on the structural properties of the crystals with the increased irradiation dosage. The diffraction pattern obtained are shown in Figure. 6.1. The peaks corresponding to the particular Braggs angles of (0 2 1), (1 -2 -2) and (1 0 3) have evoked out as the prominent one in the pure KHOOD crystal. However, the observed XRD peak intensities of the irradiated crystals with

respect to the unirradiated crystal there is a change in intensity and the intensity was increased as the irradiation dosage increased. From the intensities of the peaks obtained from the powder XRD peaks it is evident that the crystallinity of the materials was increased after the irradiation and maximum crystallinity was observed for the 20 kGy irradiated KHOOD single crystals. It was also noted that the peak intensities were shifted slightly when compared with the pure crystal inferring the possibility of the crystal strain inside the lattice due to the defects created and there is no phase change is observed after irradiation [Virk et al. 2001 Ahlam et al. 2012b Raju et al. 2016]

6.2.2 Scanning electron microscopy (SEM) analysis.

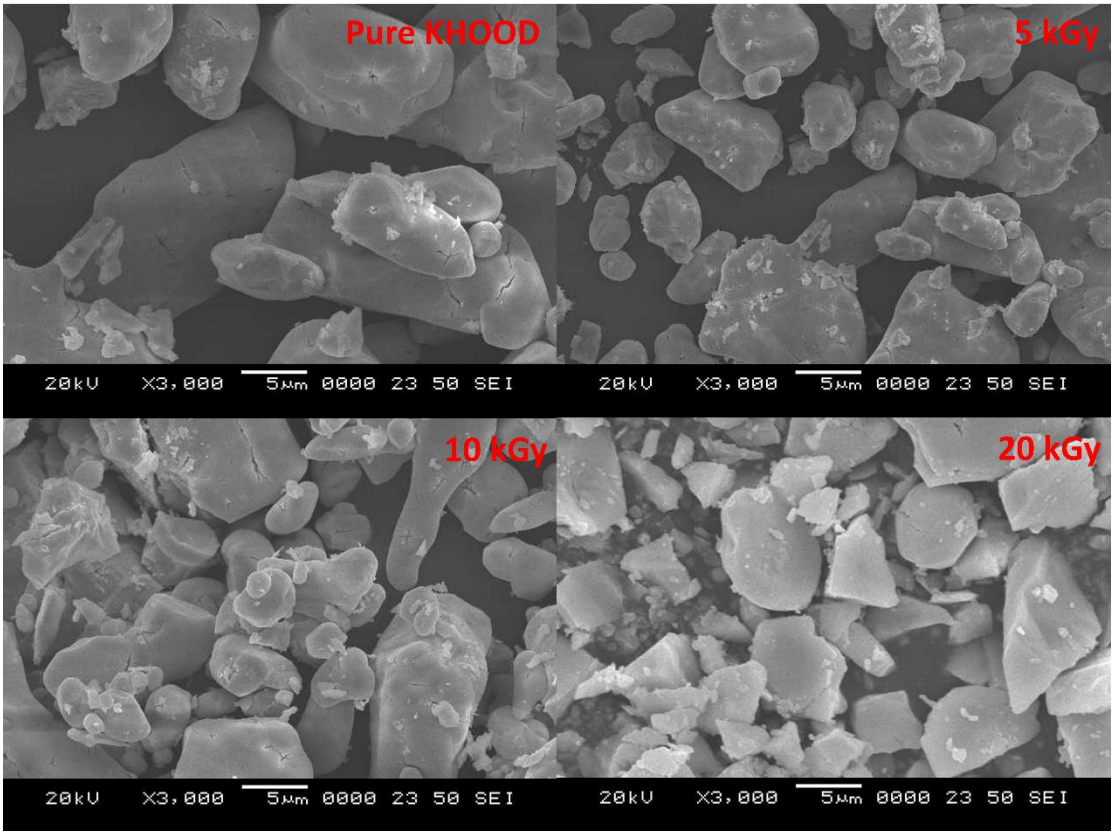

Figure. 6.2. SEM images of pure and irradiated KHOOD single crystals.

The synthesized crystals were crushed and the powders were studied structurally using SEM analysis which is shown in Figure. 6.2. The darker and brighter areas observed in the SEM images are attributed to solvent inclusions, which can be observed commonly in crystals grown from solvent evaporation techniques [Sorescu et al. 1995 Ahlam et al. 2012a]. There is a gradual increase in the crystallinity of the samples as the radiation dosage is increased from 5 kGy to 20 kGy as confirmed from

powder XRD and SEM analysis. Further, the increase in crystallinity has also affected the optical and electrical parameters as described below.

6.2.3 Optical Studies

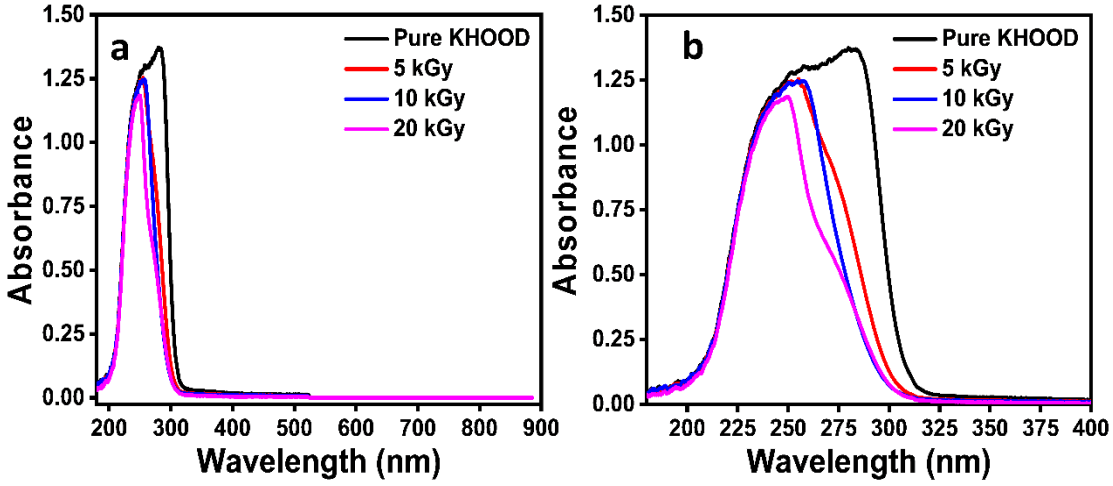

Figure. 6.3. (a) UV-vis absorption (b) Enlarged image of UV-vis absorption of pure and Gamma irradiated KHOOD single crystals.

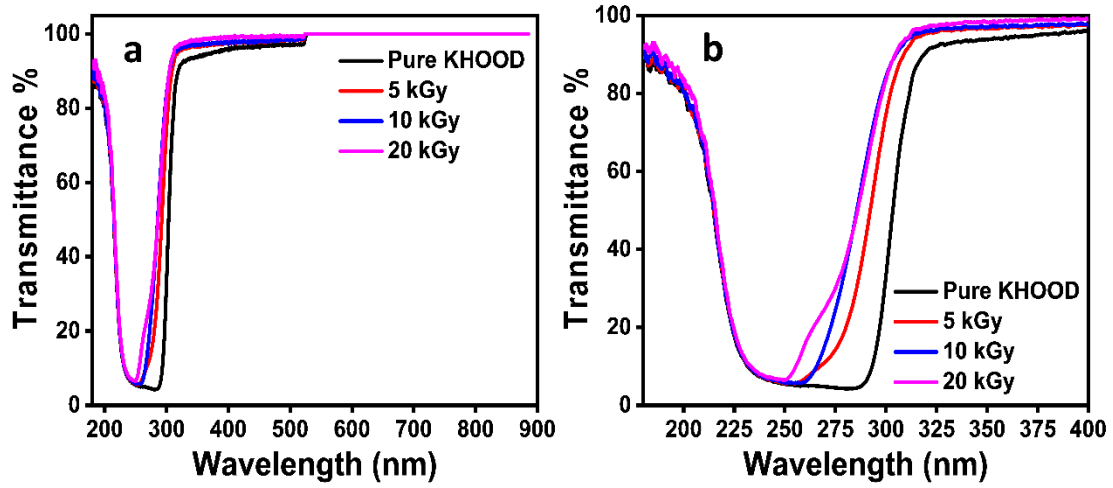

Figure. 6.4. (a) UV-vis transmittance (b) Enlarged image of UV-vis transmittance spectra of pure and Gamma irradiated KHOOD single crystals.

The absorbance and transmittance spectrum were recorded for pure and gamma irradiated crystals. Figure. 6.3 gives the absorption spectrum of pure and gamma irradiated KHOOD crystals. It was noticed that the absorption peak is slightly shifted towards the lower wavelength region as the dosage of gamma irradiation increased.

For pure KHOOD crystal there is an absorption peak at around 279 nm and the irradiated crystals show absorption peaks at around 255 nm, 257 nm and 249 nm for 5, 10, 20 kGy gamma irradiated crystals respectively. Figure. 6.4 shows the transmittance

spectrum for pure and gamma irradiated KHOOD crystals. Pure as well as irradiated KHOOD exhibit a good transmittance in the visible region. In the transmission spectrum, the cutoff wavelength decreases slightly to lower wavelength region indicating the increment in the transmission in the visible region which is the necessary condition for the application of the crystals in the optoelectronic industries.

6.2.4 Optical Constants Determination

Absorption coefficient is defined as the reduction in the intensity of incident light per unit distance in the absorption medium [Bincy and Gopalakrishnan 2014a].

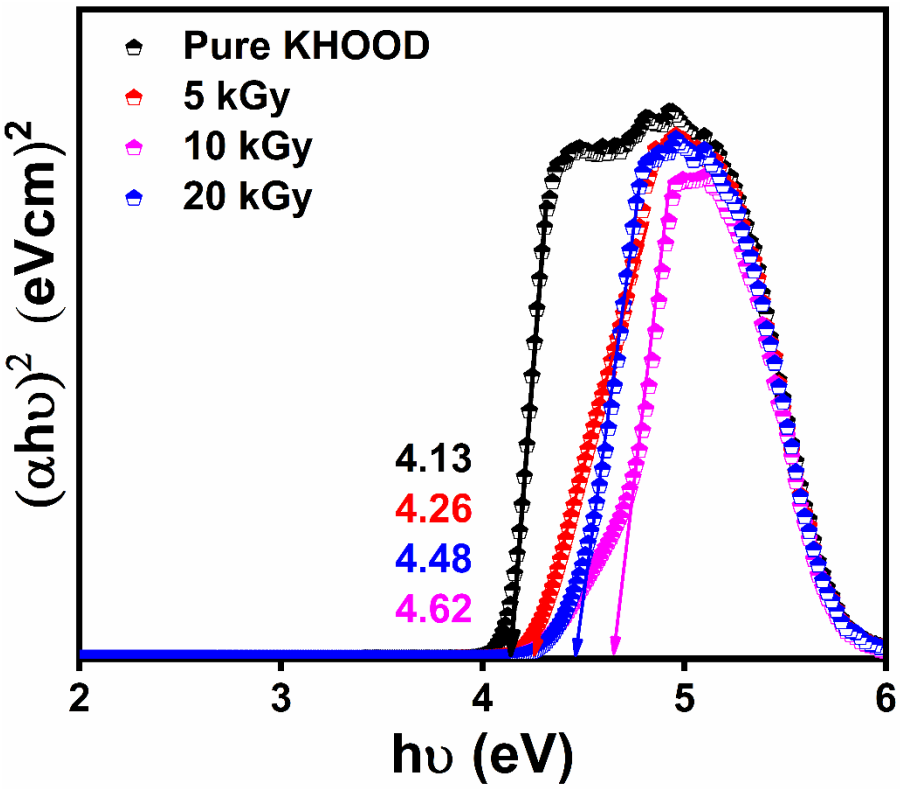

Figure. 6.5. A plot of $(\alpha h\nu)^2$ versus hν.

From the Tauc's relation (Equation 2.2) the optical bandgap can be determined by extrapolating the linear portion of Tauc's plot, a graph of $(\alpha h\nu)^2$ versus photon energy (hν). The bandgap of pure KHOOD crystal is found to be 4.13 eV as shown in Figure. 6.5 and it increased for the irradiated crystals as 4.26 eV, 4.48 eV and 4.62 eV for the 5, 10, 20 kGy gamma irradiated crystals.

Extinction coefficient of the crystal is also calculated using the Equation 2.4. And it is the amount of intensity decreased as the electromagnetic radiation travels through the material. It is directly related to the absorption coefficient as [Job et al. 2016b Shanthi

et al. 2016b],

The Extinction coefficient is plotted with respect to the wavelength and given in Figure. 6.6. It was noted that the light loss is more in the UV region and less in the visible region. The light loss is in the order of 10^{-6} indicating the light loss is negligible [Theras et al. 2016].

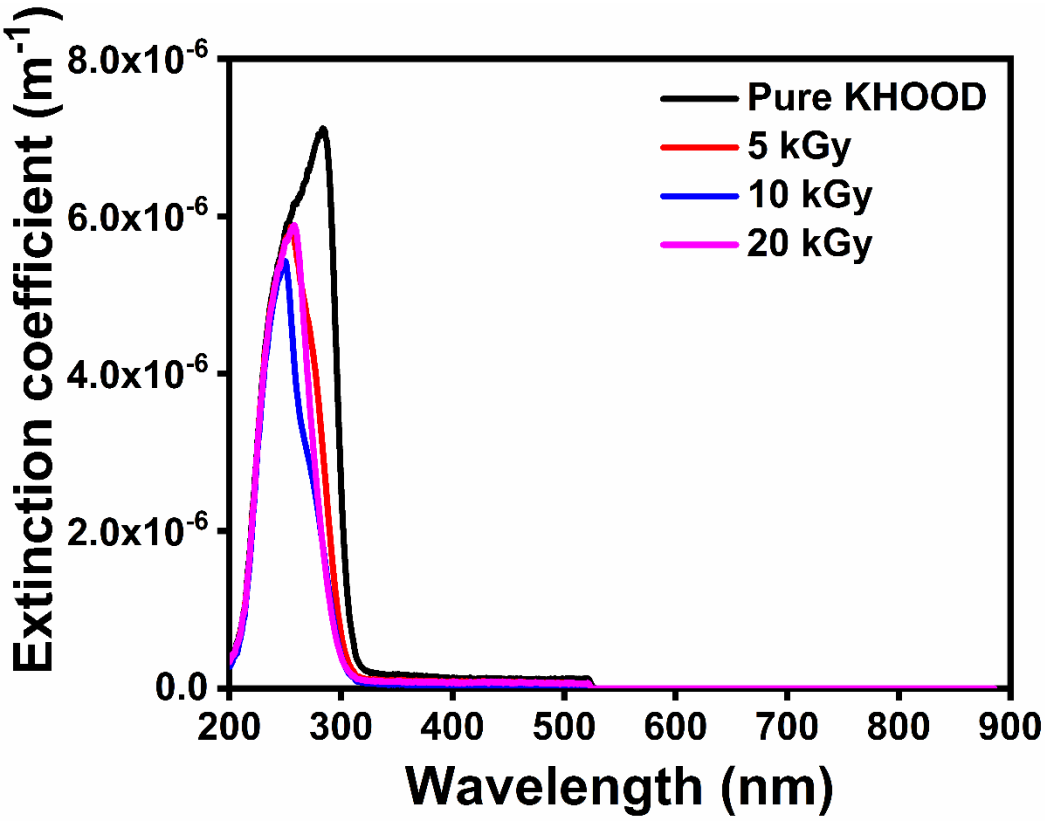

Figure. 6.6. Extinction coefficient versus wavelength.

6.2.5 FTIR analysis

The effect of gamma irradiation on the fundamental molecular vibrations of KHOOD single crystals were studied using FTIR spectroscopy, which is sown in Figure. 6.7. The stretching frequency of 3432 cm^{-1} can be attributed to the O-H stretching frequencies and conformation of water in the structure of KHOOD by the peaks of 3012 cm^{-1} and 1627 cm^{-1} peaks present because of stretching and bending vibrations [Mahalakshmi et al. 2012 Vimal et al. 2014]. Symmetric and asymmetric stretching of C=O was confirmed by the peak is present at 1705 cm^{-1} and 1627 cm^{-1} [Pasupathi et al. 2014]. The presence of metal oxygen bond was observed at the peaks obtained at 1401 cm^{-1}, 1219 cm^{-1} and 795 cm^{-1} [Ezhil Raj et al. 2008 Pasupathi et al. 2014 Chandran et al. 2017]. The presence of C-C stretching vibrations were attributed

to the peaks present at 1114 cm^{-1} and 913 cm^{-1} [Mahalakshmi et al. 2012]. Compared to the pure KHOOD crystals the irradiated crystals show small variations in the peak positions indicating that the crystal structure is not altered rather strain induced in the crystal lattice after irradiation [Raju et al. 2016]. The assignment of the peaks compared with the irradiated crystals are tabulated in the Table. 6.1.

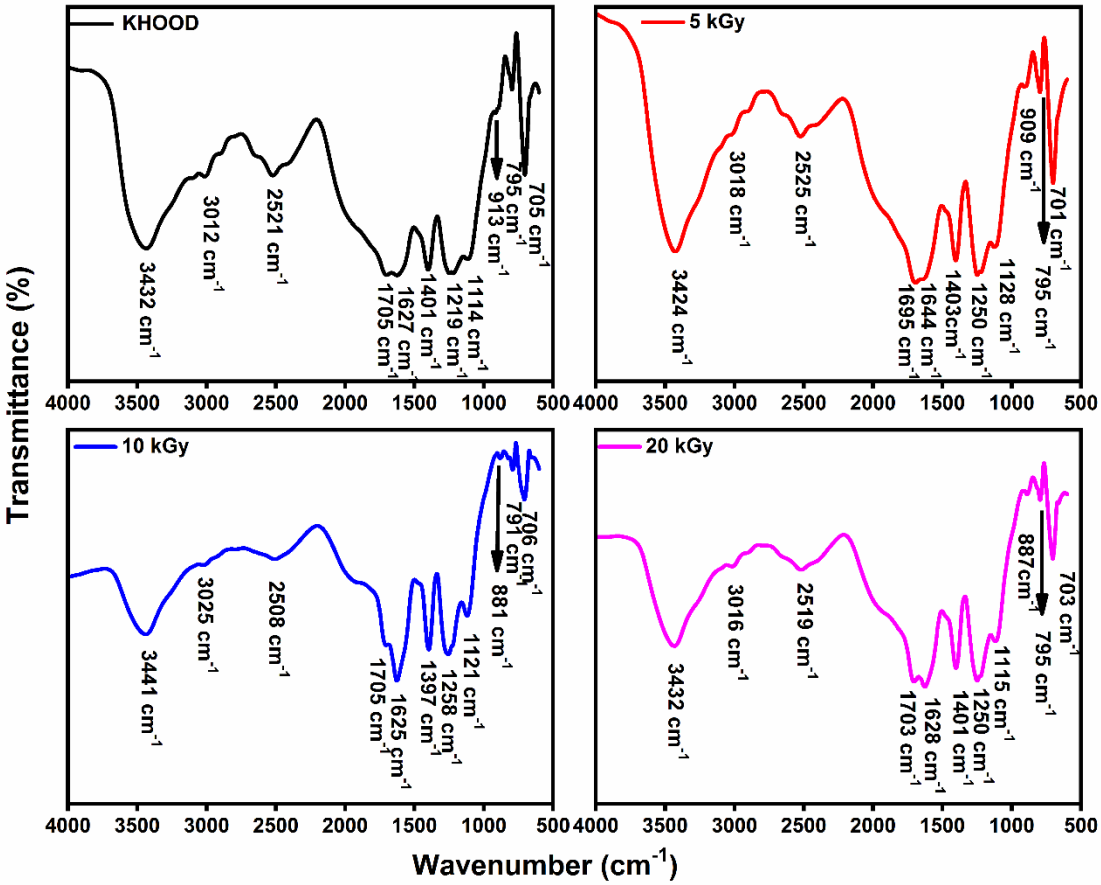

Figure. 6.7. FTIR spectrum of the pure and irradiated KHOOD single crystals.

Table. 6.1. FTIR vibrational assignments of pure and irradiated KHOOD single crystals.

KHOOD	5 kGy	10 kGy	20 kGy	Assignments
3432	3424	3441	3432	OH stretching
3012	3018	3025	3016	H_2O symmetric and asymmetric stretching
1705	1695	1705	1703	C=O stretching
1627	1644	1625	1628	C=O asymmetric stretching and H_2O

				bending
1401	1403	1397	1401	K-O asymmetric stretching
1219	1250	1285	1250	C-O stretch or K-O asymmetric stretching
1114	1128	1121	1115	C-C stretching
913	909	881	887	C-C stretching
795	795	191	795	K-O ring stretching
705	701	706	703	O-C=O deformation

6.2.6 Photoluminescence

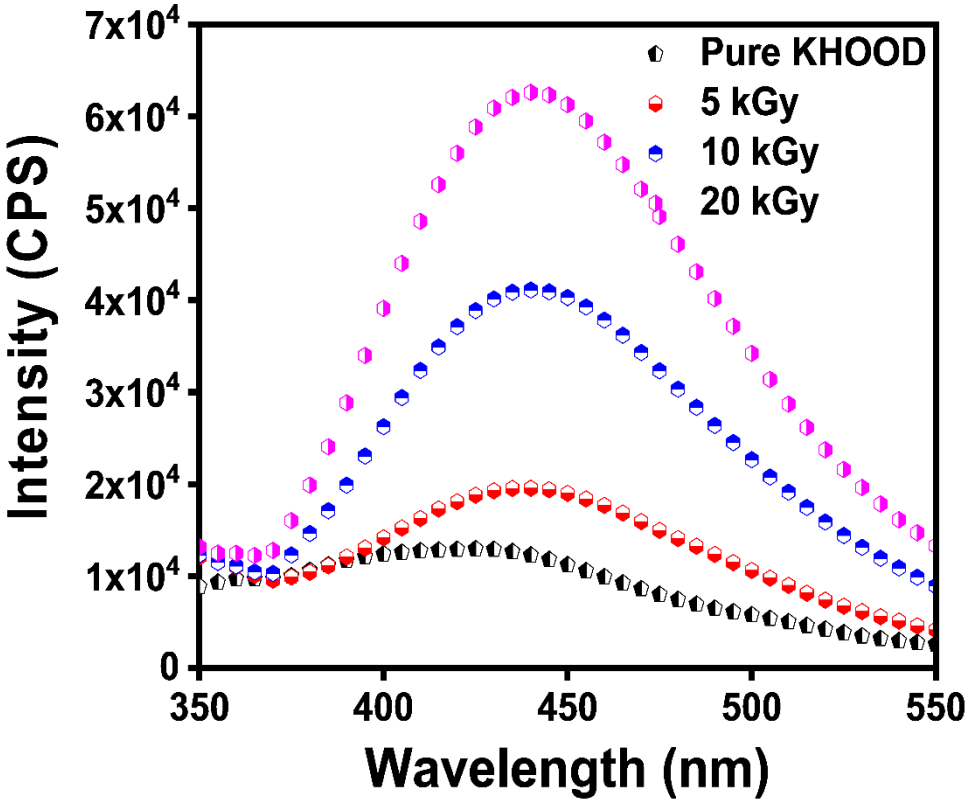

Figure. 6.8. Photoluminescence spectra of pure and irradiated KHOOD single crystals.

The photoluminescence spectra of pure and irradiated KHOOD crystals were shown in Figure. 6.8. All samples were excited at 280 nm and the emission spectrum was recorded in the region of 340 nm to 550 nm. PL spectrum reveals the enhancement in the intensity of peaks as the gamma irradiation dosage increased. The crystal also shows shift in the peak position and the peaks were observed at 390 nm, 401 nm, 403 nm and 404 nm for pure, 5, 10 and 20 kGy gamma irradiated crystals. All the crystals

emit in the UV and blue region of the electromagnetic spectrum and the emission peaks were attributed to the delocalization of the O-C=O bond of oxalic acid [Dalal and Kumar 2016].

6.2.7 IV studies (Photo conductivity)

The synthesized crystal was polished on both sides to maintain the uniform thickness throughout the sample to study the conductivity and resistivity of the crystal using I–V characteristic curve. The I–V characteristics of the crystal was studied in the dark and the presence of light which is shown in the Figure. 6.9 and Figure. 6.10. Thus I–V curves are plotted using the measured current and the applied field. From the I–V curve electrical resistance of the crystal was calculated. The dc electrical resistivity (ρ_{dc}) of pure and irradiated crystals are obtained by the relation, ρ_{dc} = RA/d [Freeda and Mahadevan 2000], where, R is the measured resistance, d is the thickness of the sample and A is the area of contact. Using the resistivity relation, the conductivity of the crystal was calculated and tabulated in Table 6.2 and 6.3. The resistivity of the pure and irradiated KHOOD crystal was observed to be in the order of 10^4 Ω.m and the conductivity of the crystal was found to be in the order of $10^{-5}\,\Omega^{-1}m^{-1}$. As the irradiation dosage increased the crystal conductivity decreases which in turn lead to increase in its resistivity which is also true in case of light irradiated crystals. Interestingly, for 20 kGy irradiated crystals, the field dependent dark and photo current values were almost identical. Which may be due to the drastic increment in the crystallinity of the KHOOD crystal for 20 kGy gamma irradiation. The improved crystallinity reduces the phonon loss in the material and lead to the decrement in the photoresistivity value.

It was observed that photocurrent is less than the dark current for both pure and irradiated crystals at every applied electric field. Generally, the photo resistive behavior is being attributed to the loss of water molecules when irradiated with intense light. The photo resistive behavior may also be due to the decrease in charge carriers in the conduction band when irradiated with light and also due to the decrease in lifetime of the material [Ashraf et al. 2004b].

The reduction in lifetime of the crystals is the presence of radiation can be attributed to the trapping and the increase in the carrier velocity, which can be explained using the Equation 6.1.

$$\tau = (vsN)^{-1} \qquad 6.1$$

where, s is the capture cross-section of the recombination centers, v is the thermal velocity of the carriers and N is the carrier concentration.

When the external photon with sufficient energy and intensity hits the material, their lifetime decreases. The generated electron hole pair in the materials will recombine these itself in the presence of intense light. Due to the recombination process the charge carriers decreased leading to less conductivity in the presence of radiation. Figure. 6.11. shows the field dependent I-V curves for dark and illuminated conditions. At room temperature, the current increases linearly for every applied field for the crystals in dark and illuminated condition. The field dependent I-V curves for all the irradiated crystals show negative conductivity under illuminated condition. The trapping of electrons inside the crystals are due to the defect states created inside the crystals owing to the gamma irradiation. The negative photo conductivity is also explained according to the Stockmann model which states that the forbidden gap in the materials will hold two energy levels. One is situated in between the conduction band and the fermi level and the other band is located near to the valance band. The band located near valence band contains high capture cross section for holes and electrons. The electrons from the conduction band and the holes from the valence band are captured in this state and the number of charge carriers gets reduced in conduction band which led to the decrease in conductivity in the presence of intense radiation.

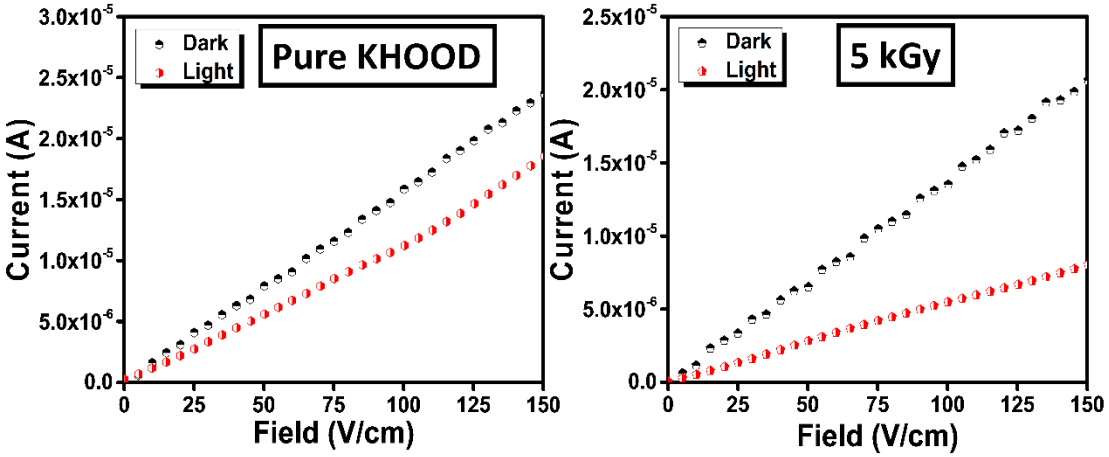

Figure. 6.9. Photoconductivity graph of pure and 5 kGy irradiated KHOOD single crystal.

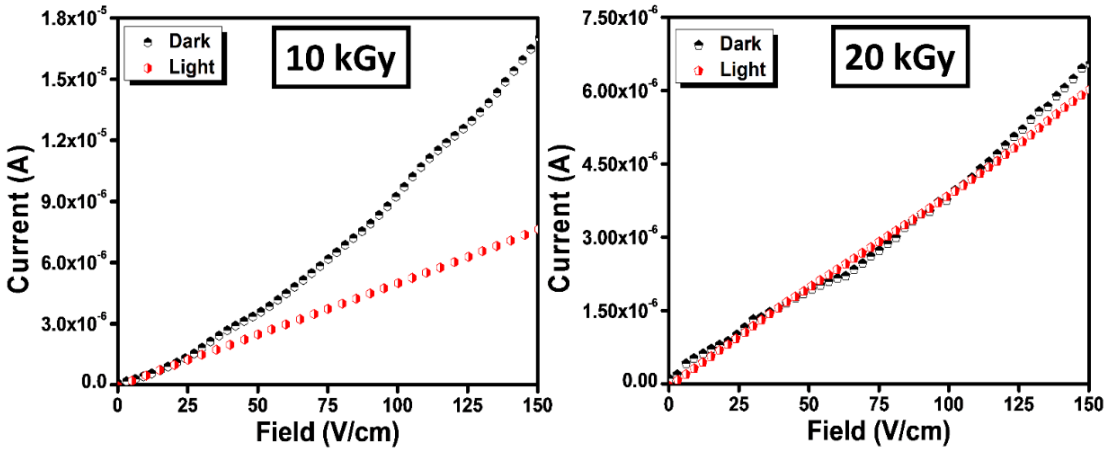

Figure. 6.10. Photoconductivity graph of 10 kGy and 20 kGy irradiated KHOOD single crystal.

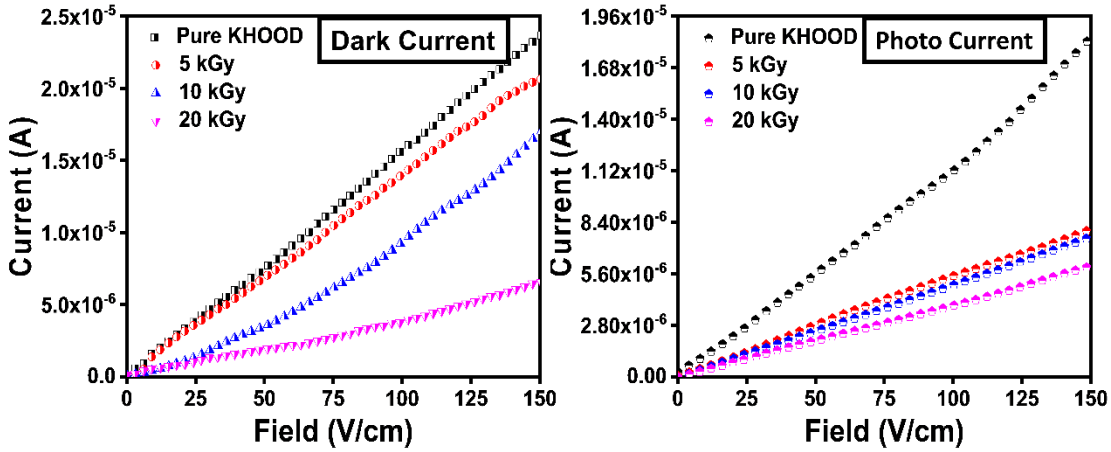

Figure. 6.11. I-V curve of crystals in dark and photo current of pure and irradiated KHOOD single crystals.

Table 6.2. Resistivity and conductivity of the pure and irradiated KHOOD single crystals in dark condition.

Name	**Resistance (Ω)**	**Resistivity (Ω.m)**	**Conductivity $(\Omega.m)^{-1}$**
KHOOD	6.30×10^{6}	1.78×10^{4}	5.61×10^{-5}
5 kGy	7.20×10^{6}	2.03×10^{4}	4.90×10^{-5}
10 kGy	8.76×10^{6}	2.47×10^{4}	4.03×10^{-5}
20 kGy	2.36×10^{7}	6.67×10^{4}	1.49×10^{-5}

Table 6.3. Resistivity and conductivity of the pure and irradiated KHOOD single crystals in the presence of light.

Name	**Resistance** (Ω)	**Resistivity** (Ω.m)	**Conductivity** $(\Omega.m)^{-1}$
KHOOD	8.37×10^{6}	2.36×10^{4}	4.22×10^{-5}
5	1.87×10^{7}	5.29×10^{4}	1.88×10^{-5}
10	1.97×10^{7}	5.56×10^{4}	1.79×10^{-5}
20	2.52×10^{7}	7.12×10^{4}	1.40×10^{-5}

6.3 Conclusions

Grown KHOOD single crystals were irradiated with gamma radiation in the dosage of 5, 10, 20 kGy. The powder XRD studies of the single crystal confirm the crystalline nature of the sample. Small shift in the position of peaks is due to the creation of defect states, inducing stress in the crystal lattice. However, the small shift observed in the peak positions of XRD and FTIR spectra signifies that the crystal structure remains unaltered even after the irradiation process. Furthermore, in the transmission and absorption spectra, we have observed a peak shift towards lower wavelength region, indicating the widening of the transmission window with the irradiation process. Light induced I-V studies on pure and irradiated KHOOD crystals exhibit negative photoconductivity phenomenon. The resistivity of the pure and irradiated KHOOD crystal is observed to be in the range of 10^4 Ω.m. It is also observed that resistivity of the crystal increases for both gamma and light irradiation process. On fine-tuning the material properties of the studied crystals, we can use them for light dependent resistor (LDR) and space applications.

CHAPTER 7

Growth and comparative studies on Oxalic acid dihydrate, Potassium oxalate hydrate and Potassium hydrogen oxalate oxalic acid dihydrate single crystals

Overview

In this chapter, the single crystals of potassium oxalate oxalic acid dihydrate ($KH_3(C_2O_4)_2.\ 2H_2O$) is compared with oxalic acid dihydrate ($(C_2O_4)_2 \cdot 2H_2O$) and potassium oxalate hydrate ($K_2(C_2O_4)_2 \cdot H_2O$) single crystals. Structural, optical, thermal and electrical properties of the crystals are compared and discussed in detail.

7.1 Introduction

Organic optoelectronics is evolving rapidly due to certain unique properties of associated devices such as light weight, good performance, low cost and process abilities [Tao et al. 1992 Pan et al. 1996 Usharani et al. 2016]. Organic single crystals have extremely good crystallinity, unprecedented structural order and very low impurity content. Organic optical materials show superior properties when compared with the inorganic materials in terms of their high nonlinearity, speed response and non-hygroscopic nature [Arivanandhan et al. 2005]. Further, Organic crystals are potential candidates for the device fabrications of organic field effect transistors, sensors, smart tags, frequency converters and light emitting diodes [Usharani et al. 2016]. Even though organic materials possess excellent optoelectronic properties, because of their poor thermal stability, inability to grow into large sizes, poor chemical and mechanical stability, device fabrications for industrial applications are still limited [Long 1995 Krishnan et al. 2008]. Whereas, inorganic materials possess better thermal stability and higher mechanical performance [Albert Irudayaraj et al. 2014]. The drawbacks of organic and inorganic materials have led to development of a new class of hybrid materials which consists of organic-inorganic hybrid compounds labelled as metalorganics or semiorganics, which revolutionized optoelectronic industries [Anbuselvi et al. 2014 Mahendra et al. 2019].

Hence, attempts have been focused in the direction of synthesizing a hybrid class of organic-inorganic combined materials, because of their interesting properties and widespread applications [Batten and Robson 1998 Yaghi et al. 1998]. In this regard, numerous attempts were carried to synthesize the hybrid materials using different

chemical synthesis methods such as hydrothermal treatment and ion exchange reactions [Pinnavaia 1983]. The ion exchange reaction is an extensively used technique to synthesize these materials where, the starting material A–B possess covalent framework, in which A is weakly bonded with the ion B, such materials can be easily exchanged via a solid-liquid reaction via organic ion. The exchange reaction leads to the formation of hybrid materials with the inorganic–organic combined complexes, which consists of parent molecule bonded with the combined molecules [Rebbah et al. 1980 Clearfield 1982]. In the hydrothermal synthesis the materials are placed inside the Teflon jar and high pressure is created by means of applying temperature and kept for couple of hours to form organic-inorganic hybrids. Organic materials play a major role in formation of hybrid compounds [DeBord et al. 1996 Serpaggi and Férey 1998].

Metal-organic hybrids have attracted many researchers to develop materials in field of crystal engineering due to their vast applications such as in high ionic or mixed conductors, solid-state batteries, sensors, capacitors, photovoltaic cells, electroluminescent diodes, electrochemical transistors and so on [Zhang et al. 2002 Sanchez et al. 2005 Matulková et al. 2012 Chouaib et al. 2016]. In view of this, significant interest in the synthesis of metal-organic materials due to their increased thermal stability, higher mechanical stability, high resistance to laser-induced damage and good optical properties [Zhang et al. 2008 Bright and Freeda 2010 Anis et al. 2014 Rajagopalan and Krishnamoorthy 2017]. In this system, metal-organic hybrid compounds were repeatedly studied by their explicit chemical physical properties, like ferroelectric transitions or magnetic, electrical properties, conductivity, electro-luminescence and photoluminescence [Bator et al. 2001 Wojtaś et al. 2004]

Oxalic acid is an interesting organic matrix modifier and its salts are of significant importance due to its interaction on human body, plants, animals and micro-organisms. Oxalic acid is a compound produced naturally inside living body when glycine and ascorbic acid metabolized. The metabolism of oxalic acid in man [Takasaki and Naito 1968 Stewart 2011] and accumulation of oxalate in plants [Yang and Loewus 1975] have been explained. Oxalic acid exists in anhydrous and dehydrated forms. Oxalic acid links to the metal atoms and forms stable metal oxalates. Crystals of oxalic acid and metal oxalates can be obtained in the crystal form with the known structure. Oxalic acid

finds applications in biological, geological and industrial applications. Metal oxalates are of interest due to its stable complex formations with the metal ions. Oxalates find applications in technical and medical fields such as stain removal in photography, coatings of metals for stainless steel, chromium, titanium, nickel and their alloys, process in bleaching and cleaning of natural fibers, dying in textile dyeing industies, anticoagulants in medical tests, and dental seals [Lalia-Kantouri and Manoussakis 1984 Cammi et al. 2003 Goforth et al. 2004 Balazs et al. 2006]. The sodium and potassium salts of oxalic acid are found in many plants (clover, sorrel, salicornia, spinach, rhubarb, bamboo shoots, cacao, roots, and tree barks). Furthermore, salts of complexes (potassium and sodium) are capable to pass the gastric mucous membrane, and consequently the foremost components of kidney stones. However, the long-lasting efforts are made to understand the characteristic physical features of the oxalate anion by means of conventional methods of chemical bonding still continues without closure. Alkali oxalates are of importance in nature and chemistry because of their interesting physical properties, medical and material functions [Lalia-Kantouri and Manoussakis 1984 Cammi et al. 2003 Goforth et al. 2004 Balazs et al. 2006].

In the present study compounds of oxalic acid dihydrate, potassium oxalate hydrate and potassium hydrogen oxalate oxalic acid dihydrate single crystals were grown using solvent evaporation technique. The grown crystals were characterized and compared to estimate physio chemical changes in its optical, structural, mechanical and electrical properties of the crystal.

7.2 Results and discussions

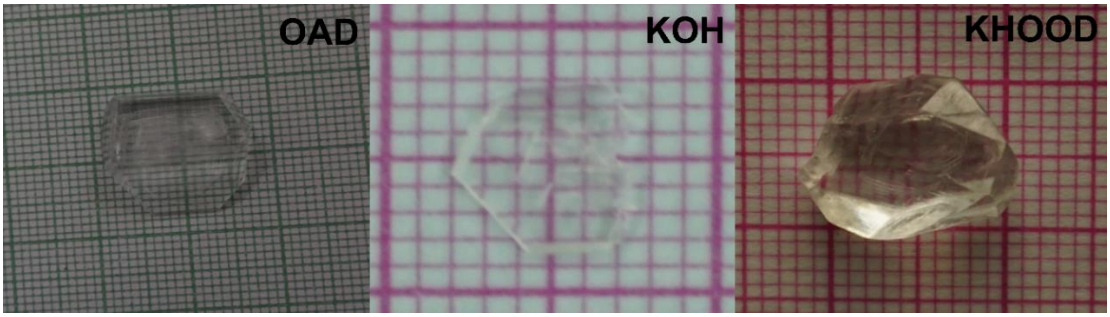

Figure. 7.1. As grown crystals of OAD, KOH and KHOOD crystals.

7.2.1 Single crystal XRD (SCXRD) and Powder XRD (PXRD) measurements

Unit cell parameters of the obtained crystals were studied using SCXRD measurements. The unit cell parameters were explored and tabulated in Table. 7.1. The obtained crystals of OAD, KOH and KHOOD single crystals are observed to be monoclinic ($P2_1/a$), monoclinic (A2/a) and triclinic ($P\bar{1}$) crystal system. The crystal orientation space group and lattice parameters were significantly altered by metal atom complexion with the OAD molecule.

Table. 7.1. The unit cell parameters of the OAD, KOH and KHOOD single crystals.

Crystal structure details	**OAD**		**KOH**		**KHOOD**
Compound	**Oxalic acid**		**Potassium oxalate hydrate**		**Potassium hydrogen oxalate oxalic acid dihydrate**
Formula	$(COOH)_2 \cdot 2H_2O$		$K_2C_2O_4 \cdot H_2O$		$KH_3(C_2O_4)_2 \cdot 2H_2O$
	Experimental	Reported [Iwasaki and Saito 1967]	Experimental	Reported [Hodgson and Ibers 1969]	Experimental
Space group	$P2_1/a$	$P2_1/a$	C2/c	C2/c	$P\bar{1}$
Density	1.63 gm/cc	1.65 gm/cc	2.127 gm/cc	2.14 gm/cc	1.856 gm/cc
a (Å)	11.9000	11.88	10.6840	10.690	6.3632
b (Å)	3.6040	3.60	6.1820	6.197	7.0291
c (Å)	6.1240	6.12	9.226	9.222	10.5984
α	90 º	90 º	90 º	90 º	93.835 º
β	103.3 º	103.5 º	110.77 º	110.70 º	101.358 º
γ	90 º	90 º	90 º	90 º	100.174 º
Volume	255.60	254	569.76	571.5	454.90
Crystal system	Monoclinic	Monoclinic	Monoclinic	Monoclinic	Triclinic

The synthesized crystals were crushed in to fine powders using motor and pestle to study its structural properties using powder X-ray diffraction technique. The indexed XRD patterns for OAD, KOH and KHOOD crystals are shown in Figure. 7.2. The obtained sharp peaks in the diffraction pattern confirms the crystalline nature of the synthesized materials. The XRD peaks obtained for the OAD and KOH crystals are well matching with standard JCPDS patterns. The OAD crystal is matching with the standard JCPDS file number 00-030-0624 and KOH matches with 00-022-1232. It was noticed that the OAD and KOH crystallizes in monoclinic crystal system with $P2_1/a$ and A2/a space group. Whereas, KHOOD crystallizes in triclinic crystals system of $P\bar{1}$ space group.

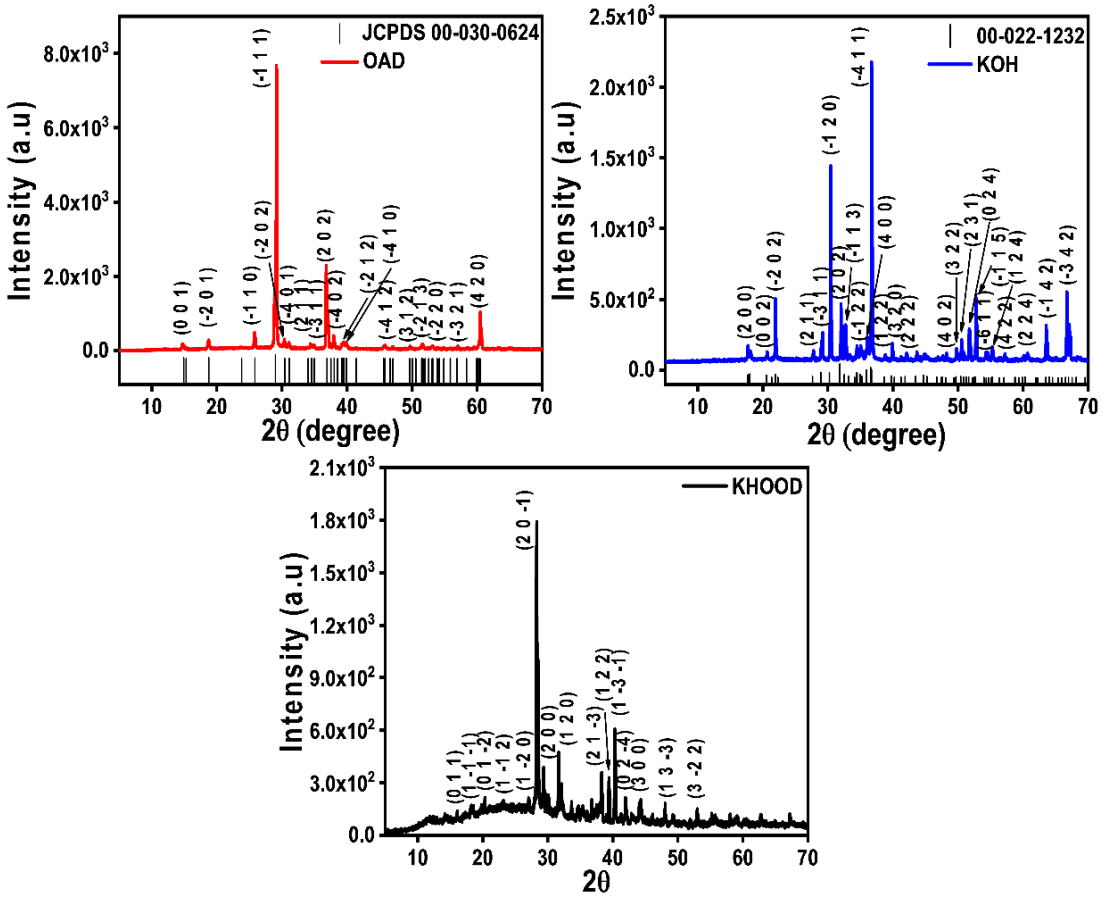

Figure. 7.2. Powder XRD pattern of the OAD, KOH and KHOOD single crystals.

7.2.2 Optical studies

The optical absorption of the OAD, KOH and KHOOD single crystals were studied in the optical range of 200 nm to 900 nm as shown in Figure. 7.3. When a crystal

is exposed to electromagnetic radiation, crystal can absorb a portion of light, can transmit some portion of light and rest is reflected from the surface of the crystal [Job et al. 2016a]. The absorption peaks for the OAD, KOH and KHOOD crystals were measured to be 286 nm, 269 nm and 280 nm. There is only one absorption peak for the crystal in the UV region, which is due to n → π* electron transfer [Bhuvaneswari et al. 2019]. The crystal does not absorb in the visible region, necessary criteria for a material to be applied in optoelectronic industries [Uma and Rajendran 2016].

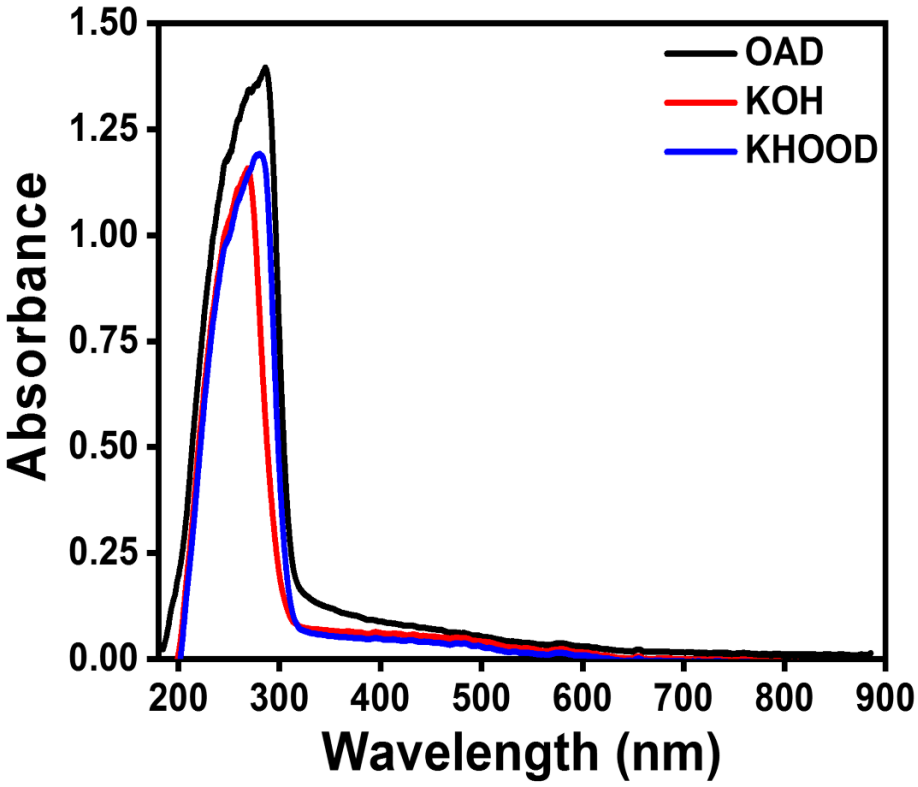

Figure. 7.3. Absorbance spectrum of OAD, KOH and KHOOD single crystals.

7.2.3 Determination of optical constants

Optical study gives information associated with the electronic band structures and compositional nature of the material [Anis et al. 2018b, 2018e, 2018a]. Optical absorption coefficient (α) is a portion of reduction in the energy of incident radiation per unit distance as the incident radiation propagates through the crystal and calculated using the Equation. 2.3

The optical absorption coefficient (α) with respect to photon energy is calculated using Tauc's relation given in Equation. 2.2.

Direct transition is selected and the plot of $(\alpha h\nu)^2$ versus hυ is shown in Figure. 7.4 (a).

Extrapolating the linear portion of the graph, optical band gap E_g is calculated. Band gap is observed to be more in the case of KOH crystal and less for OA crystal and KHOOD comes in between these crystals. The calculated bandgap for OAD, KOH and KHOOD crystals are 4.06, 4.28 and 4.10 eV respectively.

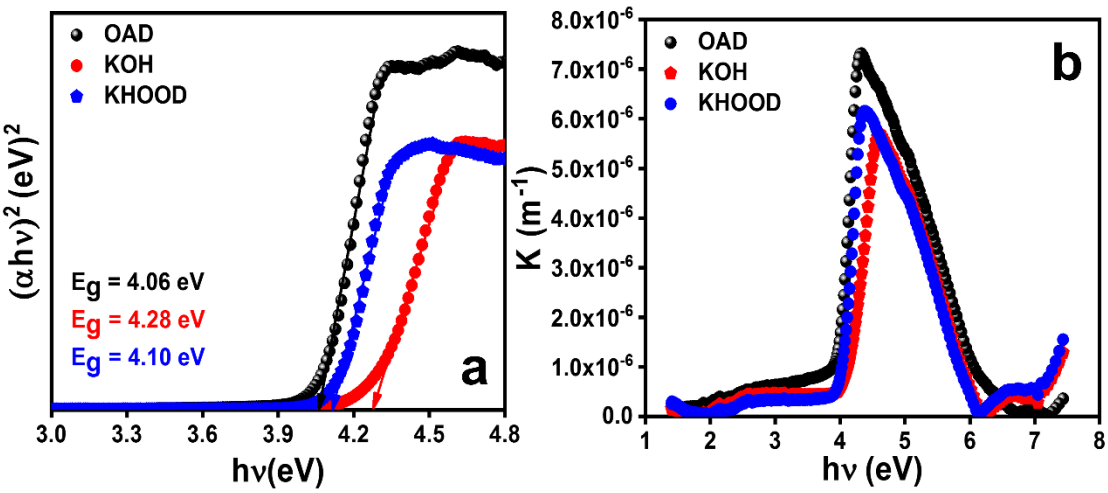

Figure. 7.4. (a) Bandgap (b) extinction coefficient of the OAD, KOH and KHOOD crystals.

Extinction coefficient (K) can be calculated using the absorption coefficient as given by the Equation. 2.4.

It indicates the loss of electromagnetic radiation by means of scattering and absorption during its propagation through the crystal [Bincy and Gopalakrishnan 2014b]. Figure. 7.4(b) shows the variation of extinction coefficient with wavelength. It was noticed that the optical loss is more in case of OAD and less for KOH crystal.

7.2.4 Photoluminescence studies (PL)

Photoluminescence (PL) is an optical phenomenon where the material is excited using optical absorption of light of particular wavelength and then allowed to undergo radiative relaxation [Rajesh et al. 2014 Shanthi et al. 2016a]. The PL emission is sensitive to defect states in a crystal structure and change in local atomic configurations [Goel et al. 2017]. The pure and doped samples were excited at a wavelength of 280 nm and PL emission spectra were recorded in the range 320 nm to 550 nm as shown in Figure. 7.5. The oxalic acid crystal does not show any emission but KOH and KHOOD crystals emits in UV and blue region. Single emission peak observed for the KOH and KHOOD crystals. The emission peak of 399 nm and 430 nm is observed for KOH and KHOOD crystals respectively. The emission intensity is more for KOH crystal when

compared with the KHOOD. And also, KOH crystal emits in broad region when compared with KHOOD crystal. It is worth noting that, KOH and KHOOD crystal emission are observed in the UV and blue region of the spectrum and can be due to delocalization effects of O-C=O bond present in oxalic acid [Dalal and Kumar 2016].

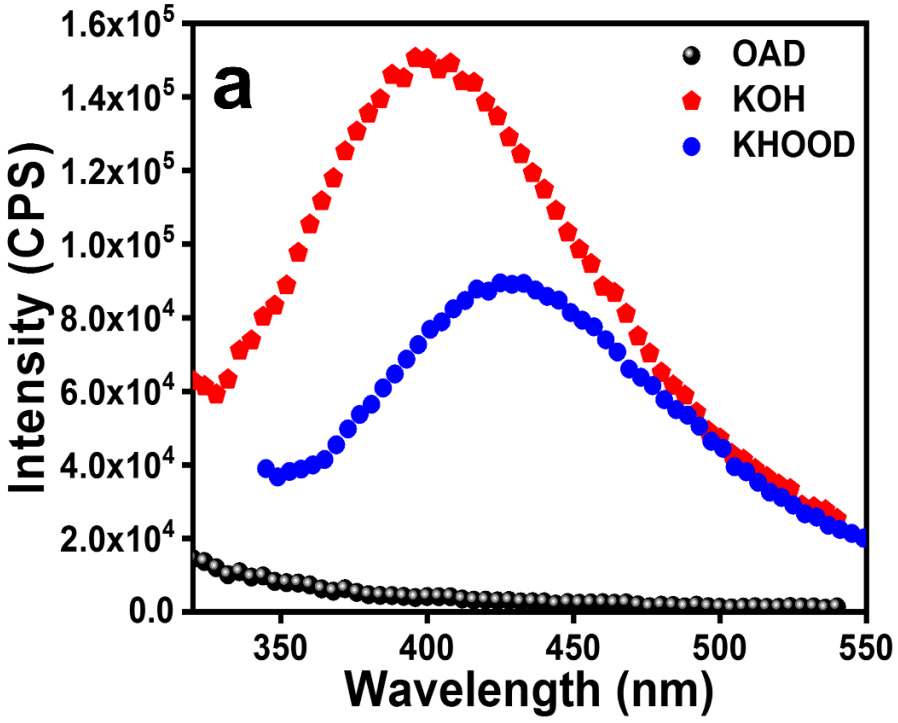

Figure. 7.5. PL spectrum of OAD, KOH and KHOOD single crystal.

7.2.5 TGA-DTA

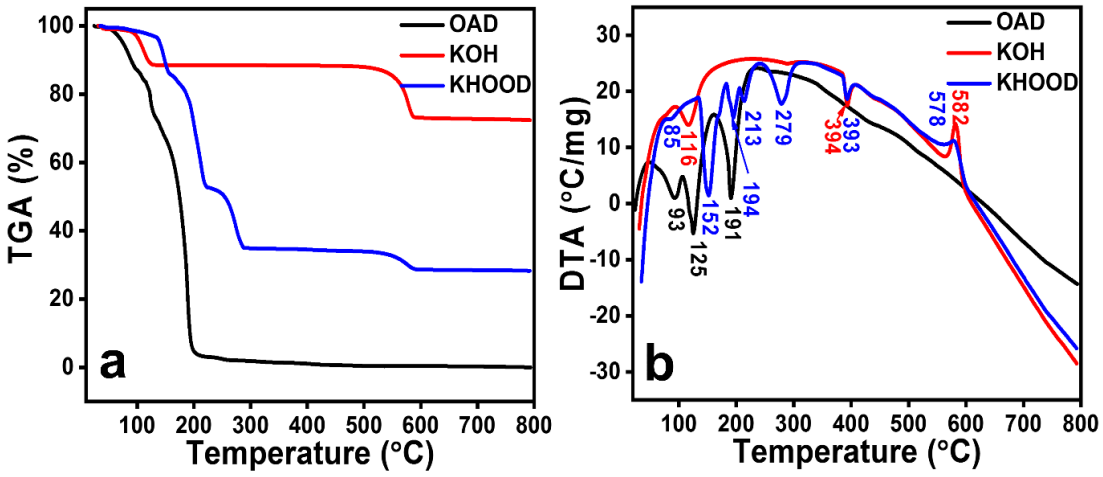

Figure. 7.6. a) TGA **b)** DTA curves of OAD, KOH and KHOOD single crystal.

The crystals of OAD, KOH and KHOOD are studied for thermal stability and decomposition mechanisms using TGA-DTA analysis. Oxalic acid decomposition

mechanisms were investigated and the mass loss observed till 130 °C in the TGA curve can be explained as due to the dehydration of oxalic acid. The DTA peaks of 93 °C and 125 °C are due to water evaporation. The maximum mass loss and decomposition of the oxalic acid starts after 130 °C to 200 °C and the CO_2, CO and H_2O will evaporate from the crystal [Higgins et al. 1997 Ma et al. 2013]. Oxalic acid completely decomposes after 200 °C. The thermal reaction of the oxalic acid dihydrate crystal is given in Equation. 7.1 and 7.2.

$$H_2C_2O_4 \cdot 2H_2O \rightarrow H_2C_2O_4 + 2H_2O \quad (7.1)$$

$$H_2C_2O_4 \rightarrow CO_2 + CO + H_2O \quad (7.2)$$

In the case of KOH single crystal the decomposition mechanism is altered due to the potassium atom in the crystal structure turns to potassium carbonate by liberating CO gas. The anhydrous potassium oxalate is stable till 520 °C. The melting point is completely changed when the potassium is formed complex with oxalic acid. The first weight loss observed for KOH can be attributed to dehydration, corresponding to the peak obtained at around 116 °C in DTA. It was interesting to note that an endothermic peak appeared at 394 °C in DTA curve and no mass loss is observed in the TGA, which can be explained as the change in physical properties [Higashiyama and Hasegawa 1971a Dinnebier et al. 2005]. The second mass loss corresponding to the DTA curve of 582 °C is explained as the liberation of the CO gas and K_2CO_3 is formed [Papazian et al. 1971 Mohamed et al. 2002]. The decomposition mechanism is mentioned below in the Equation. 7.3 and 7.4.

$$K_2C_2O_4 \cdot H_2O \rightarrow K_2C_2O_4 + H_2O\uparrow \quad (7.3)$$

$$K_2C_2O_4 \rightarrow K_2CO_3 + CO\uparrow \quad (7.4)$$

When there is an oxalic acid and potassium oxalate in the KHOOD crystal structure the melting mechanism differs from the KOH. The TGA and DTA curves of the synthesized crystals are shown in the Figure. 7.6. The initial mass loss and the endothermic peaks corresponding to 85 °C and 152 °C can be attributed to the liberation of water molecules adsorbed in the crystal [Vimal et al. 2014 Chandran et al. 2017]. The endothermic peak corresponding to 194 °C is can be attributed to the liberation of water molecules adsorbed and CO_2 liberation [Vimal et al. 2014]. The third mass loss corresponding to the DTA peak of 279 °C is explained as the liberation of HCOOH and

CO_2 gas and $K_2C_2O_4$ is remaining in the solid. The similar physical transformation is observed in the case of KHOOD crystals as compared with KOH crystal corresponding DTA peak of 393 °C**.** The fourth mass loss corresponding to 578 °C is due to the liberation of CO gas and K_2CO_3 remains [Mahalakshmi et al. 2012]. The thermal decomposition mechanism of KHOOD crystal is given in Equation. 7.5-7.8.

$$2(KH_3C_4O_8 \cdot 2H_2O) \rightarrow 2KH_3C_4O_8 + 4H_2O\uparrow \quad (7.5)$$

$$2KH_3(C_2O_4)_2 \rightarrow 2KHC_2O_4+2CO_2\uparrow+2HCOOH \quad (7.6)$$

$$2KHC_2O_4 \rightarrow K_2C_2O_4+CO_2\uparrow+HCOOH \quad (7.7)$$

$$K_2C_2O_4 \rightarrow K_2CO_3+CO\uparrow \quad (7.8)$$

7.2.6 I-V studies

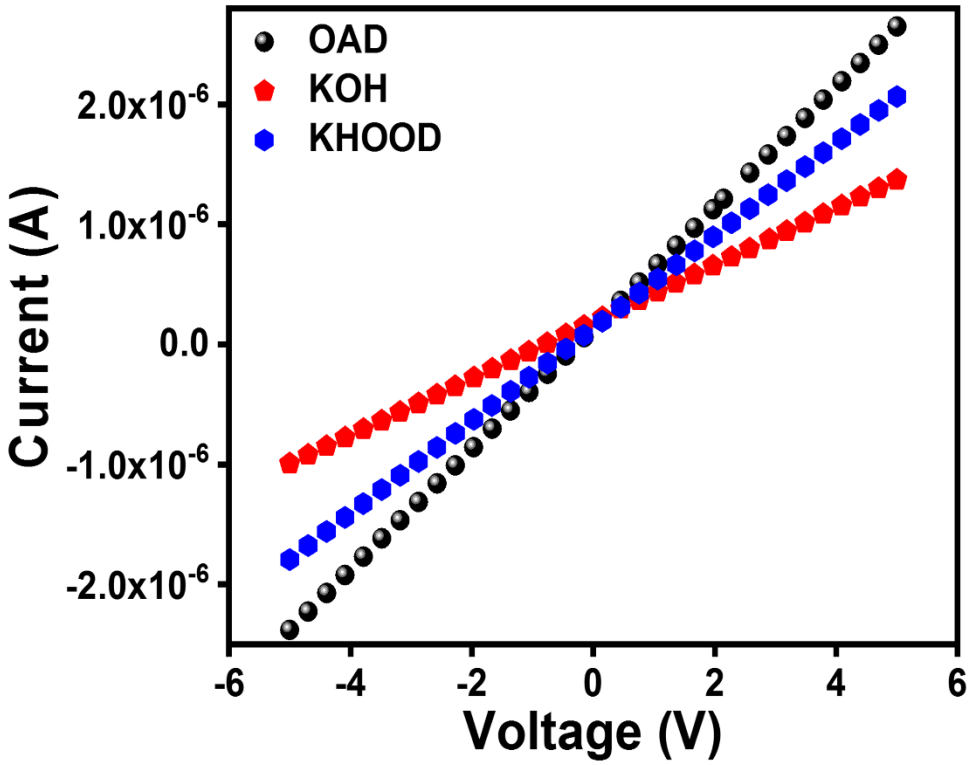

Figure. 7.7. I-V curve of OAD, KOH and KHOOD crystals.

The crystals of OAD, KOH and KHOOD were subjected to I-V studies to understand the electrical response of the material. Figure. 7.7 shows I-V curves of OAD, KOH and KHOOD single crystal. The synthesized crystals of OAD, KOH and KHOOD were polished to obtain uniform surfaces on the both sides (1 mm) to perform I-V measurements. I-V measurements were executed in the voltage range from -5 V to +5 V, and the current generated are measured. As the voltage increased current increased linearly for all the crystals. The dc resistivity (ρ_{dc}) of OAD, KOH and KHOOD single

crystals are measured using the relation 2.19 [Freeda and Mahadevan 2000],

The dc resistivity (ρ_{dc}) of OAD, KOH and KHOOD single crystals are 1.399×10^4, 2.988×10^4 and 1.8314×10^4 Ω.m respectively. The electrical studies were also supported by bandgap calculation (Figure. 7.4(a)).

7.2.7 Hardness studies

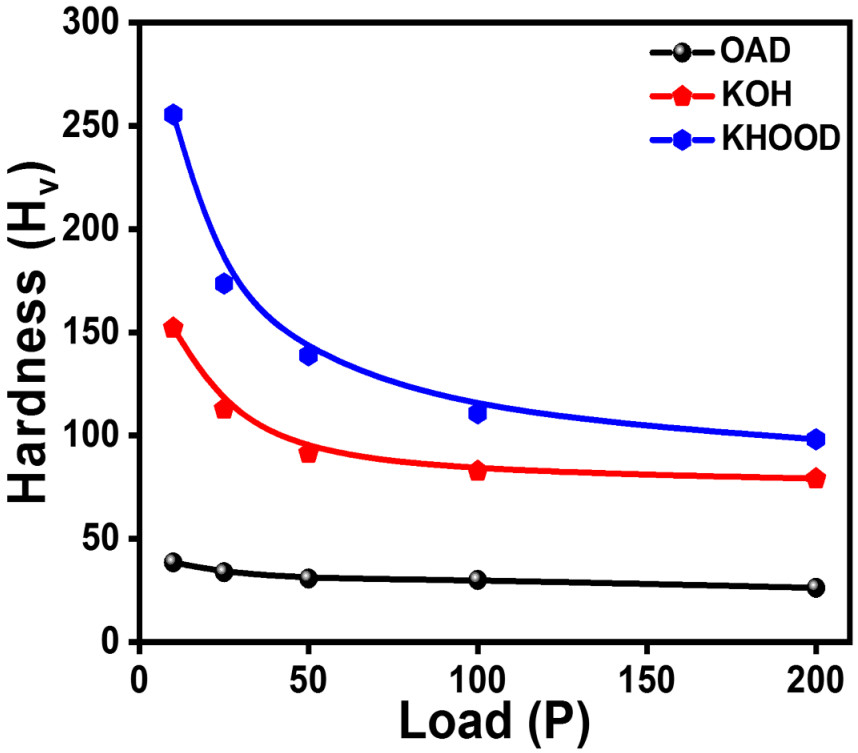

Figure. 7.8. Load (P) versus hardness number (H_v).

The hardness of the crystal can be due to combined effect of characteristic features such as Debye's temperature, internal lattice energy, interatomic spacing, heat of formation, etc and also caused due to external parameters such as inclusions, vacancies, defect centers, pores, impurities, etc [Anis et al. 2018c, 2019]. Vickers micro hardness measurement technique is used to study the microhardness of the OAD, KOH and KHOOD single crystals. Vicker's indentation mark is made on the well-polished surfaces of OAD, KOH and KHOOD single crystals. The microhardness number is measured for different loads starting from 5 g to 200 g and H_v is measured. It was noticed that the crystal hardness number decreased as the applied load increased for all the crystals which can be termed as Indentation Side Effect (ISE) [Anis et al. 2018d]. The hardness number is more for KHOOD crystal and less for OAD crystal for all the applied loads.

The Vickers microhardness number (H_v) is calculated using the Equation. 2.13 [Gao et al. 2003 Tyagi et al. 2015]

The microhardness number is plotted with respect to applied load, as shown in Figure. 7.8.

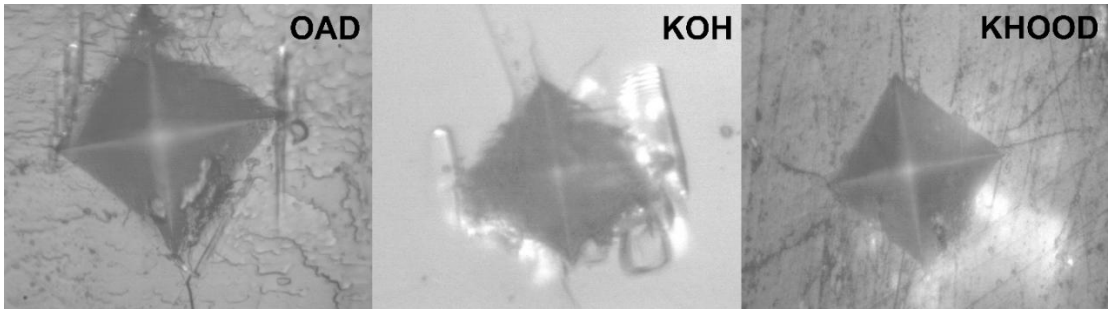

Figure. 7.9. Indentation images of 200 g applied load for OAD, KOH and KHOOD single crystal.

The molecular bond strength of the crystal is calculated using Wooster's relation (Elastic stiffness constant (C_{11})) as shown in Equation. 2.14 [Ray et al. 2017b]. The C_{11} value is calculated be calculated for OAD, KOH and KHOOD single crystals for different applied loads.

The size of the indentation and the load applied can be related using Meyer's law [Sangwal 2000] as shown in Equation. 2.15.

The n value can be calculated by taking the slope from log P versus log d graph. The obtained n values for OAD, KOH and KHOOD crystals are 1.78, 2.32 and 1.54 respectively. OAD and KHOOD crystals have n value $n < 2$ implies the materials belongs to hard material category whereas the KOH crystal possess n >2 and belongs to soft material category [Sangwal 2000 Hanumantharao et al. 2013].

The yield strength values shown in Table 7.2-7.5 are computed using the relation 2.16 [Suresh et al. 2018]

In order to understand the relation between hardness, microstructural properties and bond nature, of the fractured surfaces of OAD, KOH and KHOOD single crystals using the Equation. 2.17.

The relative measure of the material brittleness is obtained by the crack produced on the indented surface. The brittleness of the OAD, KOH and KHOOD single crystals were calculated using the Equation. 2.18.

The material hardness depends on the chemical bond strength of the molecules which

are responsible for the distinct hardness. From the results it is evident that the hardness of the material mainly depends on the bond strength of the material. Organic crystal binds with and forms complex with inorganic material and gains improved hardness number and better mechanical parameters.

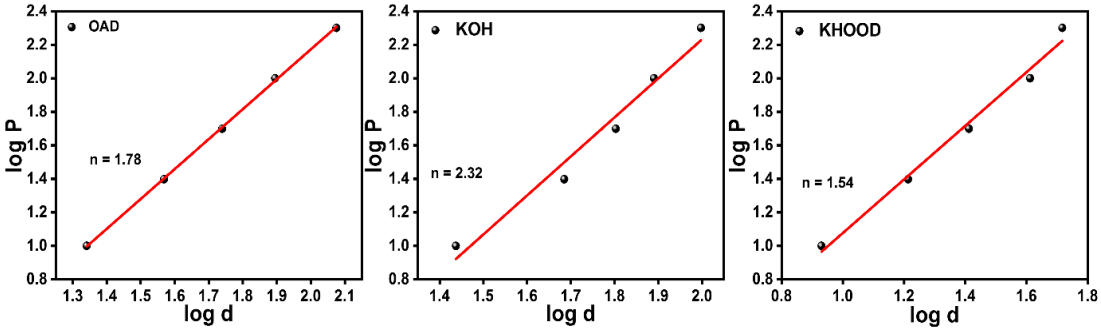

Figure. 7.10. Plot of Log P vs Log d.

Table. 7.2. Microhardness parameters of OAD single crystal.

Sl. no	Load P (g)	Hardness H_v (Kg/mm^2)	Yield Strength σ_y (Kg/mm^2)	Elastic stiffness constant (C_{11}) (Pa)	Fracture toughness K_c ($g/\mu m^{3/2}$)	Brittleness B_i ($\mu m^{-1/2}$)
1	10	38.56	12.85	596.67	–	–
2	25	33.83	11.27	474.54	–	–
3	50	30.77	10.25	401.99	–	–
4	100	30.09	10.03	386.57	–	–
5	200	26.25	8.75	304.42	0.0160	1638.57

Table. 7.3. Microhardness parameters of KOH single crystal.

Sl. no	Load P (g)	Hardness H_v (Kg/mm^2)	Yield Strength σ_y (Kg/mm^2)	Elastic stiffness constant (C_{11}) (Pa)	Fracture toughness K_c ($g/\mu m^{3/2}$)	Brittleness B_i ($\mu m^{-1/2}$)
1	10	152.12	50.70	6589.09	–	–
2	25	112.83	37.61	3906.09	–	–
3	50	91.43	30.47	2703.36	–	–
4	100	82.79	27.59	2272.27	–	–
5	200	79.18	26.39	2101.73	0.0730	1084.50

Table. 7.4. Microhardness parameters of KHOOD single crystal.

Sl. no	Load P (g)	Hardness H_v (Kg/mm^2)	Yield Strength σ_y (Kg/mm^2)	Elastic stiffness constant (C_{11}) (Pa)	Fracture toughness K_c ($g/\mu m^{3/2}$)	Brittleness B_i ($\mu m^{-1/2}$)
1	10	255.4	85.13	16316.85	–	–

2	25	173.56	57.85	8299.21	–	–
3	50	138.84	46.28	5615.65	–	–
4	100	110.7	36.90	3777.96	–	–
5	200	98.2	32.73	3063.33	0.1045	9398.92

7.3 Conclusions

The crystals of oxalic acid dihydrate (OAD), potassium oxalate hydrate (KOH) and potassium hydrogen oxalate oxalic acid dihydrate (KHOOD) were grown using solvent evaporation technique. The OAD and KOH crystals belongs to monoclinic crystal structure with space group $P2_1/a$ and A2/a respectively, where the KHOOD crystal belongs to triclinic crystal system of $P\bar{1}$ space group. From the UV-vis absorption studies it is evident that the optical absorption changes for OAD, KOH and KHOOD crystals and corresponding bandgaps are 4.06, 4.28 and 4.10 respectively. From the I-V studies the resistivity of the crystals were obtained as 1.399×10^4, 2.988×10^4 and 1.8314×10^4 Ω.m, respectively. In the emission spectra, the OAD crystal does not show emission property, where KOH and KHOOD crystals show emission. The maximum emission intensity is observed for KOH crystal when compared with KHOOD. The emission peaks of KOH and KHOOD were observed to be 399 nm and 430 nm respectively followed by a broad emission in the case of KOH crystal. Thermal studies were studied and explained for OAD, KOH and KHOOD crystals and confirmed that KOH crystal is thermally more stable than the other crystals. The microhardness measurements showed the increased hardness number for all the applied loads in the case of KHOOD single crystal and the lesser values are obtained for the OAD crystal. The Mayer's number for the crystals were calculated to be 1.78, 2.32 and 1.54 respectively and infers the OAD and KHOOD crystal belongs to hard material category, where KOH belongs to soft material category. The other mechanical properties such as Yield strength, Elastic stiffness, Fracture toughness and brittleness were calculated. The obtained fracture toughness and brittleness number for the OAD, KOH and KHOOD crystals are 0.0160 g/$\mu m^{3/2}$, 0.0730 g/$\mu m^{3/2}$, 0.1045 g/$\mu m^{3/2}$ and 1638.57 $\mu m^{-1/2}$, 1084.50 $\mu m^{-1/2}$, 9398.92 $\mu m^{-1/2}$ respectively.

CHAPTER 8

Summary and Conclusions

The overall summary of the thesis and a few directions for future work are also indicated in this chapter.

8.1 Summary and Conclusions

- Potassium hydrogen oxalate oxalic acid dihydrate crystal have been successfully synthesized using slow solvent evaporation method at room temperature.
- The crystal structure was solved using single crystal XRD analysis. The crystal belongs to centro-symmetric space group P-1 with triclinic crystal system.
- The unit cell parameters were determined using powder XRD technique which shows good agreement with data obtained from single crystal XRD.
- High optical transmittance in the visible region suggests the potential use in optoelectronic applications. Optical band gap of the crystal was found to be 4.07 eV.
- EDAX analysis confirmed the presence of potassium, carbon and oxygen in the synthesized crystal.
- The crystal was stable up to the temperature of 266 ºC which was studied using DSC analysis.
- The functional vibrations were studied using FTIR analysis and the vibrational modes present in the crystal were identified.
- Photo-excitation of the crystals resulted in emission of three distinct peaks in the UV and blue region.
- I-V studies have shown the decrease in the resistivity of the crystal on illumination suggesting their use as photoresistors.
- Time dependent I-V studies have shown negative photoconductivity of the crystal with the resistance being increased on illumination and decreasing under dark condition.
- The electrical resistivity measurements show increasing trend as the temperature increased. The activation energy of the crystal is also estimated and the crystal shows activation energy of 0.476 eV and 0.290 eV.
- The Vickers microhardness study reveals that the hardness number decreases as the applied load increases which explains the indentation side effect (ISE) behaviour of

the crystal. From Meyer's law the value of 'n' is evaluated to be 1.47 and it belongs to hard material category.

- The elastic stiffness constant and yield strength was observed to be 16.3×10^3 Pa and 85.13 (Kg/mm^2).
- The dielectric constant decreases as the frequency increases and also the lesser value of dielectric parameter and dielectric loss suggests its potential application in optoelectronic device fabrications.
- From the dielectric measurements it was observed that the space charge phenomenon is acting on the crystal as the frequency is varied.
- The single crystals of potassium oxalate oxalic acid dihydrate (KHOOD) and $Co(OH)_2$ doped KHOOD crystals were synthesized using slow evaporation technique.
- The powder XRD spectrum does not show much variations on the doped crystals due to the incorporation of the nanoparticles in the vacancy cites and it will not alter the crystal lattice. The shift in the XRD peaks after doping confirms the nanoparticle incorporation into the host lattice.
- The optical constants such as optical bandgap and extinction coefficient were estimated. The bandgap of the crystals were calculated and it decreased as the dopant concentration increased.
- The confirmation and distribution of the nanoparticles in the host crystal was studied using EDAX and the mapped images confirms the distribution of Co in the crystal.
- The fundamental vibrations of the molecules were analyzed using FTIR spectroscopy and the crystal does not show variations confirming that there is no bond formation after doping.
- The melting point of the crystal is increased as the dopant concentration increased suggesting the increased thermal stability of the crystal after doping.
- The resistivity of the crystal decreased as the dopant concentration increased leading to the better conductivity of the material after doping.
- The emission spectrum of the crystal increased as the dopant concentration increased suggesting increased number of defect states created due to the nanoparticle incorporation in the crystal lattice.

- From ac conductivity studies it was observed that the hopping mechanism is the reason behind the conductivity process and the conductivity mechanism is due to small polaron hopping mechanism.
- The dielectric measurements of the synthesized crystals were examined in the frequency range of 10 Hz to 1 MHz at room temperature and the parameters such complex dielectric constants, complex impedance, ac conductivity and loss factor were analyzed. From the nyquist plot the radius of the semicircle decreased as the dopant concentration increased and suggesting the decrease in the resistivity of the material.
- KHOOD single crystals are successfully doped with amaranth dye molecule and the results are presented systematically.
- The dye incorporation in KHOOD matrix have retained the KHOOD crystal structure.
- The extra absorption peak witnessed for the doped crystal is also present in the absorption spectrum of amaranth dye inferring the dye molecules successfully incorporated in KHOOD lattice.
- The optical bandgap of KHOOD crystal is observed to be 4.08 eV and as that of dye doped crystal is 4.04 eV.
- Increased surface roughness is obtained for the dye doped crystals inferring the larger molecules of dye in the crystal is the reason behind the roughness obtained.
- From the thermal studies the obtained crystals melting point and decomposition mechanisms are shifted for the doped crystal confirms the dye molecule present in the crystal and also mass loss is less in case of dye doped crystals (TGA) confirming dye residuals of sodium is converted to carbonate.
- Enhanced and broader emission is noticed for dye doped KHOOD crystal with emission peak of 426 nm and 430 nm for pure and amaranth dye doped KHOOD crystal.
- Increased conductivity is observed for the dye doped KHOOD crystal.
- Grown KHOOD single crystals were irradiated with gamma radiation in the dosage of 5, 10, 20 kGy.
- The powder XRD studies of single crystal confirms the crystalline nature of the sample. Small shift in the position of peaks justifies that the crystal structure has

been retained and defects states were created which induced stress in the crystal lattice due to irradiation.

- The functional groups of the crystals were studied using FTIR spectral analysis and it is evident that the crystal structure was not altered after irradiation but there is a stress induced on the crystal which causes small variations in the peak positions.
- Optical transmission and absorption spectrum reveals that the absorption peak was shifted to lower wavelength region as the irradiation dosage increased which in turn increases the transmission window.
- Pure and irradiated crystals show negative photoconductivity. The resistivity of the pure and irradiated KHOOD crystal was observed to be in the order of 10^4 Ω.m and the conductivity of the crystal was found to be in the order of 10^{-5} $\Omega^{-1}m^{-1}$. As the irradiation dosage increased, the crystal conductivity decreases which consequently led to increase in its resistivity which is also true in case of light irradiated crystals.
- The crystals of OAD, KOH and KHOOD were grown using solvent evaporation technique.
- The OAD and KOH crystals belongs to Monoclinic crystal structure with space group $P2_1/a$ and A2/a respectively, where the KHOOD crystal belongs to triclinic crystal system of $P\bar{1}$ space group.
- From the UV-vis absorption studies it is evident that the optical absorption changes for OAD, KOH and KHOOD crystals and corresponding bandgaps are 4.06, 4.28 and 4.10 respectively.
- From the I-V studies the resistivity if the crystals were obtained to be 1.399×10^4, 2.988×10^4 and 1.831×10^4 Ω.m respectively which also reflects the bandgap calculation where maximum resistivity was obtained for KOH crystal and lesser resistivity for OAD crystal.
- In the emission spectra the OAD crystal does not shows emission but KOH and KHOOD crystal shows emission and the maximum emission intensity is witnessed to KOH crystal when compared with KHOOD. The emission peaks of KOH and KHOOD are 399 nm and 430 nm respectively. Broad emission is observed in the case of KOH crystal.
- Thermal studies were carried out and explained for OAD, KOH and KHOOD crystals that KOH crystal was thermally more stable than the other crystals. The

microhardness measurements showed the increased hardness number for all the applied loads in the case of KHOOD single crystal and the lesser values are obtained for the OAD crystal.

- The Mayer's number for the crystals were calculated to be 1.78, 2.32 and 1.54 respectively and infers the OAD and KHOOD crystal belongs to hard material category, where KOH belongs to soft material category. The other mechanical properties such as Yield strength, Elastic stiffness, Fracture toughness and brittleness were calculated. The obtained fracture toughness and brittleness number for the OAD, KOH and KHOOD crystals are 0.0160 g/$\mu m^{3/2}$, 0.0730 g/$\mu m^{3/2}$, 0.1045 g/$\mu m^{3/2}$ and 1638.57 $\mu m^{-1/2}$, 1084.50 $\mu m^{-1/2}$, 9398.92 $\mu m^{-1/2}$ respectively.

8.2 Directions for future work

The investigations of the present research work can be extended further in the following directions:

- Present measurements were performed at room temperature at ambient conditions. This can be extended to temperature dependent measurements under controlled conditions. From these measurements we could estimate material stability and the effect of temperature on the material properties. This could be useful in designing temperature sensor devices.
- Piezoelectric properties of the KHOOD crystals can be studied.

References

Adhikari, S. and Kar, T. (2013). "Experimental and theoretical characterization of semiorganic nonlinear optical material l-leucine hydrobromide." Mater. Res. Bull., 48 (4), 1612–1617.

Ahlam, M.A., Ravishankar, M.N., Vijayan, N., Govindaraj, G., Siddaramaiah and Gnana Prakash, A.P. (2012a). "Investigation of gamma radiation effect on chemical properties and surface morphology of some nonlinear optical (NLO) single crystals." Nucl. Instrum. Methods Phys. Res. Sect. B Beam Interact. Mater. At., 278 (Supplement C), 26–33.

Ahlam, M.A., Ravishankar, M.N., Vijayan, N., Govindaraj, G., Upadhyaya, V. and Prakash, A.P.G. (2012b). "The effect of Co-60 gamma irradiation on optical properties of some nonlinear optical (NLO) single crystals." J. Opt., 41 (3), 158–166.

Albert Irudayaraj, A., Dhayal Raj, A. and Illavarasi, G. (2014). "Growth and characterization of BTCS and BTZA crystals grown by slow evaporation method." Opt. - Int. J. Light Electron Opt., 125 (2), 824–827.

Anand, S., Amaliya, A.P., Janifer, M.A. and Pauline, S. (2017). "Structural, morphological and dielectric studies of zirconium substituted $CoFe_2O_4$ nanoparticles." Mod. Electron. Mater., 3 (4), 168–173.

Anbuselvi, D., Jayaraman, D., Arul Martin Mani, J. and Joseph, V. (2014). "Growth and optical, thermal, mechanical and surface morphology studies of semiorganic nonlinear optical material: Dichlorobis (l-proline) zinc (II) crystal." Spectrochim. Acta. A. Mol. Biomol. Spectrosc., 127 405–414.

Anis, M., Baig, M.I., Hussaini, S.S., Shirsat, M.D., Shkir, M. and Ghramh, H.A. (2018a). "Linear and nonlinear optical analysis on semiorganic L -proline cadmium chloride single crystal." Chin. Phys. B, 27 (4), 047801.

Anis, M., Baig, M.I., Muley, G.G., Rabbani, G., Shirsat, M.D., Shkir, Mohd. and Ghramh, H.A. (2018b). "Gamma glycine crystal for efficient second harmonic generation of 1064 nm Nd:YAG laser light." Mater. Lett., 233 238–241.

Anis, M., Baig, M.I., Pandian, M.S., Ramasamy, P., AlFaify, S., Ganesh, V., Muley, G.G. and Ghramh, H.A. (2018c). "Optimizing Structural, Microhardness, Surface Growth Mechanism, Luminescence and Thermal Traits of KH_2PO_4 Crystal Exploiting

Multidirectional H-Bonding Quality of Dopant Tartaric Acid." Cryst. Res. Technol., 53 (4), 1700165.

Anis, M., Hussaini, S.S., Hakeem, A., Shirsat, M.D. and Muley, G.G. (2016). "Synthesis, growth and optical studies of novel organometallic NLO crystal: Calcium bis-thiourea chloride." Opt. - Int. J. Light Electron Opt., 127 (4), 2137–2142.

Anis, M., Muley, G.G., Baig, M.I., Rabbani, G., Ghramh, H.A. and Ramteke, S.P. (2019). "Doping effect of Ni^{2+} on structural, UV-visible, SHG efficiency, dielectric and microhardness traits of KH_2PO_4 (KDP) crystal." Optik, 178 752–757.

Anis, M., Muley, G.G., Shkir, M., Alfaify, S. and Ghramh, H.A. (2018d). "Comparative analysis on microhardness and third order nonlinear optical traits of pure and Nd^{3+} doped zinc tris-thiourea sulphate (ZTS) crystal." Mater. Sci.-Pol., 36 (3), 403–408.

Anis, M., Shaikh, R.N., Shirsat, M.D. and Hussaini, S.S. (2014). "Investigation of optical and electrical properties of l-Cystein doped zinc thiourea chloride (ZTC) crystal for nonlinear optical (NLO) applications." Opt. Laser Technol., 60 124–129.

Anis, M., Shkir, M., Baig, M.I., Ramteke, S.P., Muley, G.G., AlFaify, S. and Ghramh, H.A. (2018e). "Experimental and computational studies of L-tartaric acid single crystal grown at optimized pH." J. Mol. Struct., 1170 151–159.

Aoki, T. (2002). Photoluminescence Spectroscopy. In Characterization of Materials, (John Wiley & Sons, Inc.), p.

Aravind, G., Raghasudha, M. and Ravinder, D. (2015). "Electrical Transport Properties of Nano Crystalline Li-Ni ferrites." J. Materiomics, 1 348–356.

Arivanandhan, M., Ramyalakshmi, A., Rathikha, R., Gopalakrishnan, R., Sanjeeviraja, C. and Sankaranarayanan, K. (2005). "Ethyl p-amino benzoate (EPAB): A novel organic non-linear optical material for optical devices." Opt. Commun., 251 (1), 172–178.

Arora, S.K. and Abraham, T. (1981). "Controlled nucleation of cadmium oxalate in silica hydrogel and characterization of grown crystals." J. Cryst. Growth, 52 851–857.

Ashraf, I.M., Elshaikh, H.A. and Badr, A.M. (2004a). "Photoconductivity in Tl4S3 layered single crystals." Cryst. Res. Technol., 39 (1), 63–70.

Ashraf, I.M., Elshaikh, H.A. and Badr, A.M. (2004b). "Photoconductivity in Tl_4S_3 layered single crystals." Cryst. Res. Technol., 39 (1), 63–70.

Ashwini, L.S., Sridhar, R. and Bellad, S.S. (2017). "Dielectric and magnetoelectric properties of Li-Mg ferrite: Barium titanate composites." Mater. Chem. Phys., 200 136–145.

Balasubramanian, D., Sankar, R., Shankar, V.S., Murugakoothan, P., Arulmozhichelvan, P. and Jayavel, R. (2008). "Growth and characterization of semiorganic nonlinear optical rubidium bis-dl-malato borate single crystals." Mater. Chem. Phys., 107 (1), 57–60.

Balazs, L., Breunig, H.J., Lork, E., Soran, A. and Silvestru, C. (2006). "Isomers of a Dibismuthane, R2Bi−BiR2 [R = 2,6-$(Me_2NCH_2)_2C_6H_3$], and Unusual Reactions with Oxygen: Formation of $[R_2Bi]_2(O_2)$ and R‘R‘‘Bi [R‘ = 2-(Me_2NCH_2)-6-$\{Me_2N(O)CH_2\}C_6H_3$; R‘‘ = 2-(Me_2NCH_2)-6-$\{O(O)C\}C_6H_3$]." Inorg. Chem., 45 (5), 2341–2346.

Bamini, N.S., Vidyalakshmy, Y., Choedak, T., Kejalakshmy, N., Muthukrishnan, P. and Ancy, C.J. (2015). "Synthesis, linear optical, non-linear optical, thermal and mechanical characterizations of dye-doped semi-organic NLO crystals." Mater. Res. Express, 2 (6), 065010.

Bangera, K.V. and Rao, P.M. (1992). "Growth and characterization of barium copper oxalate single crystals in gels." Bull. Mater. Sci., 15 (4), 339–347.

Baskaran, P., Vimalan, M., Anandan, P., Bakiyaraj, G., Kirubavathi, K. and Selvaraju, K. (2017). "Synthesis, growth and characterization of a nonlinear optical crystal: l-Leucinium perchlorate." J. Taibah Univ. Sci., 11 (1), 11–17.

Bator, G., Zeegers-Huyskens, T., Jakubas, R. and Zaleski, J. (2001). "Structure and phase transitions in guanidinium halogenobismuthates(III)." J. Mol. Struct., 570 (1), 61–74.

Batten, S.R. and Robson, R. (1998). "Interpenetrating Nets: Ordered, Periodic Entanglement." Angew. Chem. Int. Ed., 37 (11), 1460–1494.

Bhandari, S., Sinha, N., Ray, G. and Kumar, B. (2014). "Enhanced optical, dielectric and piezoelectric behavior in dye doped zinc tris-thiourea sulphate (ZTS) single crystals." Chem. Phys. Lett., 591 10–15.

Bhuvaneswari, R., Vinitha, G. and Sakthi Murugesan, K. (2019). "Crystal growth, optical, physico-chemical and third-order nonlinear optical studies of morpholinium

oxalate: a new organic single crystal for optical limiting application." Appl. Phys. A, 125 (6), 385.

Bincy, I.P. and Gopalakrishnan, R. (2014a). "Studies on synthesis, growth and characterization of a novel third order nonlinear optical 4-Dimethylaminopyridinium p-Toluenesulfonate single crystal." 37 267–276.

Bincy, I.P. and Gopalakrishnan, R. (2014b). "Studies on synthesis, growth and characterization of a novel third order nonlinear optical 4-Dimethylaminopyridinium p-Toluenesulfonate single crystal." Opt. Mater., 37 267–276.

Bindu, K., Ajith, K.M. and Nagaraja, H.S. (2018a). "Electrical, dielectric and magnetic properties of Sn-doped hematite (α-Sn_xFe_2-xO_3) nanoplates synthesized by microwave-assisted method." J. Alloys Compd., 735 847–854.

Bindu, K., Ajith, K.M. and Nagaraja, H.S. (2018b). "Electrical, dielectric and magnetic properties of Sn-doped hematite (α-Sn_xFe_2-xO_3) nanoplates synthesized by microwave-assisted method." J. Alloys Compd., 735 847–854.

Bridle, C. and Lomer, T.R. (1965). "The growth of crystals in silica gel, and the unit-cell dimensions of cadmium oxalate and copper tartrate." Acta Crystallogr., 19 (3), 483–484.

Bright, K.C. and Freeda, T.H. (2010). "Growth and characterization of organometallic l-alanine cadmium chloride single crystal by slow evaporation technique." Phys. B Phys. Condens. Matter, 18 (405), 3857–3861.

Cammi, R., Lanfranchi, M., Marchiò, L., Mora, C., Paiola, C. and Pellinghelli, M.A. (2003). "Synthesis and Molecular Structure of the Dihydrobis(thioxotriazolinyl)borato Complexes of Zinc(II), Bismuth(III), and Nickel(II). M···H−B Interaction Studied by Ab Initio Calculations." Inorg. Chem., 42 (5), 1769–1778.

Chand, P., Vaish, S. and Kumar, P. (2017a). "Structural, optical and dielectric properties of transition metal (MFe_2O_4; M = Co, Ni and Zn) nanoferrites." Phys. B Condens. Matter, 524 53–63.

Chandran, S., Paulraj, R. and Ramasamy, P. (2015). "Influence of amaranth dye on the growth and properties of KDP single crystal." Mater. Res. Bull., 68 210–215.

Chandran, S., Paulraj, R. and Ramasamy, P. (2017). "Crystal growth, structural, optical, thermal and dielectric properties of lithium hydrogen oxalate monohydrate single crystal." Opt. Mater., 73 154–162.

Chen, H.-C., Huang, C.-W., Wu, J.C.S. and Lin, S.-T. (2012). "Theoretical Investigation of the Metal-Doped $SrTiO_3$ Photocatalysts for Water Splitting." J. Phys. Chem. C, 116 (14), 7897–7903.

Chouaib, H., Elfaleh, N., Karoui, S., Kamoun, S. and Graça, M.P.F. (2016). "Synthesis, crystal structure, thermal analysis and dielectric properties of $(C_8H_{12}N)_3SnCl_6.Cl$ compound." Synth. Met., 217 129–137.

Chouaib, H., Kamoun, S., Costa, L.C. and Graça, M.P.F. (2015). "Synthesis, crystal structure and electrical properties of N,N-dimethylanilinium trichloridostannate (II): $(C_8H_{12}N)SnCl_3$." J. Mol. Struct., 1102 71–80.

Clearfield, A. (1982). "Inorganic ion exchange materials (CRC press Boca Raton, FL).

Cocke, D.L. and Clearfield, A. (1987). "Design of New Materials (Springer US).

Cubillas, P. and Anderson, M.W. (2010). Synthesis Mechanism: Crystal Growth and Nucleation. In Zeolites and Catalysis, J. Čejka, A. Corma, and S. Zones, eds. (Wiley-VCH Verlag GmbH & Co. KGaA), pp 1–55.

Cyrac Peter, A., Vimalan, M., Sagayaraj, P. and Madhavan, J. (2010). "Thermal, optical, mechanical and electrical properties of a novel NLO active l-phenylalanine l-phenylalaninium perchlorate single crystals." Phys. B Condens. Matter, 405 (1), 65–71.

Dalal, J. and Kumar, B. (2016). "Bulk crystal growth, optical, mechanical and ferroelectric properties of new semiorganic nonlinear optical and piezoelectric Lithium nitrate monohydrate oxalate single crystal." Opt. Mater., 51 (Supplement C), 139–147.

Dalal, P.V. and Saraf, K.B. (2006). "Growth and study of barium oxalate single crystals in agar gel." Bull. Mater. Sci., 29 (5), 421–425.

Dardar, F., Day, C.S., El Jazouli, A., Sebti, S. and Lachgar, A. (2019). "Synthesis and Characterization of a New Layered Gallium Phosphonate Oxalate $[C_2H_{10}N_2]0.5[Ga_3(PO_3CH_3)4(C_2O_4)].H_2O$." J. Chem. Crystallogr., 49 (1), 44–51.

De, A. and Rao, K.V. (1988). "Dielectric properties of synthetic quartz crystals." J. Mater. Sci., 23 (2), 661–664.

DeBord, J.R.D., Zhang, Y., Haushalter, R.C., Zubieta, J. and O'Connor, C.J. (1996). "One-Dimensional Vanadium Oxide Chains Containing Covalently Bound Copper Coordination Complexes: Hydrothermal Synthesis and Characterization of $Cu(H_2N(CH_2)_2NH_2)[V_2O_6]$, $Cu(C_{10}H_8N_2)[V_2O_6]$, and $Cu(C_{10}H_8N_2)_2[V_2O_6]$." J. Solid State Chem., 122 (2), 251–258.

Deepa, M., Babu, K.R. and Vaidyan, V.K. (1995). "Surface topographical studies of calcium oxalate grown in silica gel." J. Mater. Sci. Lett., 14 (18), 1321–1322.

Devan, R.S., Kolekar, Y.D. and Chougule, B.K. (2006). "Effect of cobalt substitution on the properties of nickel–copper ferrite." J. Phys. Condens. Matter, 18 (43), 9809.

Devmunde, B.H., Raut, A.V., Birajdar, S.D., Shukla, S.J., Shengule, D.R. and Jadhav, K.M. (2016). "Structural, Electrical, Dielectric, and Magnetic Properties of Cd^{2+} Substituted Nickel Ferrite Nanoparticles." Journal of Nanoparticles, 2016 4709687.

Dhanjayan, R., Gunasekaran, S. and Srinivasan, S. (2017). "Synthesis, crystal structure, optical, thermal and dielectric studies of a potential novel organic material: l-histidinium fumarate fumaric acid monohydrate single crystal." Mater. Lett., 206 221–224.

Dharmaprakash, S.M. and Rao, P.M. (1985). "Growth of barium oxalate dihydrate crystals in silica hydrogel." J. Mater. Sci. Lett., 4 (6), 787–789.

Dinnebier, R.E., Vensky, S., Jansen, M. and Hanson, J.C. (2005). "Crystal Structures and Topological Aspects of the High-Temperature Phases and Decomposition Products of the Alkali-Metal Oxalates $M_2[C_2O_4]$ (M=K, Rb, Cs)." Chem. – Eur. J., 11 (4), 1119–1129.

Dong, Y., Xu, J., Zhou, G., Zhao, G., Su, L., Xu, X., Li, H. and Si, J. (2007). "Gamma-ray induced color centers in Yb:YAG crystals grown by Czochralski method." Solid State Commun., 141 (3), 105–108.

Eggeling, C., Widengren, J., Rigler, R. and Seidel, C.A.M. (1998). "Photobleaching of Fluorescent Dyes under Conditions Used for Single-Molecule Detection: Evidence of Two-Step Photolysis." Anal. Chem., 70 (13), 2651–2659.

Elangovan, K., Senthil, A. and Vinitha, G. (2019). "Growth, structure perfection and characterization of 2-methylimidazolium hydrogen oxalate dihydrate (2MIO) single crystal for NLO applications." J. Mater. Sci. Mater. Electron., 30 (14), 13664–13674.

Elwej, R. and Hlel, F. (2016). "Hydrothermal synthesis, characterization by single crystal XRD, structural discussion and electric, dielectrical properties of $(C_6H_9N_2)_2(Hg_{0.12}Zn_{0.88})Cl_4$ hybrid compound." Phys. E Low-Dimens. Syst. Nanostructures, 84 498–504.

Enculescu, M. (2010). "Morphological and optical properties of doped potassium hydrogen phthalate crystals." Phys. B Condens. Matter, 405 (17), 3722–3727.

Eriksson, A. and Nielsen, O.F. (1978). "Single crystal Raman study of potassium oxalate monohydrate, $K_2C_2O_4$. H_2O, and potassium oxalate monodeuterate, $K_2C_2O_4$. D2O." J. Mol. Struct., 48 (3), 343–351.

Ezhil Raj, A.M., Jayanthi, D.D. and Jothy, V.B. (2008). "Optimized growth and characterization of cadmium oxalate single crystals in silica gel." Solid State Sci., 10 (5), 557–562.

Fadhil, A.C., Akram, R.J. and Sabreen, A.A. (2017). "Studying Dielectric and Magnetic Properties of Nano Ferrite Functionally Graded Materials." Energy Procedia, 119 52–60.

Feigelson, R.S. (2015). 1 - Crystal Growth through the Ages: A Historical Perspective. In Handbook of Crystal Growth (Second Edition), T. Nishinaga, ed. (Boston: Elsevier), pp 1–83.

Freeda, T.H. and Mahadevan, C. (2000). "]Electrical conductivity measurements on gel grown KDP crystals added with some ammonium compounds." Bull. Mater. Sci., 23 (4), 335–340.

Gao, F., He, J., Wu, E., Liu, S., Yu, D., Li, D., Zhang, S. and Tian, Y. (2003). "Hardness of Covalent Crystals." Phys. Rev. Lett., 91 (1), 015502.

Gilmore, C.J. and Speakman, J.C. (1982). "The structure of potassium tetroxalate: a redetermination and a cautionary tale." Acta Crystallogr. B, 38 (11), 2809–2813.

Girija, E.K., Charistic Latha, S., Narayama Kalkura, S., Subramanian, C. and Ramasamy, P. (1998). "Crystallization and microhardness of calcium oxalate monohydrate." Mater. Chem. Phys., 52 (3), 253–257.

Girisun, T.C.S. and Dhanuskodi, S. (2009). "Linear and nonlinear optical properties of tris thiourea zinc sulphate single crystals." Cryst. Res. Technol., 44 (12), 1297–1302.

Goel, N., Sinha, N. and Kumar, B. (2013). "Growth and properties of sodium tetraborate decahydrate single crystals." Mater. Res. Bull., 48 (4), 1632–1636.

Goel, S., Sinha, N., Yadav, H., Joseph, A.J., Hussain, A. and Kumar, B. (2017). "Optical, piezoelectric and mechanical properties of xylenol orange doped ADP single crystals for NLO applications." Arab. J. Chem.,.

Goforth, A.M., Smith, M.D., Peterson, LeRoy and Loye, H.-C. zur (2004). "Preparation and Characterization of Novel Inorganic−Organic Hybrid Materials Containing Rare, Mixed-Halide Anions of Bismuth(III)." Inorg. Chem., 43 (22), 7042–7049.

Grachev, V.G., Vrable, I.A., Malovichko, G.I., Pritula, I.M., Bezkrovnaya, O.N., Kosinova, A.V., Yatsyna, V.O. and Gayvoronsky, V.Ya. (2012). "Macroscopic and microscopic defects and nonlinear optical properties of KH_2PO_4 crystals with embedded TiO_2 nanoparticles." J. Appl. Phys., 112 (1), 014315.

Haas, D.J. (1964). "The crystal structure of potassium tetraoxalate, $K(HC_2O_4)(H_2C_2O_4).2H_2O$." Acta Crystallogr., 17 (12), 1511–1516.

Hamdi, M., Karoui, S., Oueslati, A., Kamoun, S. and Hlel, F. (2018). "Synthesis, crystal structure and dielectric properties of the new organic -inorganic hybrid compound $[C_6H_{10}N_2]7[Bi_2Cl_{11}]2.4[Cl]$." J. Mol. Struct., 1154 516–523.

Hanumantharao, R., Kalainathan, S., Bhagavannarayana, G. and Madhusoodanan, U. (2013). "An extensive investigation on nucleation, growth parameters, crystalline perfection, spectroscopy, thermal, optical, microhardness, dielectric and SHG studies on potential NLO crystal - ammonium Hydrogen L-tartarte." Spectrochim. Acta. A. Mol. Biomol. Spectrosc., 103 388–399.

Haque, S.U., Saikia, K.K., Murugesan, G. and Kalainathan, S. (2017). "A study on dielectric and magnetic properties of lanthanum substituted cobalt ferrite." J. Alloys Compd., 701 612–618.

Hasmuddin, Mohd., Singh, P., Shkir, Mohd., Abdullah, M.M., Vijayan, N., Ganesh, V. and Wahab, M.A. (2014). "Study of pure and l-tartaric acid doped ammonium dihydrogen phosphate single crystals: A novel nonlinear optical non-centrosymmetric crystal." Mater. Chem. Phys., 144 (3), 293–300.

Helen, F. and Kanchana, G. (2015). "Growth, mechanical, dielectric, thermal and optical studies of a nonlinear optical crystal: l-Histidinium dipicrate dihydrate." Mater. Chem. Phys., 151 5–13.

Higashiyama, T. and Hasegawa, S. (1971a). "The Differential Thermal Analysis of Potassium Oxalate." Bull. Chem. Soc. Jpn., 44 (7), 1727–1730.

Higashiyama, T. and Hasegawa, S. (1971b). "The Differential Thermal Analysis of Potassium Oxalate." Bull. Chem. Soc. Jpn., 44 (7), 1727–1730.

Higgins, J., Zhou, X., Liu, R. and Huang, T.T.-S. (1997). "Theoretical Study of Thermal Decomposition Mechanism of Oxalic Acid." J. Phys. Chem. A, 101 (14), 2702–2708.

Hodgson, D.J. and Ibers, J.A. (1969a). "Refinement of the crystal and molecular structure of potassium oxalate monohydrate." Acta Crystallogr. B, 25 (3), 469–477.

Hodgson, D.J. and Ibers, J.A. (1969b). "Refinement of the crystal and molecular structure of potassium oxalate monohydrate." Acta Crystallogr. B, 25 (3), 469–477.

Hottenhuis, M.H.J. and Lucasius, C.B. (1986). "The influence of impurities on crystal growth; In situ observation of the {010} face of potassium hydrogen phthalate." J. Cryst. Growth, 78 (2), 379–388.

Hottenhuis, M.H.J. and Lucasius, C.B. (1988). "The role of impurities on the process of growing potassium hydrogen phthalate crystals from solution; A quantitative approach." J. Cryst. Growth, 91 (4), 623–631.

Hottenhuis, M.H.J. and Lucasius, C.B. (1989). "The influence of internal crystal structure on surface morphology; in situ observations of potassium hydrogen phthalate {010}." J. Cryst. Growth, 94 (3), 708–720.

Hottenhuis, M.H.J. and Oudenampsen, A. (1988). "Fe^{3+} and Ce^{3+} acting as competitive impurities in the crystallization process of potassium hydrogen phthalate from solutions." J. Cryst. Growth, 92 (3), 513–529.

Isac, J., Ittyachen, M.A. and Raju, K.S. (1996). "Praseodymium barium molybdate—its growth and structural characterization." Bull. Mater. Sci., 19 (3), 495–504.

Iwasaki, F.F. and Saito, Y. (1967). "The crystal structure of deuterated oxalic acid dihydrate, $(COOD)_2.2D_2O$, by X-ray analysis." Acta Crystallogr., 23 (1), 56–63.

Jagannatha, N. and Rao, P.M. (1993). "Studies on impurity incorporation in cadmium oxalate crystals grown by gel method." Bull. Mater. Sci., 16 (5), 365–369.

Jananakumar, D. and Mani, P. (2014a). "Growth and characterization of semiorganic crystal potassium hydrogen oxalate." J. Therm. Anal. Calorim., 115 (1), 355–359.

Jananakumar, D. and Mani, P. (2014b). "Growth and characterization of semiorganic crystal potassium hydrogen oxalate." J. Therm. Anal. Calorim., 115.

Jerusha, E., Kirupavathy, S.S. and Gopalakrishnan, R. (2016). "Spectral, optical and dielectric analyses on L-lysine p-nitrophenolate monohydrate organic crystals." Opt. - Int. J. Light Electron Opt., 127 (1), 420–427.

Job, C.B., Shabu, R. and Paulraj, S. (2016a). "Growth, structural, optical, and photo conductivity studies of potassium tetra fluoro antimonate crystal." Opt. - Int. J. Light Electron Opt., 127 (8), 3783–3787.

Job, C.B., Shabu, R. and Paulraj, S. (2016b). "Growth, structural, optical, and photo conductivity studies of potassium tetra fluoro antimonate crystal." Opt. - Int. J. Light Electron Opt., 127 (8), 3783–3787.

John, M.V. and Ittyachen, M.A. (1998). "Studies on $Ce_2(C_2O_4)_3 \cdot nH_2O$ crystals grown in hydro-silica gel." Bull. Mater. Sci., 21 (5), 387–391.

John, V., Ittyachen, M.A. and Raju, K.S. (1997). "Lanthanum samarium oxalate — its growth and structural characterization." Bull. Mater. Sci., 20 (8), 1059–1068.

Joseph, C., Ittyachen, M.A. and Raju, K.S. (1997). "Some structural aspects of neodymium praseodymium oxalate single crystals grown in hydro silica gels." Bull. Mater. Sci., 20 (1), 37–48.

Kadam, S.L., Patankar, K.K., Kanamadi, C.M. and Chougule, B.K. (2004). "Electrical conduction and magnetoelectric effect in $Ni_{0.50}Co_{0.50}Fe_2O_4$ + $Ba_{0.8}Pb_{0.2}TiO_3$ composites." Mater. Res. Bull., 39 (14), 2265–2272.

Kahr, B. and G. Shtukenberg, A. (2016). "Dyeing crystals since 2000." CrystEngComm, 18 (47), 8988–8998.

Kambale, R.C., Shaikh, P.A., Bhosale, C.H., Rajpure, K.Y. and Kolekar, Y.D. (2009). "Dielectric properties and complex impedance spectroscopy studies of mixed Ni–Co ferrites." Smart Mater. Struct., 18 (8), 085014.

Kanagasekaran, T., Mythili, P., Kumar, B. and Gopalakrishnan, R. (2010). "Effect of ion irradiation on the M-Nitroaniline single crystals." Nucl. Instrum. Methods Phys. Res. Sect. B Beam Interact. Mater. At., 268 (1), 36–41.

Kanagasekaran, T., Mythili, P., Srinivasan, P., Vijayan, N., Kanjilal, D., Gopalakrishnan, R. and Ramasamy, P. (2008). "On the observation of physical, chemical, optical and thermal changes induced by 50MeV silicon ion in benzimidazole single crystals." Mater. Res. Bull., 43 (4), 852–863.

Kanchana, P., Elakkina Kumaran, A., Hayakawa, Y. and Sekar, C. (2013). "Effect of divalent metal ion impurities (Ba^{2+}, Ca^{2+} and Mg^{2+}) on the growth, structural and physical properties of KAP crystals." Spectrochim. Acta. A. Mol. Biomol. Spectrosc., 103 187–192.

Karthigha, S. and Krishnamoorthi, C. (2018). "Synthesis, growth, crystal structure, optical and third order nonlinear optical properties of quinolinium derivative single crystal: PNQI." J. Phys. Chem. Solids, 114 133–140.

Karuppasamy, P., Senthil Pandian, M., Ramasamy, P. and Das, S.K. (2018). "Growth and characterization of semi-organic nonlinear optical (NLO) guanidinium trichloroacetate (GTCA) single crystal." Opt. - Int. J. Light Electron Opt., 156 707–719.

Khader, S.A., Sankarappa, T., Sujatha, T., Ashwajeet, J.S. and Ramanna, R. (2015). "Structural and Dielectric Studies on Magneto Electric Nano-composites." Mater. Today Proc., 2 (9, Part A), 4334–4343.

Kittel, C. (2012). "Introduction to Solid State Physics, 8ed (New Delhi: Wiley).

Korah, I., Joseph, C. and Ittyachan, M.A. (2007). "Growth and characterisation of gadolinium samarium oxalate single crystals." Cryst. Res. Technol., 42 (10), 939–942.

Kosinova, A.V., Kolybaeva, M.I., Bezkrovnaya, O.N., Tkachenko, V.F., Grishina, E.V., Levchenko, A.N., Puzikov, V.M. and Pritula, I.M. (2014). "Structural and mechanical properties of KH2PO4 single crystals with embedded nanoparticles and organic molecules." Cryst. Res. Technol., 49 (12), 965–974.

Krishnakumar, V., Manohar, S. and Nagalakshmi, R. (2010). "Semiorganic nonlinear optical l-lysine sulphate growth and characterization." Spectrochim. Acta. A. Mol. Biomol. Spectrosc., 75 (5), 1394–1397.

Krishnakumar, V. and Nagalakshmi, R. (2006). "Polarised Raman and infrared spectral analysis of L-alanine oxalate ($C_5H_9NO_6$)—a non-linear optical single crystal." Spectrochim. Acta. A. Mol. Biomol. Spectrosc., 64 (3), 736–743.

Krishnan, S., Justin Raj, C., Dinakaran, S., Uthrakumar, R., Robert, R. and Jerome Das, S. (2008). "Optical, thermal, dielectric and ferroelectric behaviour of sodium acid phthalate (SAP) single crystals." J. Phys. Chem. Solids, 69 (11), 2883–2887.

Kushwaha, S.K., Shakir, M., Maurya, K.K., Shah, A.L., Wahab, M.A. and Bhagavannarayana, G. (2010). "Remarkable enhancement in crystalline perfection, Second Harmonic Generation Efficiency, Optical Transparency and laser damage threshold in KDP crystals by L-threonine doping." J. Appl. Phys., 108 (3), 033506.

Kuznetsov, V.A., Okhrimenko, T.M. and Rak, M. (1998). "Growth promoting effect of organic impurities on growth kinetics of KAP and KDP crystals." J. Cryst. Growth, 193 (1), 164–173.

Lahlali, S., Essaleh, L., Belaqziz, M., Chehouani, H., Alimoussa, A., Djessas, K., Viallet, B., Gauffier, J.L. and Cayez, S. (2017). "Dielectric and modulus analysis of the photoabsorber Cu2SnS3." Phys. B Condens. Matter, 526 54–58.

Lalia-Kantouri, M. and Manoussakis, G.E. (1984). "THERMAL DECOMPOSITION OF TRIS(N,N-DISUBSTITU!ED DITHIOCARBAMATE) COMPLEXES OF As(lll), Sb(lll) AND Bi(lll)." J. Therm. Anal., 29 (5), 1151–1169.

Long, N.J. (1995). "Organometallic Compounds for Nonlinear Optics—The Search for En-light-enment!" Angew. Chem. Int. Ed. Engl., 34 (1), 21–38.

L. Parker, H., J. Hunt, A., L. Budarin, V., S. Shuttleworth, P., L. Miller, K. and H. Clark, J. (2012). "The importance of being porous: polysaccharide -derived mesoporous materials for use in dye adsorption." RSC Adv., 2 (24), 8992–8997.

Ma, Q., He, H. and Liu, C. (2013). "Hygroscopic properties of oxalic acid and atmospherically relevant oxalates." Atmos. Environ., 69 281–288.

Ma, Y., Teng, B., Cao, L., Zhong, D., Ji, S., Teng, F., Liu, J., Yao, Y., Tang, J. and Tong, J. (2018). "Growth, structural, thermal, dielectric and optical studies on HBST crystal: A potential THz emitter." Spectrochim. Acta. A. Mol. Biomol. Spectrosc., 190 274–282.

Macdonald, J.R. (1992). "Impedance spectroscopy." Ann. Biomed. Eng., 20 (3), 289–305.

Macdonald, J.R. and Johnson, W.B. (2005). Fundamentals of Impedance Spectroscopy. In Impedance Spectroscopy, (Wiley-Blackwell), pp 1–26.

Mahalakshmi, V., Lincy, A., Thomas, J. and Saban, K.V. (2012). "Crystal growth and characterization of a new co-ordination complex—barium tetrakis(maleate) dihydrate." J. Phys. Chem. Solids, 73 (4), 584–588.

Mahendra, K., Bhat, K.S., Nagaraja, H.S. and Udayashankar, N.K. (2019a). "Modulations of physio-chemical and electronic properties of metalorganic KHO single crystals through $Co(OH)_2$ nanoparticles doping." J. Mater. Sci. Mater. Electron., 30 (13), 12566–12576.

Mahendra, K., D'Souza, A. and Udayashankar, N.K. (2017). "Effect of Zn doping on the structural, optical, photoluminescence and mechanical properties of thiourea barium chloride (TBC) crystal." Mater. Today Commun., 13 (Supplement C), 178–185.

Mahendra, K., Kumar, H.K.T. and Udayashankar, N.K. (2019c). "Enhanced structural, optical, thermal, mechanical and electrical properties by a noval approach (nanoparticle doping) on ferroelectric triglycine sulphate single crystal." Appl. Phys. A, 125 (4), 228.

Mahendra, K., Nayak, K.K., Fernandes, B.J. and Udayashankar, N.K. (2018a). "Gamma irradiation effect on structural, optical and electrical properties of organometallic potassium hydrogen oxalate oxalic acid dihydrate single crystal." J. Mater. Sci. Mater. Electron., 29 (22), 18905–18912.

Mangaiyarkarasi, K., Ravichandran, A.T., Anitha, K. and Manivel, A. (2018). "Synthesis, growth and characterization of L-Phenylalaninium methanesulfonate nonlinear optical single crystal." J. Mol. Struct., 1155 758–764.

Manikandan, S., Sundari, A. and Manivannan, S. (2019). "Effect of Cu^{2+} ion on single crystal of nonlinear optical material (glycinium oxalate)." J. Mater. Sci. Mater. Electron., 30 (11), 10711–10721.

Martin Britto Dhas, S.A., Bhagavannarayana, G. and Natarajan, S. (2008). "Growth and characterization of a new potential NLO material from the amino acid family—l-prolinium picrate." J. Cryst. Growth, 310 (15), 3535–3539.

Mary C, M., G, V., Mani, K.P., Jose, G., P.r., B., Joseph, C., N.v., U. and M.a., I. (2016). "Growth and characterization of Sm^{3+} doped cerium oxalate single crystals." J. Mater. Res. Technol., 5 (3), 268–274.

Matulková, I., Cihelka, J., Pojarová, M., Fejfarová, K., Dušek, M., Vaněk, P., Kroupa, J., Krupková, R., Fábry, J. and Němec, I. (2012). "A new series of 3,5-diamino-1,2,4-triazolium(1^+) inorganic salts and their potential in crystal engineering of novel NLO materials." CrystEngComm, 14 (14), 4625–4636.

Mohamed, M.A., Galwey, A.K. and Halawy, S.A. (2002). "The activities of some metal oxides in promoting the thermal decomposition of potassium oxalate." Thermochim. Acta, 387 (1), 63–74.

Muenster, R., Jarasch, M., Zhuang, X. and Shen, Y.R. (1997). "Dye-Induced Enhancement of Optical Nonlinearity in Liquids and Liquid Crystals." Phys. Rev. Lett., 78 42–45.

Murakoshi, K., Kano, G., Wada, Y., Yanagida, S., Miyazaki, H., Matsumoto, M. and Murasawa, S. (1995). "Importance of binding states between photosensitizing

molecules and the TiO_2 surface for efficiency in a dye-sensitized solar cell." J. Electroanal. Chem., 396 (1), 27–34.

Nancollas, G.H. and Gardner, G.L. (1974). "Kinetics of crystal growth of calcium oxalate monohydrate." J. Cryst. Growth, 21 (2), 267–276.

Nandhakumar, R. and Radhakrishnan, T. (2016). "Growth and Study of ADP Crystal Doped with Acridine Orange." Open J. Appl. Sci., 06 (03), 177.

Pan, F., Bailey, R.T., Cruickshank, F.R., Pugh, D., Sherwood, J.N., Simpson, G.S. and Wilkie, S. (1996). "The birefringence of the optically nonlinear crystal 4-amino benzophenone." J. Appl. Phys., 80 (8), 4649–4654.

Panchapakesan, S., Subramani, K. and Srinivasan, B. (2018). "Growth, spectral, thermal, electrical, mechanical and nonlinear optical properties of organic single crystal 4–Amino–(1–methylphenyl) pyridinium bromide." Opt. - Int. J. Light Electron Opt., 157 774–786.

Papazian, H.A., Pizzolato, P.J. and Patrick, J.A. (1971). "Thermal Decomposition of Oxalates of Ammonium and Potassium." J. Am. Ceram. Soc., 54 (5), 250–254.

Pasupathi, G., Murugadoss, K., Senthilkumar, M. and Ramachandraraja, C. (2014). "Synthesis, growth, vibrational, optical and thermal studies of potassium diboro oxalate single crystals." Opt. - Int. J. Light Electron Opt., 14 (125), 3389–3392.

Patil, P.S., Shkir, M., Maidur, S.R., AlFaify, S., Arora, M., Rao, S.V., Abbas, H. and Ganesh, V. (2017). "Key functions analysis of a novel nonlinear optical D-π-A bridge type (2E)-3-(4-Methylphenyl)-1-(3-nitrophenyl) prop-2-en-1-one chalcone: An experimental and theoretical approach." Opt. Mater., 72 427–435.

Pedersen, B.F. (1972). "The crystal structure of ammonium oxalate monoperhydrate." Acta Crystallogr. B, 28 (3), 746–754.

Perkowitz, S. (1993). "Optical characterization of semiconductors: infrared, raman, and photoluminescence spectroscopy (Academic Press).

Pinnavaia, T.J. (1983). "Intercalated clay catalysts." Science, 220 (4595), 365–371.

Prabukanthan, P., Lakshmi, R., Harichandran, G. and Kumar, C.S. (2018). "Synthesis, structural, optical and thermal properties of N-methyl-N-aryl benzamide organic single crystals grown by a slow evaporation technique." J. Mol. Struct., 1156 62–73.

Pring, A. (2006). "Sunagawa, I. 2005. Crystals. Growth, Morphology and Perfection, 295 pp. Cambridge, New York, Melbourne: Cambridge University Press, Volume 143 Issue 5." Geol. Mag., 143 (5), 749–750.

Punniyamoorthy, R., Manimekalai, R., Uma, K. and Pasupathi, G. (2019). "Synthesis and Investigation on Structural, Thermal, Mechanical, Linear Optical, and Nonlinear Optical Nature of Potassium Sulphato Oxalate Single Crystals." Cryst. Res. Technol., 54 (3), 1800203.

Raguram, T., Rajni, K.S., Shanmugam, P. and Meiyazhagan, S. (2016). "Synthesis and characterisation of undoped and methyl orange (dye) doped L-alanine acetate single crystal." 9 678–687.

Rahman, M.A. and Hossain, A.K.M.A. (2014). "Electrical transport properties of Mn–Ni–Zn ferrite using complex impedance spectroscopy." Phys. Scr., 89 (2), 025803.

Raj, A.M.E., Jayanthi, D.D., Jothy, V.B., Jayachandran, M. and Sanjeeviraja, C. (2008). "Growth aspects of barium oxalate monohydrate single crystals in gel medium." Cryst. Res. Technol., 43 (12), 1307–1313.

Raja, R., Seshadri, S. and Saravanan, R.R. (2014). "Crystal growth, spectral, thermal and optical properties of an organic single crystal – Dye doped hippuric acid." Opt. - Int. J. Light Electron Opt., 125 (3), 916–919.

Rajagopalan, N.R. and Krishnamoorthy, P. (2017). "A systematic approach to physico-chemical analysis of tris (thiourea) zinc selenate — A semi-organic nonlinear optical crystal." Opt. - Int. J. Light Electron Opt., 129 118–129.

Rajasekaran, R., Ushasree, P.M., Jayavel, R. and Ramasamy, P. (2001a). "Growth and characterization of zinc thiourea chloride (ZTC): a semiorganic nonlinear optical crystal." J. Cryst. Growth, 229 (1), 563–567.

Rajesh, P., Silambarasan, A. and Ramasamy, P. (2014). "Effect of crystal violet dye on the optical, dielectric, thermal and mechanical properties of <001> directed KDP single crystal." Mater. Res. Bull., 49 (Supplement C), 640–644.

Raju, K.S., Krishna, K.N., Issac, J. and Ittyachen, M.A. (1994). "Structural characterization of gel-grown neodymium copper oxalate single crystals." Bull. Mater. Sci., 17 (7), 1447–1455.

Raju, R.K., Dharmaprakash, S.M. and Jayanna, H.S. (2016). "Gamma irradiation effects on crystalline and optical properties of pure and doped Potassium Hydrogen

Phthalate (KHP) single crystals." Opt. - Int. J. Light Electron Opt., 127 (24), 11649–11656.

Rajyalakshmi, S., Ramachandra Rao, K., Brahmaji, B., Samatha, K., Visweswara Rao, T.K. and Bhagavannarayana, G. (2016). "Optical investigations on Tb^{3+} doped L-Histidine hydrochloride mono hydrate single crystals grown by low temperature solution techniques." Opt. Mater., 54 74–83.

Ramajothi, J. and Dhanuskodi, S. (2007). "Crystal growth, thermal and optical studies on a semiorganic nonlinear optical material for blue-green laser generation." Spectrochim. Acta. A. Mol. Biomol. Spectrosc., 68 (5), 1213–1219.

Ramki, C. and Ezhil Vizhi, R. (2017a). "Growth, optical, electrical and mechanical properties of sodium hydrogen oxalate hydrate ($NaHC_2O_4 \cdot H_2O$) single crystal for NLO applications." Mater. Chem. Phys., 197 70–78.

Ramki, C. and Ezhil Vizhi, R. (2018). "Study on the mechanical properties of potassium sodium hydroxide borate hydrate (KSB) single crystals by using Vickers microhardness tester." Mater. Lett., 215 165–168.

Rao, G.B., Rajesh, P. and Ramasamy, P. (2017). "Enhanced optical, thermal and piezoelectric behavior in dye doped potassium acid phthalate (KAP) single crystal." J. Cryst. Growth, 468 411–415.

Rathika, A., Prasad, L.G. and Raman, R.G. (2016). "Physicochemical properties of dimethylammonium p-nitrophenolate– p-nitrophenol: A nonlinear optical crystal." Phys. B Condens. Matter, 485 29–34.

Ray, G., Kumar, S., Sinha, N. and Kumar, B. (2017a). "Enhanced dielectric piezo-/ferro-/electric properties of dye doped sodium acid phthalate crystal." Curr. Appl. Phys., 17 (5), 813–819.

Ray, G., Kumar, S., Sinha, N. and Kumar, B. (2017b). "Enhanced dielectric piezo-/ferro-/electric properties of dye doped sodium acid phthalate crystal." Curr. Appl. Phys., 17 (5), 813–819.

Rebbah, H., Borel, M.M. and Raveau, B. (1980). "Intercalation of alkylammonium ions and oxide layers |TiNbOt|−." Mater. Res. Bull., 15 (3), 317–321.

Rosso, K.M., Smith, D.M.A. and Dupuis, M. (2003). "An ab initio model of electron transport in hematite (α-Fe2O3) basal planes." J. Chem. Phys., 118 (14), 6455–6466.

Ruby Nirmala, L. and Thomas Joseph Prakash, J. (2013). "Habit modification of bis-thiourea zinc chloride (ZTC) semi organic crystals by impurities." Spectrochim. Acta. A. Mol. Biomol. Spectrosc., 110 249–254.

Rudolph, P. (2003). Thermodynamic Fundamentals of Phase Transitions Applied to Crystal Growth Processes. In Crystal Growth Technology, H.J. Scheel, and T. Fukuda, eds. (John Wiley & Sons, Ltd), pp 15–42.

S., N.S.D. and E.k., G. (2018). "A comparative study on the effect of l-tartaric acid and sodium bicarbonate on the growth and characterization of KDP single crystals." Optik, 164 498–509.

Sagadevan, S. (2016a). "Optical and electrical studies of non-linear optical crystal: Potassium boro-oxalate." Opt. - Int. J. Light Electron Opt., 127 (14), 5613–5621.

Sanchez, C., Julián, B., Belleville, P. and Popall, M. (2005). "Applications of hybrid organic–inorganic nanocomposites." J. Mater. Chem., 15 (35–36), 3559–3592.

Sangwal, K. (2000). "On the reverse indentation size effect and microhardness measurement of solids." Mater. Chem. Phys., 63 (2), 145–152.

Sankar, R., Raghavan, C.M., Mohan Kumar, R. and Jayavel, R. (2007). "Growth and characterization of a new semiorganic non-linear optical thiosemicarbazide cadmium chloride monohydrate ($Cd(NH_2NHCSNH_2)Cl_2 \cdot H_2O$) single crystals." J. Cryst. Growth, 305 (1), 156–161.

Santhi, G. and Alagar, M. (2016). "Growth and Characterization of Single Crystals of Thiourea and Tartaric Acid Based Compounds." 2 2454–1362.

Saritha, P. (2013). "Growth and Analysis of Urea Thiourea Sodium Sulphate Crystal." IOSR J. Appl. Phys., 4 38–41.

Sasi, S., Robert, R., Arumugam, S. and Inmozhi, C. (2016). "Growth, optical and spectroscopic studies of l-cysteine doped KDP single crystals." Opt. - Int. J. Light Electron Opt., 127 (4), 2366–2369.

Sass, S.L. (2011). "The Substance of Civilization: Materials and Human History from the Stone Age to the Age of Silicon (Skyhorse Publishing Inc.).

Senthil Pandian, M. and Ramasamy, P. (2010). "Conventional slow evaporation and Sankaranarayanan–Ramasamy (SR) method grown diglycine zinc chloride (DGZC) single crystal and its comparative study." J. Cryst. Growth, 312 (3), 413–419.

Serpaggi, F. and Férey, G. (1998). "Hybrid open frameworks (MIL-n). Part 4 Synthesis and crystal structure of MIL-8, a series of lanthanide glutarates with an open framework, $[Ln(H_2O)]_2[O_2C(CH_2)_3CO_2]_3 \cdot 4H_2O$." J. Mater. Chem., 8 (12), 2737–2741.

Shahil Kirupavathy, S., Stella Mary, S., Mythili, P. and Gopalakrishnan, R. (2008). "Growth and characterization of pure and doped cadmium thiourea acetate single crystals." J. Cryst. Growth, 310 (10), 2555–2562.

Shaikh, R.N., Anis, M., Shirsat, M. and Shuakat, H. (2013). "Investigation on the Linear and Nonlinear Optical Properties of L-Lysine Doped Ammonium Dihydrogen Phosphate Crystal for NLO Applications." IOSR J. Appl. Phys., 6.

Shakila, K. and Kalainathan, S. (2015). "Synthesis aspects, structural, spectroscopic, antimicrobial and room temperature ferromagnetism of zinc iodide complex with Schiff based ligand." Spectrochim. Acta. A. Mol. Biomol. Spectrosc., 135 1059–1065.

Shanthi, D., Selvarajan, P. and Perumal, S. (2016a). "Growth, linear optical constants and photoluminescence characteristics of beta-alaninium picrate (BAP) crystals." Opt. - Int. J. Light Electron Opt., 127 (6), 3192–3199.

Shanthi, D., Selvarajan, P. and Perumal, S. (2016b). "Growth, linear optical constants and photoluminescence characteristics of beta-alaninium picrate (BAP) crystals." Opt. - Int. J. Light Electron Opt., 127 (6), 3192–3199.

Shenoy, U.S., Bantawal, H. and Bhat, D.K. (2018). "Band Engineering of SrTiO3: Effect of Synthetic Technique and Site Occupancy of Doped Rhodium." J. Phys. Chem. C, 122 (48), 27567–27574.

Shkir, M., AlFaify, S., Abbas, H. and Muhammad, S. (2015). "First principal studies of spectroscopic (IR and Raman, UV-visible), molecular structure, linear and nonlinear optical properties of L-arginine p-nitrobenzoate monohydrate (LANB): A new non-centrosymmetric material." Spectrochim. Acta. A. Mol. Biomol. Spectrosc., 147 84–92.

Shkir, M., Ganesh, V., AlFaify, S., Maurya, K.K. and Vijayan, N. (2017a). "Effect of phenol red dye on monocrystal growth, crystalline perfection, and optical and dielectric properties of zinc (tris) thio-urea sulfate." J. Appl. Crystallogr., 50 (6), 1716–1724.

Shkir, Mohd., Patil, P.S., Arora, M., AlFaify, S. and Algarni, H. (2017b). "An experimental and theoretical study on a novel donor-π-acceptor bridge type 2, 4, 5-

trimethoxy-4′-chlorochalcone for optoelectronic applications: A dual approach." Spectrochim. Acta. A. Mol. Biomol. Spectrosc., 173 445–456.

Shoba, M. and Kaleemulla, S. (2017). "Structural, optical and dielectric studies of Er substituted zinc ferrite nanospheres." J. Phys. Chem. Solids, 111 447–457.

Singh, D.V., Kumar Bhargava, Dr.G., Dhiman, P., K. Kotnala, R., Shah, J., Batoo, K. and Singh, M. (2014). "Structural, Dielectric And Magnetic Properties Of Nanocrystalline BaFe12O19 Hexaferrite Processed Via Sol-gel Technique." Adv. Mater. Lett., In press.

Sinha, N., Bhandari, S., Yadav, H., Ray, G., Godara, S., Tyagi, N., Dalal, J., Kumar, S. and Kumar, B. (2015a). "Performance of crystal violet doped triglycine sulfate single crystals for optical and communication applications." CrystEngComm, 17 (30), 5757–5767.

Sinha, N., Goel, N., Singh, B.K., Gupta, M.K. and Kumar, B. (2012a). "Enhancement in ferroelectric, pyroelectric and photoluminescence properties in dye doped TGS crystals." J. Solid State Chem., 190 180–185.

Sinha, N., Goel, N., Singh, B.K., Gupta, M.K. and Kumar, B. (2012c). "Journal of Solid State Chemistry Enhancement in ferroelectric , pyroelectric and photoluminescence properties in dye doped TGS crystals." J. Solid State Chem., 190 180–185.

Sorescu, M., Knobbe, E.T., Martin, J.J., Barrie, J.D. and Barb, D. (1995). "Excimer laser and electron beam irradiation effects in iron-doped lithium niobate." J. Mater. Sci., 30 (23), 5944–5952.

Spring-Thorpe, A.J. and Pamplin, B.R. (1968). "Growth of some single crystal II–IV–V2 semiconducting compounds." J. Cryst. Growth, 3–4 (Supplement C), 313–316.

Stewart, R.D. (2011). "The function of oxalic acid in the human metabolism." Clin. Chem. Lab. Med., 49 (9), 1405–1412.

Subramani, K., Joseph, P.S. and Shankar, G. (2013). "Optical, electrical and ac conductivity measurements of nonlinear optical Dimethylaminomethylphthalimide doped with cadmium chloride single crystal for nano applications." Opt. Commun., 300 12–16.

Sujatha, T., Cyrac Peter, A., Vimalan, M., Merline Shyla, J. and Madhavan, J. (2010). "Thermal, mechanical, optical and conductivity studies of a novel NLO active l-

phenylalanine l-phenylalaninium dihydrogenphosphate single crystal." Phys. B Condens. Matter, 405 (16), 3365–3370.

Suresh, T., Vetrivel, S., Gopinath, S. and Mullai, R.U. (2018). "A new metal-organic nonlinear optical material: L-Asparagine Indium chloride (LAIn) for photonics application." Chin. J. Phys., 56 (6), 2773–2781.

Takasaki, E. and Naito, Y. (1968). "[Studies on a microdetermination of oxalic acid (Zarembski and Hodgkinson's method]." Nihon Hinyokika Gakkai Zasshi Jpn. J. Urol., 59 (12), 1117–1120.

Tao, X.T., Yuan, D.R., Zhang, N., Jiang, M.H. and Shao, Z.S. (1992). "Novel organic molecular second harmonic generation crystal: 3-methoxy-4-hydroxy-benzaldehyde." Appl. Phys. Lett., 60 (12), 1415–1417.

Thaila, T. and Kumararaman, S. (2012a). "Growth and characterization of Glycine Magnesium Chloride single crystals for NLO applications." Arch. Appl. Sci. Res., 4 (3), 1494–1501.

Thaila, T. and Kumararaman, S. (2012b). "Growth and characterization of Glycine Magnesium Chloride single crystals for NLO applications." 4 (3), 1494–1501.

Theras, J.E.M., Kalaivani, D., Mercina, M., Jayaraman, D. and Joseph, V. (2016). "Characterization of l-threonine phthalate crystal for photonic and nonlinear optical applications." Opt. - Int. J. Light Electron Opt., 127 (6), 3397–3401.

Tsay, C.-Y., Lin, Y.-H., Wang, Y.-M., Chang, H.-Y., Lei, C.-M. and Jen, S.-U. (2016a). "Electrical transport properties of $CoMn_{0.2-x}Ga_xFe_{1.8}O_4$ ferrites using complex impedance spectroscopy." AIP Adv., 6 (5), 055909.

Tyagi, N., Sinha, N., Yadav, H. and Kumar, B. (2015). "Pyroelectric properties and conduction mechanism in solution grown glycine sodium nitrate single crystal." Phys. B Condens. Matter, 462 18–24.

Uma, J. and Rajendran, V. (2016). "Growth and properties of semi-organic nonlinear optical crystal: L-Glutamic acid hydrochloride." Prog. Nat. Sci. Mater. Int., 26 (1), 24–31.

Usharani, S., Natarajan, V., Judes, J., Arivanandhan, M., Anandan, P. and Natarajan, S. (2016). "Crystal growth, structural and optical properties of a novel benzophenone derivative: 2-Chloro 5-nitro benzophenone." Opt. - Int. J. Light Electron Opt., 127 (15), 5887–5893.

V. Kannan, N.P.R. (2004). "Growth and characterization of Bisthiourea-zinc Acetate, a new nonlinear optical material." J. Cryst. Growth - J CRYST GROWTH, 269 (2), 565–569.

V Mary Sheeja, O. (2013). "GROWTH AND CHARACTERIZATION OF CdS DOPED KDP SINGLE CRYSTALS." Int. J. Res. Eng. Technol., 02 738–748.

Varghese, G., Ittyachen, M.A. and Issac, J. (1990). "Studies on La1–xCux · 3C2O4 · nH2O crystals grown in hydro-silica gel." Cryst. Res. Technol., 25 (7), K153–K159.

Vidotti, M., Greco, C. van, Ponzio, E.A. and Córdoba de Torresi, S.I. (2006). "Sonochemically synthesized Ni(OH)2 and Co(OH)2 nanoparticles and their application in electrochromic electrodes." Electrochem. Commun., 8 (4), 554–560.

Vimal, G., Mani, K.P., Jose, G., Biju, P.R., Joseph, C., Unnikrishnan, N.V. and Ittyachen, M.A. (2014). "Growth and spectroscopic properties of samarium oxalate single crystals." J. Cryst. Growth, 404 20–25.

Virk, H.S., Chandi, P.S. and Srivastava, A.K. (2001). "Physical and chemical changes induced by 70 MeV carbon ions in polyvinylidene difluoride (PVDF) polymer." Nucl. Instrum. Methods Phys. Res. Sect. B Beam Interact. Mater. At., 183 (3), 329–336.

Vizhi, R.E. and Vijayalakshmi, M. (2016). "Bulk growth and characterization of novel organic piperazinium (bis) hydrogen succinate single crystals." J. Cryst. Growth, 452 204–212.

Weber, W.H. and Eagen, C.F. (1979). "Energy transfer from an excited dye molecule to the surface plasmons of an adjacent metal." Opt. Lett., 4 (8), 236–238.

Whittaker, E.J.W. (1981). CHAPTER 8 - The Basis of X-ray Crystallography. In Crystallography, (Amsterdam: Pergamon), pp 121–129.

Wojtaś, M., Jakubas, R., Ciunik, Z. and Medycki, W. (2004). "Structure and phase transitions in $[(CH_3)_4P]_3[Sb_2Br_9]$ and $[(CH_3)_4P]_3[Bi_2Br_9]$." J. Solid State Chem., 177 (4), 1575–1584.

Wu, D., Wei, Y., Ren, X., Ji, X., Liu, Y., Guo, X., Liu, Z., Asiri, A.M., Wei, Q. and Sun, X. (2018). "Co(OH)2 Nanoparticle-Encapsulating Conductive Nanowires Array: Room-Temperature Electrochemical Preparation for High-Performance Water Oxidation Electrocatalysis." Adv. Mater., 30 (9), 1705366.

Yadav, H., Sinha, N., Tyagi, N. and Kumar, B. (2015). "Enhancement of Optical, Piezoelectric, and Mechanical Properties in Crystal Violet Dye-Doped Benzophenone Crystals Grown by Czochralski Technique." Cryst. Growth Des., 15 (10), 4908–4917.

Yaghi, O.M., Li, H., Davis, C., Richardson, D. and Groy, T.L. (1998). "Synthetic Strategies, Structure Patterns, and Emerging Properties in the Chemistry of Modular Porous Solids." Acc. Chem. Res., 31 (8), 474–484.

Yang, J.C. and Loewus, F.A. (1975). "Metabolic Conversion of l-Ascorbic Acid to Oxalic Acid in Oxalate-accumulating Plants." Plant Physiol., 56 (2), 283–285.

Zhang, L., Ma, Y. and Li, Y. (2017). "Preparing crystalline silicon from Si-Sn solvent by zone melting directional solidification method." Mater. Sci. Semicond. Process., 71 (Supplement C), 12–19.

Zhang, X.-M., Tong, M.-L. and Chen, X.-M. (2002). "Hydroxylation of N-heterocycle ligands observed in two unusual mixed-valence Cu(I)/Cu(II) complexes." Angew. Chem. Int. Ed Engl., 41 (6), 1029–1031.

Zhang, Y., Li, H., Xi, B., Che, Y. and Zheng, J. (2008). "Growth and characterization of l-histidine nitrate single crystal, a promising semiorganic NLO material." Mater. Chem. Phys., 108 (2), 192–195.

Research Output

Journal Publications

1. **Mahendra K**, Nayak K.K, Fernandes B.J. and Udayashankar N.K. (2018). "Gamma irradiation effect on structural, optical and electrical properties of organometallic potassium hydrogen oxalate oxalic acid dihydrate single crystal" *J Mater Sci: Mater Electron*, 29 (22), 18905–18912 DOI:10.1007/s10854-018-9888-0.
2. **Mahendra K,** Bhat K.S, Nagaraja H.S. and Udayashankar N.K. (2019). "Modulations of physio-chemical and electronic properties of metalorganic KHO single crystals through $Co(OH)_2$ nanoparticles doping" *J. Mater. Sci. Mater. Electron.*, 30 (13), 12566–12576 DOI: 10.1007/s10854-019-01617-1.
3. **Mahendra K** and Udayashankar N.K. (2019). "Growth and comparative studies on oxalic acid dihydrate, potassium oxalate hydrate and potassium hydrogen oxalate oxalic acid dihydrate single crystals" *J. Phys. Chem. Solids*, 109263 DOI: 10.1016/j.jpcs.2019.109263.
4. **Mahendra, K.** and Udayashankar, N.K. (2020). "A study on structural, optical, thermal and electrical properties of the amaranth dye-doped KHOOD single crystal." International Journal of Modern Physics B, 34 2050002.
5. **Mahendra, K.** and Udayashankar, N.K. (2020). "Investigation on mechanical and temperature dependent electrical properties of potassium hydrogen oxalate oxalic acid dihydrate single crystal." Physics Letters A, 384 (19), 126475.
6. **Mahendra K** and Udayashankar N.K. "Investigation on Crystal Structure, Structural, Optical and Thermal Properties of Organometallic Potassium Hydrogen Oxalate Oxalic Acid Dihydrate Single Crystal" (*Inorganic and Nano-Metal Chemistry*, Taylor and Fransis Publisher (Under Review))
7. **Mahendra K**, Nayak K.K. and Udayashankar N.K. "Negative photoconductivity in metal-organic potassium oxalate oxalic acid dihydrate single crystal" (Submitted)

8. **Mahendra K,** Kumar H.K.T. and Udayashankar N.K. (2019). "Enhanced structural, optical, thermal, mechanical and electrical properties by a noval approach (nanoparticle doping) on ferroelectric triglycine sulphate single crystal." *Appl. Phys. A*, 125 (4), 228 DOI: 10.1007/s00339-019-2499-7.
9. **Mahendra K,** Fernandes J. M. and Udayashankar N.K. "A Novel Approach to the Synthesis of Nonlinear Organometallic Ammonium Hydrogen Oxalate Oxalic acid Dihydrate Single Crystal and its Characterization" (Submitted)
10. **Mahendra K,** Fernandes J.M. and Udayashankar N.K. "Effect of Gamma Irradiation on the Structural, Mechanical, Optical and Electrical Properties of Organometallic Ammonium Hydrogen Oxalate Oxalic acid Dihydrate Single Crystal" (Submitted)

Conferences participated

1. International conference on Recent Advances in Materials, Mechanical and Civil Engineering held at MLRIT Hyderabad 1-2nd June 2017.
2. International conference on Multifunctional Materials for future applications (ICMFA) held at IIT BHU 27-29 Oct 2015.
3. International conference on advanced materials (SCICON 16) held at Amrita Vishwa Vidhyapeetam University Coimbatore 19-21 Dec 2016.
4. International conference on advanced materials (SCICON 16) Amrita Vishwa vidhyapeetam University Coimbatore **(Best Paper award).**
5. International workshop on Advaned Materials (IWAM) 2017 19-21st Dec 2017 Behrampur Odisha.
6. International conference on nanotechnology: Ideas, Innovations and Initiatives held at IIT Roorkee 6-8 Dec 2017.

Scientific activities and Workshops participation:

1. Three dimentional structure (DRUG) determination Using X-Ray Crystallography, Manipal, 26th February 2013.
2. Computational Materials Science, NITK, 17-18th April 2015.
3. Asia Students Photonic conference, Manipal, 12-14th December 2016.
4. Nano-structured materials and their applications in catalysis and fuel cells

(NMFC-2016), NITK, 29-1st October 2016.

5. GIAN sponsored program on "Novel functional materials for energy conversion" conducted Chemistry department, NITK, 04- 07th October 2016.
6. DST-PURSE Laboratory - National Workshop on Theory and Practice of Molecular Structure Determination using X-ray Crystallography, Mangalore University, 3-5th, March 2016.

Mahendra K

Research scholar, Department of Physics, National Institute of Technology Karnataka, Surathkal, Mangalore-525 025, India

Mob: +91 9743997789

Email: manukolya@gmail.com

Education

Course	Institution	Year of completion
PhD	National Institute of Technology Karnataka, Surathkal	2019
MSc-Photonics	Manipal University, Manipal	2013
BSc-(Physics, Mathematics and Computer Science)	Canara College, Mangalore, Karnataka	2011
XII (Pre-university Board)	St. Sebastian Pre-University College, Thokkottu, Karnataka	2008
X (SSLC)	Anandashrama High School, Mangalore, Karnataka, India.	2006

Research Experience

- Crystal growth and nanomaterials laboratory, Department of Physics, National Institute of Technology, Surathkal. (2013-present)
  Research Scholar
  Thesis title: "Synthesis and characterization of semiorganic potassium hydrogen oxalate oxalic acid dihydrate single crystals"
  Supervisor: Dr. N.K. Udayashankar
- Department of atomic and molecular Physics, Manipal University, Manipal, Karnataka, India.
  MSc-II (2012-2013)
  Project: "Crystallization trials using optical forces"
  Supervisor: Dr. Abdul Ajees

Achievements and awards

- Secured 2nd position in the CHESS event held at NITK, Surathkal.
- Participated in Annual Training Camp, Combined Annual Training Camp, National Integration Camp, Pre Vayu Sainik I and Pre Vayu Sainik II Camps in NCC activity.
- Cleared NCC 'B' and 'C' examination.

Teaching Experience:

- Teaching Assistant (August 2014-July 2018), Department of Physics, National Institute of Technology Karnataka, Surathkal, India.
  - Tutorials for MSc students.
  - B.Tech Physics experiments and MSc-I Physics experiments.
- Guest faculty (August 2013-December 2013), Department of Electronics, Field Marshal K M Cariappa College, Madikeri, Karnataka, India.
  - M.Sc. – Molecular spectroscopy, Mathematical Physics and MSc laboratory.
  - B.Sc. – Physics theory and experiments.

Instrumental knowledge

- Hands on experience on,
  1. Optical tweezer Setup.
  2. Handling solution growth apparatus for crystal growth.
  3. Rigaku miniflex-600 X-ray diffractometer.
  4. Ocean optics UV-visible spectrometer and Diffuse reflectance spectrometer.
  5. Sigma photoluminescence spectrometer.
  6. Keythley I-V Sourcemeter.
  7. Agilent LCR meter.
  8. Clemex microhardness tester.
  9. Vacuum furnace.
  10. Vacuum coating systems.
  11. Vacuum Sealing Unit.
  12. Photocatalysis system.
  13. Optical microscope.

Computer knowledge

- Experience in analysing data using Panalytical Xpert highscore plus and Origin software.

Publications

Peer-reviewed Journal publications:

1. **Mahendra K**, Nayak K.K, Fernandes B.J. and Udayashankar N.K. (2018). "Gamma irradiation effect on structural, optical and electrical properties of organometallic potassium hydrogen oxalate oxalic acid dihydrate single crystal" *J Mater Sci: Mater Electron*, 29 (22), 18905–18912 DOI:10.1007/s10854-018-9888-0.
2. **Mahendra K,** Bhat K.S, Nagaraja H.S. and Udayashankar N.K. (2019). "Modulations of physio-chemical and electronic properties of metalorganic KHO single crystals through $Co(OH)_2$ nanoparticles doping" *J. Mater. Sci. Mater. Electron.*, 30 (13), 12566–12576 DOI: 10.1007/s10854-019-01617-1.
3. **Mahendra K** and Udayashankar N.K. (2019). "Growth and comparative studies on oxalic acid dihydrate, potassium oxalate hydrate and potassium hydrogen oxalate oxalic acid dihydrate single crystals" *J. Phys. Chem. Solids*,

109263 DOI: 10.1016/j.jpcs.2019.109263.

4. **Mahendra, K.** and Udayashankar, N.K. (2020). "A study on structural, optical, thermal and electrical properties of the amaranth dye-doped KHOOD single crystal." International Journal of Modern Physics B, 34 2050002.
5. **Mahendra, K.** and Udayashankar, N.K. (2020). "Investigation on mechanical and temperature dependent electrical properties of potassium hydrogen oxalate oxalic acid dihydrate single crystal." Physics Letters A, 384 (19), 126475.
6. **Mahendra K** and Udayashankar N.K. "Investigation on Crystal Structure, Structural, Optical and Thermal Properties of Organometallic Potassium Hydrogen Oxalate Oxalic Acid Dihydrate Single Crystal" (*Inorganic and Nano-Metal Chemistry*, Taylor and Fransis Publisher (Under Review))
7. **Mahendra K**, Nayak K.K. and Udayashankar N.K. "Negative photoconductivity in metal-organic potassium oxalate oxalic acid dihydrate single crystal" (Submitted)
8. **Mahendra K,** Kumar H.K.T. and Udayashankar N.K. (2019). "Enhanced structural, optical, thermal, mechanical and electrical properties by a noval approach (nanoparticle doping) on ferroelectric triglycine sulphate single crystal." *Appl. Phys. A*, 125 (4), 228 DOI: 10.1007/s00339-019-2499-7.
9. **Mahendra K,** Fernandes J. M. and Udayashankar N.K. "A Novel Approach to the Synthesis of Nonlinear Organometallic Ammonium Hydrogen Oxalate Oxalic acid Dihydrate Single Crystal and its Characterization" (Submitted)
10. **Mahendra K,** Fernandes J.M. and Udayashankar N.K. "Effect of Gamma Irradiation on the Structural, Mechanical, Optical and Electrical Properties of Organometallic Ammonium Hydrogen Oxalate Oxalic acid Dihydrate Single Crystal" (Submitted)

Conferences attended:

1. International conference on Recent Advances in Materials, Mechanical and Civil Engineering held at MLRIT Hyderabad 1-2nd June 2017.
2. International conference on Multifunctional Materials for future applications (ICMFA) held at IIT BHU 27-29 Oct 2015.
3. International conference on advanced materials (SCICON 16) held at Amrita Vishwa Vidhyapeetam University Coimbatore 19-21 Dec 2016.
4. International conference on advanced materials (SCICON 16) Amrita Vishwa vidhyapeetam University Coimbatore **(Best Paper award)**
5. International workshop on Advaned Materials (IWAM) 2017 19-21st Dec 2017 Behrampur Odisha.
6. International conference on nanotechnology: Ideas, Innovations and Initiatives held at IIT Roorkee 6-8 Dec 2017.

Scientific activities and Workshops attended:

1. Recent Advances in Photonics, Manipal, 10th March 2012.
2. Recent Advances in Photonics, Manipal, 23rd February 2013.
3. Three dimentional structure (DRUG) determination Using X-Ray Crystallography, Manipal, 26th February 2013.
4. Computational Materials Science, NITK, 17-18th April 2015.
5. Asia Students Photonic conference, Manipal, 12-14th December 2016.

6. Nano-structured materials and their applications in catalysis and fuel cells (NMFC-2016), NITK, 29-1st October 2016.
7. GIAN sponsored program on "Novel functional materials for energy conversion" conducted Chemistry department, NITK, 04- 07th October 2016.
8. DST-PURSE Laboratory - National Workshop on Theory and Practice of Molecular Structure Determination using X-ray Crystallography, Mangalore University, 3-5th, March 2016.

Hobbies:

Riding, exploring new places, trekking and playing outdoor games are my hobbies.

Working Style:

- Begin with basic and easy tasks, and move on to complex things.
- Good problem analysing and solving skills.
- Strong independent worker and excellent in team work.
- Well organized and fast learner.

References:

1. Dr. N. K. Udayashankar
   Professor
   Department of Physics
   National Institute of Technology Karnataka
   Surathkal-575025
   Email: nkuday_01@yahoo.com;

2. Dr. Abdul Ajees
   Associate Professor
   Department of Atomic and Molecular Physics
   Manipal University
   Manipal- 576104
   Email: abdul.ajees@manipal.edu;